3D Design Process of Clothing for Women Applied in Corsetry and Ballistic Protection using 3D Warp Interlock Fabrics

Doctoral dissertation by

Mulat Alubel ABTEW

In the partial fulfilment of Erasmus Mundus Joint Doctor of Philosophy Program

On

Sustainable Management and Design for Textiles

Jointly Organized by

University of Lille, FRANCE

"Gheorghe Asachi" Technical University of Iași, ROMANIA

Soochow University, CHINA

Jury Composition
President: **Professor Emilie DREAN**
Examiners: **Professor Dr.ing.Cătălin FETECĂU**
                             Professor Antonela CURTEZA
Thesis director: **Professor Pascal BRUNIAUX** (*ENSAIT-GMTEX*)
*Thesis co- director***:**   **Professor Carmen LOGHIN** (*GATU*)
                             Professor Yan Chen (*Soochow University*)
                             Professor François Boussu (*ENSAIT-GMTEX*)
                             Dr. Irina Cristian (*GATU*)
                             Dr. Lichuan Wang (*Soochow University*)

Date of thesis defence: - 29 June, 2020

Processus de conception 3D de vêtements pour femmes appliqués en corsetterie et protection balistique à l'aide de tissus 3D Warp Interlock

Thèse de doctorat de

Mulat Alubel ABTEW

Dans le cadre des réalisations partielles du programme Erasmus Mundus de doctorat en philosophie

Sur

Gestion et conception durables pour les textiles

Organisé conjointement par

Université of Lille, FRANCE
"Gheorghe Asachi" Technical University of Iași, ROMANIA
Soochow University, CHINA

Composition du jury
President: **Professor Emilie DREAN**
Examinateurs: **Professor Dr.ing.Cătălin FETECĂU**
Professor Antonela CURTEZA
Thèse directeur: **Professor Pascal BRUNIAUX** (*ENSAIT-GMTEX*)
*Thèse co- directeur***:** **Professor Carmen LOGHIN** (*GATU*)
Professor Yan Chen (*Soochow Université*)
Professor François Boussu (*ENSAIT-GMTEX*)
Dr. Irina Cristian (*GATU*)
Dr. Lichuan Wang (*Soochow Université*)

Date de soutenance de thèse : - Juin 29, 2020

3D Design Process of Clothing for Women Applied in Corsetry and Ballistic Protection using 3D Warp Interlock Fabrics

Abstract

The number of women participation in different perilous tasks including law enforcement and related fields shows an increment. However, they are still forced to wear either small-sized man's body armour or traditionally designed women-based armour system during fieldwork. This ultimately puts them in danger by bringing poor ballistic impact protection, bad fitness as well as less comfort. These problems mainly ascend from using both less accurate sizing system and involvements of darts during armour design to accommodate the bust area. This ultimately creates weak parts at a seam while ballistic impact and discomfort by the accumulated fabrics. Nowadays, significant efforts have been made to improve its overall performance. However, still designing women's soft body armour which properly accommodates the different women body shape for better ballistic impact protection without conceding fitness and comfort are in great demand. This thesis proposed a novel 3D designing (CAD) technique for generating patterns for seamless women body armour. Besides, an appropriate textile (3D woven) fabric structures were engineered to accommodate the design for better performances.

In the design process, various approaches have been utilised to develop the required pattern for women's seamless frontal soft body armour. The first steps devised new techniques to model the adaptive bust on a 3D virtual mannequin (having 90B cup size) using the 3D design process. The developed adaptive bust assisted for easy generations of 3D bra patterns from different bust volumes of same women body size. Later, an adaptive bust cup was associated with other frontal parts of 3D women virtual mannequin to develop a 2D block pattern for first layers of women seamless soft body armour panel using reverse engineering approach (2D-3D-2D pattern generation). This approach also used to attain the required bust volume in the pattern by eliminating the involvement of design element including darts. However, since the body armour comprises multiple panel layers, determining the pattern for each successive panel layer was very important. For this, a systematic 3D design approach through parametrisation process based on each layer's thickness was then utilized to generate block patterns for each successive armour panel's layer. Through experimental validation, such a 3D design approach and its manufacturing system were found precisely to generate the different multi-layer panel's pattern for developing seamless women's soft body armour.

Besides, due to its excellent moulding ability, 3D warp interlock p-aramid fabrics based on various parameters including warp yarn interchange ratios were designed and manufactured to accommodate the proposed design through a dome-formation (moulding) process. Moreover, the developed 3D warp interlock and corresponding traditional 2D plain weave p-aramid fabric were investigated for its mechanical behaviour and ballistic impact performance against NIJ-standard Level IIIA. Based on the result, the woven fabric type (2D and 3D woven), panel impact conditions and layers number show a great effect on ballistic impact performances of target panels. Unlike a higher number of layers, 2D plain weave fabric panels

revealed higher energy absorption with corresponding 3D warp interlock O-L p-aramid fabric at a lower number of layers due to its rigid and stiffness property. However, based on the previous result, we enhanced the ballistic performances of the 3D warp interlock by designing and manufacturing the fabrics by re-arranging the different warp yarn ratios inside the structure. Based on the result, 3D warp interlock fabrics made with equal or a higher interchange ratio of binding: stuffer warp yarn inside the 3D fabric, i.e. 66.7% binding and 33.3% stuffer warp yarns revealed much lower back face signature values and higher energy absorbing capability with minimum number panels layer penetrations compared with its corresponding 2D plain weave and other 3D warp interlock fabric variants. The moulding behaviour and its recovery values of the 3D warp interlock fabrics toward hemispherical punching were also greatly affected by the binding-stuffer warp yarns interchange ratio inside the 3D warp interlock fabric variants. A perform with an optimised proportions of stuffer and binding warp yarns ratio revealed better drawing-in and in-plane shear values than other preforms. In conclusion, it was also possible to achieve the 3D warp interlock structure which could both accommodate the women's body contour with better ballistic impact performances compare to the conventional 2D plain woven fabrics.

Processus de conception 3D de vêtements pour femmes appliqués en corsetterie et protection balistique à l'aide de tissus 3D Warp Interlock

Résumé

Au cours des dernières décennies, le nombre de femmes participant à des tâches périlleuses dans les domaines de l'armée, de la police et de domaines connexes ont augmenté. Celles-ci portent toujours un gilet pare-balles conçu pour une morphologie masculine, ce qui les met potentiellement en danger en apportant une mauvaise protection balistique, moins adaptée à leur morphologie féminine, donc inconfortable. De tels problèmes surviennent suite à un système de taille moins précis lors de la conception des vêtements, à cause des pinces qui permettent le moulage du buste mais qui entraîne des parties amoindries à l'impact balistique au niveau des coutures et de l'inconfort dû à la difficulté de pliage des multicouches de tissus. D'importants efforts ont été réalisés pour améliorer les performances globales de ces gilets pare-balles au niveau de la matière, de l'architecture du tissu et de la conception de ses vêtements. Cependant, la conception de gilets souples qui s'adaptent à la morphologie de l'ensemble des personnels féminins pour une meilleure protection balistique et un meilleur confort semble très demandée. Dans cette thèse, une nouvelle technique de conception numérique 3D associée à des structures de tissu appropriées a permis de développer un gilet pare-balles adapté à la morphologie féminine. Dans le processus de conception, diverses approches ont été utilisées pour développer le modèle requis pour les gilets pare-balles frontaux souples sans couture pour femmes. Les premières étapes ont été la mise au point de d'un modèle de buste adaptatif à partir d'un mannequin de mode scanné (ayant une taille de bonnet 90B) en utilisant un processus de conception 3D. Le buste adaptatif développé à faciliter la création de modèles fittés de soutien-gorge 3D pour différents volumes de buste et pour une même taille de corps. Par la suite, une buste de femme avec bonnets adaptatifs a été associée à la partie frontale du buste du précédent mannequin afin de développer un patronage de base 2D pour les premières couches du gilet pare-balles souple sans couture en utilisant une approche de rétro-ingénierie. Cette approche permet de mouler parfaitement le buste avec la poitrine à différents bonnets sans pince. Le gilet présentant plusieurs couches, les autres couches ont été générées automatiquement à partir du premier patronage par le biais d'un processus de paramétrage basé sur l'épaisseur de chaque couche.

De plus, en raison de son excellente capacité à se déformer, des tissus 3D interlock chaîne à base de fils de para-aramide ont été conçus et fabriqués pour s'adapter à la morphologie féminine grâce à un processus de mise en forme 3D. De plus, des solutions de protection à base de multicouches de tissus 2D et de différentes structures de tissu 3D interlock chaîne ont été caractérisés par différents essais mécaniques et testés à l'impact balistique au niveau IIIA de la norme NIJ 0101.06. Sur la base de ces résultats, les conditions d'impact sur les solutions de protection et leurs nombres de couches influent fortement sur les performances d'impact balistique. Initialement, les solutions de protection à base de multicouches de tissus 2D ont permis d'absorber plus d'énergie à l'impact que les premières solutions de tissus 3D interlock chaine O-L à base de fils de para-aramide. Une nouvelle approche de conception et de fabrication de tissus 3D interlock chaîne a alors été engagée pour réorganiser en interne les différents rapports entre les fils de chaîne utilisés au sein de la structure. Ces nouveaux essais

d'impact réalisés sur un tissu 3D interlock chaîne, possédant une proportion de 66.7% de fils de chaine de liage et 33.3% de fils de chaine de renfort, ont révélé des valeurs de traumas mesurées dans la plastiline et une capacité d'absorption d'énergie plus élevée avec un nombre minimum de pénétrations de couches par rapport à la solution de protection à base de multicouches de tissus 2D. La capacité de mise en forme par un poinçon hémisphérique des tissus 3D interlock chaine sont fortement influencées par les rapports en permutation entre les fils de chaine de liage et de renfort. Des valeurs de rapports optimisées entre les fils de chaine de liage et de renfort pour une solution de tissu 3D interlock chaine ont révélé de meilleures valeurs de cisaillement dans le plan du tissu que pour les autres solutions tissées. En conclusion, à l'issue de ces différents travaux de recherche, une structure de tissu 3D interlock chaine a été optimisée pour s'adapter à la fois aux contours féminins et posséder de meilleures performances à l'impact balistique que la solution à base de multicouches de tissus 2D

Mots-clés: conception assistée par ordinateur (CAO), Processus d'ingénierie inverse 2D-3D-2D; Gillet pare-balle pour femme; Impact balistique; Caractérisations mécaniques; Structure tissée 3D à haute performance.

Procesul de proiectare 3D a îmbrăcămintei pentru femei aplicat în corsetărie și protecție balistică Utilizând țesături 3D interlock

Rezumat

Cu toate că numărul femeilor care participă la diferite sarcini periculoase în cadrul Armatei, Ministerului de Interne sau în alte domenii conexe a crescut semnificativ în ultimele decenii, vestele de protecție balistică pe care acestea le poartă sunt, de cele mai multe ori, mărimile mai mici ale vestelor proiectate pentru bărbați. Există și veste proiectate special pentru femei, volumul în zona bustului fiind realizat prin procedee clasice de proiectare. Acest mod de proiectare a vestelor de protecție pentru femei prezintă dezavantaje - protecție balistică redusă lipsa de ajustare pe corp și lipsă de confort. Proiectarea clasică a vestelor de protecție balistică pentru femei implică nu numai un sistem de gradare mai puțin precis, ci și executarea de pense, pentru a crea volum în zona bustului. Prezența penselor determină rezistență balistică redusă în zona cusăturii și disconfort crescut cauzat de suprapunerile de material. În ultimii ani s-au depus eforturi semnificative pentru îmbunătățirea performanțelor generale ale vestelor de protecție pentru femei, prin utilizarea de materii prime performante, noi structuri textile și tehnici avansate de proiectare a îmbrăcămintei. Cu toate acestea, nu există încă un proces clar de proiectare a vestelor de protecție balistică ușoară pentru femei, care să ia în considerare crearea volumului pentru zona bustului pentru diferite variante morfologice și care să ofere simultan protecție balistică și confort. Teza de față prezintă o nouă tehnică de proiectare (3D, asistată de calculator) a acestui tip de echipament de protecție, împreună cu structurile textile corespunzătoare acestui procedeu.

În procesul de proiectare s-au utilizat diferite tipuri de abordări pentru procesul de construcție a tiparul pentru partea din față a vestelor de protecție balistică ușoară fără cusături, destinate femeilor. Primii pași au constat în stabilirea de noi tehnici pentru modelarea adaptivă a bustului pe un manechin 3D virtual (cu dimensiunea cupei 90B), folosind procesul de proiectare 3D. Procedeul de modelarea adaptivă a bustului a facilitat generarea tiparelor pentru diferite mărimi de sutien, corespunzătoare aceleiași siluete, urmărind perfect liniile de contur ale corpului.

Mai târziu, o cupă cu bust adaptiv a fost asociată cu o altă parte frontală a manechinului virtual pentru femei 3D pentru a dezvolta un model de bloc 2D pentru 1 straturi de panou de armură pentru corpuri moi, fără probleme, folosind abordarea de inginerie inversă (generarea modelului 2D-3D-2D). Această abordare a utilizat, de asemenea, pentru a atinge volumul de bust necesar în model, eliminând implicarea elementului de design, inclusiv săgeți. Cu toate acestea, având în vedere că armura corpului cuprinde mai multe straturi de panou, a fost foarte importantă determinarea modelului pentru fiecare strat de panou succesiv. Pentru aceasta, a fost utilizată apoi o abordare sistematică de proiectare 3D prin intermediul procesului de parametrizare bazat pe grosimea fiecărui strat pentru a genera modele de blocuri pentru fiecare strat succesiv de panou de armură. Prin validare experimentală, o astfel de abordare de proiectare 3D și sistemul său de fabricație s-a dovedit precisă pentru a genera diferite tipuri de panouri cu mai multe straturi pentru a dezvolta o armură de corp moale pentru femei.

Pentru realizarea din p-aramidă a vestelor de protecție conform modelului de proiectare propus pentru cupă, s-a optat pentru clasa de țesături multistrat 3D-interlock, care prezintă

capacitate de punere în formă excelentă. Astfel s-au proiectat și realizat diferite variante structurale de țesături 3D-interlock, cu diferite proporții între firele de urzeală de legare și de umplutură. În plus, țesături 2D cu legătura pânză, utilizate tradițional pentru veste de protecție balistică și variante de țesături 3D-interlock au fost testate mecanic și balistic, cu scopul evaluării comparative a performanțelor balistice, conform Standardului NIJ, nivelul IIA. Rezultatele au arătat că tipul țesăturii (2D, 3D), condițiile de impact și numărul de straturi au avut influențe semnificative asupra performanțelor la impact al panourilor balistice testate. Spre deosebire de cazul panourilor cu număr mare de straturi, panourile cu număr redus de straturi realizate din țesături 2D au prezentat capacitate mai mare de absorbție a energiei de impact, comparativ cu panourile din țesături 3D-interlock tip ortogonal/strat-cu-strat. Acest fapt se datorează rigidității mai mari a straturilor din țesături 2D testate. Pe baza acestei concluzii, s-a încercat îmbunătățirea proprietăților balistice ale țesăturilor 3D-interlock, prin creșterea procentului de fire de umplutură (cu grad de ondulare zero), comparativ cu procentul de fire de urzeală pentru legarea straturilor. Au fost proiectate și realizate diferite variante structurale referitor la procentul de fire de urzeală de umplutură/de legare conținut. Rezultatele testelor balistice au arătat că panourile realizate din țesături 3D-interlock care conțin în structură fire de urzeală de umplutură în proporții de până în 50% (de ex. 66.7% fire de legare și 33.3% fire de umplutură), chiar chiar dacă au un număr redus de straturi, prezintă capacitate de absorbție mai mare a energiei de impact comparativ cu panourile din țesături 2D sau alte variante de țesături 3D-interlock.

Capacitatea de punere în formă în matrițe hemisferice și capacitatea de menținere a formei după scoaterea din matriță sunt de asemenea influențate de raportul procentual între firele de urzeală de umplutură/de legare din structura țesăturii 3D-interlock, dar în sens invers decât cel exercitat asupra rezistenței balistice. Alegerea unei proporții optime între firele cu grade de ondulare diferite plasate în structura 3D-interlock, poate influența pozitiv rezistența balistică, menținând în același timp în parametri optimi contracția și rezistența la forfecare, care trebuie să fie reduse, pentru ca materialul să fie format în matriță. În concluzie, a fost posibilă obținerea unei structuri 3D-warp interlock care să poată fi modelată fidel după forma corpului femeilor și care prezintă proprietăți balistice superioare comparative cu țesăturile 2D clasice pentru veste antiglont.

Cuvinte cheie: Proiectare asistată de calculator (CAD), proces de inginerie inversă 2D-3D-2D; Garnitura antiglonț pentru femei; Impact balistic; Caracterizări mecanice; Structura țesută 3D de înaltă performanță.

经线接结三维织物的女性防弹胸衣设计研究

在过去几十年中，参与各种危险任务的女性人数有所增加，其中包括军事、执法和相关领域。然而，在各种危险场景工作中，她们仍然穿着小号型的男式防弹服装或根据传统方法设计的女式防弹服装。这种情况会给她们带来不良的弹道冲击防护、不良的适体性以及较差的舒适度，从而给着装者带来一定的危险与伤害。这样的问题产生不仅是因为在服装设计过程中使用了不太合适的尺寸系统，而且还涉及到没有很好地应用省道结构以适应胸围面积。这样不仅会在弹道冲击时在接缝处产生薄弱环节，同时由于连续的织物平面而引起不适感觉。目前，通过改进材料、织物结构和服装设计体系，已在提高其整体性能方面有了很大的改善。然而，考虑到不同女性的形态差异，仍然需要设计能适应胸部结构变化的女式软性防弹衣，以便在不降低适体性和舒适度的情况下，更好地进行弹道冲击防护。本文提出了一种利用计算机辅助设计（CAD）知识和工程设计合理的织物结构以适应设计要求的新型设计技术，为开发无缝女式软性防弹服装提供了更好的综合性能。

在设计过程中，采用了多种方法来开发女性无缝正面柔软的防弹衣所需的样板。首先提出了设计新技术，利用三维设计过程在一个三维虚拟人体模型（90B罩杯）上模拟自适应半身像。开发的自适应胸围模型有助于生成不同胸围体积的三维胸罩样板，适合对应的女性体型，完全符合人体廓形。随后，将一个自适应胸部模型与三维女性虚拟人体模型的其他前身部位相关联，使用逆向工程方法（2D-3D-2D模式生成）为女性无缝软式防弹服装的表层开发二维样板。这种方法还用于通过消除设计元素（包括省道）的方法来获得所需的胸围尺寸。然而，由于防弹服装包含多层织物，因此确定每个连续织物层的样板就非常重要。为此，采用基于各层厚度的参数化处理的系统化三维设计方法，为各连续防弹服装织物层生成样板。通过实验验证，找到了一种适合于开发无缝女式软性防弹服装的三维设计方法及其制造系统。

此外，由于其具有优异的成型性能，设计并制造了不同接结经纱排列比等参数变化的聚芳纶经线接结三维织物，以适应通过曲面成型（模塑）工艺的设计。此外，还研究开发了三维经接结织物和二维平纹对芳纶织物的力学性能和冲击性能。结果表明，机织物类型（2D和3D机织物）、靶板冲击条件和织物层数对靶板的冲击性能有很大影响。与层数较多的情况不同，二维平纹织物在层数较低的情况下，由于其刚性和刚度特性，比相应的经线接结三维O-L p-芳纶织物具有更高的能量吸收能力。在前人研究的

基础上，我们通过在织物结构内部重新安排不同的经纱排列比，设计和制造出了织物试样，提高了经纱接结三维织物的防弹性能。在此基础上，本研究采用相同或更高的上下层互换频率，在三维织物中填充经纱，制成经线接结三维织物，即66.7%的接结纱线和33.3%的填充经纱与相应的二维平纹织物和其他经线接结三维织物相比，具有更低的背面痕迹和更高的能量吸收能力，具有较小的织物层穿透率。经线接结三维织物在半球形曲面的可模塑性及其回复性也受到经线接结三维织物的接结经纱在织物内部换层比例的影响。与其他模塑件相比，通过优化填充纱线和接结经纱的比例，展示出更好的拉伸和剪切值。综上所述，与传统的二维平纹机织物相比，还可以实现既能适应人体轮廓又具有较好的冲击性能的经线接结三维织物结构。

关建词：计算机辅助设计（CAD），2D-3D-2D逆向工程过程；女用防弹背心；弹道冲击；机械特性高性能3D编织结构。

Acknowledgements

My parents also deserve to be acknowledged. I am extremely grateful to my lifetime role models my mother, Sisay G/Yesus, my father, Alubel Abtew. They paid a big price for me to become who I am today. I would like also to thank all my families back home and abroad for their endless love, pray and support.

Last but not the least; my sincerest appreciation goes to my caring, loving and supportive wife, Tihitena Teshome (Tina) and our adorable children Kaleab, Mariamawit and Amanuel. Having you all during my PhD process was invaluable. You were always showing me love and support during good and rough times. You deserve special acknowledgement. My elder son, Kaleab, asked me 'Pourquoi toujours travailler sur votre ordinateur portable? I finally have this document to show him why I usually work in my laptop.

<div align="right">

Lille, France
Sincerely
Mulat Alubel ABTEW
May 2020

</div>

Table of Contents

List of Figures

List of Tables

General Introduction

Protective textiles refer to garments and other fabric-related items designed to protect the wearers from various threats that may result in injury or death. Among the various protective garment, ballistic protection is a class of which aims for guarding the individuals from the projectiles and exploding ammunition [1]. Body amours are one of the most important items of personal protective wear used as police and military protective equipment in battlefields as well as the civilian subjected to fragments of materials in the working place. Soft body armour is a category of body armour, mainly composed of a fabric carrier vest that holds a front and back ballistic panel which are made of very strong fibres such as aramid or ultra-high molecular weight polyethylene made fabrics to absorbs the projectile impact energy. There are many instances in which such equipment has prevented and saved many law enforcement officers from serious and potentially fatal injuries from criminal conflicts, physical assaults traffic accidents, and in battlefield confrontation [2]. Even, various countries law enforcement agencies have decided to make it mandatory for their officers to wear body armour while on the field duty. Besides its ballistic resistance, designing light-weight and comfortable ballistic body amour becomes extremely important especially to those officers wearing the vest for long hours. For example, according to Federal Bureau of Investigation (FBI) statistics and the National Law Enforcement Officers Memorial Fund, in the USA around 2011, more than 54,000 U.S. police officers were assaulted in the line of duty and more than 160 who died, about 53 per cent were not wearing body armour, due to non-comfortable of the armour for officers to be worn [3]. This is because wearing a heavy and inflexible vest for long hours while on duty could build-up heat which in turn gives uncomfortable for the wearer. Adding many protective layers while developing body amour can offer greater projectile protection for higher threat levels, but also add undesirable weight and inflexibility of the vests [4][5]. The commercial success of the soft flexible vest has greatly increased in the last several decades due to several numbers of factors[6]. Previously, various conventional materials like cotton, silk, nylon, polyester etc. have been employed for ballistic protection with only limited satisfaction without realizing the underlying mechanism of ballistic impact. Nowadays, even if the requirements seem contradicting, it is possible to develop lightweight, flexible and comfortable soft body armour by using high-performance fibres such as Kevlar®, Nomex®, and Twaron®, Spectra® (Allied) HDPE fibres and other materials to prevent high-velocity ballistic impacts of projectiles high-powered rifles and satisfying the requirements of the wearer [1][7][5][8]. However, still, efforts have been made by scientists and researchers even to design and develop protective body amour at much-reduced weight with better fitness.

On the contrary of developing men's ballistic protection vests, design and manufacturing for women encounter problems due to their curvilinear body shape. Designing women's body armour would be quite challenging both due to their unique body shape and even affected by various factors including race, geographic locations, etc. For the last many decades, women personnel and officers were forced to wear small-sized body armour which was designed for men personnel. Fitting such male-based body armour to the women's body shape could not be acceptable not only due to the physiological difference but also imposes some disproportionate on fitness, comfort, and worse ballistic protection. However, according to the various research

data, nowadays the number of women personnel involved in different dangerous tasks including law enforcement, privet security, and military forces are significantly increased from time to time across the world. For example, in 2008, 16.7 % of police officers in the EU were women. In the recent year of 2016, among the total of 324 police officers per 100,000 people in the EU, women police officers' percentages were increased to 21 %. This means that one in five polices officers is a woman [9]. Like other countries, the entire UK police forces were also male at the start of the 20th century and even their numbers were very small since the 1970s. However, the number of women law enforcement members has been recent increases and make up a significant minority. According to the study, in March 2016, 28.6% of police officers in England and Wales were women. This was an increase from 23.3% in 2007 [10]. Besides, in March 2017, the percentage of women officers even increased to 29.1% in England and Wales, 29% in Scotland and 28.5% in Northern Ireland [10–12]. The women were made up of a 61% majority of non-sworn police staff and 45% of Police Community Support Officers. Moreover, the percentage of women was 5.0% in 1980 and 9.8 % in 1995 for the police force in the United States [12, 13]. This number even grew further and recorded 11.2% in 2005 and 11.9% in 2014 [14, 15].

An increment of women in the field of law enforcement and other related fields enforces armour manufacturer and military organizations to develop the well-fitted women-based body armour. Thus, the various designing technique was involved to design woman body armours to minimized the different problems with the involvements of proper material applications [16–23] [16][22]. Such woman body armour designing techniques were mainly used to form the curvilinear shape and accommodate the bust area. Even though the different methods had their drawbacks, designing through such methods were found much better than the male-based body armour in terms of proper bust accommodation with better fitness and comfort. The women's body armour designing techniques include cut-and-sew, fabric folding and stretch-moulding of the conventional fabrics. Among all, cut-and-sew is the most common method to form the shape of women for proper accommodations of the bust area through dart making. Even though using such a unique woman-based design technique was found better than male-based body armour, however, still, such designing techniques also brought a disadvantage on both ballistic protection and comforts of the wearer. For example, the traditional cut-and-sew technique develops the dome shape to accommodate the bust regions, but it also affected the continuity of yarns inside the fabric while cutting. Fabric folding also helps to form the domes to accommodate the curvaceous body shape of women but it also has a drawback on wear comfort and personnel mobility due to much allowance for body armour deformation which makes thicker panel near the armpit region than other areas. Overlapping methods are using a seam with better and stronger stitching in the fabric while dome formation, but still, the small ballistic projectile could break the stitch yarn and the loop of threads among the seams. Apart from using the proper designing techniques, the above protection and comfort problem arises from the difficulty of obtaining accurate surface data for women's bust surface, since the borderline of the bust is ambiguous at the skin surface. Moreover, the effectiveness of the women's body armour also depends on the adaptiveness of the panel to the human morphology. The more the ballistic vest resembles the required shape of the body, the more the fitness and efficient protection will be obtained. So, to avoid the fitness, comfort and ballistic performance problem

due to the traditional designing methods, the frontal women panel pattern should be three-dimensional which can properly accommodate the bust area. Therefore, further developments of women's frontal body armour panel which need proper accommodations of bust area with better impact performance, comfort and fitness for different women morphological differences are very important.

Nowadays, moulding techniques become the most effective techniques to develop the women soft body armour to avoid the above-mentioned problems. It develops the required women shape without the need for cutting, stretch folding or folding. Such developments not only give proper comfort but also good ballistic protection [24]. However, even though the moulding process gives better performance, special consideration should be given for appropriate multi-layer panel pattern generation and the different material behaviour while moulding. In the moulding process, the textile material might possess different moulding characteristics such as surface shear angle, drawing-in values, material recovery and corresponding mechanical damages that need to be considered [25][26–28]. Thus, before applications of such techniques, involvements of the 3D design process for the generations of proper body armour panel patterns and selecting of an appropriate ballistic material which comprises better moulding is very important.

Developing women's soft body armour with the conventional pattern-making systems is less accurate and lack of standardization between brands which conveys finding a comfortable, well-fitting bra becomes more a matter of guesswork, trial, and error than of precise measurements. This is due to different labelling systems of brassiere measurement standards set in different countries, manufacturer etc. For example, considering the relationships between the heights and girths of the human body, the shape and size of woman bust could be varied significantly with no correlations to the other measurements [29]. Unlike the conventional (2D-3D) pattern making systems, the 3D design process, a recent technology applied in the garment making application, helps various researchers, designers and developers to encounter the challenges in terms of new product development processes. The researcher has nowadays used 3D modelling and 3D shaping in women's body armour design by employing the scanning process, which leads to woman bust separated from the body, parameterized and then adapted to individually in the relationship of given customer's morphology.

Besides modelling and developing an armour panel pattern, using appropriate ballistic fabrics that could properly accommodate the bust area while applying dome-formation on the developed pattern without compromising the ballistic impact performance is very important. Even though the conventional 2D plain woven and UD fabrics are commonly used in the developments of soft body armour, but they could not perform the desired level of moulding capability without stretching the fibres. This brings a disadvantage on the ballistic performance of the protective fabrics due to fibre stretching, imparts residual stress onto the material. Even if its architectural and geometrical complexity makes it very difficult for numerical modelling [32], 3D interlock warp interlock fabrics is a promising ballistic fabric structure which can substitute the conventional 2D fabric structures in the field of ballistic protection due to its low shear rigidity, ballistic performance and extraordinary moulding ability [33][34]. One of the research studies revealed its better ballistic performance than the conventional plain woven fabrics with good moulding ability to form the front panel of women's body armour [35]. Besides, due to its excellent moulding behaviour, it has been also successfully demonstrated in

making one-piece composite helmets without creating wrinkles and the necessity of cutting the fabric [36][37][36][37]. Another study also revealed its ballistic performance is not less than the conventional fabric constructions for body armour development with optimum warp and weft densities [2]. On the contrary, few studies also report its weak performance against conventional fabrics. For instance, one study stated that due to its less friction that keeps the fabric structural stable during the impact, the projectile penetrates easier the fabric [32]. Another study also shows angle-interlock woven fabrics show low ballistic resistance with less energy absorption due to the fabric possesses less interlacement between yarns than the other woven structures. It is also noticed that unlike 2D plain weave fabrics, 3D angle-interlock woven fabric not only displays normal features of energy absorption mechanism, like yarn slippage, fibre fracture and cone formation, but also the weaker gripping power on the constituent yarns [38]. Possessing such contradictory and unclear reports toward the ballistic performances of the 3D warp interlock fabric might be due to the various complex factors involved in the structure during the design and manufacturing process. In general, the ballistic impact performances and the effectiveness of the different textile fabric against ballistic impact depend on various internal and external factors. Its structural response and performances are not evaluated only by individual fibre properties or other parameters, but the combinations of several factors [39]. The different external and internal parameters, but not limited, includes fabric characteristics (fibre and yarn properties[40] [41], textile weave construction [42][43][44][45][46][47], areal density [48] and fabric thickness [49], number of plies [50], etc.), ballistic impact parameters (projectile velocity, angle, and geometry [51][52][53], etc.), target finishing [54][55][56][57][58][59], target dimension and ply layering sequence [60][61], friction between projectile, yarn and filament and boundary conditions [62][63][64][65][66][67][68][69][70], hybridization of layers in the panel systems [71][72][73][74], etc.

More focused and related parameters with our research will be discussed in detail in the state of the art section. Therefore, designing, developing ad characterizing the 3D warp interlock fabrics considering the fabric structure and other parameters not only give a clear understanding toward its ballistic performances but also enhance its overall performance as well.

In conclusion, both the developments of proper frontal women body armour pattern and applying appropriate fabrics structure are very important. The panels should be then tested for ballistic impact performance against ballistic test standard-NIJ (National Institute of Justice) standards) with different threat levels. This would greatly help to solve the above-mentioned problems before applying in the final seamless women's body armour.

Thesis Purpose and Objectives

This thesis has mainly two major parts:

1st Part - The automatic pattern generation techniques for developing seamless woman soft body armour with different 3D design approach on the 3D adaptive woman mannequin to achieve better fitness along with good ballistic performance.

The main objectives of this part of the work are:

- Devising new techniques to model the adaptive bust on a 3D virtual mannequin (having 90B cup size) using a 3D design process for easy generations of 3D bra patterns of different bust volumes for the same women body size.
- Sewing (Associations) of an adaptive bust volume with the rest upper torso frontal 3D woman virtual mannequin. Then, applying a reverse engineering process (2D-3D-2D pattern generation) to develop a 2D block pattern for the top (first) layers of women seamless soft body armour panel.
- Developing a systematic 3D design approach through the parametrization process based on each layer thickness to generate block patterns for each successive armour layers.
- Experimental validation of multi-layer panels pattern and its manufacturing system on the real mannequin of the same size. This has been done through observation by aligning the different layers on the seam contour after shaping the woman's soft body armour using moulding process on 3D warp interlock fabric.

2nd Part - To engineer, manufactured and investigate the performances of different 3D warp interlock fabric structure for developing the seamless woman soft body armour through domed-formation without cutting or folding the fabrics.

The objectives of this part of the thesis are:

- To design, develop and manufacture different 3D warp interlock p-aramid fabrics based on various parameters including yarn density, stuffer-binding warp yarns interchange ratios, etc.
- To experimentally investigate the moulding ability behaviours and its recovery effect of the engineered 3D warp interlock fabrics.
- To investigate the ballistic impact performances of the engineered 3D warp interlock fabrics and its counterpart traditional 2D plain weave fabric against NIJ standard Level-IIIA before applying for the seamless woman body armour.
- To enhance the ballistic impact performance along with good moulding ability of the 3D warp interlock fabrics with different warp yarns interchange ratios for seamless woman body armour application against NIJ standard Level-IIIA.
- Characterizing the mechanical behaviours of the engineered 3D warp interlock fabrics.

Thesis Outline
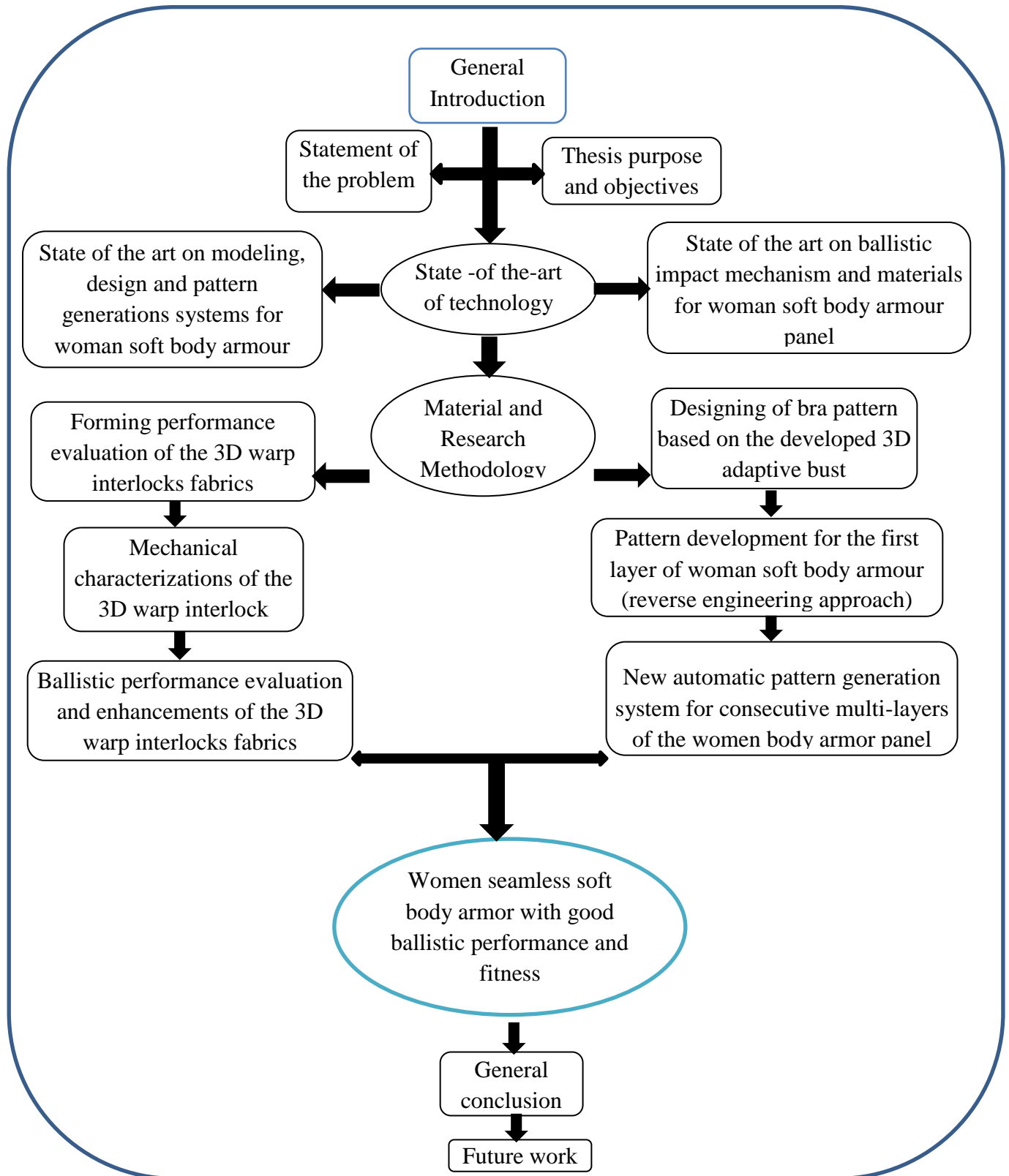
Figure 0.1 General outlines of the thesis

1 State of the art

1.1 Personal ballistic protection type, material, mechanism, and evaluations

1.1.1 Introduction

The human being was protected their body from different kinds of threats including sharp, spike, heat, flame, etc. dates back to the history of mankind. Nowadays, there are different types of personal protection kinds and categories depending on the type and level of threats. Body armour is one kind of personal protection garment wore by law enforcement, police personnel, military soldiers, journalist, personal bodyguards, etc. while on the field. The different types of body armour personal protection types will be briefly studied in section 1.1.2. In previous times, peoples wore clothes made of different kinds of materials such as animal skin (leather), wood, stones, copper, steel, etc. to protect themselves from various kinds of threats. Later, textiles and composite laminates made of traditional fibres including linen, cotton, silk and nylon are involved as protecting materials [75][76][77]. For instance, cloth made of leather on the Grecian shields, various layers of silk in ancient Japan and, armour suits with chain mail during the Middle Ages was used in different ways for protection. Nowadays, the current modern military operations impose the development of advanced damage-resistant, flexible, lightweight with good energy-absorbing ballistic protection armour systems [78]. The revolution of modern ballistic vests arose in the late 1960s, with the developments of novel synthetic fibrous having high-strength and high-modulus properties. Among the developed fibres, para-aramid fibres (Twaron® with a registered trademark of Teijin and Kevlar® with a registered trademark of DuPont) and ultra-high molecular weight polyethylene (UHMWPE) (Dyneema® with a registered trademark of DSM) and Spectra® with a registered trademark of Honeywell) are well-known to produce protective textile materials [79][80][81][82]. Besides, Zylon (Toyobo); Spectra® (Allied Signal), M5 Vectran (Hoechst Calaneses), and Technora (Teijin), etc. are also another commonly used high-performance fibres. These brought a new era of fabric-based protection system with better performances for different threat levels. 2D plain woven and UD fabrics made of those polymeric yarns are widely used in protective for defence personnel armour and armour vehicles [83][84][85][86][87]. Nowadays, 3D warp interlock fabric also becomes a promising fabric structure in ballistic protection world due to its performance and excellent moulding abilities, especially for woman body armour [88]. Different fabric type used in the developments of body armour will be outlined in section 1.1.3.

Due to the complexity of the responses of the above mentioned fibre-based armour panel against ballistic impact, section 1.1.4 will discuss in detail the ballistic impact mechanism and wave propagations for better understanding at a different level. Also, besides an exclusive property of the fibres, fabrics and laminates, various factors could influence the final target performances of the material. For example, increasing the number of fabrics in the panel might improve the ballistic performance [89][90][91][92], but it also affects the total weight and flexibility of the final panel [93][94][95]. The different parameters which affect the material ballistic impact performances of the textile materials will be discussed in section 1.1.5.

1.1.2 Body armour and its category

Body armour is the commonly used ballistic and sharp weapon protecting garment that has been used for the last many decades by military and civilian which are subjected to fragments [1]. Nowadays, various law enforcement agencies have also made it mandatory for their officers to wear body armour while on the field. Such requirements have contributed not only to its huge need but also on progressive improvement of the body armour in terms of material and design aspects. A wide variety of body armour is nowadays available on the market to protect the wearer with different threat and protection level. In general, body armour can be classified as covert and overt based on their flexibility, wearing styles and wearing situations. For example, covert body armour is designed as thin as possible to be worn comfortably under standard uniforms or other garments (**Figure 1.1 (a)**). It is applied where the work requires only a certain level of protection such as security operatives, cops, and close protection officers. Whereas, overt body armour is a usually thicker and bulkier design made from harder panels and wore over the garments (**Figure 1.1 (b)**). Such body armour styles are used in a work where an officer was put in a lot of pressure and high-risk on the security operative including riot control, military operations, war zone journalism, humanitarian missions, and security operations. However, all the mentioned body armour composed of three sections, namely carriers, panel cover and ballistic panels (**Figure 1.1 (c)**).

Figure 1.1 (a) Compositions of typical body armour, (b) covert and (c) overt body armour [65]

The carrier is used to support and secure the panels to the wearer's and the cover mainly protect the ballistic materials from the environment, whereas, ballistic panels help to provide ballistic protection. Besides, depending on the level of firearm threats, modern body armour was worn by police, law enforcement agencies and military categorised into two categories, namely, soft body armour and hard body armour [6].

1.1.2.1 Soft body armour

Soft body armour is a kind of body armour that could suffice to perform against low to medium level firearm threats (Level IIA, II and IIIA) which could go up to velocity 500 m/s according to the National Institute of Justice (NIJ) standards. It usually comprises multiple layers of flexible

dry woven fabric arranged and stitched together in different forms (**Figure 1.2 (a) and (b)**). The soft body armour offers not only significant contributions to ballistic protection but also tailored to conform very well to the body contour to provide good levels of comfort. However, it is commonly designed to protect from small arms fire (handgun bullets). Unidirectional (UD) fabric is other types of textile fabrics which used to develop an improved and desirable soft body armour systems in terms of higher protection without sacrificing mobility and comfort [96]. Besides the fabric type, all the different multi-scale structural hierarchy of soft body armour determines not only the ballistic impact performances but also can cause a probabilistic penetration response (**Figure 1.2 (c)**).
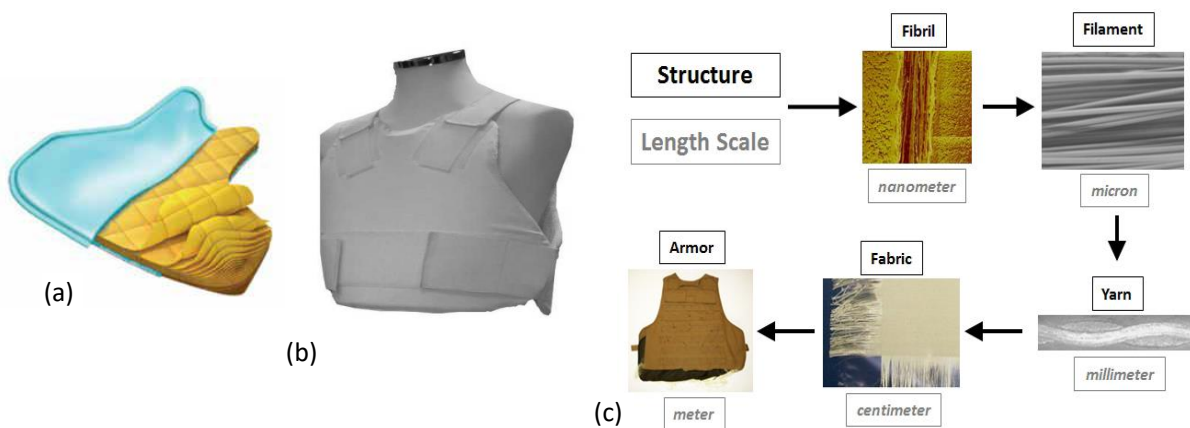
Figure 1.2 (a) Panels, (b) soft body armour, (c) structural scales in Kevlar fabric armour [67]

Conventional soft body armour is usually made up of a large number (20–50) and weighing (below 4.5 kg) of woven fabric layers made of yarns of high-performance fibres. Thus, it becomes even heavy, bulky, and inflexible, interfering which affects the mobility and comfort of the wearer. This puts a great challenge for researchers and armour development to device appropriate methods and materials for achieving lightweight, flexible, and comfortable armour panels, with enhanced impact performance to resist the new firearm technology [97].

1.1.2.2 Hard body armour

Hard armour is another category of body armour which delicately designed to resist the projectile having a velocity of more than 500 m/s according to the NIJ standard (beyond level IIIA). It is worn at a high risk of attack not only to stop the projectile but also fragments from explosions as well as bullets from handguns. Hard armour usually composed of different materials including metallic plates, ceramic tiles, silicon carbide or boron carbide plates, laminated composites, etc. in conjoined with soft body armour to ensure sufficient protection (**Figure 1.3**). The hard armour plate could weigh by itself up to 1.4 kg to 3.0 kg. Ceramics such as alumina (Al_2O_3 and silicon carbide (SiC)) are commonly used armour plates for hard armour ballistic applications. Moreover, the hard armour also composed of ceramics parts combined with composite reinforcement with epoxy resin to obtain better flexibility, light-weight and ballistic performance as compared with pure ceramic tiles [78].
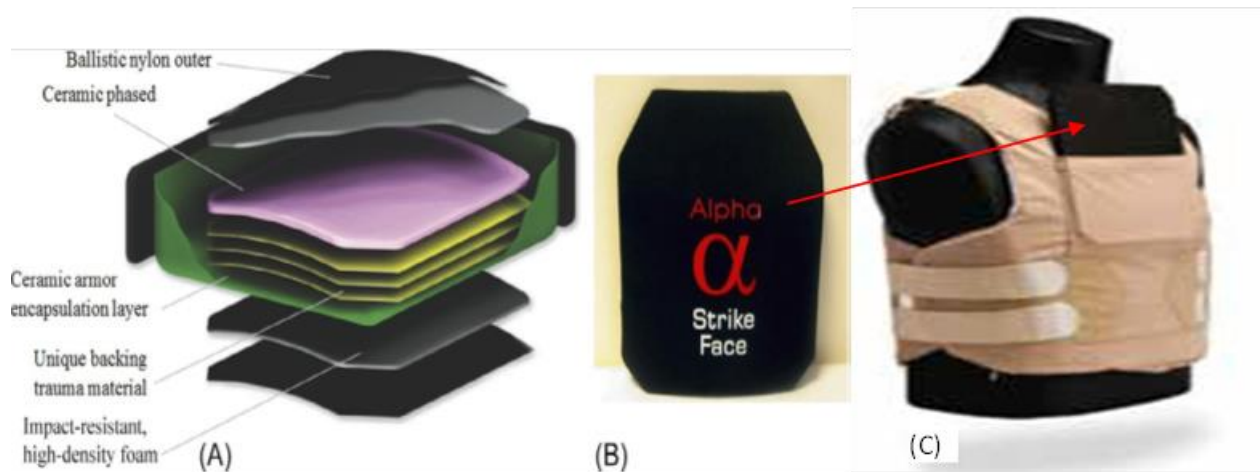
Figure 1.3 Commercial hard ballistic armour (A) VestGuard [65], (B) Alpha™ [69] (C) hard body armour with hard steel plates.

Nowadays, fibre-based textile laminated composite systems (woven fabrics impregnated with resin) become the widely used armour panel materials in the market and gets higher attention for researchers mainly due to its reduction of weight by maintaining the impact resistance. However, characterizing the composite material before the application will help to obtain an armour plate with better ballistic resistance and comfort. For example, a small amount of resin (20%) while impregnating the woven fabrics gives better energy absorption by maintaining flexibility than higher resin values. This is due to the resin restricted yarns not to share the load effectively [98]. Incorporations of vinyl ester resins coated Dyneema® fabrics in the soft body armour (NIJ-level II) could also give a ballistic resistance up to NIJ standard level III (approximately up to 840 m/s). Moreover, various research studies have also intensively investigated and characterized the ballistic impact performances and flexibility properties of the different fibre-based textile composite used as hard body armour.

1.1.3 Ballistic impact protection materials

In the late 1960s, high-strength, high- modulus fibres has been invented to escort the new era of protection through producing body armour system against different ammunition including small projectiles. USA army has early introduced body armour with Interceptor, by which it consists of the outer tactical vest (OTV) by inserting hard ceramic to stop the high-speed rifles and handguns. Nowadays, military personnel and law enforcement officers use different kinds of body armour with rigid ceramics plates throughout the world. Depending upon the threat level, these two types of material can be combined to protect various parts of the human body. Even though armours with heavier inserts are essential to protect against armour piercing, it also results in excessive weights in the armour system, which will affect the mobility of a soldier in the field. Today, soft body armour vests are also utilized by military personnel and law enforcement officers made of high-strength/modulus fibres based woven fabrics [99]. The following section will be briefly discussed some of the currently applied protection fibre materials in body armour and other ballistic protection solutions. Various companies including DuPont, Honeywell, and DSM have developed various kinds of high-performance fibres to

improve the ballistic performances of the body armour. Para-aramids and ultra-high molecular weight polyethylene (UHMWPE) are commonly used and well-known high-performance fibres to produce soft body armour. High-performance fibres usually possess high modulus, high resistance-to-impact damage, and high breaking strength with great capacity of absorbing the impact energy of high-velocity projectiles [50][79][80]. Twaron®, Kevlar®, Dyneema®, and Spectra® a registered trademark of Teijin, DuPont, DSM, and Honeywell respectively are among the well-known high-performance fibres which extensively used for flexible body armour due to their desired engineering properties [44][81][82]. Zylon, Spectra®, M5 Vectran, Technora, and Nextel are also other commonly used high-performance fibres from Toyobo, Allied Signal, Hoechst Calaneses, Teijin, and 3M Ceramic Fibre Products. Moreover, even though it is costly, a very recent material such as PBO (p-phenylene-2, 6-benzobisoxazole) and M5® (polyhydroquinone-diimidazopyridine) are also used to improve the ballistic performance [100].

1.1.3.1   Fibre materials

The ballistic-resistance armour system helps to stop the projectile from penetrating and absorbed its kinetic energy by converting it into different forms of ballistic absorbing mechanisms. The properties of fibres such as strength, modulus, and elongations at break are some of the factors which influence the performances of the final protective materials. The following sections will discuss some of the common fibre types and properties used in the ballistic protection world.

1.1.3.1.1 Traditional fibres

For many years (ancient times), materials such as animal skin, leather, silk in a combination of metal plates were used in body armour systems for better protection until the Korean War [101]. During World War II, new ballistic vests were also designed and developed from E-glass fibre/ethylcellulose composite to provide both bomb and grenade fragments protection. Nylon fibres have also used as ballistic material in the Second World War especially for the development of 'flak jacket' along with steel plates by the American army. Even though Nylon absorbed twice the amount of energy than p-aramids, but it was found inefficient to protect. Still, E-glass and nylon fibres are used due to their low cost. Later, based on the above problems, researchers and the relevant organization have worked to produce lightweight, flexible with good performance ballistic materials for developing next generation ballistic systems. Such ballistic materials from high-performance fabrics mainly depend on high tenacity yarns made from fibres with high modulus, high strength, and excellent anti-degradation traits [78]. Such high-performance fibres become the standard for most fabric-based vests and other fibre- reinforced armour applications.

1.1.3.1.2 Para-aramid fibre

P-aramid fibre is commonly used for high-strength and high modulus fibres with good resistance to melting at high temperatures. Such fibres have also a low affinity for water but affected by ultraviolet light (UV). The first p-aramid fibre which was introduced by DuPont™ in the early 1960s was a class of synthetic fibres with strong and heat resistant. Besides, the strong adhesion between their amide and aromatic groups provide much better thermal

resistance and traction compared to nylon fibres [102]. This specific property makes the p-aramid fibres to easily replace the Nylon fibres in military armour. Nowadays, it is recognized as one of the widely used polymeric fibres in protective applications. Unlike their high strength, high modulus and good tenacity properties, ballistic material from these fibres are relatively expensive [103]. Such fibres are also produced a ballistic material with inherently flexible and lightweight properties along with excellent protective performances to develop a comfortable ballistic vest. In general, p-aramid fibres are 43 per cent lighter than fibre glass (at a density of 1.44 g/cc compared to 2.55 g/cc for fibre glass), twice as strong as E-Glass, ten times as strong as aluminium, same strength as of high strength carbon on a specific tensile strength basis. It also displays excellent dimensional stability with a slightly negative coefficient of thermal expansion (-2.4 X 10-6/°C) and could resist chemicals except for a few strong acids and alkalis. Moreover, the aramids fibre exhibited excellent stability over a wide range of temperatures for prolonged periods with, no strength loss at temperatures as low as -320ºF (-196ºC) and do not melt but will start to carbonize at approximately 800ºF (427ºC). Kevlar® and Twaron® fibres are commonly used and known fibre type marketed under the p-aramid names in the development of bulletproof vests [104]. Both measures five times stronger than steel but yet flexible and perform good heat resistant, cut resistant, chemical resistant, and can handle high ballistic impacts [105]. Among others, Kevlar® production was refined properly due to its early development. The initial Kevlar® 29 makes the protective panels flexible, concealable and lightweight. Even, Kevlar® 129 which was invented in 1988 by DuPont™ found lighter than Kevlar® 29 with improved ballistic resistance to resist high-velocity projectile including 9 mm FMJ. Kevlar® Correctional (Introduced in 1995) used to develop a multi-threat vest to protects against projectile and stab attacks. In general, regarding their ballistic impact behaviour, the properties of para-aramids includes Same compressive strength as E glass fibres, Good resistance to abrasion, Good chemical resistance, Good resistance to thermal degradation (-42 ° C to + 180 ° C), excellent dimensional stability with a negative coefficient of thermal expansion, constant high temperature stability and ballistic resistance restored to wet fibers after drying can be summarize as follows [106].

1.1.3.1.3 *Ultra-High-Molecular-Weight Polyethylene (UHMWPE) fibres*

Another high-strength and high-modulus fibres which are widely used for the developments of ballistic panels are UHMWPE. They were first introduced around the mid-1980s by the Allied-Signal, now called Honeywell Advanced Fibres and Composites (Colonial Heights, Va., U.S.A.), and DSM High-Performance Fibres (Heerlen, The Netherlands) and obtained from thermoplastic polyethylene's of great mass molecular [6]. The fibre composed of polyolefin with extremely long polyethylene chains and shows nearly similar properties to para-aramids, fibre. They are produced mostly through compression moulding and ram extrusion methods. Besides, the fibre also produced through the gel-spinning process by creating a gel material of drawing dissolved ethylene through some tiny holes. This greatly helps to attain high fibre molecular orientation with good toughness, chemical resistance and abrasion properties for body armour production. The UHMWPE fibres could resist up to a 144ºC-152ºC melting point but its tenacity and modulus could decrease at higher temperatures and increase at sub-zero temperatures. According to the manufacturer's research demonstration, the strength-to-weight

ratios of UHMWPE are as much as 40 per cent higher than para-aramid fibres with a similar weight basis [107]. This property gives the UHMWPE a strength-to-weight advantage over aramids in terms of lighter ballistic armour with larger energy absorption capacity[108]. However, UHMWPE has shown also some disadvantages in weak softening, low melting temperature and easy creep high loading [109]. Dyneema^{TM} (DSM) and Spectra^{TM} (Honeywell) are the two common commercially available and widely used UHMWPE fibres. Spectra fibres are ten times stronger than steel and 40 % stronger than aramid fibre which also capable of withstanding high-load strain-rate velocities [110]. The brief description of the properties related to the ballistic performances of the HMPE fibres is good resistance to abrasion and chemical, good thermal degradation (+ 50 ° C to + 100 ° C), low permeability and good resistance mention below [106].

1.1.3.1.4 Poly (p- phenylene-2, 6-benzobisoxazole), or PBO fibres

Zylon is another high strength and modulus fibre with remarkable thermal stability produced by Toyobo Co. Ltd. (Osaka, Japan) around 1998 and first used to develop the Second Chance Body Armour Inc. (Central Lake, Mich., U.S.A.) and others ballistic vests [111]. As compared to p-aramid fibres, Zylon woven fabrics not only absorb nearly twice the energy per unit areal density when the panel is clamped at all 4 edges but also it is almost 12 times that of the aluminium fuselage skin. However, the cost of the Zylon materials is much more than aramid or polyethylene fibres. The ballistic vest made with PBOs gives equivalent protection level compared to vests made of aramid fibres with half the thickness. However, PBO was not becoming popular in soft body armour developments due to its performance degradations not only at environmental conditions of moisture [112] and sunlight heat [113] but also in acid and UV- radiation. Loosening of fibre morphology to increase the number and size of defects was observed while exposed to moisture. The presence of aqueous acid brings both loosenings of fibre structure and hydrolysis of the oxazole ring structure, whereas UV radiation affected the hydrolysis of material near the fibre surface with attendant formation of amide linkages [114]. Considering such poor shear modulus and strength properties of high modulus and high strength fibres due to their weak transverse bonds, a new types of fibre, M5 (poly {2,6-diimidazo(4,5-b 4050-e) pyridinylene-1,4-(2,5-dihydroxy)phenylene}) was also invented with stronger intermolecular bonds to increase their corresponding transverse bond [115].

1.1.3.1.5 Other High-performance fibres

There are also various fibres which are used for the applications of the ballistic, composite reinforcement, filtration, insulation, and other related fields. Glass fibre is one of the most versatile industrial material produced by fusing silica with minerals, then rapidly cooling the molten mass to prevent crystallization and formed into glass fibres by a process also known as fibrillation [116]. E-glass, S-Glass, C-Glass, M-Glass, A-Glass, and D-glass fibres are mostly available in the market with their specific properties [116][117]. E-glass and S-Glass have commonly used glass fibres. E-Glass is made of CaO, Al_2O_3, and SiO_2, conditionally with B_2O_3 from 0 to 10 wt. %, with suitable mechanical, electrical and chemical stability [118][119]. S-glass which composed of silica (SiO_2), alumina (Al_2O_3), and magnesia (MgO) was developed in the 1960s primarily for high-temperature applications and later in 1970s for ballistic protection

applications. The advantages of glass fibres are low cost, high tensile and impact resistance, and high chemical resistance, whereas its disadvantages include low modulus, high-fibre abrasiveness, low fatigue resistance, and poor adhesion to matrix resins [120]. Carbon fibres are another polymer fibre used in the ballistic applications and mainly made up of acrylic fibre with high tensile strength, high stiffness for weight, and very low thermal expansion. As compared to steel, it is five-times stronger and twice as stiff with better lightweight which makes it ideal for ballistic and other application in different forms. Graphite fibres sometimes knowns as carbon fibres with special structure in which adjacent aromatic sheets overlap with one carbon atom at the centre of each hexagon [121][122]. Ceramic fibre is another fibre with high-temperature resistance, low density, high compressive strength, and high hardness. This makes them the most important materials for lightweight ballistic personal armour and vehicle protection applications [123]. It has also a drawback of high cost, processing hindrances, and lack of proper ballistic performance prediction due to the material property [124]. Different research study has also investigated the performances of commercially available monolithic ceramic materials such as Carbide (SiC), Boron Carbide (B4C), Silicon Alumina (Al2O3), and Titanium Diboride (TiB2) for personnel and vehicular ballistic protection armour applications [125][126][127][128]. Even though Al2O3 is an economical ceramic fibre with high modulus of elasticity and refractoriness and high hardness, but it possesses heavyweight due to the highest density and lowest ballistic efficiency than other types. Other special fibres such as metallic and boron fibres are also used for ballistic protection [129]. Besides, different cellulose-based natural fibres including Jute [130][131], hemp, flax, and sisal are recently claimed to be used in the form of composite and rigid plate applications due to not only to their low cost but also their environmental friendly and recycling properties [78][132][103].

1.1.3.2 Ballistic fabrics

Textile fabrics are one of the widely used materials in either soft or rigid forms for personal and equipment protection against different kinds of ballistic and related impact threats. Lightweight, high protecting performance and low cost as well as comfort are the parameter to select the required textile fabrics [133]. Thanks to the dedicated researchers and companies, now it is possible to fulfil these requirements by using high-performance fibres/matrices and layered different types of textile structures such as two-dimensional (2D) and three-dimensional (3D) preforms. Nowadays, ballistic fabrics made of various types of materials are used in various technical applications including ballistic protections. Moreover, the developments of high tenacity yarns made from fibres with high modulus, high strength, and excellent anti-degradation traits play a significant role in the manufacturing of high-performance ballistic fabrics for the next generation ballistic protective body armour and armour vehicles. The structural responses of such fabrics are also widely used in engineering applications due to their lightweight, impact resistance and high-energy absorption ability properties. However, in addition to fibre properties, combinations of various parameters including the fabric structure and geometry play an important role in determining the ballistic performance of fabrics and its composite [39]. Currently, various types and structures of ballistic fabrics are available in the market for such applications. In general, textile structures used in ballistic protection are woven fabrics, unidirectional (UD) structures, and nonwoven fabrics [72]. In particular biaxial 2D

woven fabrics (including plain, basket, etc.), tri-axial fabrics and unidirectional laminates are the most common and widely used in the different technical applications including bulletproof vest and composite industry [47]. However, such fabric has faced low impact performances due to their crimp formation; low delamination and low in-plane shear properties. Even though it shows low in-plane properties, 3D woven fabrics have been widely used in various technical applications since it confiscates the problems of delamination due to the presence of Z-fibres in the structure. However, multi-axis 3D woven fabrics with multiple layers could solve both delamination problems due to the presence of Z-fibres and enhanced in-plane properties due to the bias yarn layers [134]. The following section will be tried to discuss some of the textile fabrics widely used in the ballistic fabrics or/and its corresponding composite applications.

1.1.3.2.1 2D woven fabrics

2D Plain weave fabric is the simplest and commonly used 2D woven structure fabrics in the ballistic applications. It is produced by interlacing the two types of yarns, namely yarns run along the length of the fabric (warp) and yarns that run from selvedge to selvedge (weft) based on the predefined checkerboard pattern. Multiple 2D woven fabrics can be layered to design structures with a range of thicknesses. Alternatively, these layered structures can be stitched in one or more directions to enhance the ballistic and stabbing resistance, especially by decreasing the back face deformation [135][136]. 2D woven fabrics can be coated with elastomers to improve the fracture toughness of the structure. On the other hand, it was claimed that para-aramid fabric becomes more flexible and resistant to ballistic penetration/stabbing when impregnated with shear thickening fluid made of Nano silica particles dispersed in ethylene glycol [58]. In the woven fabrics, especially in plain weave, the percentage of gross area, which is covered by the fabrics, also known as covers factors, played an important role in the ballistic protection performances. A researcher has suggested that ballistic fabrics with cover factors of more than 0.95 and less than 0.6 will not give better ballistic protection due to degrading yarns by the weaving process and to the looseness of the fabric respectively. On the contrary, fabrics with the cover factors between 0.6 to 0.95 values will be ideal and more effective while utilizing in ballistic applications [137]. **Figure 1.4** shows the creations of 'wedge through' effect on the woven fabrics while impacting by the ballistic projectile. The 'wedge through' exists higher in the loose fabrics than the tight one.

Such a phenomenon occurred not only through fabric structure but also the sizes of the ballistic projectile could affect it and were studied widely by various researchers [138][139][140][141]. 2D knitted and nonwoven structures are other 2D fabrics, which are also used for various technical applications. For example, knitted fabrics could be used for cutting and stabbing-resistant materials due to their structural flexibility and their ability to bring more yarns by shearing during cutting or slashing, whereas non-woven structures are also engaged mostly in the low-speed projectile applications due to its stick-slip mechanism of the short fibre-to-fibre crossing.
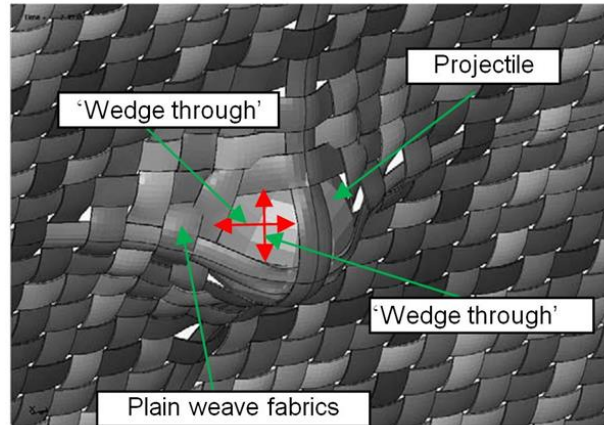
Figure 1.4 Projectile trapping by plain weave fabrics and ''wedge through'' formation [114]

1.1.3.2.2 Unidirectional laminates

It is another widely used fabric structure for the ballistic applications, which comprises a non-woven structure composed of unidirectional-layered sheets that are mutually rotated and bonded together. Sheets also are known as prepregs are produced by a process of pre-impregnation of straight and parallel fibres with the use of resin or rubber. Fibres in unidirectional laminates have different orientations in different layers and the same orientation in a single layer [142].

1.1.3.2.3 3D woven fabrics

Apart from an appropriate designing system, applying appropriate material to accommodate the required women's body contour without affecting the overall performance is inevitable. The body armour should be also developed with effective and resistive response material structures during the dynamic ballistic impact process. Besides, apart from the ballistic performance, the soft body armour material should possess sufficiently light in weight and flexible without affecting the final performances of the product to afford a relatively normal movement. As discussed earlier, 2D woven and UD textile fabrics made from high-strength fibres are the most commonly used textile material for body armour development due to their excellent mechanical properties and ballistic performances [151][152][153][49][154][155]. However, those fabrics are not suitable to form the three-dimensional body contours without the involvement of darts. On the contrary, 3D woven fabrics, such as 3D warp interlock, has been proved its capability of shaping deep dome designs without cutting due to its specific characteristics including extraordinary moulding properties [32][38]. The fabrics have also good elastic behaviour [156], due to their low shear rigidity as compared to other woven fabric structures. For protection against ballistic projectile or combined threat type, soft vests made of 3D orthogonal woven, 3D angle interlock woven and 3D fully/partly interlaced woven as well as multi-axis 3D woven or knitted preforms have been also employed [134][143]. 3D woven fabrics (mostly 3D warp interlock) have also shows not less ballistic protection over 2D woven structures [2][147]. This makes the fabric a promising material to develop the frontal women's soft body armour panel by properly accommodating the upper torso shape and the bust [157, 158]. Such behaviour then gives both the comfort and enhanced ballistic performance by removing the stitching and other

material weakening surface during traditional manufacturing. However, understanding the different formability characteristics and ballistic impact performances of the intended fabric before applying to any kind of technical application i.e. body armour and composite parts are very important. Various research studies have investigated and compared the forming characteristics of 3D warp interlock fabrics. Besides, for better understand, various researchers have defined and classify the 3D warp interlock fabric [159–161]. However, due to its complex structure, it creates some confusion among various researchers, scientists, and weaving technologists. Considering such problems, unlike other woven structures, some researchers have studied dedicatedly on detail descriptions, components and general design specification of 3D warp interlock fabrics for better clarification and understanding [148]. One of the research studies has proposed a more clear description of 3D warp interlock based on orientation and interlacing angles of the different weft layers by binding yarns [148]. **Figure 1.5** shows the proposed classifications of the 3D warp interlock fabrics with the same weft yarn layer (5) but different steps(x) and depths(y) of the binding warp yarn.

(a) Interlock A − T 5 9–5
$x = 9; y = 5; n_{wft} = 5$

(b) Interlock A − L 5 3-2
$x = 3; y = 2; n_{wft} = 5$

(c) Interlock O − T 5 1-5
$x = 1; y = 5; n_{wft} = 5$

(d) Interlock O − L 5 1-2
$x = 1; y = 2; n_{wft} = 5$
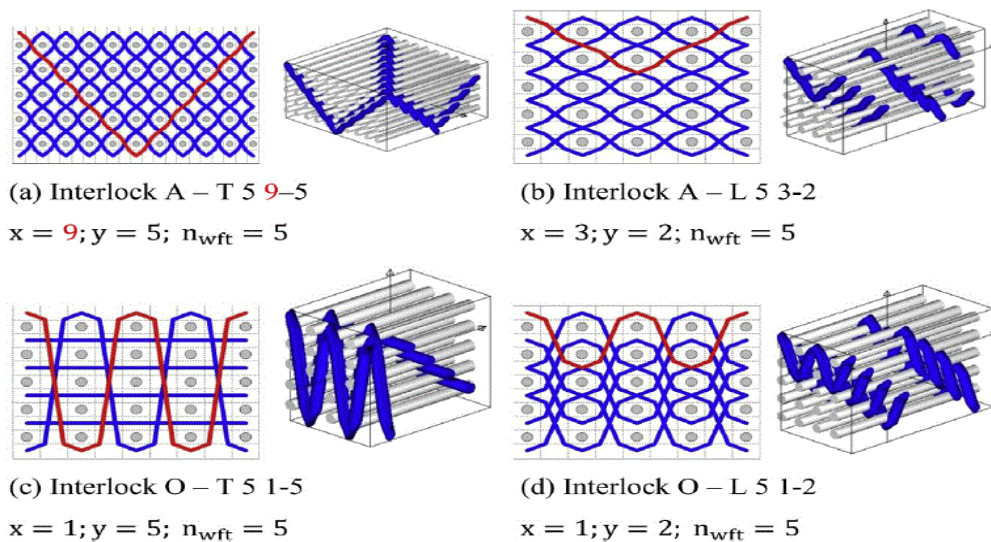
Figure 1.5 Classifications of 3D warp interlock fabrics [148]

Based on the study, it is classified into four categories; namely, orthogonal layer to layer (O-L), orthogonal throughout the thickness (O-T), angle interlock layer by layer (A-L) and angle interlock throughout the thickness (A-T). The binding warp yarn was used to interlace either for complete or different weft layers of the structure following a diagonal direction in the A/T and A/L configuration respectively. Whereas, the different binding warp yarn tried to link the entire thickness or some of the layers following an orthogonal direction for O/T and O/T configuration respectively. Due to such structures, the 3D warp interlock fabric could provide good mechanical properties and deliver good ballistic performance along with good delamination properties [24, 132, 148] as compared to the traditional (2D and UD) fabrics. This is mainly due to its different structure inside the fabrics that could give various advantages including low shear rigidity and excellent formability behaviours [33]. For example, studies have successfully worked on developing a single piece of the helmet using the 3D warp interlock reinforcement

composite by avoiding cutting the fabric [36, 84, 162–164]. The 3D warp interlock structures also exhibited less fabric damage mechanisms during forming processes [165][166].

1.1.4 Ballistic impact mechanisms

High-performance structure material made of high specific stiffness and strength needs resistance to high-velocity impact since it is an important requirement during ballistic impact [167]. The ballistic impact is normally a low mass with the high-velocity impact caused by a propelling source. For the effective use of such materials in structural applications, the material ballistic behaviour under high-velocity impact should be clearly understood. However, while impacting, the ballistic material passes into very complex ballistic penetration mechanisms which need a complete and quantitative analysis for better understanding. This complete understanding of the ballistic process would help not only for current ballistic material application but also for further reliable design and development of an improved and appropriate ballistic material. Researchers and scientists have done extensive researches to better understand the ballistic impact mechanisms of different materials with various parameters.

1.1.4.1 Ballistic impact responses of textile materials

1.1.4.1.1 Ballistic impact responses and wave propagations of yarns and fabrics

Woven fabric has been used for the last many decades to develop soft ballistic vests [168][152]. However, understanding the wave propagation and response of the textile material against the ballistic impact to enhance the soft body armour performance is very important. Different methods have been used to derive relations and model the overall fabric ballistic behaviour against ballistic impacts for better understanding before using in different applications. Normally two kinds of yarn, namely primary and secondary are mainly involved against projectile during ballistic impact as shown in **Figure 1.6**.
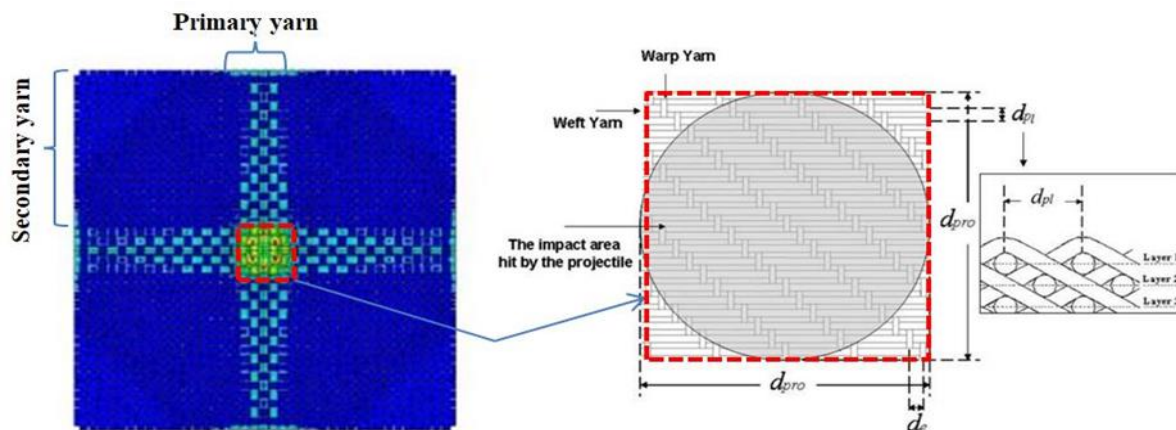
Figure 1.6 Fabric impact area by the projectile [131][132]

Principal (primary) yarns are the yarn that has direct contact with the projectile, whereas the rest yarn in the fabric which is not in direct contact is known as secondary yarns [42]. The projectile impact mostly generates not only a transverse deflection on the primary yarns but also longitudinal stress waves which propagate at the sound's speed away from the impact point

along the axes of principal yarns. However, the energy absorbing capability of the fabric becomes complex even knowing the exact type and number of yarns involved during the impact. Even the process becomes more complex when the impact takes place only on few yarns.

Moreover, the impact may take place on the yarn itself, interlacements, or between yarns. In a very ideal situation where the projectile end fully touches the fabric, the number of yarns involved during projectile impact is calculated as:

$$N_e = {d_{pro}}/{d_e} \tag{1.1}$$

$$N_p = ({d_{pro}}/{d_{pl}}) \times n_1 \tag{1.2}$$

Where,

N_e - is the number of warp yarns involved during projectile impact,

N_p - is the number of weft yarns involved during projectile impact,

d_{pro} - is the diameter of the projectile,

d_e - is the distance between the neighbouring warp yarns,

d_{pl} - is the distance between the neighbouring weft yarns,

n_1 - is the number of weft layers.

Besides, if the impact area of the projectile is equal to the fabrics' impacted area, then the diameter of the projectile, d_{pro} help to decide both the fabric length and width [169]. For the single weft layer fabric, the numbers of warp and weft yarns directly hit by the projectile is calculated as:

$$N_e = {d_{pro}}/{d_e} \tag{1.3}$$

$$N_p = {d_{pro}}/{d_{pl}} \tag{1.4}$$

$$d_e = {1}/{n_e} \quad \text{and} \quad d_{pl} = {1}/{n_p} \tag{1.5}$$

Where

n_e - is the warp yarn density respectively,

n_p - is the weft yarn density.

So, the number of warps and wefts in a single layer involved by the projectile impact will be calculated as:

$$N_e = d_{pro} \times n_e \tag{1.6}$$

$$N_p = d_{pro} \times d_{pl} \tag{1.7}$$

Where

N_e - is the involved number of warp yarns in a single layer impacted by the projectile,

N_p - is the involved number of weft yarns in a single layer impacted by the projectile.

The following section helps to understand the very complex projectile impact process by discussing from single yarn to fabric structure wave propagation during ballistic impact.

1.1.4.1.2 Wave propagation in yarn under ballistic impact

When a single yarn is impacted by the projectile, a conical-shaped transverse deflection with time is developed due to the yarn is enforced to move forward along with the projectile as shown in **Figure 1.7 (a)(b).** A longitudinal wave also developed in the yarn which rapidly propagates away from the impact centre and travelled into the direction of the axis of the yarn at the velocity of sound. In the longitudinal wave, the yarn material is forced to move inward toward the impact centre by stretching and continues until the strain in the yarn reaches its breaking strain.
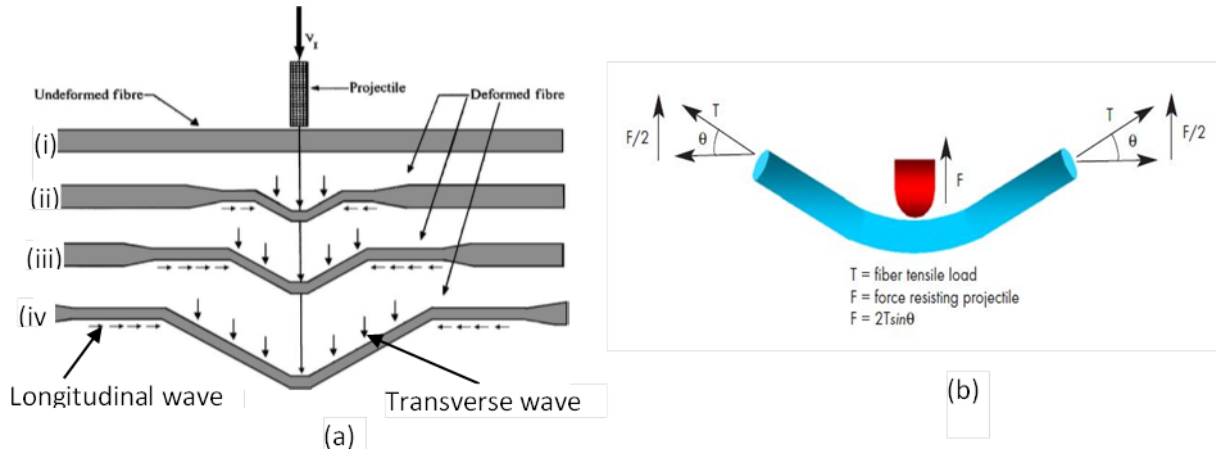
Figure 1.7 (a) different yarn configuration before and after the transverse impact [128], and (b) Single fibre energy absorbing mechanism [133]

The theory and mechanics of yarn on the transverse [170][171][172] and longitudinal [173][174] wave propagations during the ballistic impact of the single yarn with different characters has been intensively studied. The ballistic behaviour of a single yarn subjected to projectile impact will be calculated as follows [170].

$$(\varepsilon) = \sqrt{(\rho/\sigma\varepsilon)} \text{ for non} - \text{elastic yarn} \tag{1.8}$$

$$C = \sqrt{(E/\rho)} \quad \text{for elastic yarn} \tag{1.9}$$

Where,

C - is the longitudinal wave velocity;

E - is fibre young's modulus and

P - is volume density of yarn;

$$u_{lag} = \sqrt{(\varepsilon/(1 + \varepsilon))} \tag{1.10}$$

$$u_{lab} = \sqrt{(\varepsilon/(1 + \varepsilon))} - \varepsilon \tag{1.11}$$

$$V = \sqrt{2\varepsilon \times (\varepsilon/(1 + \varepsilon)) - \varepsilon^2)} \tag{1.12}$$

Where,

C - is the transverse wave velocity;

u_{lab} - is the transverse wave velocity in yarn [175] laboratory coordinates;

ε - is the instant strain level between strain wave front and point of impact;

σ - is the stress,

V - is the impact velocity of the projectile.

The amount of energy absorbed by fibres is largely dependent upon their strain to failure as depicted in **Figure 1.7 (b)**. The primary yarn transverse deflection generates a longitudinal stress wave on the secondary yarns. Later, the textile fabric transverse deflection reaches its limit when the primary yarn fails at its breaking strain [138]. The majority of the projectile energy will be absorbed by the primary yarn in the form of kinetic and strain energy, whereas, the secondary yarns are involved after ply failure [39].

1.1.4.1.3 *Wave propagation in a fabric under ballistic impact*

Normally the ballistic response and wave propagations of the fabrics revealed similarities with the single yarn [42][168]. During the impact, the heterogonous and anisotropic material including fibre-based materials (woven fabrics) faces both transverse and longitudinal strain waves out-of-plane and in-plane fabric directions respectively. A described in **igure 1.8 (b) and (c)** both the transverse deflection and longitudinal wave propagation away from the impact centre with the axes of the primary yarns has been build-up when the projectile impacted the single-layer fabrics.
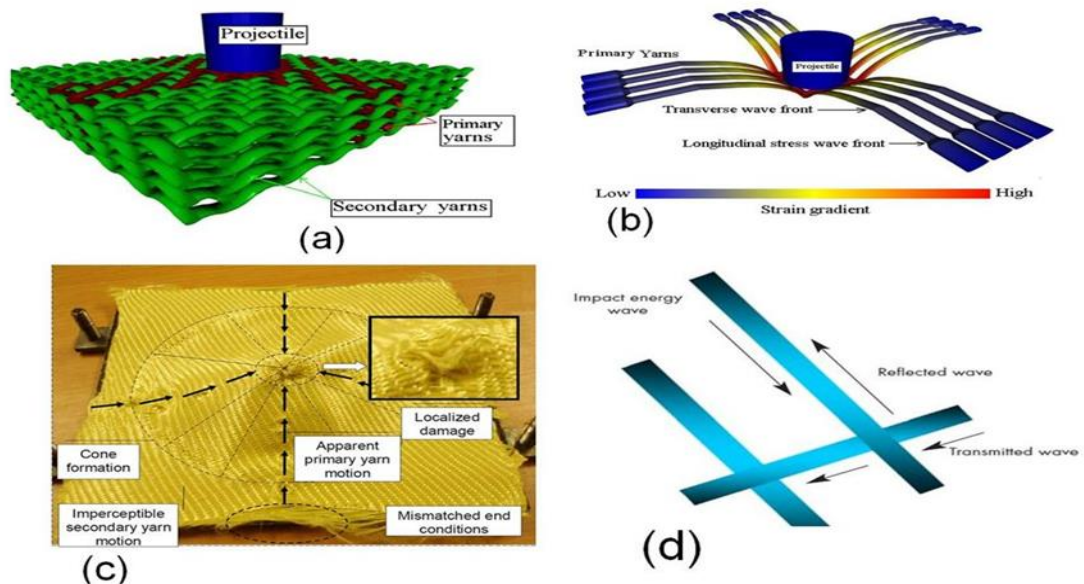
Figure 1.8 (a) Models of multi-layered fabric (b) Responses of primary yarns of first layer [140], (c) Impacted fabrics [132] and, (d) energy-absorbing mechanism [133]

While impacting, the fabric faces a small amount of wave strain at the beginning around the impact region, and then the wave starts to propagate to the adjacent points along the yarn axis

while the stress [176]. The longitudinal strain waves were considered to have uniform distribution toward the length only for the lower projectile velocities. This means that the strain wave varies from minimum to higher (breaking) values elsewhere which contribute to the stress-strain curve. Whereas, considering the transverse wave, the yarn mass generally flooded to the thickness direction away from fabric impacted areas depending upon the amount of impact energy.

The correlation between the projectile velocity and fabric strain [172] will be given as:

$$\varepsilon = V/c \qquad\qquad (1.13)$$

$$c = \left[1/\rho * E \right]^{1/2} \qquad\qquad (1.14)$$

Where

ε is the material strain upon impact;

V is the projectile velocity (m/s);

c is the impacted velocity (m/s);

ρ is the material density (g/cm^3) and

E is the tensile modulus of material (GPa)

The fibre properties and fabric amount mainly influence the speed of stress wave propagation formed on the fabric. Fibre with higher young's modulus of elasticity and lower density propagates the stress wave faster through the yarns and transmits quickly to the adjacent yarns in the fabric. So, as the number of yarn involved during the ballistic impact process increases, the higher amount of energy will be dissipated [177][178]. Besides, as shown in the above equations (1.13 and 1.14), higher tensile modulus and material density bring faster stress waves propagation through the yarns and the fabrics. The energy absorbed by the fibre-based woven fabrics will be calculated as follows: Such an equation is normally used to determine the ballistic limits of soft body armour panels.

$$E_m = 1/2 \, m \, (v_i^2 - v_e^2), \qquad \text{if } v_i > v_p \qquad\qquad (1.15)$$

$$E_m = 1/2 \, m \, v_i^2, \qquad \text{if } v_i < v_p \qquad\qquad (1.16)$$

Where,

m is the projectile mass (kg),

v_i is the impact velocity of the projectile (m/s),

v_e is the exit velocity of the projectile (m/s),

v_p is the penetration velocity of the projectile (m/s),

E_m is the projectile energy loss (joule).

1.1.4.1.4 *Wave propagation in composite laminates under ballistic impact*

Beside dry fabrics, a significant application of polymer matrix composites was also used in the different advanced technical applications. However, such material structure applied in defence and military fields could be also subjected to a localized projectile impact by different calibre bullets and blast fragments. Though, it is very important to understand the protection capability of the structure against penetration before using in specific applications. Various researchers were studied to understand the ballistic impact behaviour of polymer matrix composites both experimentally [179][180][181] numerically and analytically [182][183][184][185].

As homogenous and isotropic material, it possesses waves of stress which propagates around the impacted location with some velocity under impact load. Such wave propagations of the composite material can be expressed as [186]:

$$c_1 = \left[E/\rho\right]^{1/2} \tag{1.17}$$

$$c_2 = \left[E/\rho\right]^{1/2} \left[\frac{(1-2v)}{2(1-v)}\right]^{1/2} = c_1 \left[\frac{(1-2v)}{2(1-v)}\right]^{1/2} \tag{1.18}$$

Where

c_1 is the velocities of propagation of the plane wave of longitudinal dilatation,

c_2 is the velocities of propagation of the plane wave of transverse distortion,

E is the tensile modulus of the material,

v is the Poisson's ratio of the materials.

During the impact, the composite system has also faced a sequence of possible events to resist the impacting projectile. For example, the different sequences of ballistic events while impacting the composite armour systems by a 10g bullets steel core (grey) with a lead nose (black) and a gliding metal surface (copper colour) are shown in **Figure 1.9 (a).** The different bullet deformation sequence was taken from X-ray experiments [187][188].
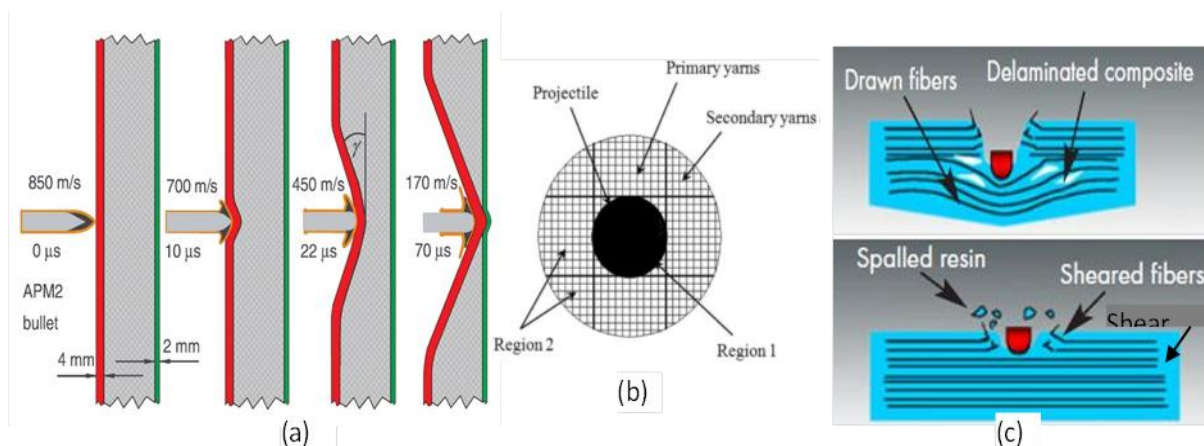
Figure 1.9 Schematic layered fibrous structure of a typical 2D woven fabric (a) side view [154], (b) Front view of different impact regions [155], and (c) Energy Absorption [133]

Even though it depends on various parameters, in general, three conditions might occur during impact.

(i) Complete perforation with certain residual velocity - The projectile impact energy is higher than the absorbed energy by the target.

(ii) Complete perforation with zero residual velocity - All the impact energy is completely absorbed by the target and the impact velocity with the given mass is considered as a ballistic limit.

(iii) Partial perforations of the target - The impact energy is lower than the target absorbed energy and the projectiles are trapped inside or bounce back by the target.

Besides, more or less the projectile impacted kinetic energy will be absorbed by the target by various damage and energy-absorbing mechanisms. Among them:

(a) *Compression of the target directly below the projectile*: The target compression takes place in the region directly below the projectile when compressive wave propagates in the thickness direction (**Region 1 of Figure 1.9 (b)).**

(b) *Compression surrounding the impacted zone*: The region which surrounds the impacted zone up to which the transverse stress wave travels along with the in-plane directions (**Region 2 of Figure 1.9 (b)).** This region also experiences compressive strain along thickness direction due to transverse shear wave propagating in the in-plane directions.

(c) *Conical deformation:* Due to the sudden drop of the contact impact force, only a few upper layers are failed due to shear plugging as the shear wave propagates along the thickness direction. Whereas the rest layer absorbs the projectile residual kinetic energy by forming a cone-shaped deformation when the shear wave reaches the target back-face [189][190].

(d) *Tension in primary yarns:* The direct projectile force and its penetration were resisted by absorbing some of the energy mainly by the primary yarns with higher strain and tension. Mostly, those primary yarns tend to fail when its tensile strain exceeds the ultimate strain during the ballistic impact.

(e) *Deformation of secondary yarns*: Secondary yarns are mostly responsible to absorb some of the energy which was not absorbed by the primary yarn. Such energy is absorbed based on strain distribution within the yarns and its highest values are found near the top face of the deformed cone.

(f) *Friction between the projectile and the target:* Some parts of impact energy can be also absorbed by the frictional coefficient between the projectile and the target [191].

1.1.5 Ballistic material performance affecting parameters

For the last many decades' ballistic materials from stone to metal and fabrics to composite have been used for various applications including body armour. Nowadays, besides steel, new and innovative materials including fibres, fabrics, composites, laminates, and ceramics have been extensively exploited to accomplish the requirement of modern military and other technology-driven applications. As discussed earlier, textile fabrics have been used as ballistic since World War II and now the high-strength fabric is used as personnel protection systems against small arms projectiles for military and police personnel [41]. An understanding of the characteristics of high-strength fabric under ballistic impact would provide useful insights for fabric armour design. However, the effectiveness of different textile material performance against ballistic impact depends on various parameters. In this section, we tried to discuss some of the important internal and external parameters which affect the ballistic impact performances of given materials and directly related to our thesis works.

1.1.5.1 Fabric properties

Among the different affecting mechanisms, textile properties including the type of fabric, fabric architecture, weave construction; yarn densities, fabric thickness, and fabric crimp are some of the major factors. Various research has studied the effect of those parameters considering various fabrics not only on their ballistic performance [192][193][194][195] but also flexibility [157][25]and mechanical properties, such as tension wave speed [196], tensile and tear strength [197][198][199][200][201]. The weaving architectures of the fabric could affect not only the

flexibility and durability but also the impact resistance and energy absorption of the final targets [202][203][204][205]. One of the studies investigated the effect of fabric construction considering made similar p-aramid fibres material, density on their ballistic behaviour and constant speed against different projectiles [202]. For this, various fabric construction such as 1/1 plain, weave, twill weave, 2×2 basket, and satin was prepared and tested at a lower speed. A 1/1 Plain weave was revealed better performance against both armour-piercing (AP) and Full Metal Jacket Rifle Bullets (RB) than other constructions. On the contrary, the 2×2 Basket weave demonstrated better performance than plain and twill construction at higher speeds. The influence of woven architectures toward the ballistic resistance of single and multilayer Twaron® fabrics has been studied with numerical models at the mesoscale level [152]. Besides, experimental investigations were carried out only on plain weave fabrics to determine the residual velocity, fabric deformation, and failure patterns. Based on the study, both fabric architectures and fabric firmness show a higher effect on the overall ballistic protection of single-ply panels systems than multi-plies. The effect of fabric structure (plain weave, basket weave and knitted fabrics) against ballistic resistances of textile material have also numerically investigated using finite element analysis (FEA) [203]. Considering all the structures with similar mass per unit area, knitted textile possessed the worst performance than other fabrics. A 2/2 basket weave demonstrated similar performance with knitted fabrics but exhibited more shearing and flexibility compared to the rigidity of the plain weave. The numerical results of plain weave and knitted structures in terms of impact-induced damage patterns were also supported experimentally. Besides, as shown in **Figure 1.10 (c) (iii) and (d) (ii),** the propagation of crack was consistency along the 'course' direction of the knitted fabric.
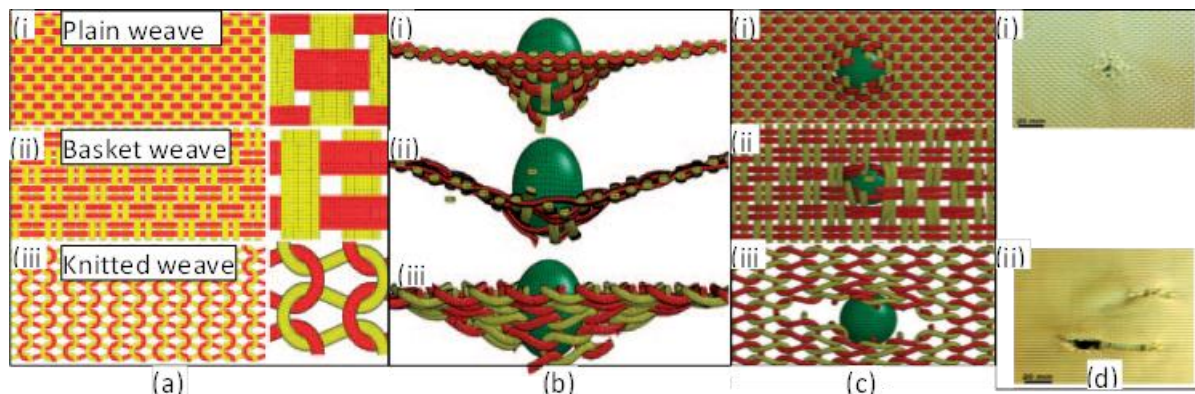
Figure 1.10 Ballistic mechanisms of different textile materials (a) different fabrics, (b) and (c) Side and bottom view of p penetrating fabrics at time=0.4 ms respectively, and (d) Experimental ballistic results of (i) woven and (ii) knitted fabrics [129]

The ballistic response of different woven fabrics was also supported by the above investigation through a numerical modelling study [204]. The study involves plain, twill and satin fabric structure, and the result revealed that plain-woven fabric has better energy absorption capability because of having higher yarn interlacing points. This helps to transmit stress to a larger area of fabric by involving more secondary yarns. The ballistic performances of between cross-ply and woven fabric architecture made of high strength fibres based on depression depth and energy transferred to the backing are also studied both experimentally and numerically [205]. Based on

the result, multi-axial and plain woven fabrics revealed higher and least blunt trauma resistance respectively. Besides, the ballistic performance of cross-laminated and woven aramid fabrics based on energy dissipation and projectile arrest of the material were also experimental investigated [47]. Cross-ply laminated aramid showed higher ballistic performance than woven fabrics with similar fibre material. Another study also revealed that the ballistic performances of panels made of K-Flex UD non-woven fabric structure shown 16% lighter and more flexible than panels made from 100% woven (Twaron CT-710 type) and 100% unidirectional non-woven (K-Flex) para-aramid fabric panels (Kevlar 129 yarns) at various ply numbers while tested against NIJ standards [153]. Moreover, the K-Flex UD non-woven fabric panel showed less trauma depth values than Twaron woven fabric panels at dry state because of the absence of crimp for better propagation of ballistic impact energy as shown in **Figure 1.11 (a) and (b)**.
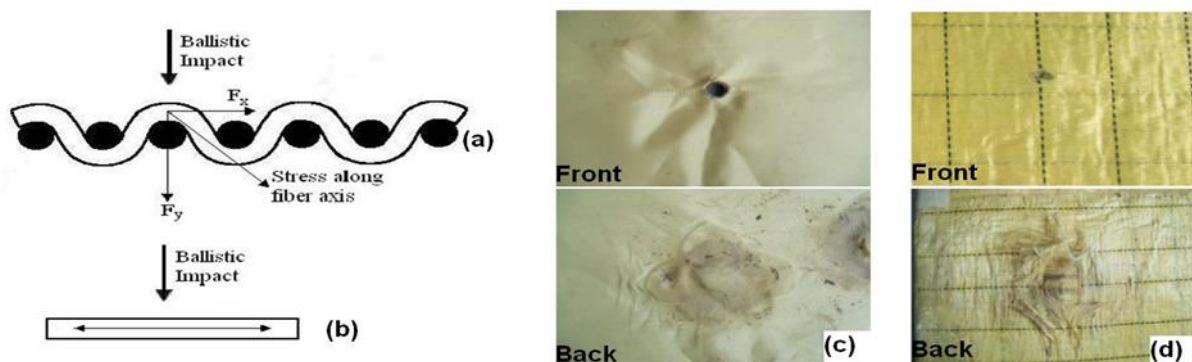
Figure 1.11 Ballistic impact of fabric structures (a) woven fabric and (b) UD non-woven fabric, (c) and(d) deformation after shooting on the front and backside of woven Twaron and K-Flex fabric panels respectively [192]

UD fabric panels absorbed around 12.5–16.5% more energy with higher fabric deformation as compared to woven fabric panels for the unit panel weight. Beside a dry fabric stage, the fabric structure also shows a great effect on the ballistic performance of composite laminates. One of the studies investigates its effect on the ballistic performances of the final composite laminate developed using UD, 2D plain-woven and 3D woven single-ply orthogonal fabrics [49]. Composite laminates made of UD fabrics display higher ballistic impact velocity and energy absorption than others. Whereas, laminates reinforced with 2D plain and single-ply 3D orthogonal woven fabric shown localized damages with little delamination and UD composite faces plugging friction for the thin laminate and delamination, fibre tension and bulking for thick laminate. Besides, adding a yarn gripping effect while productions of narrow plain woven fabrics show a great effect on the ballistic performances of the final material[206][48]**.** Another ballistic test on plain-woven narrow fabrics revealed that fabric with narrower width demonstrates higher performance in lower impact energy due to possessing better weft yarn gripping effect at the selvedges [206]. However, it shows less performance at higher impact energy due to its fabric discontinuity not allowing dissipating more energy than wider fabrics. So, fabric possessing both yarn gripping and continuity will have better back-face deformation and projectile penetration resistance. The panel arrangement (cut and fold form) and (offset and stacked) of the narrow fabrics also influenced the ballistic impact performances. For example,

cut and offset panel arrangements revealed less performance than folded panels due to their less fabric continuity arrangement.

Weave types and weave density are also other influential fabric properties that should be considered while ballistic impact resistance [207][208]. The effect of weave types on the ballistic performance was experimentally investigated on various fabrics made of aramid, ultrahigh molecular weight polyethylene (UHMWP), and hybrid (aramid–ultrahigh molecular weight polyethylene) [207]. The ballistic performances of fabrics made of UHMWP and hybrid were independence of the weave types while considering the combined projectile, yarn count and denier, whereas aramid fabrics are found insensitive with a higher variation. The fabric panel thickness also shows a great effect independently on the ballistic impact behaviour such as energy absorption and failure mechanisms on each dry fabric [155]. The area density of 3D woven angle-interlock fabric also showed a great effect on the ballistic performances while used in various ballistic applications. One of the studies investigated the ballistic performances of two 3D woven angle-interlock fabrics having the same and different area density of panels on the non-perforation ballistic test approach. According to the result, panels with heavier fabric density demonstrated higher overall ballistic performance than a panel with lower density [209].

1.1.5.2 Fibre and yarn properties

The ballistic impact performance of the textile materials also greatly depends on the fibre and yarn properties. Various researchers have investigated its effects on ballistic performances using different methods and materials. For example, the effects of high-modulus organic fibres (X-500) on the ballistic protection were investigated using three fabrics having a yarn with different physical properties. Based on the result, materials with the most ductile property showed considerable promised and higher ballistic resistance than normal material with modest tensile strength [210]. The yarn's physical properties also played their effect on the ballistic performances of the final ballistic materials. One of the studies demonstrated its effect in terms of the number of multifilament in the yarn [211]. A higher number of multi-filament fibres inside the fabric helps not only to facilitate dissipations of energy from a high-speed ballistic projectile but also optimized the final fabric ballistic performances. Another study also computationally investigated the effects of the statistical yarn strength distribution on the final fabric impact response by using five strength distributions with differing mean strengths and distribution widths [212]. According to the study, the distributions of yarn strength were found as the major determinants of the probabilistic fabric penetration behaviour. While prediction, the reduction of the yarn mean strength decrement in fabric V50 velocity, meanwhile an increase of the yarn strengths standard deviation led to an increase in the standard deviation of the probabilistic velocity response. The effect of yarn properties on the ballistic performance of high-strength plain-weave Kevlar KM2 fabric was also numerically studied [213]. The result shows that its ballistic performances mainly depended on the friction, elastic modulus and strength of the yarns. Yarn friction improved the performances by maintaining the integrity of the weave pattern, whereas yarn Poisson's ratio, transverse and shear modulus shows various role on the ballistic impact behaviours of the final materials [214]. The application of coating mechanism of fibre and yarn surface with a specific chemical normally increases the ballistic performances of its corresponding fabric panels in body armour due to its ability to favour the

formation of different forms of frictional behaviour which in turn gives a superior distribution of ballistic energy than fibres that were not coated [215][216][217].

1.1.5.3 Ply arrangement, sequence, and orientation in the ballistic panel

As discussed in the previous section, arranging different layers in the face and backside depending on their material properties while developing the hybrid ballistic panel is very important. Besides, the arrangements, continuity, sequence, and orientations of layers in the panel are also one of the methods to improve the ballistic performance and its weights of the final target [218][219][220]. For example, according to the study, arranging the sequences of the layer improved the ballistic performance of STF impregnated fabric hybrid multi-layer panels both the BFS value and ballistic limit [55]. Even the arranging sequences of the layer in the same thickness of hybrid armour shows a significant effect on their final ballistic performance [154]. The effect of the layering sequences of UD and woven fabric on the BFS values and perforation resistance (V50) of hybrid panels against 5.56 mm FSP and .44 Magnum projectile were studied [221]. Placing the neatly woven fabric behind UD or STF-impregnated woven fabric provides an improved perforation resistance due to the reduced out-of-plane constraint. Interestingly, smaller BFS values were recorded when the neatly woven fabric is placed on the front positions of UD or STF-impregnated woven fabrics due to its better coupling of yarn elongation in the front and rear layers. The arrangements of ply with different ply angles while developing the panel are also studied numerically to investigate its effect in terms of deformation and energy absorption capabilities of multi-ply woven fabric panels as shown in **Figure 1.12** [222]**.** Besides, the model was also considered impact velocity, panel construction and number of layer in the panels. Based on the result, plies orientation and stacking sequence significantly affects the energy-absorbing capacity of the multi-ply fabric panels. Moreover, multi-panels arranged with more ply angle demonstrated higher energy-absorbing capacity than panels with aligned layers (**Figure 1.12 (b) and (c)).**

For instance, the panels arranged with different ply angles show up to 20% more energy absorption capability depending on the number of layers than panels with aligned layers. The models predicted the optimized sequences of the different layers in the panel to achieve the maximum energy-absorbing capability (**Figure 1.12 (d)).** The same researchers have also studied experimentally the effects of ply orientation and layering sequence of plies with different laying angles against ballistic impact performance of the multi-ply fabric panels. The result revealed that multi-ply which is arranged in an angle exhibit a significant improvement in the energy-absorbing capacity as compares to panel with aligned ply. The angled layered panels showed a 14% improvement of impact energy absorption over the aligned layer panel. Moreover, the optimized stacking sequence of the angled plies provides a 15% improvement of impact energy absorption than other sequences [61]. Another study was also numerically investigated the effect of different angled ply-orientation on ballistic performances and failure mechanism of 3-ply align-laid [0/0/0] and angle-laid [0/30/60] UHMWPE plain-woven fabric panels. According to the result, the angle-laid panel absorbed more energy than the align-laid panel at a certain level of impact velocity. Besides, critical velocity was found for 3-plies fabric panels, and under this velocity, the enhanced inter-ply isotropy in the angle-laid panel contributes to improve the energy absorption [223].
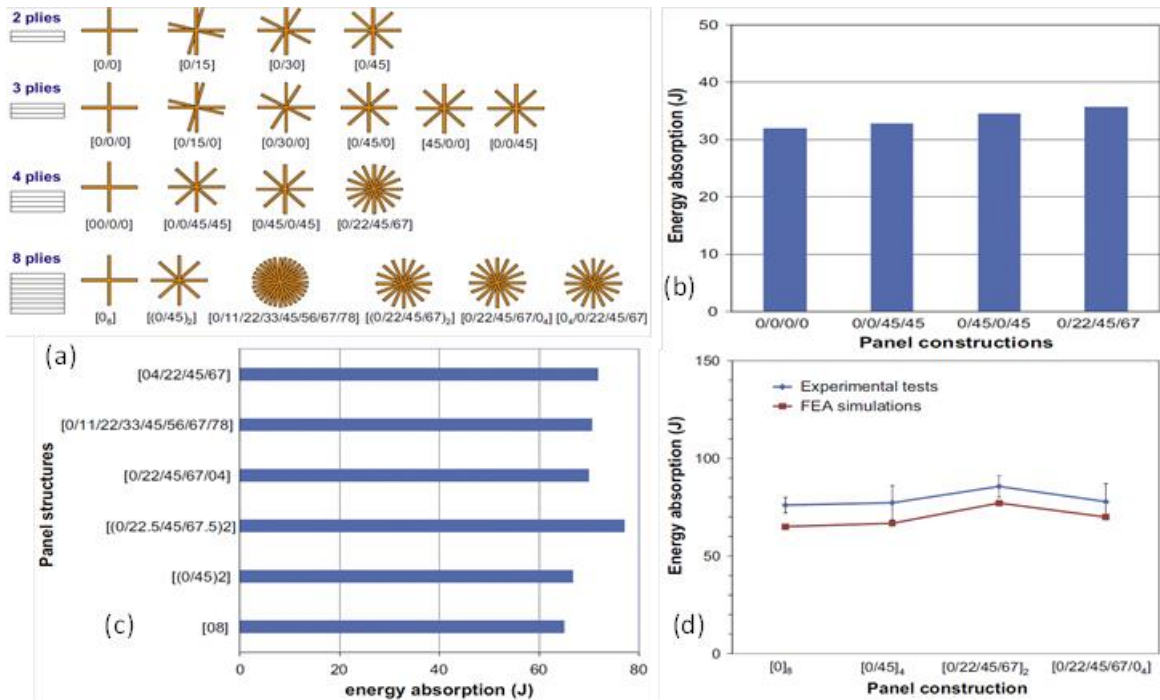
Figure 1.12 (a) Ply arrangement (b) 4-plies panel energy absorption (c) 8-plies panel energy absorption, and (d) numerical and experimental values validation for 8-ply [224]

1.1.5.4 Effects of panels' layer bonding system

Various layers of fabric layers are laminated together in different forms for developing the ballistic panel. However, such bonding systems of different layers also affected its final ballistic performances [224][225][226][227]. Besides, the moulding, flexibility and other mechanical properties of multi-layered p-aramid panels were also affected by the stitch binding parameter [25]. One of the research studies has investigated the effect of stitching types on the ballistic performances of plain-woven aramid fabrics (Twaron CT-710) panel against NIJ standards [94]. For such study, three different stitches were selected to laminate the various layers while forming the panel as shown in **Figure 1.13 (a)**. The energy absorbed by the panel and transmitted to the back of the panels was found significantly influenced by the type of stitch. For instance, the energy transmitted difference among stitching Types A and C was significant and the difference was recorded by 11.5%. However, not as such difference was found in energy absorption between the different stitched panels (**Figure 1.13 (b)**). Higher stitch density of Type B and C also increases the panel strength, but, it also brought higher panel rigidity which makes it difficult for easy movements of the wearer. Besides, a 6.7% reduction of BFS depth was recorded for stitch Type C than Type A for the same fabric ply number as shown in **Figure 1.13 (c)**.
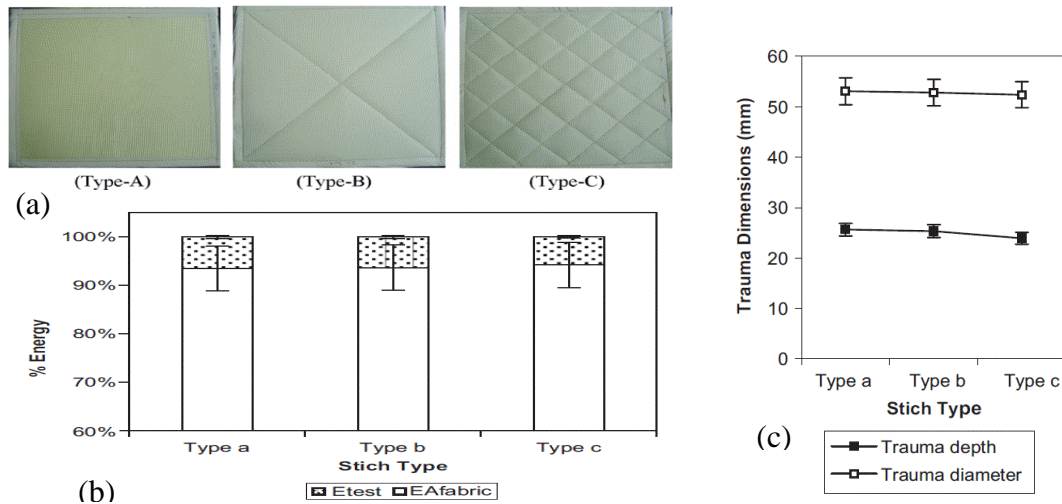
Figure 1.13 Stitching effects on ballistic performances of plain fabrics (a) different stitches (Type A: sewn 2.5 cm from edges; Type B: 2.5 cm from edges & diamond; Type C: 2.5 cm from edges & 5 cm intervals in bias, (b) energy absorption, (c) BFS values [63]

Another study also demonstrated the effect of stitching pattern on ballistic limit performance of panels made of differently arranged 8-neat and 8-natural rubber (NR) coated layer as shown in **Figure 1.14 (a)** [228]. The result shows that not all stitching patterns enhanced the ballistic resistance of the panel systems. For instance, the non-stitched panel revealed better ballistic performance than 1-in. diamond-stitched panels but lower compared to the other stitching systems. Among all the 2-in. diamond-stitched panels exhibited the highest ballistic limit and even show some improvement in reducing of BFS (**Figure 1.14 (b)**). Higher ballistic limit results indicate higher energy absorption by the fabric systems. The research also agrees on enhancements of ballistic resistance by stitching due by forming stiffer panel but it still recommends further study to improve the flexibility of the panel which is negatively affected by the stitch.
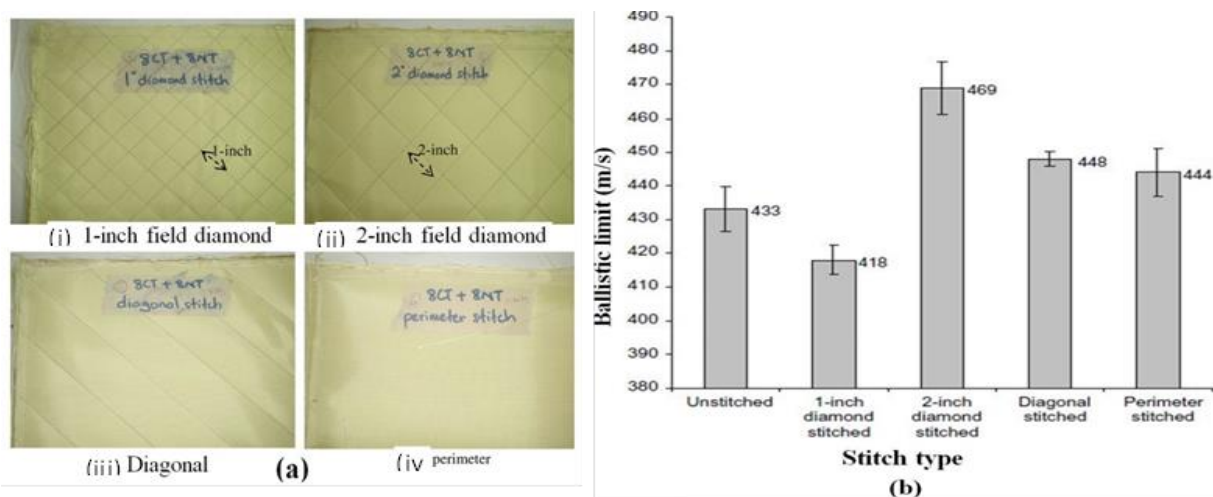
Figure 1.14 Stitching effect on ballistic resistance of natural rubber-coated fabric systems (a) Photographs of stitching pattern (1-in. diamond, 2-in. diamond, diagonal, and perimeter stitching patterns) (b) Ballistic limit of fabric systems [230]

1.1.5.5 Effect of projectile parameters

The different projectile conditions such as the projectile size and mass [229][230], impact trajectory [231], shape and geometry [232][233], nose angle [234][235][236][237][238], velocity [239][240] are also affected the ballistic performances of the materials. One of the research tried to study the effects of projectile nose geometries (high-carbon steel razor blade, 0.30 calibre rounded head and 0.30 calibre chisel nosed Fragment stimulated projectile (FSP)) on 3 yarn type such as Kevlar® KM2, Dyneema® SK76, and AuTx® [236]. According to the study, the 3 yarn was influenced by the projectile head geometry differently. The razor blade impact showed minimum critical velocity for all yarns. Unlike AuTx® yarn, the Kevlar®KM2 and Dyneema® SK76 face a decrease in critical velocity when impact by FSP geometry. AuTx® and Kevlar®KM2 yarns exhibit a cutting fracture surface when impacted by razor blade geometry. Also, AuTx® and Kevlar® KM2 demonstrated a high degree of fibrillation when impacted by FSP and RN projectile whereas, Dyneema®SK76 exhibited yarn cutting by razor blade projectiles impact but faced a high degree of melting when impact with FSP and round projectiles at all impact velocities.

Another study also revealed that the conical-shaped projectile produces highest ballistic limit followed by the flat, hemispherical and the fragment simulating projectile while applying on satin weave carbon/epoxy laminates with 3.2 and 6.5 mm laminate thickness [241]. The effects of projectile characteristics on the probabilistic impact response of fully-clamped single-layer flexible woven fabrics are numerically studied using a yarn-level fabric model with a statistical implementation of yarn strengths. While impacting with six small and large-sized spherical, cylindrical, and conical projectiles of the same mass, the probabilistic fabric impact response is observed to be strongly dependent on the shape of the projectile's impact face [229]. Other research is also numerically studied the effect of nose angle of a projectile on ballistic performance by modelling the angle from 30° to 180° with the difference of 15° [235]. The projectile with a nose angle of 60° generates the maximum efficiency to make the maximum damage on the fabric than the other nose angles. The projectile impact obliquity is also another important projectile parameter that greatly affects the material ballistic performance and damage mechanisms [242][243]. The effect of different projectile shapes on energy absorption and perforation of plain-woven single-ply fabrics (Twaron® CT-716) were also experimentally investigated [65]. The applied different projectile shapes are shown in **Figure 1.15 (a)**. A similar trend of energy absorption values with increment until critical velocity and then starts to decrease for all projectile shapes. However, various failure mechanisms were observed while impacting with different shapes. For example, other than flat shape, all other projectile generates broken yarns that end with messy and disorder structures. Besides, conical and ogive shape brought least yarn pull-out due to their ability to slip through the fabric, whereas, hemispherical shape causes disorder yarn pull-out. Bowing were occurred by hemispherical rather than flat-head projectile impact.
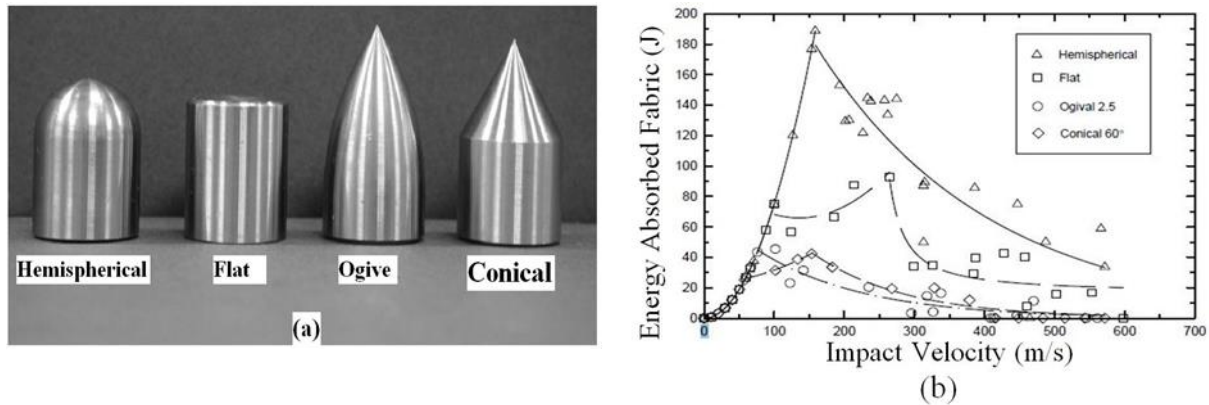
Figure 1.15 (a) Types of projectiles used and (b) energy absorbed by fabric against impact velocity of projectiles [210]

 Besides, the round and blunt shape also create bowing through emerging more stresses on the fabric before yarn breakage whereas, due to their narrower and sharper profiles both ogive and conical-head develop bowing by pushing yarns aside while penetration than creating stresses on the fabrics. The continuation of these studies is also investigating the effect of the mentioned projectile shapes on the ballistic performances of double-ply fabric (Twaron CT 716) systems [232]. In general, the failure mechanisms of a double-ply system were found similar to the single-ply system, but the degree of damage of the impact and distal plies differs. The effect of impact obliquity (with different angle of inclination) on the ballistic limit and energy absorption capability of square shape plain-woven (CT-716) and pliable Spectra Shield® laminate mounted atop and bottom were also investigated [244]. Based on the observation by high-speed camera, increasing of the Twaron® specimen obliquity tends to decrease the ballistic limit at the beginning and then decrement due to weft yarn asymmetric deformation and projectile slide inside the panel. On the contrary, the ballistic limit was first increases then decrease due to competition between the weakening effect of asymmetric deformation and strengthening via projectile sliding in the fabric and pulling out of horizontal yarns of Spectra Shield® specimen. Moreover, for both fabric types, the effect of impact obliquity on the energy absorption will be reduced as impact velocity increases and finally vanishes at higher impact velocity. Another research also applied different projectile shapes, weight, and impact velocity to study their influence on ballistic performances of Kevlar woven fabric. Based on the result, the pointed projectile is highly slow down while impacted at a lower speed than a higher speed compared to blunt projectile due to it hit the target with an angle that results in higher impact energy absorption than expected [141]. More BFS values were also recorded in blunted projectile than pointed because it involves fabric mass to absorb and propagate higher energy.

1.1.5.6   Target impact situations and boundary conditions

Other factors which affects the ballistic impact performance of different material were also studied by various researchers including impact point (at yarn and between yarn (gap)), panel condition (wet, dry, moulded, non-moulded, panel size, panel shape) [245][246], environmental conditions, boundary conditions (clamping condition, clamping size, clamping shape, clamping pressure, frame type, etc.) [247][248][249][250]. Even though ballistic testing standards have

put their own specific armour target mounting procedures for the ballistic testing, researchers have also designed various target conditioning methods to study its effect. Another numerical study has analysed the effects of boundary conditions on failure mechanisms of 3D interlock weaved fabric with 49.8 µs at 200 m/s velocity. Two-panel boundary conditions, one fixed on two edges of weft direction and others on warp direction have been used as shown in **Figure 1.16**. The yarns at non-clamped edges were slip-on other yarns and pulled out from fabric by the projectile. However, such a phenomenon brings damage zones at free edges as described in **Figure 1.16 (a) and (b)**.
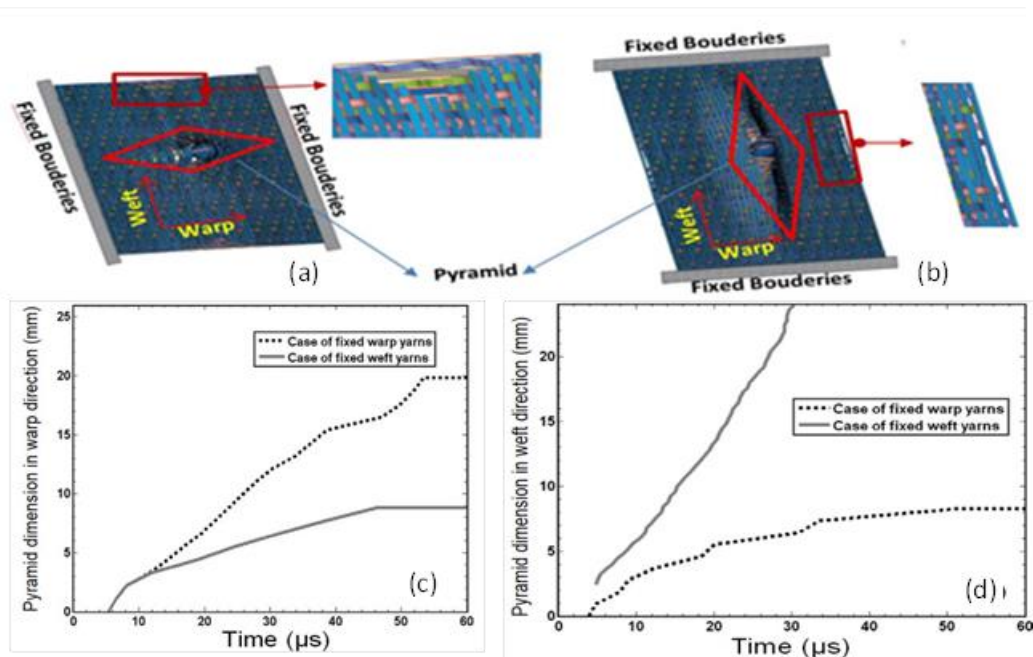
Figure 1.16 Configurations of 3D fabric both a global view and its damage at free edges for boundary fixation only at (a) warp direction, (b) weft direction and their deformational pyramid dimension in (c) warp direction and (d) in weft direction [253]

On the contrary, yarns at fixed edges were tensioned and faced friction with projectile and then ruptured [251]. Besides, as shown in **Figure 1.16**, both numeric and visual result shows that higher deformational pyramid was observed in the direction where the yarns were fixed.

Another research also numerically investigated the influences of frame size, frame type, and clamping pressure of a 10-layers woven Kevlar body armour against a 9 mm FMJ, 124-grain projectile. Using a smaller frame size for armour panels where each edge is clamped reveal an increase in residual speed and kinetic energy of the projectile and vice-versa. Moreover, the speed of the residual projectile will increase with higher clamping pressure for armour panel clamped at both 2 and 4-bar frames. Armour panel clamped at 4-edge also exhibits lesser impact resistance than a panel that fixed in a 2-edge bar frame [252].

The effect of clamping design (4-sided, 2-sided, circular, diamond and corner-clamped) on the ballistic performances of non-backed soft body armour panel made of woven aramid fabrics impacted both at yarn and between the yarn gaps were studied as shown in **Figure 1.17 (a))** [247]. Even though clamping design generally shows an effect on panels ballistic performances, the circular frame revealed maximum V50 velocity followed by diamond clamped fabric

regardless of the impact location. Whereas corner plates and corner points clamp revealed tearing at the corners and deformational failure mechanisms respectively at various impact velocity. Besides, diamond or circular clamp design exhibited uniform but gradually-varying fabric deformation and less fabric creasing compare to 4-sided, 2-sided, and corner clamp (**Figure 1.17 (b)).**
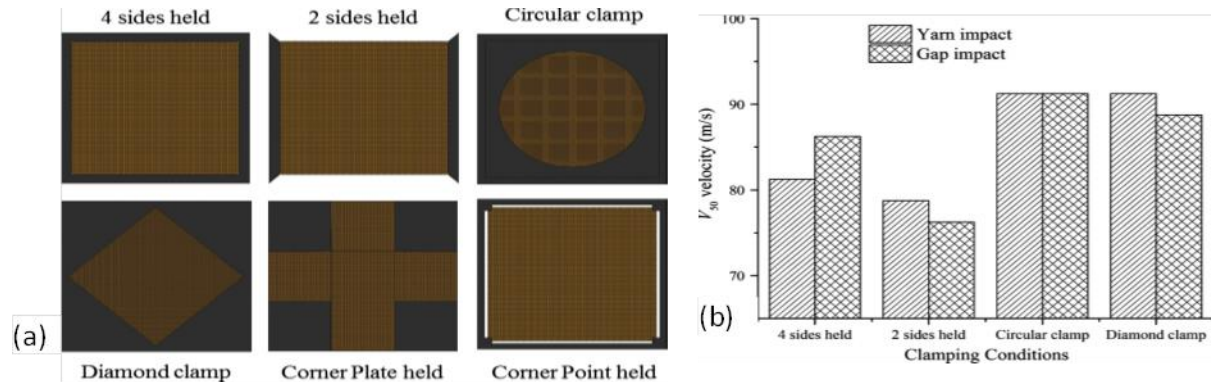
Figure 1.17 (a) clamping configurations for the fabric impact testing and (b) Effect of precise impact location on V50 velocities [249]

Yarn pull-out was also highly occurred in the panel which was not clamped at the edges. Even though such clamp orientation gives better panel energy dissipation through yarn pulling, but at least two edges or sufficient fabric areas at the 4 corners. This clamp helps not only to produce higher inter-yarn normal contact forces but also to create the force which is required to pull the yarns out of fabric weave. Failing these conditions might face less energy dissipation similar to corner point clamped. Moreover, orientations of fabric show no difference in a circular clamp due to its symmetry. But, a 4-sided clamp with a 0/90° orientation is the same as a diamond clamp with a ±45° orientation and vice versa. The panel dimensions, the projectile size relative to yarn width and extra length (de-crimping) also affect the fabric failure modes. One of the studies was intensively studied the effects of panel shape and size (5 to 525 cm^2), impact location (yarn-based and impact-based), clamp design (4-sided, circular, and diamond) on non-backed woven aramid fabrics against V_{50} ballistic impact response [246]. All clamping conditions show an initial sharp rise for V_{50} velocity and become plateaus as panel cross-areas increase. This clearly shows that for impact velocities of each clamped panel shape around V_{50} velocity, there is a critical fabric size by which the projectile residual kinetic energy shows a sharp jump in magnitude, and to grow as fabric sizes increases. This indicates that panel with smaller size facilitates projectile decelerations with higher residual velocities compared to the larger size. Besides, projectile impact at a yarn-based location revealed higher energy dissipations than gap-based regardless of fabric size. Moreover, the V_{50} velocities panel clamped in circular and diamond were found similar but higher than 4-sided clamped panel. The effect of clamping considering 3-different conditions, namely 2- edges-clamped, 0° 4- edges-clamped and 45° 4- edges-clamped was numerically modelled and studied on the ballistic resistances of plain-woven fabric targets (Twaron® CT-716) while tested against 12 mm, 7 g spherical projectile at striking velocities ranged V50 to 500 m/s as shown in **Figure 1.18** [253]**.** Not only the clamping conditions but also targets yarn orientation were both sensitive toward targets' ballistic resistance.
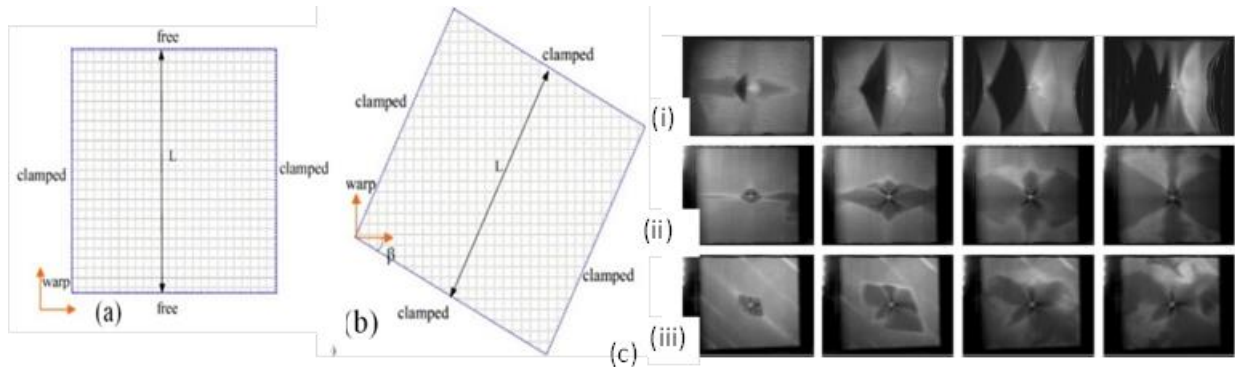
Figure 1.18 Schematic diagram of fabric systems (a) 2-clamped-edges (b) 4-clamped-edges at angle β and (c) High-speed images of fabric deformation at (i) two-clamped-edges (122 m/s), (ii) 0° 4-clamped-edges (110 m/s), (ii) 45° 4-clamped-edges(103 m/s) [255]

For example, 2-edges clamp panel can absorb more impact energy than 4- edges clamp panel with different angles and even clamp panel still improved its absorption capability through orienting the yarns at 45°. **Figure 1.18 (c)** shows the high-speed photographic images of the target which is arranged in different angles and edge clamps. The observations revealed that as panel ends clamped with the yarns parallel to the edges, primary yarns face both higher stresses with rapid impact point failure and fewer energy absorptions (**Figure 1.18 (c) (ii))**. However, the energy dissipation could be facilitated for better energy absorption of 4-edges clamped panel through arranging the yarn 45° to the clamping edges. Another research also claims that ballistic panels conditioning such as wet or dry, and some ply in the target also affects the BFS depth and ballistic properties of aramid fabrics [94]. According to this study, a 3.6% BFS depth value difference was recorded between the dry and wet panels. Besides, 5.0% transmitted energy increments and no significant change in energy absorption was recorded in wet than dry panels due to wetting so long as good water-repellent treatment is applied.

1.2 Personal women ballistic vest design systems

1.2.1 Introduction

Nowadays different countries have made ballistic vests mandatory for their officers to wear. Ballistic body armour with good ballistic resistance, lightweight and comfortable is extremely important for the officer working for long hours. For example, body armour with many protective layers may offer greater protection against projectiles, but it also adds undesirable weight and inflexibility [4][5]. Moreover, unlike men, designing women's body armour encounters more problems due to the curvilinear body shape. A various designing system including cut-and-sew has been used to form this shape, but it still faces weakness at the seams and also difficult to obtain accurate surface data for women's bust due to its ambiguous borderline of the bust at the skin surface. So far different research scientist has tried to design, develop and patented the women soft body armour using different design approaches.

1.2.2 Women soft body armour design techniques

Even though various countries make mandatory to wear body armour by their officers, many personnel's did not feel comfortable to wear the vests while on duty. This is due to as you increase the panel's ballistic protection; it becomes much heavier and rigid. Unless it is designed with light weighted, comfortable and fitted along with the ballistic resistance performances, wearing a heavy and inflexible vest for long hours could generate excessive heat and bring less mobility [4][5]. This problem even became worse while developing women's body armour due to the curvaceous shape of their body [52]. Moreover, as mentioned in the introduction section, the participation of women in different dangerous tasks including in the field of law enforcement, privet security, and military forces has been also significantly increased across the world for the last few decades [254][255]. Such increments of women's participation in the law enforcement and police office department make it mandatory to uniquely develop a dedicated designing and manufacturing woman soft body armour based on their unique morphological shape. Such features of body armour optimization specifically for women enable them more protected without conceding fitness and comfort while wearing the body armour. As discussed earlier, designing women's body armour would be quite challenging due to their unique body shape and even affected by various factors including race, geographic locations, etc. However, for the last many decades even though the numbers of women personnel are significant, they were fitted with small-sized male-based body armour systems. Such fitting of male-based armour for women personnel could be not acceptable not only due to the physiological difference but also imposes the disproportionate on fitness, comfort, and worse ballistic protection. Nowadays, after considering the body difference, various research studies have brought solutions to reduce such problems through either designing techniques or designing with proper material applications [16–23]. The woman body armour designing techniques were mainly used to form the curvilinear shape and accommodate the bust area. Even though the different methods had their drawbacks, designing women's body armour through such methods is far better than the male-based body armour by forming the curvilinear shape and accommodates the bust shape properly and provides better fitness and comfort. This subsection

will discuss briefly some of the most common designing techniques for developing women body armour.

1.2.2.1 Cut-and stitch methods

For the last many years, traditional cut-and-sew designing methods are commonly used design methods in the industry to develop women's body armour to form the required domed bust shape for better comfort. This method involves different kinds of dart designs in different forms to accommodate mainly the women's body bust area. So far various research scientists and armour developers have a design, develop and patented the women's soft body armour using cut-and-stitch design approaches. However, designing women's soft body armour with such a design principle faces weakness points at the stitches of the dart seams line against projectile during impact. This could ultimately reduce the ballistic performance of the material. Moreover, the accumulated material at darts areas also cinches the body near-certain positions of the bust and creating uncomfortable when worn by the wearer [35][19]. Some of the research studies even further studied on the optimizations of ballistic performance and the comforts of women body armour design designed by the cut-and-stitch methods. For example, concealable soft body armour was designed using a plurality of layers of ballistic material, where the different layers of the material include a series of folded pleats arranged at selected angles and intervals along with the layer and sewn along their length [4]. Another woman's body armour having dual cups has been also designed for accommodating, protecting and supporting the breasts and protecting the woman torso from trauma [20]. Body armour with contoured front panel, all-fabric, lightweight panel composed of a plurality of superposed layers of protective plies of fabric made of aramid polymer yarns has been also developed. This panel was contoured using overlapping seams joining two side sections to a central section of the panel to the curvature of the bust of a female wearer to convey good ballistic protection and comfort [17]. Ballistic vest with front and the rear ballistic panel which also has elongated side portion to provide ballistic protection for the side of a female wearer's breast conformed to the body of a wearer by a stretchable outer garment located over the ballistic panels has been also developed [22]. One of the studies also optimize the protection zones for tailor-made bullet-proof vest using a virtual body given by the body scanner for more comfort and to accelerate the sizing process through improving the measurement process [256] as shown in **Figure 1.19.**
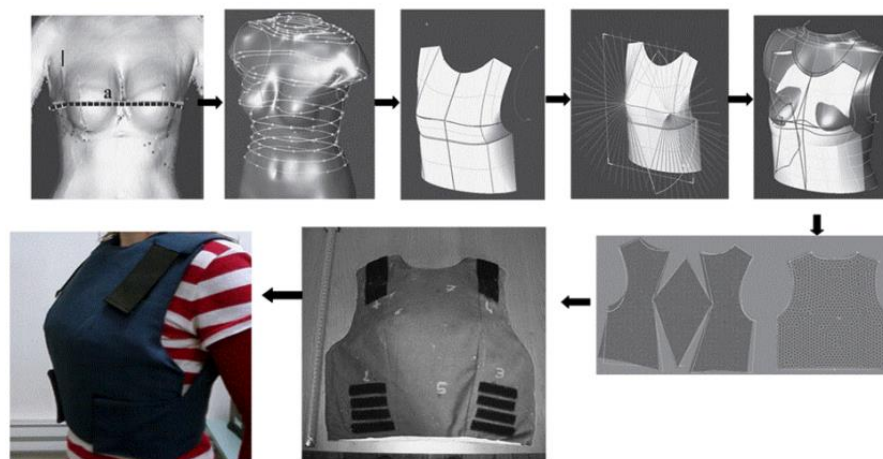
Figure 1.19 Production process of women ballistic vest with dart
rotation methods [38]

Here, it was tried to replace the traditional two-dimensional design method by three-dimensional design process using the darts rotation techniques for better fitness based on the different female morphology. Even though the three-dimensional shape has been developed on the two-dimensional flat fabric using different darts and seams, apart from improved fitness by getting precise dart design, location, and quantity because of the 3D design process but it leaves difficulty to get the desired level of ballistic performance. This was mainly the methods still used many darts and seams to create the required shape, which does not overcome the same issue that the traditional method meets. Another approach was also proposed a new geometric definition of the vest by introducing different body parameters (**Figure 1.20**). The 3D virtual body was generated using Body Scanner to makes the tailor-made bullet-proof vest more comfortable and improve the measurement process during sizing. Such a study was mainly focused on the optimization of the different protection zones of the basic vest by materials distribution based on the vulnerability of the body toward the impact as shown in **Figure 1.20** *(a)* and *(b)* [257]. While material distribution various parameters that affect the garment cost, ballistic performance, weight, and comforts were considered. The correct pattern was generated and draped on the attained virtual 3D female dummy using Design Concept (**Figure 1.20** *(c))* and its various protection zone was delimited with the help of various darts positions (**Figure 1.20** *(d)*).
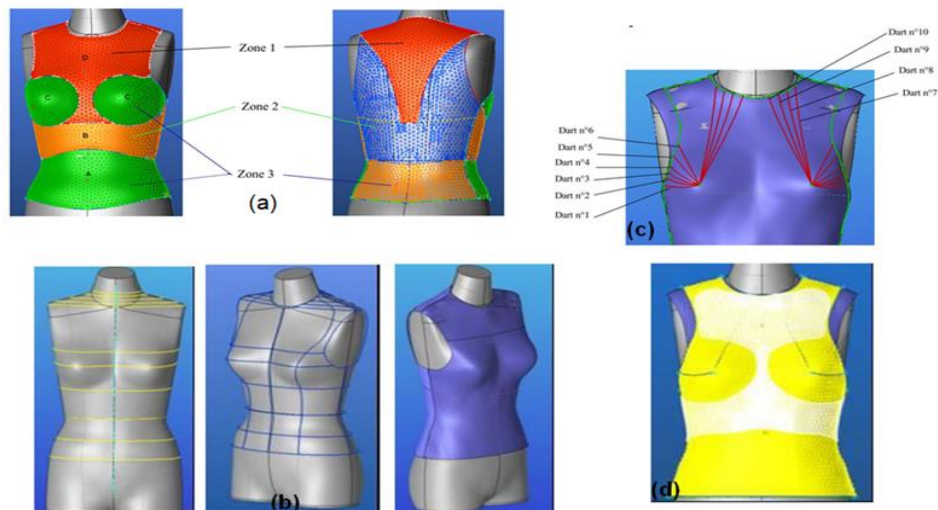
Figure 1.20 Design processes of a ballistic vest with various protection zone (a) protection zones on front and back of the virtual body, (b) measurement values, fit and final fitting, (c) distribution of darts (d) Set of layers (12th) while alternation of darts [264]

1.2.2.2 Folding and overlapping Methods

Fabric folding and overlapping are barely used designing techniques to develop the women's body armour [258][4]. For example, the folding technique is mainly used to shape the materials into a three-dimensional form by folding the materials and stitched at the side in a certain shift. This also revealed the limitation of ballistic performance due to material discontinuities and weak stitching area around folded material. One of the women's body armour with multiple layers of penetration-resistant material was designed using a series of V-shaped darts in successive layers to shape and fit the bust of women. The V-shaped material was then folded on

itself to form a pleat and is angularly offset from one another in directions so that the added thickness is distributed substantially evenly, thereby avoiding bulges or stiffness and improving the wearing comfort [258]. However, one of the disadvantages of folding techniques is that many folded fabrics at the side with sharp edges create thicker panels while folding which causes itching, less personal mobility, and discomfort.

Another method of developing women's body armour is superposing the layers of ballistic material to develop contoured surfaces to accommodate the frontal women part called overlapping. The methods are also applied overlapping seams to join the different superimposed layers. Even though involving overlapping seams could give both the contour surface to accommodate the frontal body and much strength in fabric stitching; however, the small ballistic missiles still can penetrating by severing the loop of threads among the seams [259][17]. One of the patents tried to develop a light-weight, all-fabric and contoured body armour panel to protect the torso of a woman against small arms missiles using overlapping methods [17]. The frontal panels were contoured to the curvature of the women bust using overlapping seams while joining the two side section to the centre section of the panel as shown in **Figure 1.21**. The multiple layers which were superimposed were comprised of ballistic-resistant fabric made of aramid polymer yarns.
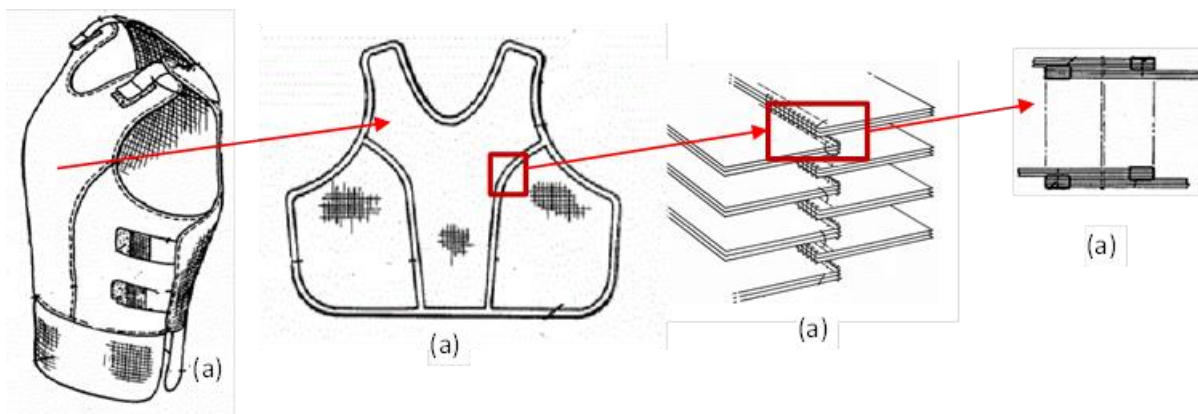
Figure 1.21 Women body armour with overlapping seams, (a) Perspective view (b) plan view (c) exploded perspective view of different ply joined with overlapping and (d) a vertical section through the overlapping seams [8]

1.2.2.3 Moulding Methods

The cut-and-stitches, folding and overlapping designing techniques provide better fitness and comfort as compared with fitting the women personnel with the unisex outfits. However, the above-mentioned designing techniques also face a problem of obtaining an accurate surface data for women's bust due to its ambiguous borderline with the skin surface. Normally, the effectiveness of the women's ballistic protection depends on the adaptiveness of the body armour to the human morphology. The more the ballistic vest resembles the required shape of the body; the better fitness and efficient protection will be obtained. Therefore, developing women's body armour which properly accommodates the bust area and fitting of the different curvilinear areas with the required dome-shape will improve not only the fit and comfort but also its ballistic protections for different women morphology [24][158]. Besides, to avoid the

fitness, comfort and poor ballistic performance problem, the pattern for the frontal women ballistic vest should be three-dimensional which can properly accommodate the bust area. Moulding is a new developing technique that usually creates the required dome-shape through the forming process without applying any kind of cutting and stitching to develop women's soft body armour. Thus, it helps to develop seamless frontal body armour by mimicking the bust area without the need of cut-and-stitch or any other finishing methods. However, the methods need not unique designing techniques but also proper materials to accommodate the required shape without facing shear deformation, panel thickness variations, and wrinkles on the material and body size limitations.

Figure 1.22 Female body armour through the moulding process [268]

Various body armour developers and researchers have been used such designing techniques to develop women's soft body armour. For example, Teijin Aramid in collaboration with Triumph International claims the concept of manufacturing the women's body armour through the moulding process as shown in **Figure 1.22**. The moulding process was carried out using pressure and heat on the 2D woven p-aramid (CT709) fabric to create the moulded panels [260]. Each moulded layers were then kept one over the top of the other to obtain a garment part and, joined by a base seam, e.g., in the middle of the panel as shown in **Figure 1.22** *(b)*. Another women's body armour for ballistic protection, increased comfort, and ease of movement using a 3D melded multilayer laminated woven structure was also developed with better retaining and conforms of the female torso [19]. Moreover, some researchers have also used a 3D pattern for the frontal panels of women's body armour to avoid the problem of the traditional designing method. 3D modelling shaping of women's body armour using the scanning process leads to woman's chest separated from the body, parameterized and then adapted to individually in the relationship of the given customer's morphology. For example, parametric design methods for generating human body models of varying sizes according to different anthropometric measurements in the 3D domain and 3D presentation were used to develop warp-knitted seamless garments [261]. A new design approach has been also proposed for developing women's body armour by introducing the different personal parameters of the body inside the new geometric definition of the vest. It uses the real 3D body measurement to optimize the assembly process and projection zone, which later leads to the reduction of weight and waste quantity during the cutting operation. Afterwards, it can be possible to create a base virtual

dummy with scalable measurements, depending on a certain number of measures to recreate the internal surface of the bullet-proof vest [257]. Other three-dimensional seamless women body armour (both loose-vest and bra-vest) were also designed by researcher combining CAD software for design and seamless knitting technology for production [262]. Such a method claimed to eliminate the traditional cut-and-sew method since it has a negative effect on the protective and comfort performance while accommodating the bust contour. Some researchers have also used 3D warp interlock fabric to accommodate their women's body armour design due to its good moulding ability. For example, among the different patented women armour design, a moulding process on the base functional materials made of multi-layer laminated woven structure to substantially conform the intended women's frontal body morphology was invented [19] as shown **Figure 1.23**. The thermoplastic material was applied during the moulding process to fuse the fibres within the 3D woven material for better lamination and improved ballistic impact performances. The material forming on the upper and lower panel shape was designed based on the women's frontal shape to provide not only good ballistic resistance but also comfort and ease of movement of the wearer. Such design was claimed for its capability of retaining the moulded shape for better comfort and ease of movement when the protective wear is in use.
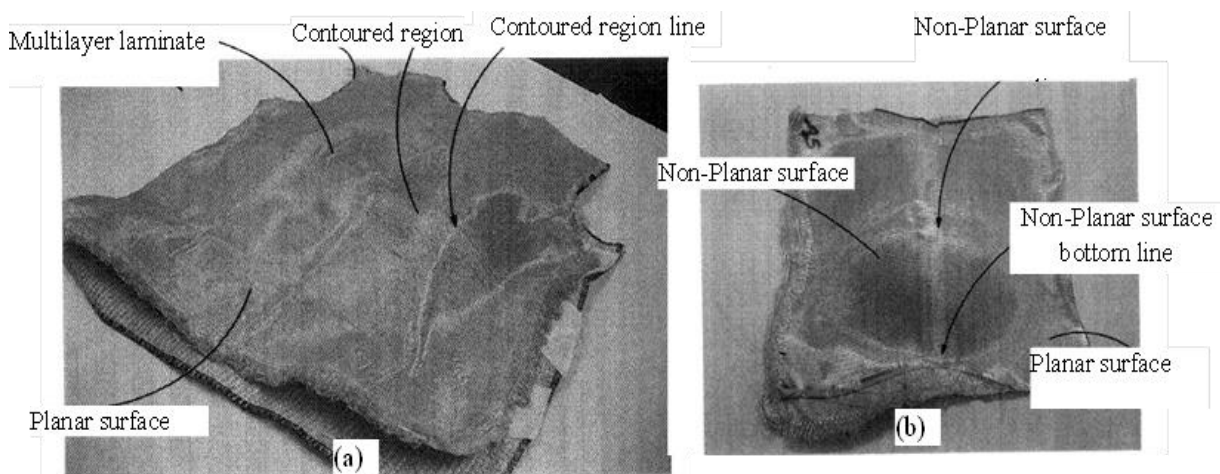
Figure 1.23 (a) multilayer laminate for ballistic protective wear in vest form constructed to conform to the natural curvature of a female torso, and (b) its sectional or component form

A contoured, form-fitting and flexible panel through the moulding process using three-dimensional woven material was also invented (**Figure 1.24**). The required number of layer fabric is placed jointly and substantially parallel with each other and moulded to adapt to the women's torso. To facilitate the torso conforming feature of the product, each layer of the fabric was made of weft and warp yarns with long float weave in one or more directions. The Adhesive resin can be used for the impregnations of yarn in each sheet. As shown in **Figure 1.24** *(a)* the multiple woven ballistic fabric layers are placed on the preformed mould between the upper and lower portion to conform to the desired body contour. Then, the fabric sheets with applied adhesive will be compressed between the two portions and subsequently the long floats of the fabric weave help to conform to the required shape of the mould. Even though such methods provide better ease of movement and comfort, however, it also creates different creases

and folds due to the inflexibility of fabric which ultimately might cause problems with fit and comfort [263].
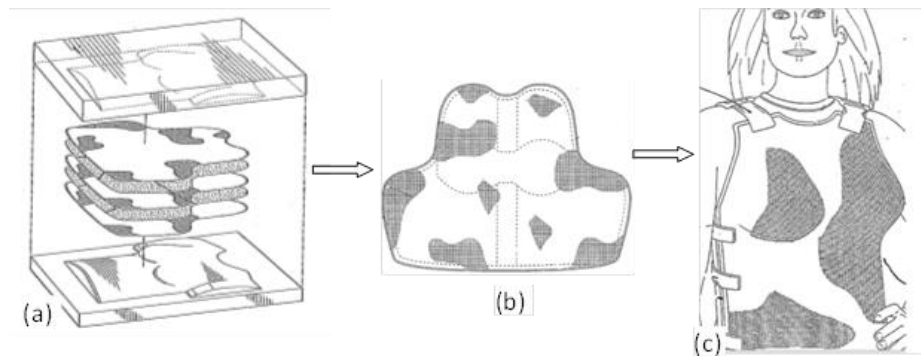
Figure 1.24 Moulding process for developing flexible women body armour with 3D woven material [263].

For example, one of the research studies presented mathematical modelling to determine the pattern to develop seamless women body armour frontal panel considering both body size and bra size for better ballistic performance in speedy pattern development [35]. The mathematical model was constructed by combining both the bust-cup (model) and no bust-cup areas (block projection) based on the classic coat block pattern by omitting the dart. Then, the bust area was geometrically modelled with the help of Rhinoceros software. According to the study, three different models (as shown in **Figure 1.25** *(a-c)*) to represent and accommodate the bust-cup areas of the women were tested.
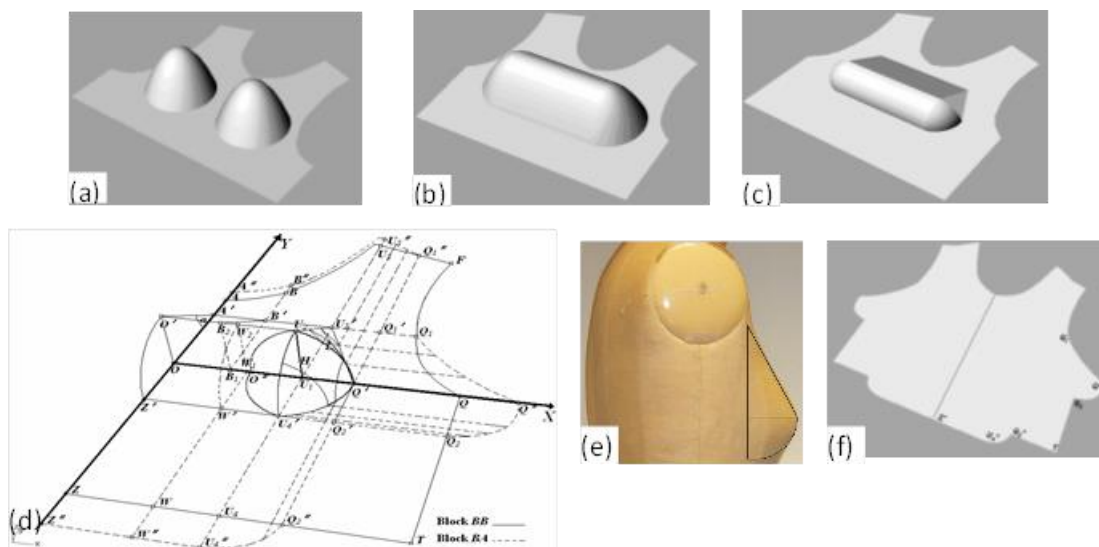
Figure 1.25 (a), (b) and (c) different geometrically models to represent the bust area, (d) mathematical model of half front panel of the women body armour, (e) size 12 standard mannequin and (f) the developed pattern

The first two-dome-shaped model to accommodate the bust area (**Figure 1.25** *(a)*) was found not appropriate due to excessive fabric creation while flattening of the domed area during the pattern making the process. The second model was designed to illuminate the excessive fabrics exists in the first model by linking the two doomed shape entirely (**Figure 1.25** *(b)*). Even such models were impractical for real body armour developments. The last model (**Figure 1.25** *(c)*)

was likely appropriate developed considering the shape of both the frontal mannequins and bust area and dividing it into seven different geometrical shapes (**Figure 1.25** (*d*)). Finally, the mathematical model based on half of the female body armour front panel was computed based on a size 12 standard mannequin (**Figure 1.25** (*e*))*.* A simple pattern for the first layer of the panel was generated for the frontal part (**Figure 1.25** (*f*)) and fitted with 3D warp angle-interlock fabric (**Figure 1.26**(*a*)) to validate the model through a moulding process.
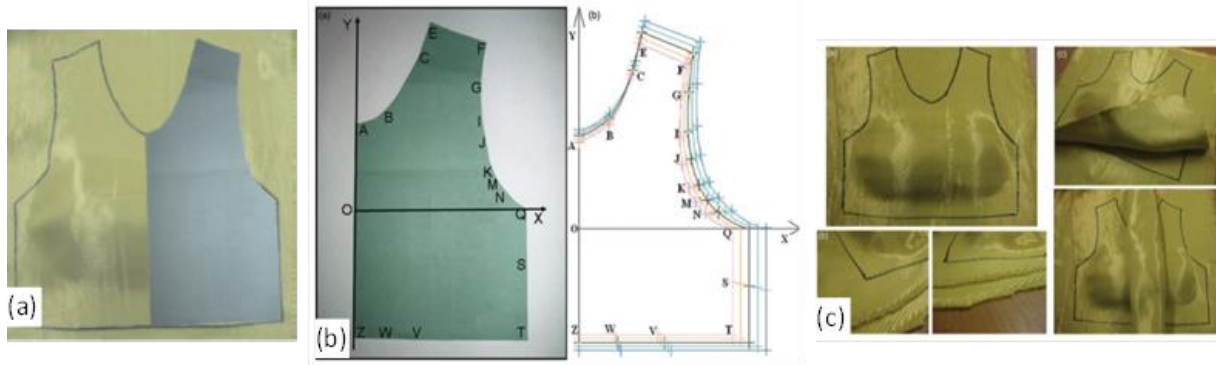
Figure 1.26 (a) Single-layer validations (b) pattern development process for multiple layers and (c) experimental validation for multiple layers of the front panel of the female body armor using 3D warp angle interlock fabrics

In continuation of this work, a pattern for various layers of the panel was developed considering the relationship between the thickness of the fabric and the pattern block projection as shown in **Figure 1.26** (*b*) [24]. 3D warp interlock woven fabric was used and moulded to shape the frontal women's body armour of different layers according to the design as shown in **Figure 1.26** (*c*). Even though the result shows a satisfactory result for the given body size, however, the methods use a traditional bra sizing system which may still bring fitness problems on the wearer. Moreover while flattening; the deformational stress on the fabrics might not be uniform throughout the front panel. This might have a problem with the final ballistic performances of the body armour [29].

1.2.3 CAD and human body modelling for soft body armour design

Different researchers have used 3D surfaces of body modelling for designing different garments. A customized cloth making method was involved in body dimension collection, pattern generation, and fabric cutting, etc. The researchers tried to generate clothing patterns using CAD techniques from collected body dimensions. The 3D design process, recent technology is one of the processes which help the researchers to meet the challenges in terms of new product development processes. Even if the development of virtual custom models is a challenging process, it is a very important accompaniment to the field "ready to wear" and mass customization, crucial to direct garment design in the 3D environment [30][31]. Therefore, the researcher has started to approach 3D modelling and 3D shaping including women's body armour design by employing the scanning process, which leads to woman chest separated from the body, parameterized and then adapted to individually in the relationship of given customer's morphology.

1.2.3.1   CAD applications

Nowadays computer-aided design (CAD) is an established technique for generating practical designs for most engineering applications. Unlike the early systems, modern CAD systems not only incorporate various analytical tools for optimizing the functionality of their designs but also assist to generate manufacturing information efficiently [264]. It is used for shortening the product development cycle by improving pattern accuracy and grading sampling [265]. CAD can also offer an opportunity for more accurate sizing, measuring and able to draft a design virtually to reduce material waste. Commercially available 3D CAD software for virtual prototype garment design is mainly identified into 2D-3D and 3D-2D approach. 2D-3D approach refers draping of digital 2D pattern pieces onto a 3D mannequin. Whereas, 3D-2D approach indicates the development of garment design on a 3D body and subsequently flattening the shape into 2D pattern pieces [266]. The 3D-2D method includes a parameterization process on a scanned body to create a parameterized model. Based on this model a basic wireframe aligned with body features will be developed to achieve the desired fit. The 3D-2D flattened pattern is simple for implementation and can generate patterns for fit-ensured mass-customized apparel products as compared to conventional 2D-3D patternmaking methods [267]. Besides, unlike the typical approach of 2D-to-3D CAD systems where 2D patterns pieces are pulled towards the human model for virtual sewing simulation, a new CAD approach has been proposed by involving from cross parameterization up to editing for virtual try-on, fitting evaluation and style editing to speed up the clothing design [268]. The methods use a cross parameterization technique for mapping the clothing pattern pieces on a model surface with low distortion and then a new hybrid pop-up for deformation to approximate the virtual try-on shape. Moreover, CAD application in the 3D garment design process and manufacture engineering has been also used in a different range of process i.e., digital human modelling, 3D garment design and modification, numerical integration of draping, 2D pattern generation, geometric details modelling, etc. [269]. However, the pattern generation processes in the textile industry ignored some important constraints which affect the accuracy of the final patterns. This can be solved by generating a 2D block patterns method directly from the 3D model body using 3D-2D approaches. Various researchers have made a very good contribution to this field. Moreover, while designing the women soft body armour through the 3D design process, it is very important to review and understand the 3D human modelling, Bust volume, and bra pattern generation and manufacturing process.

1.2.3.2   Human body modelling

In the last few decades, human-centred design has got immense attention in the product design process. For such purpose, a lot of efforts have been made on generating an accurate and reliable digital human model for analysing the effects between human users and products. Modelling the outside human body shape is one of the key techniques for realizing proper garment product design. A lot of researchers have devoted to proposing a solution to the development of the human body model using parameterization algorithms either with creative or reconstructive approaches. One of the studies has developed a human body model template using the parametric design method and anthropometric measurement [261]. It was parametrised by extracting feature information from the template model combining 3D geometry and human

semantic analysis to generate the different sizes of human models for the 3D presentations of warp-knitted seamless garments. Another method is also presented to generate 3D human body shape by appointing a set of semantic values using an exemplar-based method [270]. It mainly deals with design and manufacturing aspects rather than focusing on body modelling for human pose generation. The method allows generating a new 3D human body by a new set of semantic parameters input in the database which greatly improves the design automation of human-centric products. Another study has also convinced the 3D human model can be constructed from 2D images which are a cost-effective approach to visualize digital humans in a virtual environment [271]. The study proposes a systematic approach for constructing a 3D human model using the front and side images of a person. The method includes detecting the silhouettes of the human body, feature extraction on the silhouettes and 3D model construction. Another parametrization approach of human bodies using unorganized cloud points has been also proposed for generating human models [272]. The method involves both semantic feature extraction technique and symmetric human body mesh surface for developing human body wireframe and moulding respectively. The produced symmetric mesh surface was claimed as efficient compared to other template fitting based approaches due to the sample models had a chance to be synthesized to convert to the new human body based on user input dimensions. Another geometric modelling method has been also introduced to automate the customized product design for specific customers by mapping the designs onto different reference model shapes and then unfolds them into 2D pattern pieces [273]. This method becomes more important for designers and developers to automate the product from design to fabrication which later uses a map-guided algorithm to positions the pieces automatically according to industrial requirements. Another parametric human body shape modelling framework for integration into various product design has been familiarized. This mainly involves database construction for structuring the 3D body scan data, statistical analysis for investigating the different characteristics of the human body shape variation and their correlations. It appealed to be accurate with better visual fidelity due to its correlating ability of body shape and body sizes through parameter optimization technique [274].

Various researchers have also further used different human models for different garment designs. For example, one of the studies has developed different garments din a 3D virtual environment using garment modelling and numerical simulation of mannequins. The method starts with defining a strategy for virtual garment development to create virtual tailoring. The model incorporated the ease of the garment model to define the priority concepts of draping and proper fit of the garment considering the real deformation of the fabric [275]. Beyond the sole use of CAD modelling, an integrated physics-based model within CAD systems for highly accurate garment shape in virtual garment design, simulation, and quality evaluation has been also presented to allow the designer to validate their design option through garment virtual prototypes and simulation analysis for reducing the physical prototype used [276]. Besides, a general 3D Automatic Made-to-Measure approach has been used for designing customized apparel products. [277].

1.2.3.3   Bra pattern designing for women body armour development

While developing seamless women's soft body armour through the 3D designing process on the adaptive virtual mannequin and using moulding process on the material, first it is imperative to find the right bust volumes depending on the different cup sizes. However, the intimate apparel product including the bra designing stage passes through a very complex process to achieve proper sizing, fit and comfort. Ill-fitting bra and insufficient bust support can lead to not only unpleasant appearance but also the development of musculoskeletal pain while developing bra or further used for soft body armour development[278]. In general, as cup size is not homogeneous for different band sizes, it is recommended that women should not consider themselves to be an isolated cup size, but rather a combination of a band and cup size [279]. However, commercial bra designs are inadequate in overcoming all the bra's physical and physiological problems that arise due to poor bra components design i.e. pressure from tight shoulder straps, pain rashes resulting from rigid underwire, irritation by bra cup seams, etc. [280]. Some researcher has discussed thoroughly to analyse bra design problems to provide suitable methods to alleviate those problems. In doing so the current professional design methods to ascertain the details of the commercial bra design process have been studied with the discussion of designers and other relevant professionals [281]. The result shows that this design process relies heavily on the expertise of the designers and involves a high level of heuristics knowledge. Apart from this, even if the woman's breast is a very complex 3D geometry, still the commercial bra sizing system has been working based on bust girth and under bust girth for bra design [280][282][283]. This situation makes the system inappropriate to categorize breast sizes and results difficult for women to find their correct bra size.

Moreover, unlike another human body part due to ambiguous and lack of a standard method of measurement, the borderline of the breast with the skin surface is difficult to obtain accurate surface data for women's breasts. For better comfort and fitted brassieres, a new appropriate measurement protocol with a reliable boundary of the breast has been explored for providing new shape parameters of breasts by scanning different women's nude breasts [284]. This method uses a folding line method for finding a continuous and natural boundary for the breasts, so the breast base and volume could be measured more accurately. Breast volume determination is important not only for fitted and comfortable bra design but also for the diagnosis and treatment of breast disease. The comparisons of breast volume calculation between 3D scanning and three different classic methods namely nuclear magnetic resonance imaging (MRI), thermoplastic castings, and anthropomorphic measurements show 3D scanning provides acceptable accuracy for breast volume measurements [285]. The traditional methods of breast volume measurement have been also carried out using different approaches [279]. However, those different methods will be incomparable if the breast boundaries are different. Another study on different traditional methods of bra sizing revealed that mammography found the most accurate method of breast volume measurement followed by the Archimedes method [286].

Considering the problem of the current standard bra sizing method for proper size and bra design, some researchers came up with different proposals. A study has developed a novel approach of personalized bra cup dart quantization in the 3D virtual environment. This approach tried to meet the customer demand of made-to-measure well-fitted bra. With this method realization of the virtual magic, the female breast shape archive provided a favourable 3D

environment with a theoretic foundation for bra pattern design [287]. Another solution has proposed for the bra sizing scheme by taking the entire shape information into account based on surface scan data. It took the breast's volume on a robust and automatic algorithm based on measuring the volume difference of a torso with and without the breasts for breast shape approximation. Using this bra sizing method, the development of the actual bra is greatly simplified and less expert knowledge as per the bra designer requirement [288]. Another systematic design process has been also introduced for the development of a prototype sports bra for large-busted women by draping and flat pattern based on several research studies as input to resolve specific comfort, support, and aesthetic issues. While product development fabric choices, design modifications, and fabric layering were considered to accommodate these specific issues [289]. Other than the traditional measurement of the volume of the breast, a novel breast volume measuring method by using a rapid and accurate mesh projection based on three-dimensional (3D) point cloud data derived from a [TC]2 3D scanners have been used. It is established as a simple and standard land marking procedure to determine and avoid the arbitrariness of the definition of breast boundary. Comparing with the water displacement method for validation, the proposed method was found accurate to calculate breast volume. Meanwhile, measuring breast size has been also developed from three-dimensional (3D) body scans image data. An anthropometric bra cup sizing system with the breast arc length and the new bra cup size was highly correlated with breast depth [290]. Another approach with parametric design and process parameter optimization of bra cup moulding has been defined by integrating several advantages including 3D scanning via reverse engineering, parameterized-based meshing, non-linear mathematical prediction models, a model of foam shrinkage and example-based bra cup design and grading to optimize the bra cup development and production process. Based on experimental results the proposed method is highly effective and more time-saving in the design of new products and providing consistent quality control of the bra cup moulding process [291].

Nowadays seamless moulded bras have become more and more popular. The manufacturing of a seamless 3D bra cup using foam sheet moulding by one-step forming technology is an important manufacturing technique for the familiar apparel industry. The process of bra cup moulding is booming not only reduces the production cost of cutting and sewing but also gives the smooth surface of a moulded cup [292]. Moreover, due to the continual need for brassieres that provide enhanced comfort and readily adjustable fitness for constant comfort and support, and improved brassiere providing very comfortable and readily adjustable fit to the wearer's torso has been invented [293]. In comparison with traditional cut-and-sewn bra cups, the moulded foam cups give better support and fit by maintaining the cup shape after repeated washing and wearing [294]. Another robust algorithm for 3D surface reconstruction of a bra fitted to an underlying mannequin projecting the patch to a plane in the current viewing direction via scanned polylines has been developed. However, instead of a physically-based approach, they use a geometrically based bra pattern flattening method using linear least squares optimization. Considering the complex surface characteristics of the female breast region, the method has consumed relatively lesser time than the traditional one. Moreover, even though bra pattern grading is also a highly complicated procedure due to higher number of commercial sizes ranging, using this new procedure grading of the bra size can be achieved by simply controlling the gap between the

mannequin surface and the poly lines of chest girth [295]. In the new bra product design process, brassiere manufacturers work on consumer co-design to develop new design bra products which are suitable for individual consumers. This co-design process will indicate the different most important parameter of bra that has to be included in the designing process [296]. Some studies also scanned bra cup specimens to characterize the 3D shapes of the convex surface of the scanned bra cups to determine different sizes through grading the wireframe model. This might help to produce product of new bra cups which was conventionally very time-consuming and ineffective but still will not give the proper breast shape due to not following directly the body contour. Moreover, unlike another human body part due to ambiguous and lack of a standard method of measurement, the borderline of the breast with the skin surface is difficult to obtain accurate surface data for women's breasts.

In traditional clothing design, different researcher has worked on standard sizing systems to fit different groups of the population based on their demographic and anthropometric data [297][298]. However, only a few types of research have been involved in analysing breast shapes and come out with different solutions for developing better bra sizing systems. Based on different investigation regardless of how good the design of the bra, using the appropriate sizing is very critical for the effective support of the breast [299]. This hypothesis has been supported using a comparison between women's bra size as measured by the traditional bra fitting method with their recommended bra size based on professional bra fitting criteria [282]. Another study used relatively different breast measurements and propose a new bra sizing system that gives better fitness for Chinese women [283]. Another research group also tried to design the ergonomic brassiere wire that should fit the curve of under breast and thorax by applying the 3D measurement of human body structure [300]. The traditional breast sizing system was complained due to its erroneousness because a woman's who have the same underbust and bust measurement can have a different body shape. For this, a researcher has developed a new system of bra measurement in which band size is still determined by the industry standard of "underbust chest circumference plus 5," but cup size is determined by direct measurement of the breast in proportion to underbust circumference [301].

2 Materials and Methodology

2.1 Introduction

As it has been described in the last chapters, the main objective of this research work is to solve the current problems of women's soft body armor. The research approach mainly involves both the developments of the new design system for generating women's frontal panel patterns with specific body shapes and developing an appropriate fabric structure. Involving both approaches help us to develop the final seamless soft body armour for a woman not only to accommodates the body shape for better fitness but also providing better ballistic impact protection. A new designing approach and various experimental works have been carried out. Among this, designing of an adaptive bust on the 3D virtual model, integrations of this adaptive bust in the other part of the woman frontal body to develop the first layers of the panel using reverse engineering (2D-3D-2D flattening) and generating of pattern for the multi-layer panels for the final seamless woman body armour based on the developed block patterns are some of the designing approach we devised. Moreover, the study tried to design, manufacture and introduced the 3D warp interlock fabric structure not only due to their excellent moulding behaviour for accommodating the design properly but also its good ballistic performances. Even though the two complementary approaches (pattern designing system and experimental ballistic testing on engineered fabric) are used to realize the research objectives, however this section mainly discussed the design, developments and quasi-dynamics experimental testing parameters and protocols of the engineered fabrics. The designing process and its methodology of the pattern generation system were included in their respective chapter.

This chapter will discuss different materials used and the research methodology for realizing the research aims and objectives. First, a comprehensive description of the design and development of different 3D warp interlock fabric using different parameters will be discussed. The different methods protocol, parameters, and procedures to measure, test against the mechanical and forming behaviour for characterization will be outlined. Besides, the procedures and parameters of the ballistic testing equipment and different methods to extract and analyse the ballistic performances of the tested materials will be explained. The protocols and testing parameters for testing of the engineered fabric at the final women body armour panels according to NIJ standard Level – IIIA will be also outlined.

2.2 Materials

For the last many years, researchers have been studied and investigate various material for their performances including mechanical, ballistic and flexibility in terms of different parameter for ballistic protection, i.e. soft body armour [302][61][50]. Moreover, different fabrics type felts, metals and composite materials have been involved for the applications armoured systems [303]. Among the fabric type, 2D woven and UD laminated made from high-strength fibres are widely used for the developments of soft body armour due to their excellent mechanical and better fatigue life properties[304][305]. Those fabrics are commonly made of the well-known high-performance fibres, such Twaron®, Kevlar®, Dyneema® and Spectra® which is

61

extensively used in flexible personnel ballistic protection due to their high resistance-to-impact damage [50][79][80], high strength, high tenacity, good chemical resistance and lightweight characteristics [44][81]. Besides, research studies have also proposed 3D woven fabrics for ballistic protection due to the enhanced mechanical properties in the thickness direction [304][305]. In this section, the design, development, and manufacturing of 3D warp interlock fabrics used for the applications of women soft body armor will be introduced. Those fabrics will be later experimentally investigated for the ballistic, formability and other mechanical characterisations.

2.2.1 2D plain weave fabric

A significant number of industries have used 2D woven fabrics perform for many technical applications. Plain weave is one of the most commonly used two-dimensional weave patterns for soft body armour design which consists of weft yarn (0° or x-direction yarns) that interlaces over the warp yarn (90° or y-direction yarns) [306] by applying different binding systems i.e. stitching. For our study, a plain weave para-aramid fabric, Twaron CT-709, with areal density 200 g/m^2 was chosen material for the investigation (**Figure 2.1**).
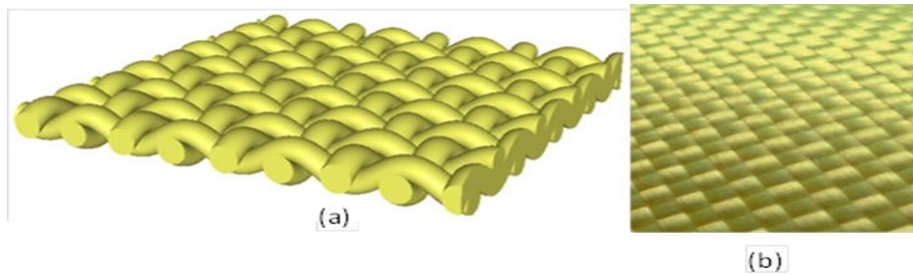
Figure 2.1 2D plain weave para-aramid fabric structures, Twaron CT-709 (a) Design schematic representation, and (b) 2D plain weave fabrics

The mentioned fabric structure also consists of 930dtex yarns with warp and weft density of 105 yarns per 10 cm. The fabric was obtained from Teijin Aramid, a subsidiary of the Teijin Group, Netherland. Apart from fabric properties, the yarns were taken from the fabric structure and tested to determine their mechanical properties. The detail specification of para-aramid CT-709 fabric used for this research purpose is given in **Table 2.1.**

Table 2.1 Specification of the fibre and 2D plain weave p-aramid fabrics (CT-709)

Fabric style	Twaron Type	Linear density [dtex]	Yarn Properties			Fabric properties		
			Tenacity at break [mN/tex]	Strength at break [N]	Elongation at break [%]	Areal density [g/m^2]	Yarn densities([Warp/ Weft per cm]	Fabric thickness [mm]
CT-709	2040 microfilament	930 f 1000	2.35	225	3.45	200	10.5/10.5	0.31

The fabric was also mainly recommended and used for manufacturing body armour due to its ballistic protection performance combined with a high level of flexibility and comfort as per the manufacturer.

2.2.2 3D warp interlock fabrics structure design and manufacturing

Various researchers have claimed 3D warp interlock structures show not less ballistic protection performance and display good formability behaviour and lightweight as compared to its counterpart 2D structures [46][147]. Today, three-dimensional (3D) textiles are enormously involved not only in the ballistic protection but also in various applications [34] due to the enhanced mechanical properties in the thickness direction [304][305], good elastic behaviour properties [156], good formability and moulding ability capacity [2] and low shear rigidity as compared to other woven fabric structures [33]. Besides, due to their excellent forming capability, the 3D warp interlock fabric could substitute the conventional plain woven fabrics for developing woman body armour design. However, the fabric should be carefully developed and investigated their forming capability along with their ballistic performance before considering for woman body armour design. This section discussed how the different 3D warp interlock fabrics have been designed and manufactured for application of woman soft body armour. The main aims were to find the better 3D warp interlock by investigating their forming, ballistic and mechanical performance for better forming ability to accommodate the shape along with better ballistic protection to produce the woman seamless soft body armour. During our research, different production campaign has been taking place to produce the different 3D warp interlock fabrics depending on the different parameters and characterisation. The general flow diagrams for 3D warp interlock production and testing are shown in **Figure 2.2**.
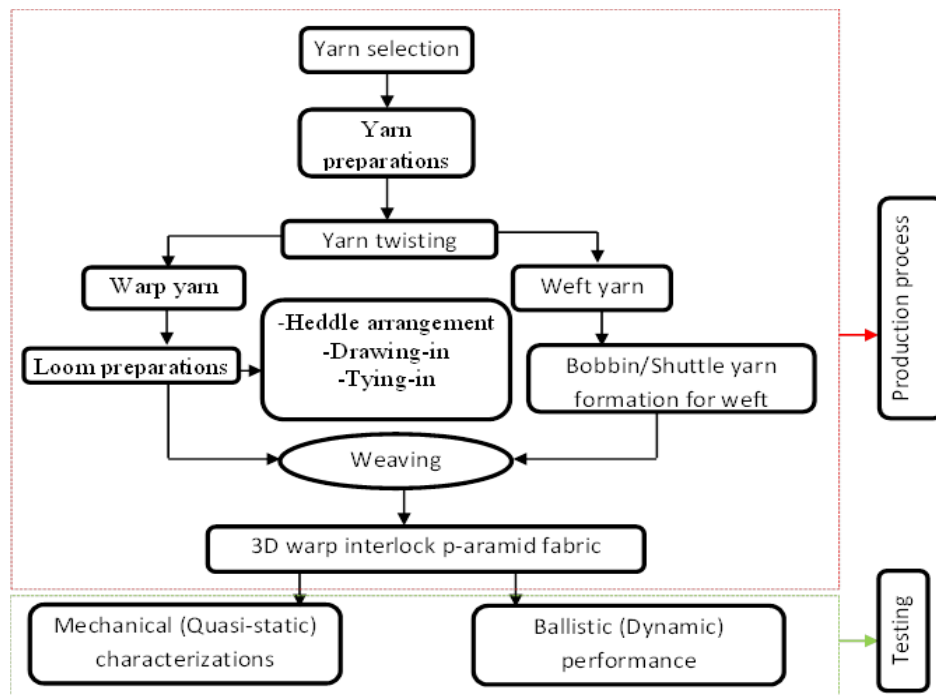
Figure 2.2 General flow diagrams for 3D warp interlock fabric production and testing.

The first campaign was produced four different 3D warp interlock p-aramid fabrics having different yarn density to investigate the effects of fabric density on their formability and mechanical properties. The second campaign involves in designing and developing of the 3D warp interlock p-aramid fabrics with similar the fibre types of the commonly used 2D plain weave p-aramid fabrics (CT-709) for the woman soft body armour application. Both fabrics were then prepared with the same fabric weight to compare for their ballistic performance according to NIJ Level-IIIA. The third campaign was designed and develops different 3D warp interlock fabric considering the ballistic results of the 2nd campaign. In this campaign, the interlock fabric was developed considering the warp yarn interchange ratio for enhancing the ballistic performance without affecting the forming capabilities of the fabrics.

The next sub-section will explain the design, preparation, machine used and manufacturing processes for developing different 3D warp interlock p-aramid fabrics in the different campaigns for its mechanical formability and ballistic property characterisations before applying for women soft body armor. All the fabric belongs to different 3D warp interlock fabric category and produced either in the automatic dobby and ARM semi-automatic weaving machine.

In the first production (*Campaign one),* we have produced two 3D warp interlock fabric structure having 5 and 7 weft layers with different yarn density to investigate the effects of yarn/fabric density on the forming and other mechanical behaviours of 3D warp interlock fabric structure. Researchers have somehow exploited, designed and used various materials for the developments of soft body armour based on different parameters. Moreover, the soft body armour should be design not only considering the material's ballistic performance but also other mechanical properties including bending and forming capability without affecting its mechanical performance for better protection, fit and comfort of the wearer**.** Besides, designing woman body armour needs good material formability to accommodate different curvy parts including the bust area without compromising the ballistic performances. The density of the fabric is one of the most important factors which could affect the ballistic performances of the materials. However, it also has a great effect on material formability and mechanical properties. In this production campaign, two 3D warp interlock (O-L) fabric structure with different layers namely, 5 and 7 weft layers, considering yarn densities were manufactured using an automatic dobby loom (DORNIER) in ENSAIT, GEMTEX laboratory. From the two 3D warp interlock fabric weave structures, four variants with 7 layers and one with 5 layers considering different weft and warp density were developed. All the fabrics were manufactured based on the geometrical design of the architecture generated on Wisetex© software. **Table 2.2** show structural characteristics and different parameters of the produced 3D warp interlock fabrics.

Table 2.2 Structural characteristics and parameters of the produced 3D warp interlock fabrics

Parameters	Sample preforms			
Sample designation	$3DS_1$	$3DS_2$	$3DS_3$	$3DS_4$
Total density of warp yarns (yarns/cm)	30	32	42	64
Total density of weft yarns (yarns/cm)	30	49	38	35
No. of warp layers	6	8	8	8
No. of weft layers	5	7	7	7
Warp density per layer (yarns/cm)	5	4	5	8
Weft density per layer (yarns/cm)	6	7	5	5
Fabric areal density(g/m^2)	3115	4526	4543	5074
Fabric thickness (mm)	0.55	0.654	0.68	0.72

Figure 2.3 shows the schematic, 3D view and weave patterns of the developed 3D (O-L) warp interlock fabrics with 5 and 7 weft layers. The proposed 3D woven structure was obtained by interlacing warp yarns with perpendicular weft yarns in the width direction. In the structure, the binding warp yarns were used to build a link between the different layers of the fabric following a diagonal direction but not through the thickness of the entire structure. The fabric peg plans were designed and transferred to the machine using DB-weave® software.

The weaving loom was set-up with 24 heddle shafts to accommodate the 12 warp zones. All the produced fabrics were used similar 168Tex linear density high-performance yarns and 25 turns/100 cm yarn twist in the Z direction for both warp and weft yarns. **Figure 2.4 (a), (b), (c) and (d)** shows the different 3D warp interlock fabric production process, whereas **Figure 2.4 (e)** shows both 5 weft layers fabric (with 30 yarns/cm) and 7 weft layers fabric (49 weft yarns/cm & 32 warp yarns/cm, 38 weft yarns/cm & 42 warp yarns/cm and 64 weft yarns/cm & 35 warp yarns/cm) structure**.** The second production (campaign two) of 3D warp interlocks p-aramid O-L (orthogonal layer by layer) was also performed in GEMTEX, ENSAIT laboratory using an automatic dobby loom**.** In this production, the structure of the 3D warp interlock fabric was chosen to compare its ballistic performance and forming capability to the commonly used 2D plain weave p-aramid fabrics (CT-709) for woman soft body armour**.** The 3D interlock fabric structure was carefully designed with the help of WiseTex and TexGen software® as shown in **Figure 2.5**. DB weaves® software was then used to generate the lifting plans which later imported manually to the control panel box of the Dornier automatic dobby loom for production. The DB-WEAVE is one of the commonly used programs for the shaft weaving. It also helps in designing the weave patterns and weaves them on a computer-controlled loom. The peg plan was prepared with straight drawing-in for the dual-beam.
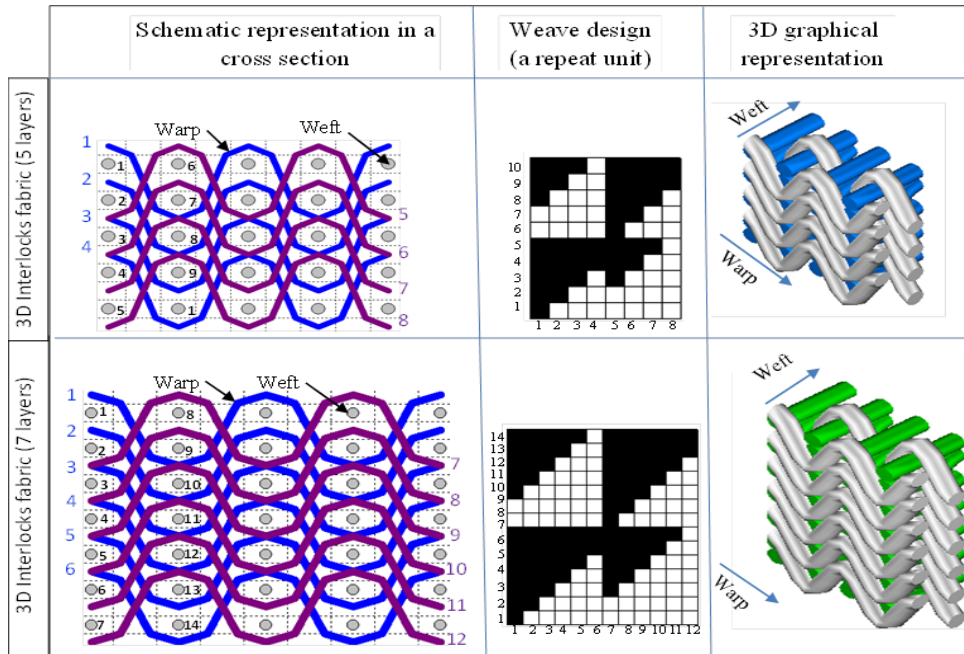
Figure 2.3 Designing of the weave structure design for 3D orthogonal layer-to-layer interlock woven fabric design using Wisetex® and DB weave® software

Unlike the previous production, the fabrics were made of high-performance p-aramid yarns (Twaron) having 2040 microfilament and 930dTex for the warp and weft direction. The yarns were supplied by the Teijin Aramid, the Netherland. **Table 2.3** shows the different specifications of high-performance p-aramid yarns (Twaron) used in this production campaign. While production, the 3D warp interlock fabric design which consists of only the binder warp yarn to have the same degree of crimp (yarn intake) was chosen. Besides, the weft yarn which was arranged systemically in the thickness direction with the help of at least one warp yarn system was considered. This design will also help to reduce the difficulty during weaving production by using dobby loom. The actual production width of the loom was 130 cm. According to the denting and its reed count, the total number of warp yarns in a centimetre was 52 ends. The total number of warp ends to produce the given fabric width was found 6,760 warp ends. These numbers of warp yarns were found very huge to accommodate in one warp beam. So, to accommodate such a higher number of warp yarns in the specified width (130 cm), two warp beams with an equal number of threads were installed for the production.
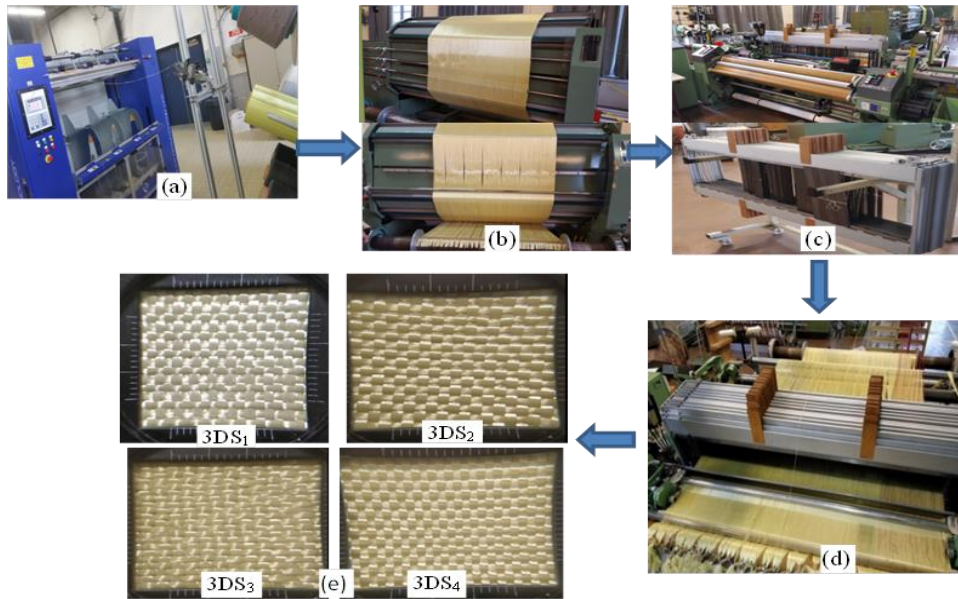
Figure 2.4 3D warp interlock fabric production process (a) yarn twisting (b) Yarn warping (c) Loom preparation and (e) fabric pre-production (drawing-in) and production (d) produced fabrics

Each warp beam was then accommodated 3800 warps each and the warp was carefully threaded and dented according to the lifting plan and denting order from the two beams as shown in **Figure 2.6 (a).** Besides, it was also very important to consider and use the proper number of reed and denting orders of the warp yarn during weaving. Using proper reed number will avoid excessive friction between the reed and yarn and breakage of yarn, whereas the reed denting provides an advantage of accommodating the proper design of the fabric weave geometry.

Table 2.3 The specifications of high-performance p-aramid yarns (Twaron)

Twaron fibre type	Filament	Linear density [dtex]	Tenacity at break [mN/tex]	Breaking force [N]	Elongation at break [%]	Chord Modulus
2040 microfilament	1000	930	2.35	225	3.45	89

In our production campaign, the number of reed and the denting order were optimised for better results. Based on the conception, to get the good yarn movement while shedding, the reed was selected as 8.5 dents/cm with racking of 6 yarns/dent. On each warp yarn, a warp break needle was also placed before the harness to stop the machine while warp yarn breakage or loss tensions as shown in **Figure 2.6 (c)**. The conceived fabric consists of weft yarns with low undulation degree and warp yarns with higher waviness degree throughout the length direction as described in the 3D weave design. The specifications of the produced fabrics are given in **Table 2.4.** While manufacturing using the automatic dobby loom, the different 3D warp interlock fabrics structure faces drawback of yarns damage due to abrasion [307], yarn to yarn friction [64], friction between loom part with yarns [149][308].
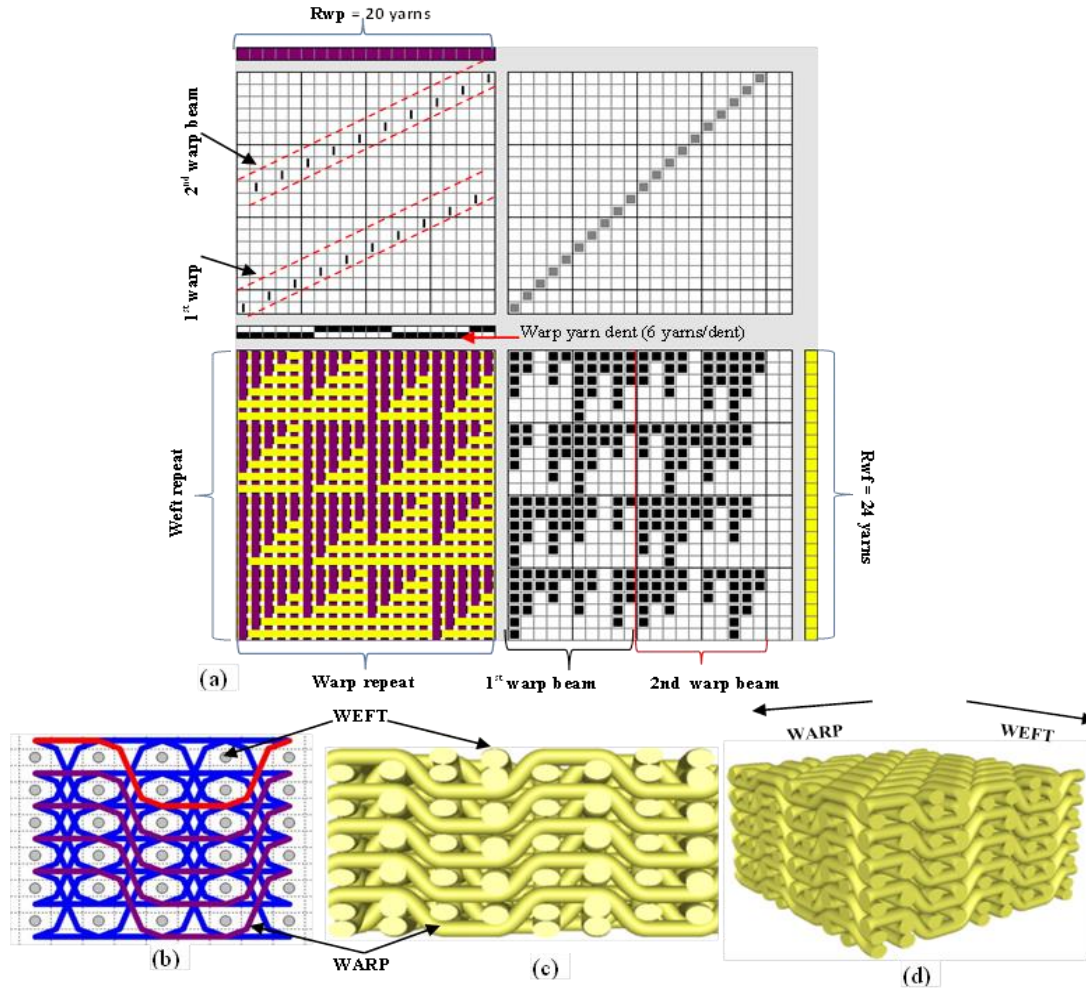
Figure 2.5 3D warp interlock design (a) Weave pattern and lifting plan (DB-weave software), (b) Orthogonal weave structure (c) Schematic representation of the fabrics in a cross section (TexGen software); and (d) 3D graphical representation (TexGen software).

Besides, accommodating higher number of warp yarn in only two beams for the different warp systems brings lots of weaving difficult during production. This definitely affects the overall mechanical performances of the fabrics and also faces a problem of producing huge amount due to its high production cost.

Table 2.4 Specification of the 3D warp interlock O-L p-aramid fabric produced

Fabric style	Fabric designation (one panel)	Linear density [dTex] (warp/weft)	Fabric areal density [g/m^2]	Total density [yarns/cm] (warp/weft)	Fabric thickness [mm]
3D warp interlock (O-L)	3D-5	930 (2040 micro-filaments)	1000	52.5/52.5	1.55

To avoid such problems, the ARM semi-automatic dobby loom has been used for our next production campaign to involve and accommodate a higher number of warp beams (24) for better controlling and lifting of the yarn based on the lifting plan of the design. Besides, the involvement of the higher number of warp beams also helps to separate the warp yarn sufficiently to avoid the friction between the yarn to avoid yarn degradation and breakage.
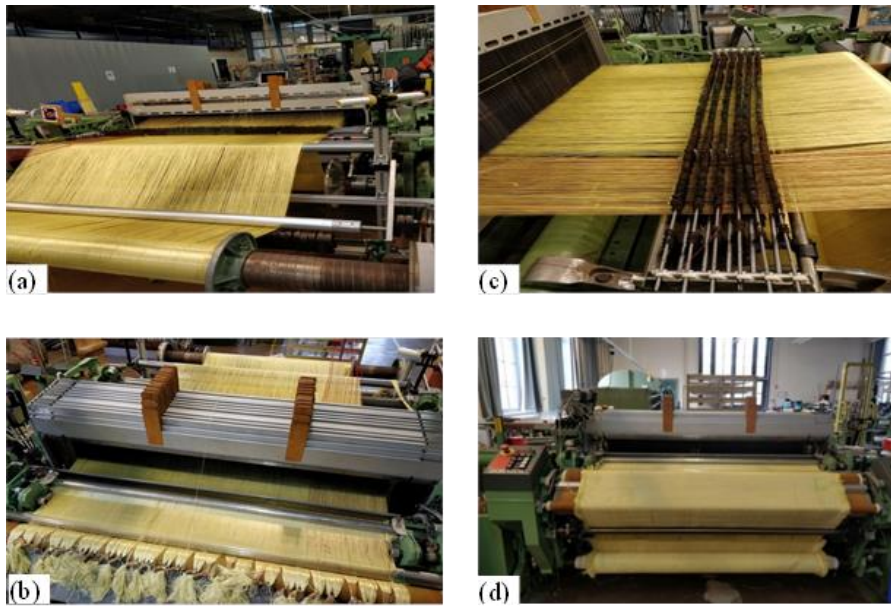
Figure 2.6 Weaving loom set-up (a) arrangements of warp yarn in the two beams (b) threading and denting of warp yarn, (c) tension and breakage control and (d) weaving of the 3D warp interlock fabrics in the dobby loom

The developed fabrics were compared with the corresponding 2D plain weave fabric against ballistic performance for developing the woman soft body armour panel. However, considering the ballistic test result of the previously produced 3D warp interlock fabric, a new production (production campaign three) was then set up considering the warp yarn compositions system inside the 3D warp interlock fabric structure for enhancing the ballistic performances without compromising the forming properties. The ARM semi-automatic weaving machine which could attain 24 warp beams was utilized to avoid some limitation of the Dornier dobby loom while producing 3D warp interlock fabric in the 2nd production campaign. Based on the result of the previously produced 3D warp interlock ballistic tests, developing a more rigid structure could enhance ballistic performances. However, the moulding ability of the fabrics should not be also compromised while increasing the ballistic performance through the fabric rigidity. The involvement, movement and deformational behaviours of different warp (stuffer and binding) and weft yarns could affect the overall properties of the fabrics. For example, stuffer and binder warp yarns could delineate the longitudinal and through-out-the thickness properties of the final fabric respectively [148]. Based on our previous result and in a combination of different research studies on effects of warp yarn type on the final fabric property, four different 3D warp interlock fabric architecture based on their binder and stuffer warp yarn interchange ratios were considered. These different compositions of warp yarn will give us a better idea of the final performances of the architecture not only on ballistic performance but also on other mechanical properties. The four designs include 100% binder and 0% stuffer (8:0), 66.7% binder and 33.5% stuffer (8:4), 50% binder and 50% stuffer (8:8) and 33.3% binder and 66.7% stuffer inside the 3D warp interlock fabrics. The different interlock fabric architectures were designed by using the similar commercial fabric weave-design software (TexGen®) which is usually used for designing different 2D and other complex 3D woven fabric architecture. Such a warp yarn interchange ratio inside the fabric could affect both the weave repeat unit and the overall fabric

structures. The geometrically developed 3D models of the fabrics were then transferred to Pointcarre® software to prepare the lifting plan for the fabric productions. The 3D graphical representation and its unit weave repeat pattern with the different sectional views of the 3D warp interlock fabric with different interchanging ratios between binder and stuffer warp yarn are shown in **Figure 2.7**.

The weave repeat unit which is the smallest constituents of the fabric structure will be combined to develop the overall fabric structures. For time-saving and simplicity purposes, all the fabrics were designed and prepared in the same weave drafting/lifting plan and similar weaving loom adjustment but weave the different fabrics by only changing the weave designs. Similar to the previous production, high-performance p-aramid fibre, Twaron® with 930dtex (which was purchased from Teijin Aramid, a subsidiary of the Teijin Group) was used for producing all the fabrics (**Table 2.1**). All the yarns were twisted at room temperature using Twistec machines with 25 twists per meter (TPM) throughout the fibre. The selected yarn is commonly used to produce the 2D woven fabrics (Twaron CT-709) by the Teijin Company and recommended to develop women ballistic vests due to its good ballistic performance and high level of moulding ability. **Figure 2.9** shows the production process of the 3D warp interlock structure and its produced fabrics.24 warp beams with a sufficient warp yarn length were prepared using the warping machines (**Figure 2.9 (a)**) to produce all the fabric. An adapted and modified ARM dobby loom was used to manufacture all the 3D warp interlock fabric architecture. A 50 cm long reed made of metals having a reed count of 12 dents /cm was used for the productions. A total of 24 beams with adjusting weight for warp yarn tension controlling were loaded in a good sequence on the adapted warp beam creel which could accommodate more than 24 warp beams (**Figure 2.9 (b)**).

Variant (Weaver/ Stuffer ratio)	3D graphical representation	Sectional view		Weave pattern Rwp – warp repeat Rwf – weft repeat
	○ - Weft yarns ◉ - Warp yarns (weavers) ● - Warp yarns (stuffers)	Longitudinal	Transversal	
3D-40-8/0 (8:0)				Rwf = 10 yarns, Rwp = 8 yarns
3D-40-8/4 (8:4)				Rwf = 10 yarns, Rwp = 12 yarns
3D-40-8/8 (8:8)				Rwf = 10 yarns, Rwp = 16
3D-40-4/8 (4:8)				Rwf = 10 yarns, Rwp = 12 yarns

Figure 2.7 The 3D graphical representation and weave pattern of the repeat unit and the sectional (longitudinal and cross-sectional) view for the 3D warp interlock fabric with different interchanging rations between binding(weavers) and stuffer warp yarns

While loading, the arrangement of the beams was carefully considered based on not only the lifting plan of the different warp yarn type but also avoiding the yarn contact with each other and friction during weaving. Moreover, every warp yarns from each warp beams were also passed separately in the guide of horizontal yarn tension control device for adjusting and controlling the warp yarn tension during the weaving process as shown in **Figure 2.9 (c)**. Moreover, 24 heddle shafts in which each shaft consists of 100 heddles were installed on the machine for better accommodations of the ends from one beam in respective one shaft (**Figure 2.9 (c)**).
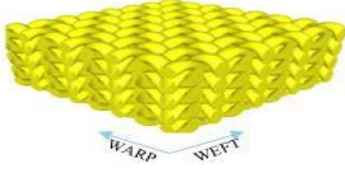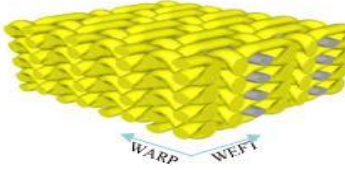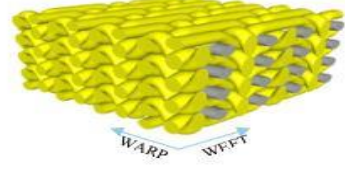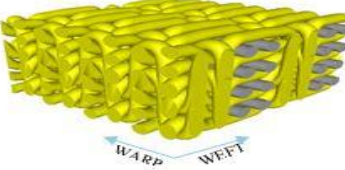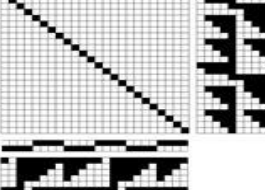
Variant (Weaver/ Stuffer ratio)	3D woven fabric simulation (Isometric View)	Lifting plans
3D-40-8/0 (8:0)		
3D-40-8/4 (8:4)		
3D-40-8/8 (8:8)		
3D-40-4/8 (4:8)		

Figure 2.8 The 3D graphical representation (isometric view) and lifting plans of the different 3D warp interlock fabrics

For better comparisons, all the fabrics architecture were produced with the same warp (48 ends/cm) and weft (50 picks/cm) density, same high performance p-aramid yarn (Twaron®) having a linear density of 930 dTex with 25 turns/100 cm yarn twist in the Z direction. Besides, all the fabrics were also produced with weft layers of 5 and a theoretical areal density of 970 g/m^2 was considered.
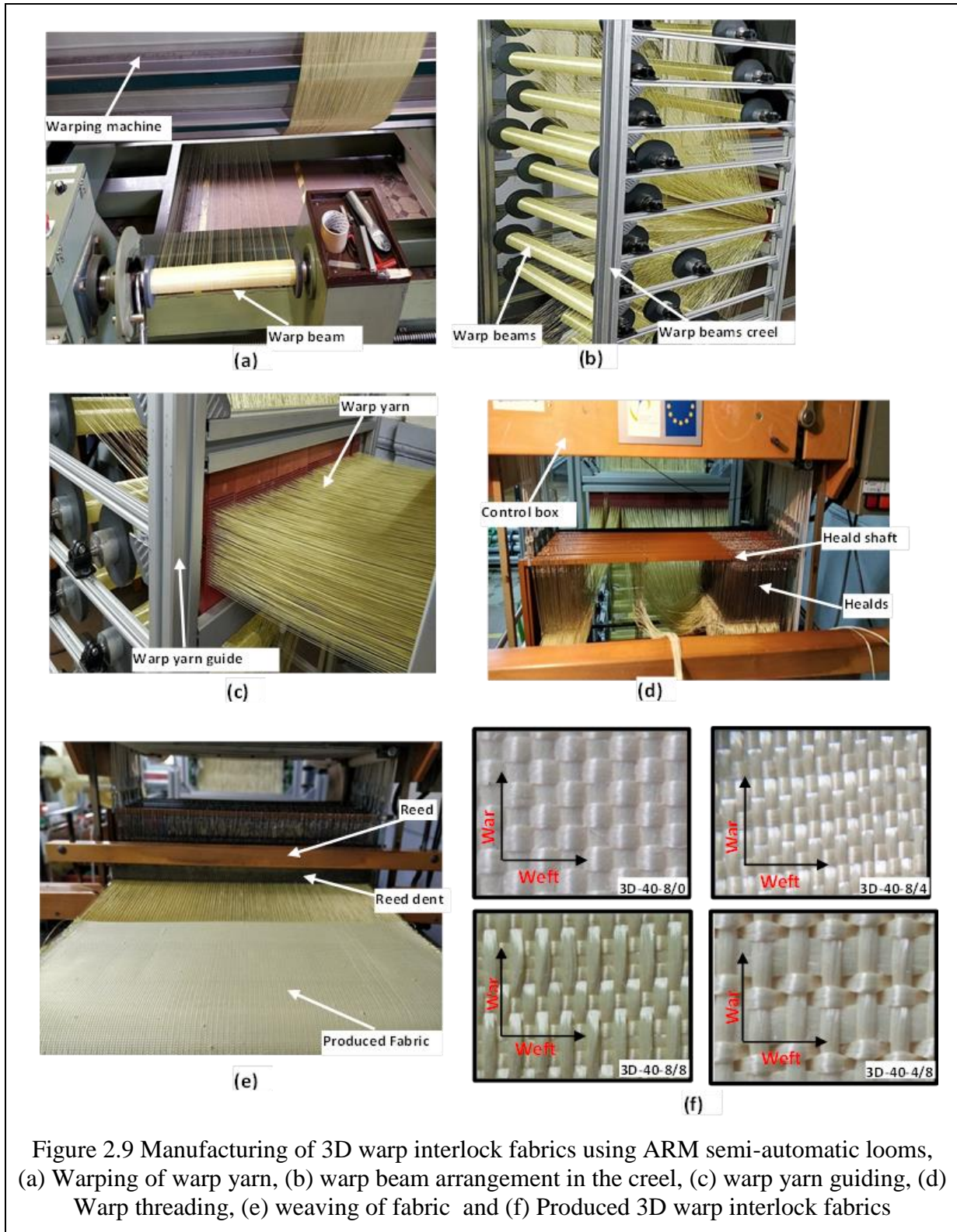
Figure 2.9 Manufacturing of 3D warp interlock fabrics using ARM semi-automatic looms, (a) Warping of warp yarn, (b) warp beam arrangement in the creel, (c) warp yarn guiding, (d) Warp threading, (e) weaving of fabric and (f) Produced 3D warp interlock fabrics

Table 2.5 shows the specifications of the produced fabrics. However, as shown in **Table 2.5**, fabric weight was found slightly different after the production due to the degradation and other factors were used while manufacturing all the intended fabrics. (Effect of weaving on mechanical properties)

Table 2.5 Specification the produced 3D warp interlocks fabrics

Fabric designations	Warp yarn (binder: stuffer) interchange ratio	Theoretical fabric weight [g/m²]	Actual fabric weight [g/m²]	yarn density (Warp/Weft) [yarns/cm]	Average Fabric thickness [mm]
3D-40-8/0	8:0	970	900	48/50	1.42
3D-40-8/4	8:4	970	920	48/50	1.44
3D-40-8/8	8:8	970	952	48/50	1.52
3D-40-4/8	4:8	970	944	48/50	1.63

2.3 General methods and methodology

The previous chapter tried to briefly discuss the different literature and related research work of the background, designing techniques, ballistic material, influencing parameters and mechanism on soft body armour, particularly for a woman. This sub-section mainly deals with the different methods and methodologies adopted to achieve the aims and objectives of the thesis study. In particular, the methodology mainly helps to define the ballistic performance, forming behaviour and quasi-static mechanical characteristics of the selected materials including 3D warp interlock fabrics. However, the general methodology and its designing framework for the body armour design part **(Chapter 3)** have been included in the respected chapters.

2.3.1 Formability behaviour characterizations

Formability, also called "drapability" or "moulding ability", is the ability of a planar textile structure to be directly deformed to fit a three-dimensional surface without the formation of wrinkles, kinks or tears [313]. It is also referred to as shear deformations at the macro-scale when the shearing angle between warp and weft yarns are changed at crossover points [314]. In the design and manufacturing of women soft body armour components, the material should have not only greater properties in terms of dynamic absorptions, strength-to-weight ratio and modulus but also formability of the material are one of the most important characteristics of textile mechanical performance to fit the three-dimensional body shape [315]. This section will discuss the forming apparatus, testing parameters and methods and analysing approaches of different ballistic materials.

Forming bench- A specific and modified pneumatic based dry fabric forming bench which is adapted to a fast, safe and ambient temperature for stamping process was applied to characterize the forming behaviour of the different ballistic materials [316][317]. The forming bench mainly composed of a static blank holder and an open die. The preform was placed and firmly held by these two parts while forming. The four actuators located on the top part of the forming machine provide the pressure at the top edges of the preform to firmly clamped/hold the blank holder, the preform and an open die while forming process. Besides, the non-heating and predefined punch with low stamping process could be used at the bottom to form the samples in a desired shape. The vertically controlled movement of the four pneumatic jacks at the bottom of the device helps not only control and measure punch position and speed but also the forces applied by the punch to the performing material. The force applied and its variations on the preforms by the

punch are normally detected and measured by the load sensor (500 N ± 0.3%) which is attached to the jack. Moreover, the punch displacement mainly depends on punch shape but set to be constant throughout the movement for a better punching process. For our study, we choose to use a semi hemispherical shaped punch not only to ensure a symmetric double curvature deformation but also has approximately similar forming shape with women bust for future comparison. Besides, the punch was used along with appropriate blank holder and open die with specific conditions and parameters to investigate the forming behaviours of the intended ballistic materials. The utilized dry fabric hemispherical forming test device with its different parts is shown in **Figure 2.10.**
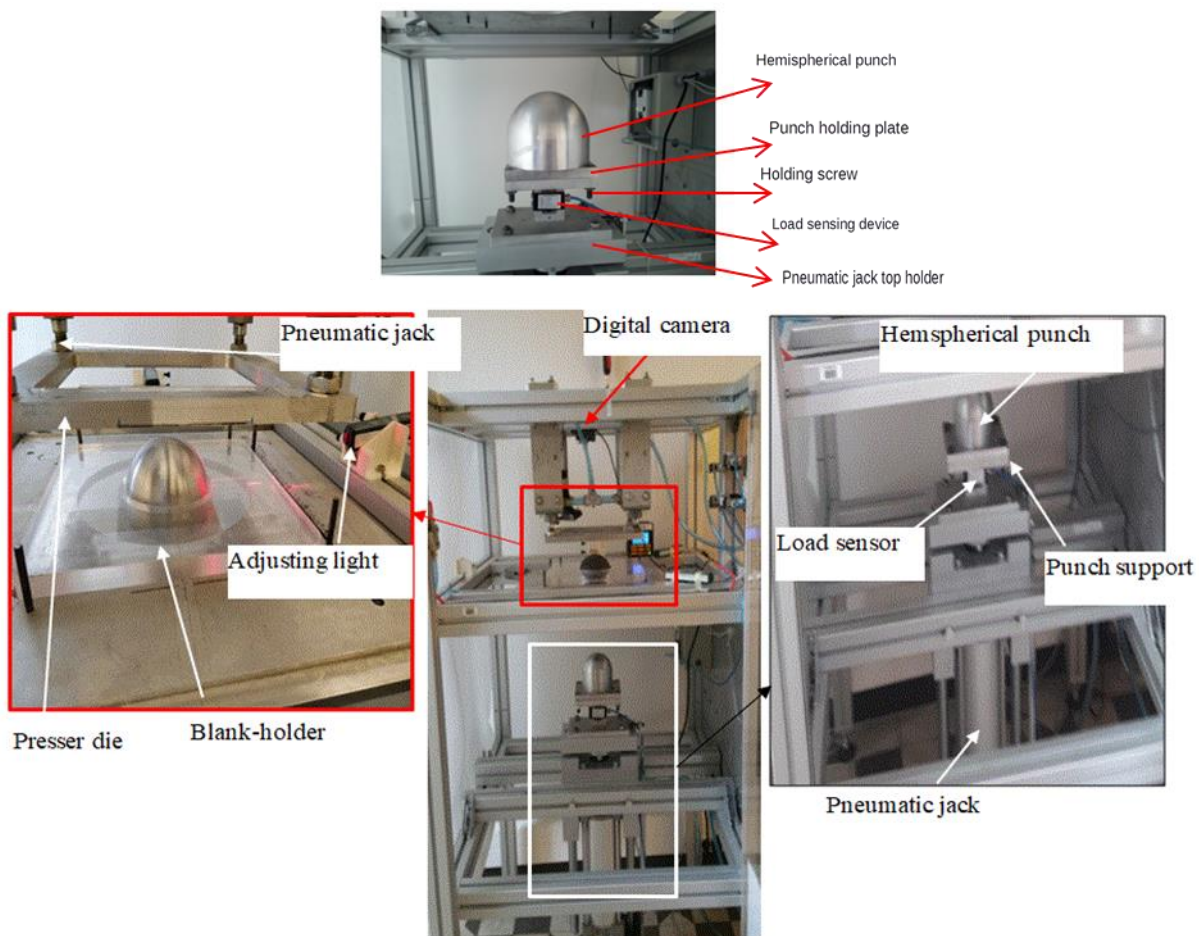
Figure 2.10 Photographic diagrams of the formability testing machine set up with its hemispherical punch [293][294]

Testing parameter - The forming device is mainly designed to experimentally investigate the single-curved shape punch to analyse the formability of dry textile materials at various dependent parameters. Those different important and dependent parameters such as blank holder pressure, stamping velocity, punching force, shapes of punch, punching depth, testing conditions, etc. which affects the formability behaviours of the material should be considered and maintained throughout the forming study to obtain a better and comparable deformability results [318]. The blank holder pressure shows a significant effect on the formability properties due to bringing different frictional force differences between the preforms and the holders.

For example, applying an appropriate blank-holder pressure helps to maintain the preform onto its deformed shape and avoid unnecessary folding, wrinkling defects, slippage, and yarn breakage during the punching process (reference). The forming device also allows regulating the values of the blank holders' pressures found at the side of the machine based on the forming test conditions. Too high or too low blank holder pressure may bring sample folds and yarn breakage respectively. All the preforms were also tested with a constant stamping velocity and hemispherical punch depth of 45 mm/s and 65 mm respectively. Unless specified in the respective experimental part, the complete and different considered parameters while investigating the forming behaviours of the different preforms during this study are listed in **Table 2.6**.

Table 2.6 Different parameters of the hemispherical punch performing

No.	Performing parameter	Value
1.	Punch shape	Hemispherical
2.	Hemispherical Punching depth	65 mm
3.	Hemispherical punch diameter	100/150 mm
4.	Blank-holder pressure	0.4 MPa
5.	Stamping velocity	45 m/s

Testing procedure - It is known that the results of mechanical and other tests on textile materials are affected by the amount of moisture present in the materials. In our study, both before and after forming testing, all textile samples were kept in the standard atmospheric condition (20°C and RH 63%) to avoid the effects of moisture content and regain. Before a test, a preliminary test with different blank holder pressure was applied to observe and decide the suitable pressure which gives the required form to avoid fold or yarn breakage during forming. In this case, different experimental work might use specific blank-holder pressure in the future experimental sections. The particular sizes of hemispherical punch were properly installed to observe the local and global fabric deformations through the path of warp and weft yarns in the structure. **Figure 2.11** shows the formability process at different views with hemispherical deep drawing tool geometry.
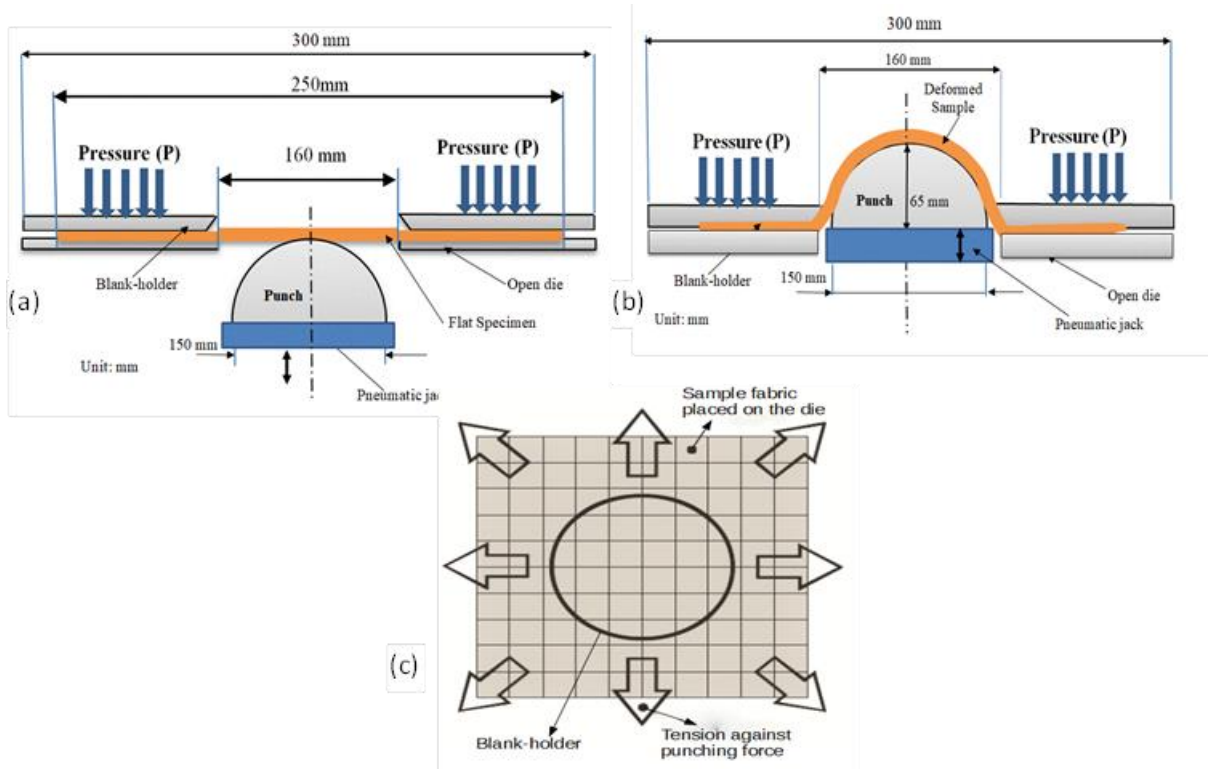
Figure 2.11 Formability process of the sample with its hemispherical deep drawing tool geometry and specimen position (a) and (b) side view before and after forming process respectively, and (c) top view

For better and balanced deformational results, each testing preforms was kept between the blank-holder and transparent open die turn by turn at its exact position with the help of the two adjustable sides inbuilt projection light. A transparent open-die also helps to achieve optical measurements to analyse the different important forming parameters such as material draw-in, the in-plane shear, the inter-layer sliding, etc. The four actuators on the top applied a sufficient and specified pressure at the four peripheral edges areas to firmly clamp the preform between the blank holder and open-die. The preform was then punched by the hemispherical punch at a constant speed from the bottom at the specific displacement or depth (65 mm) which is governed by electric jack. After forming, a deformed sample was slowly and gently removed for further formability properties assessment and analysis.

Forming behaviour analysis- Different forming characteristics of the specimens while forming including sample surface failure, and their deformation recovery corresponding to the different material parameters was observed and discussed. However, while spotting such forming behaviour of the preform associated with local and global information, it is important to capture the whole practice during the forming process. In our study, the local and global moulding behaviour at different positions was studied using a non-contact measurement method by recording a video of the forming process using a digital camera. The camera was installed at the centre top of the device to record and capture the whole fabric forming process. The formability behaviour analysis was made considering material while deformation and after full relaxation. The different forming parameters such as in-plain shear angle and material draw-in with their recovery can be then executed and optically measured by extracting the relevant information

from the recorded video using dedicated software called **ImageJ** with precisions of ±0.1°. In general, the average time spent to perform the image processing observations was shorter than the physical measurements for statistical treatments.

2.3.2 Dynamic (Ballistic) Impact performance testing methods

The ballistic impact test provides a good and direct understanding of how the tested soft body armour panel could absorb and dissipates the ballistic projectile energy. Moreover, the test also helps to investigate the amount of the back-face signature on the back of the material after each tested projectiles. In the current research two campaigns of ballistic tests have been taking place. Both campaigns were carried out in the same testing facilities with the same ballistic testing standards. However, some parameters including the ballistic monitoring set-up might be different among the two campaigns for better analysis. Moreover, the ballistic performances of the tested panels in both campaigns were evaluated based only on non-penetration test methods. This means that the ballistic performance evaluation of the tested panels was carried out only for those shots where not projectile perforation was recorded. In the non-perforation case, some amount of energy is absorbed by the panels and the remaining is transferred to the backing materials and creates the back-face signature. Based on this phenomenon, the depth and volume of the back-face signature greatly help to determine the overall ballistic performances of the particular perform. In this case, the energy absorption by the panel and energy transmitted to the back of the panels were computed based on the volume of the back-face signature, whereas, the depth of the back-face signature assists to determine the trauma level.

2.3.2.1 Ballistic test approach, testing parameters, and procedure

Testing approach and parameters – There are different methods of testing and evaluating the ballistic performance of the material. In our ballistic performance study, the non-penetration test approaches have been used to evaluate the panel's ballistic performances in terms of backface signature at the backing clay and panel's energy absorption capabilities. The ballistic testing parameter, procedure, and apparatus were adapted according to the National Institute of Justice (NIJ) Standard-0101.06 Level IIIA [319]. Such a standard level would give the highest level of ballistic protection for testing the soft body armour panel category [319] (appendixes). All our ballistic samples were undergoing the same testing standard and procedural conditions throughout the study. For example, each tested panel was examined with six shots at different points according to Level IIIA, NIJ standard. The SMG (Sub Sterling Gun) gun systems with standard 9 X 19 mm Full Metal Jacketed Round Nose (FMJ RN) bullets were used to fire at velocities of 426 ± 9 m/s. The sample holding frames were positioned at a distance of 10 meters from a 280mm longer firing gun barrel nozzle position as shown in **Figure 2.12.**

Two types of projectile velocity, initial and impact velocity were obtained through the Doppler radar system (WEIBEL of model SL-52OP with 10,525 GHz) and chronograph which were positioned at the 5 m and 9 m between the firing gun barrel and the tested panel respectively. Model 414 Sabre ballistic laser barriers were also placed at a distance of 5 m from the target sample to detect the missed velocity from the radar. The chronograph was detecting and measuring the impact speed of the projectile through the photoelectric principle. For the second ballistic campaign, two very high-speed cameras each positioned at 45° in front were installed

additionally to capture the ballistic phenomenon during the test. Both cameras of Phantom V1212: 56,000 fps, sensor 384 x 400 pixels and its focal length 280 mm were used both on the right and left axis of shooting at a distance of 3.65 m from the target.
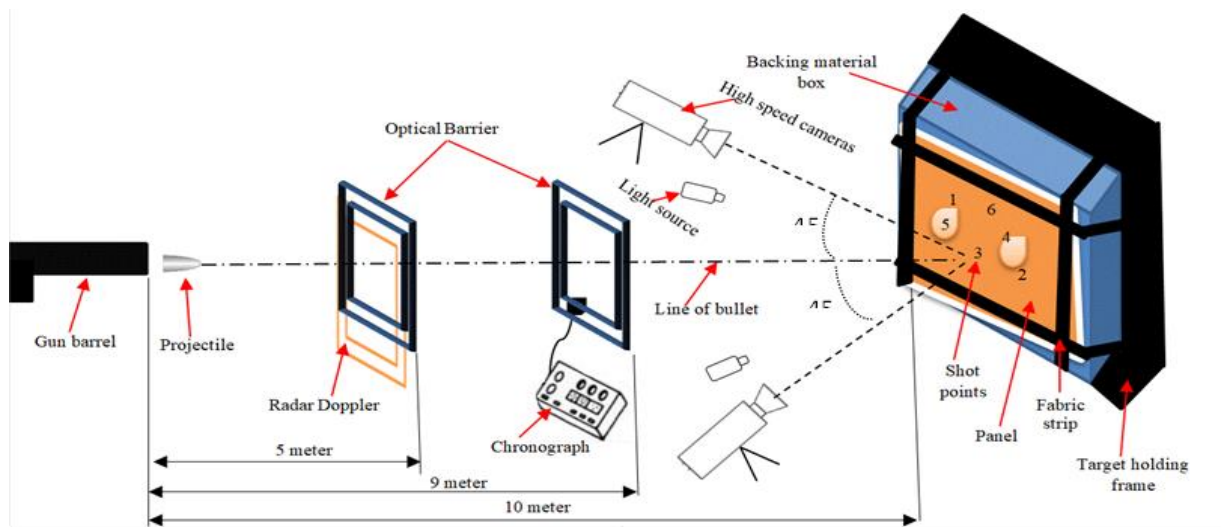
Figure 2.12 Schematic diagrams of ballistic testing set-up

The distance between the cameras was 1.40 m (0.7 m for each axis of fire). Besides, the projector type HMI with the power of 1.2KW was also used. On the other hand, projectors type HMI, power 1.2 kW. Besides, the specific and different test parameters were critically considered during the test as listed in **Table 2.7.**

Table 2.7 Ballistic impact test apparatus, parameters, and its specification

Parameters during ballistic impact:	Description:
Testing level	NIJ 0101.06 standard Level-IIIA
Gun type	Delcour N°2 with blocked 280 long tube Gun barrel
Calibre type	9 X 19 mm
Model and theoretical bullet mass	DM11A1B2, 8.0g/ 124gr
Projectile type and initial velocity	Full Metal Jacket Round Nose (FMJ RN), 440m/s
Shooting distance	10 meters
Shooting angle	0°
Shots per target	06
Radar Doppler position	5 meters from the gun nozzle
Optical Barrier	5 and 9 meters from the gun nozzle
Chronograph position	9 meters from the gun barrel
Experimental conditions	T = 24.1°C and RH = 53%

All testing bullets were provided by CREL (Centre de Recherche et d'Expertise de la Logistique of France), where the ballistic tests were carried out. The ballistic test for all panel target was performed in an indoor ballistic shooting compound with defined and standard atmospheric conditions (T° = 24.1°C RH = 53%). The firing system was also controlled automatically and guided by the laser pointer which helps to precisely shoot on the intended target point. Roma Plastilina # 1 moulding clay was also used as the backing material through the entire test due to

it is cheap, readily available, and attained higher deformation with time compare to other backing material [320].

General testing procedure- The standard clay material (plastilina no.1) was properly filled in the panel supporting wood box. The volume of plastilina inside the box measures 50 cm tall, 50 cm wide and 10 cm deep (Appendix). Besides, the bust-shaped (bust size-90B) moulded plastilina was also prepared to fit the bust-shaped moulded panel.

The hardness of plastilina filled box was regulated and calibrated around the human body temperature (37°C) according to the Standard-0101.06 Level IIIA. This calibration helps to compute the absorbed energy and transmitted by each panel. In general, all the panels in the first and second testing campaign were moulded before testing to resemble the frontal shapes of the women bust (90B size). For this, a manual based adapted bust-shaped punching bench was designed and developed. **Figure 2.13** shows the schematic, photographic adapted punching bench and sample preparation through moulding process for the ballistic test. However, the fabric type (2D and 3D warp interlock), the architecture of the 3D warp interlock fabric and number of layers in each tested panels were different. Each moulded panels made of different fabric layers (2D and 3D warp interlock) were then properly placed and mounted using narrow fabrics on the four sides of plastilina box with uniform clamping pressure as much as possible.
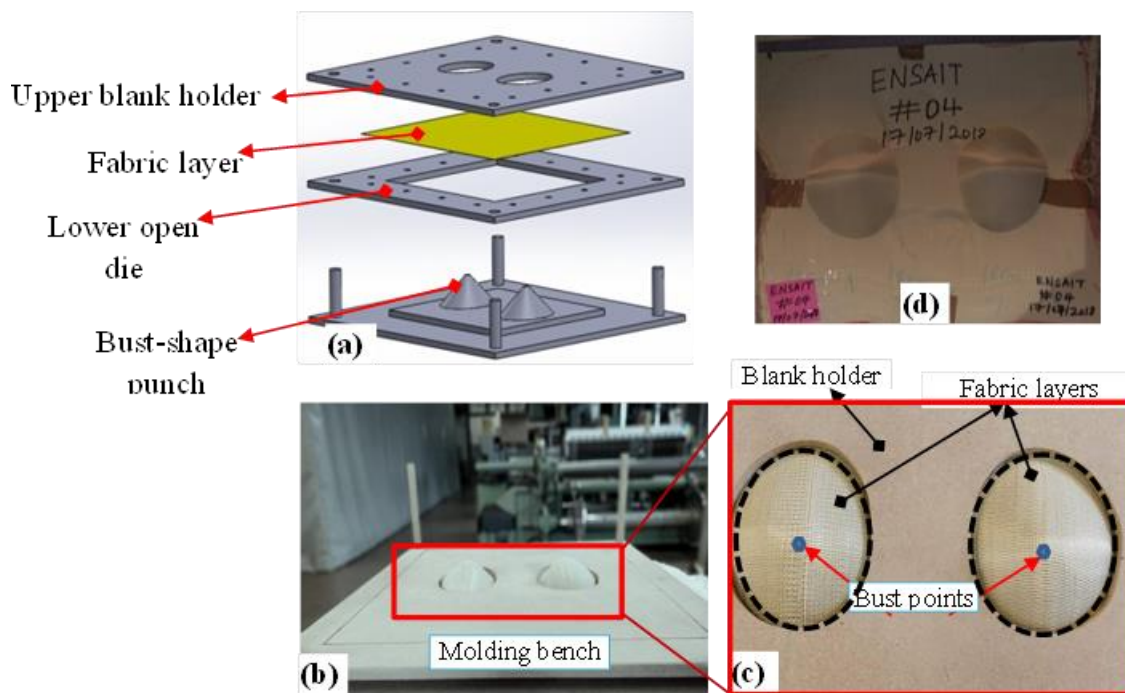
Figure 2.13 Panel preparations, (a) and (b) Schematic diagrams and a photograph of adapted moulding apparatus respectively; (c) moulding of the panel and (d) final panel for the ballistic test.

This is because the higher or lower clamping pressure difference during clamping brings inconsistent result during ballistic impact. Besides, the sample with the backing materials was carefully fitted on its sample holding frames before every shot. The preliminary test was also carried out to check and solve the different problems of testing conditions before the real target test. For all samples of our two campaigns, a total of six bullet shots per panel at a different

location (3 shots on and around the deformed bust area and the other 3 shots on the non-deformed panel surfaces) were performed following NIJ standard. However, the location and numbering of the different shot points were different for each investigation for better analysis. The numbering and location of the different shot for each investigation will be discussed in their respective chapters. This proper and even distributions of the intended shots in a different part of the panels would help us to assess the performances of the various parts while ballistic testing.

2.3.2.2 Methods for measuring and analysing the back-face signature (BFS)

After the ballistic impact test, the entire sample panel went to a non-destructive post-mortem measurement and examination to determine the different phenomenon including their ballistic performance and damage mechanisms. In our study, only the non-penetrated panels were considered for analysis according to the NIJ standard. Digital microscopic picture and microphotographs (brands) were used to analyse different panel's damage mechanism. For the non-penetration method of the ballistic evaluation method, the depth, diameter and volume of BFS also play a great role in determining the ballistic performances of the material. Therefore, the BFS of the backing material after each panel test should be precisely measured and analysed to determine not only whether the intended armour panels will provide adequate protection against the projectile but also indicate how the bullet kinetic energy with the specified velocity is absorbed by the panel target and transmitted to the backing materials. In our study, the BFS on the backing material was measured by involving different process. This sub-section will discuss the different involved methods and processes to measure the back-face signatures from each P-BFS test of the different panel. This will later help to determine their respective energy absorption capabilities and trauma values of the panel. The method mainly involves three processes namely: scanning, modelling and measuring of the BFS.

Scanning of the back-face signature (BFS) **-** The back-face signature measurement is normally created on the back of the ballistic material during the ballistic impact. Their computed measurement helps to assess the energy absorbed and other ballistic performance capabilities of tested fabric panels. According to NIJ-standard, the back-face signature depth values should not be greater than 44 mm; otherwise, it will bring a fatal injury in the vital organ of the wearer. During the impact, the projectile might perforate the panel and pass throughout the thickness or stuck inside the fabric panel. In the non-perforation testing, the projectile will be stopped inside the panel or rebound back by creating some back-face indentation on the backing material. This indentation should be measured after each panel shootings for analysing the ballistic performances of the target. Before scanning process, the target along with backing material box was detached from the fixed ballistic box holder, and then the tested target will be removed carefully from the backing material not to distort the back face signature on the surfaces of the backing material. Besides, various reflecting marks were employed on the backing material surface as reference for easy detection and modelling of the back-face signature. The back-face signature indentation on the backing materials was then carefully scanned using a hand scanner as shown in **Figure 2.14**.
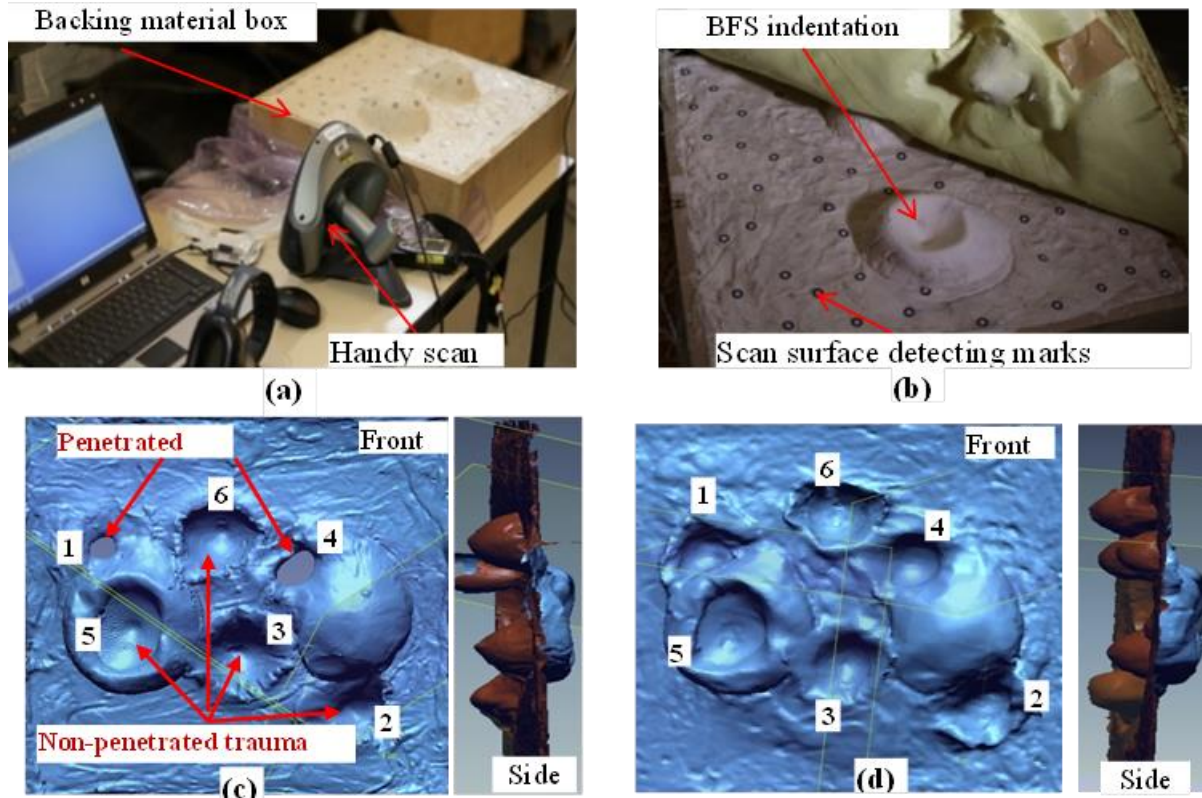
Figure 2.14 Scanning process of the indentations (a) hand scanner (b) indented backing material, (c) and (d) the different scanned backing material in front and side view

***Modelling of the back-face signature (BFS)**:-* Before conceiving the scanned surface of the backing material by the 3D modelling software, the inner and outer back face indentation contour frame-line was conceded following the exact BFS surface using Rapid Form software (**Figure 2.15 (a)**). This will greatly help to map the shell of the BFS surface indentation. Moreover, the outer and inner surface meshes were developed based on the BFS shell, and stitched together to develop the exact BFS volume.

The handy scanner helps not only for its portable, very lightweight design for easy handling but also to scan the surface in a very clear and precise 3D model representations in a short time**.** Besides, scanning methods also helps to make an easy visual comparison of the back-face indentation among the different tested panel target. The scanner captured the whole backing material surface without any physical contact to give precise values for further back face signature measurement and related analysis. The scanner had a very good resolution with accurate high- and low-resolution scan modes. The resolution measures 0.050 mm with an accuracy of 0.040 mm. The volumetric accuracy and laser cross area are 0.020 mm + 0.100 mm/m and 210 mm x 210 mm respectively. Then, the modified scanned BFS surface of the backing materials was then transferred to the 3D modelling software (3D design concept) to precisely model and measure each target tests of back face signature.
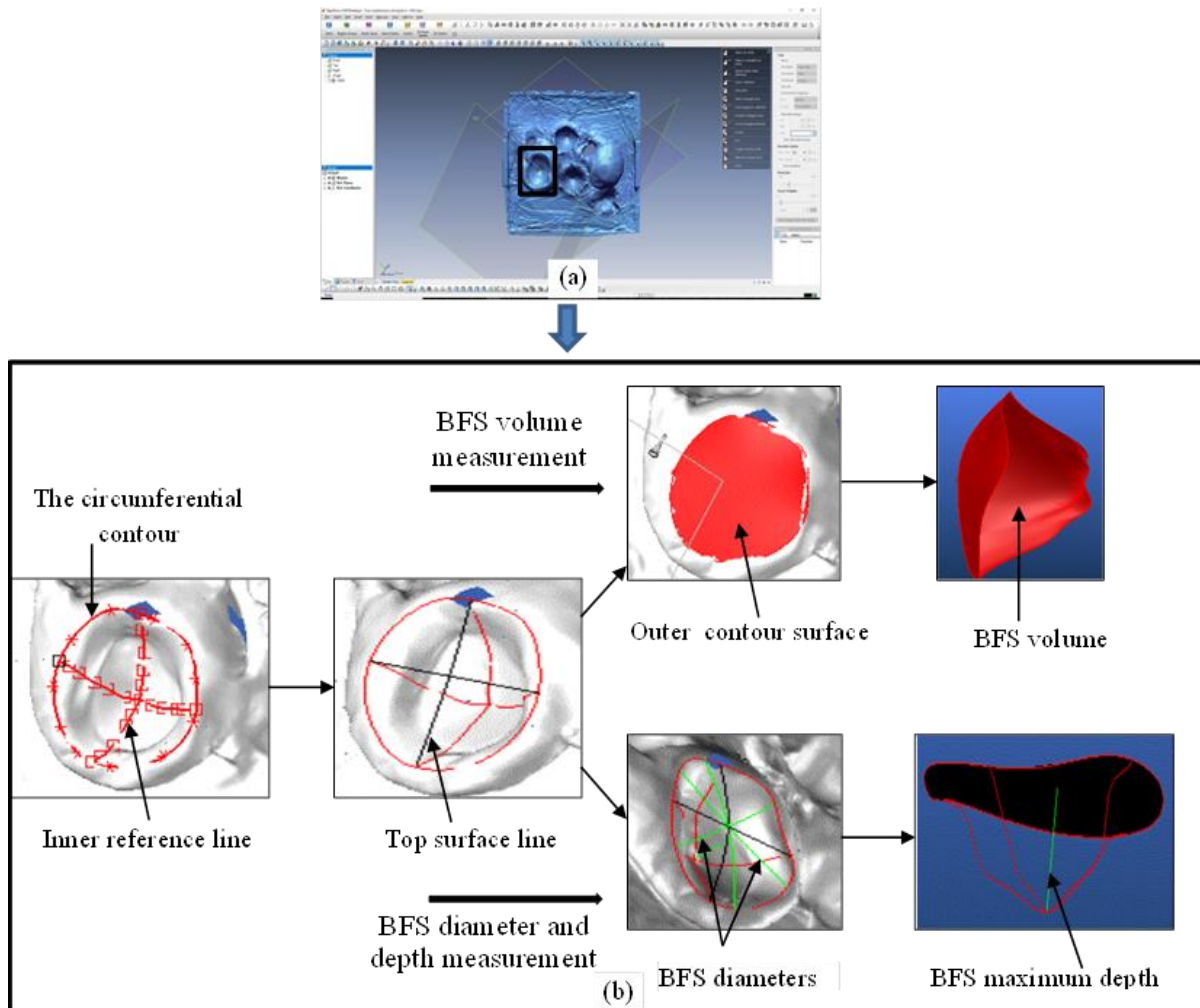
Figure 2.15 Examples of modelling process of one target shots' back face signature using 3D design software (Rapid form (a) and Design concept(b)) for measuring the depth, diameter and volume values

Measuring of the back face signature (BFS):- After modelling, as shown in the **Figure 2.15**, the different back face signature measurements such as depth, diameter and volume which are formed on non-penetrated panels' backing material will be measured and computed as follows.

The depth and diameter measurements of the back face signature (BFS) – The depth and diameter of the BFS were measured precisely on the developed model (3D modelling software) with high precision as shown in **Figure 2.15.** While measuring the depth and diameter of back face signature, the perpendicular surface axis on the depth was placed based on the most upper and lower surface. Using this perpendicular surface axis, it is possible to properly pre-define the different points that will help to measure the depth and various diameter values for each target. The average data values of both the depth and diameter for each panel at every target point were recorded. According to NIJ-standard, the BFS depth should not be greater than 44 mm; otherwise, it will bring a fatal injury in the vital organ of the wearer.

Volume determinations of the back-face signature - The energy absorption capacities of the targets were mainly computed based on the backing material BFS volume. Thus, modelling the exact back face signature volume of each target for every shot is very crucial. The 3D modelling

software helps to define the inner-outer most and upper surfaces shell of the different target shot model and then stitch together the surface to define the specific BFS volume automatically.

2.3.2.3 Calibrations of the consistency of backing material

The backing clay should be calibrated before the actual ballistic testing to determine the exact values of absorbed energy by each target. This calibration further helps not only keeps consistency throughout the test but also helps to compute the energy exerted on a unit volume of BFS (J/mm^3) in the moulding clay material. In the calibration process, a cylindrical shape with semi-spherical tipped steel bar having a mass of 1 Kg and a diameter of 60 mm were dropped freely and properly on the indicated drop point of conditioned backing material from 2.0 m height through the confined hollow tubes based on NIJ standard [319] as shown in **Figure 2.16.** The drop-test validation was carried out on the backing material before every six-shot P-BFS test sequence. Failure to meet the requirements of this drop-test depth results in additional conditioning of backing material and drop test validation. In our validation after each drop test, the BFS depth and volumes were scanned and measured with precision. The arithmetic average values of five drop test BFS depth and volumes values of the conditioned backing material were recorded 22 mm and 23 mm^3 respectively.
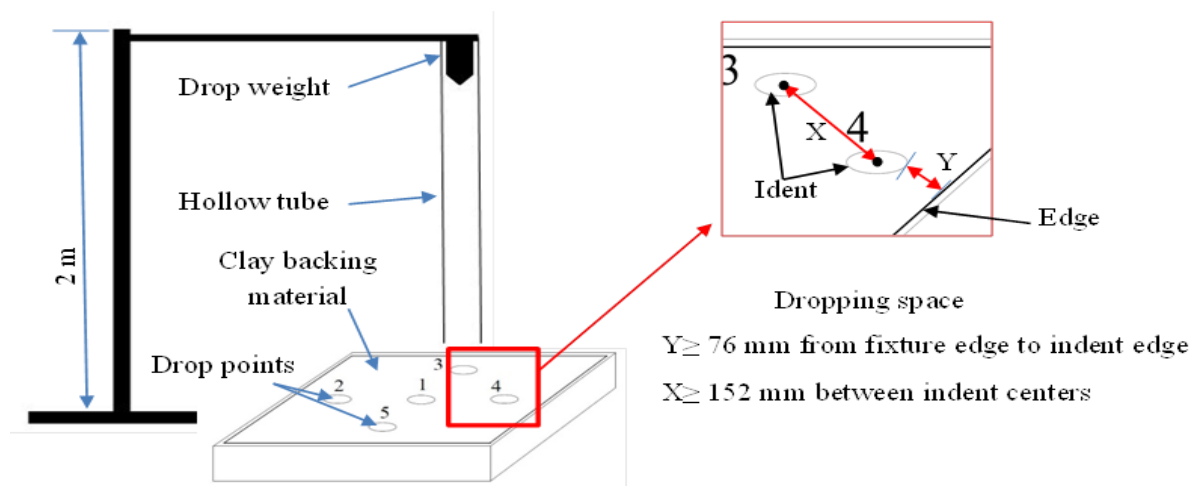
Figure 2.16 Calibrations of backing clay material

These arithmetic numbers were found similar in the range of the values recommended by NIJ 0101.06 standards at 2 m height (19 mm ± 2 mm or 16 ≤ x ≤22, x is allowed BFS depth).

Base on the average volumes of the BFS obtained from the scanning during validation with the mentioned height (2 m), it is now possible to compute the unit BFS energy ((E_{volume}) (J/mm^3) transmitted to the backing material as shown in **Table 2.8**.

This unit trauma potential energy of the dropped weight ($EP_{measured}$) was calculated using the following classical formula:

$$EP_{measured} = m \cdot g \cdot h \quad [J] \tag{2.1}$$

Where,

    m - is the mass of the semi-spherical tipped iron bar [kg],

    g - is the gravitational acceleration [m/s^2] and h - the dropping height [m].

Table 2.8 Average unit BFS energy determinations from the drop test

Height (m)	Drop test	BFS depth(mm)	BFS volume(mm^3)	EP$_{measured}$ (J)	E$_{unit\ volume}$ (J/mm^3)	E$_{ave\ unit\ volume}$ (J/mm^3)
	Test 1	24.1	24.665	19.62	7.95 x 10^{-4}	
	Test 2	23.5	23.599	19.62	8.31 x 10^{-4}	
2	Test 3	20.15	22.756	19.62	8.62 x 10^{-4}	8.3 x 10^{-4}
	Test 4	21.22	22.158	19.62	8.85 x 10^{-4}	
	Test 5	22.11	25.164	19.62	7.8 x 10^{-4}	
	Average	22.24	23.665	19.62	8.3 x 10^{-4}	

The unit volume energy of each drop test (E$_{unit\ volume}$) was calculated using the following formula:

$$E_{unit\ volume} = \frac{EP_{measured}}{V_{trauma\ calculate}}\ [J/mm^3] \tag{2.2}$$

Where,

EP$_{measured}$ - is the calculated potential energy by the drop mass for each test [J],

V$_{trauma\ calculate}$ - the BFS volume formed by weight dropped on backing material [mm^3].

Determination of the average BFS volume (V$_{average\ trauma\ calculate}$ (23.665mm^3)), on the backing material, helps to compute the average unit potential energy (E$_{ave\ volume}$). According to the test result and shown in **Table 2.8**, the average unit volume energy (E$_{ave\ unit\ volume}$) was found 8.3 × 10^{-4} J/mm^3. According to the computed result, it is now possible to calculate and correlate the values with the energy absorbed by the target panel and transmitted by the panel target while ballistic impact testing. The energy absorbed by the target panel during the ballistic test (E$_{ballistic}$) mainly depends on the BFS volume for every target tested and calculated as follows:

$$E_{ballistic} = V_{trauma\ ballistic} \cdot E_{ave\ unit\ volume} \tag{2.3}$$

Where,

V$_{ballistic}$ -is the trauma volume created while ballistic test

E$_{ave\ volume}$ - the potential energy developed by the trauma volume during dropping test.

Moreover, the kinetic energy of the ballistic bullet just before it hits the first layer of the panel target (Ek$_{ballistic}$) is computed as follows:

$$Ek_{ballistic} = \frac{m \cdot v^2}{2}\ [J] \tag{2.4}$$

Where,

m -is the mass of the bullet [kg],

v - is the speed of the bullet [m/s].

During the ballistic test, the target tried to prevent the bullet from penetration through different mechanisms. However, some portion of kinetic energy will be absorbed by target and the rest passes beyond the target to generate an indentation on the backing materials. Computing such absorbed and transmitted energy values would help to compare the performance of different fabric panel target. This makes possible to compute the energy absorbed by the target panels

($Ea_{ballistic}$) considering both the calculated kinetic energy ($Ek_{ballistic}$) and the amount of energy transmitted ($Et_{ballistic}$) to the backing material

$$Ea_{ballistic} = Ek_{ballistic} - Et_{ballistic}$$ (2.5)

Where,

$Ek_{ballistic}$ - is the energy from the kinetic energy of the bullet,

$Et_{ballistic}$ -is the energy transmitted beyond the panel target.

2.3.2.4 Post-impact panel failure mechanisms and projectile deformations analysis

The post-impact failure mechanism is another method of assessing the ballistic performance behaviours of the material. After the ballistic testing, the tested sample surface was examined for its various surface failures using an optical microscope, digital and ultra-high-speed cameras. For example, back face, front face and inter-laminar failure views were interpreted by different failure region including damaged, fibrillated, bowing and broken yarns of the samples. Pyramid formation has been also observed on the back face after most of the shooting tests as predicted in literature reviews [251]. This will be more distinctive on the targets that absorbed higher energy than in the slide-through (the sliding of the projectile between the yarns of the fabrics) phenomenon. Delamination effect between the different layers within the panels while the ballistic impact was also observed. Besides, the post-mortem projectile deformations percentage after impacting the panels at different shot points was also discussed. The shape, length and diameters of the projectile before and after impact were measured using a Vernier scale. The number of layers/panels responsible for arresting the projectiles was also investigated to interpret the ballistic behaviour mechanisms of the different ballistic materials. Using the high-speed camera images, the different surface strains of the tested panels were also discussed.

2.3.3 Quasi-static mechanical characterization

2.3.3.1 Fabric properties measurement

The crimp (shrinkage) was computed based on the relative difference between the yarn inside the fabric and of extended yarn lengths of yarn extracted from the fabrics according to standard NF ISO 7211-3 [309]. The average actual fabric thickness and weight of the different 3D warp interlock fabrics were precisely measured according to standard NF EN ISO 5084 [310] and NF EN 12127 [311] respectively. The top and cross-sectional views of the produced 3D warp interlock fabrics were examined using a portable optical microscope (DNT-Professional LCD Digital Microscope Portable camera equipped with USB/TFT 5 MPix zoom 20 to 500 x dents DigiMicro Lab5.0).

2.3.3.2 Yarn and fabric uniaxial tensile test

When the textile material is intended to apply in the technical application where better mechanical behaviour is in great demand i.e. ballistic impact, investigation of its mechanical properties at the yarn and fabric level is very important. This section will discuss the different testing parameters and protocols used for characterising the mechanical behaviours for different ballistic materials will be outlined.

Yarn uniaxial tensile test - Testing and analysing of the mechanical behaviours of ballistic fabric at the yarn level would greatly help to understand the different yarn mechanics during

applications. The yarn uniaxial tensile tests were conducted on an INSTRON 8516 universal testing machine with a 5 KN load cell at a velocity of 50 mm/min. All the yarn tests were performed at ten replicas for each specimen both in the warp and weft directions to guarantee the results repeatability. Each yarn specimen was prepared with 250 mm total length and firmly fixed in both ends at 200 mm distance using the two adapted steel clamps to avoid any slippage while testing. The uniaxial tensile tests at the yarn level also help to attain the different parameters including Load-time, Load-strain relations, Elastic modulus (E), maximum load (σmax) and maximum strain (εmax) in the yarn longitudinal direction both machine (warp) and cross (weft) directions. For such experimental investigations, 10 yarns from each 3D warp interlock fabrics in both warp (stuffer and binder) and weft (at different weft layers) directions were drawn carefully without damaging the fibres/filaments. **Figure 2.17** shows the uniaxial yarn (a) and fabric (b) tensile machine experimental set-up with the clamped specimen at the initial state.

Fabric uniaxial tensile test - The tensile property characterizations of the different ballistic fabric specimen were performed following standard EN ISO 13 934-1 using an INSTRON 5900 tensile testing machine with a 250 KN load cell [312]. The two jaws of the testing machine were initially 200 mm apart and having a speed of 100 mm/min at room temperature. All the tensile specimens were tested in the machine (warp, MD) and cross (weft, CD) orientations until fracture. During testing, the force and the deformation values were measured and recorded for all samples. Moreover, the tensile machine was checked and verified for each test to avoid sliding between the sample and the grip to attain the good values.

Testing protocols- A rectangular 300 mm × 50 mm specimen adhesively bonded with resin on both ends with an extension of 50 mm to avoid slippage between the specimens and the clamp was prepared. Before every test, the two jaws (the top clamp is movable the lower one is fixed) of the uniaxial testing machine were set with 200 mm apart.
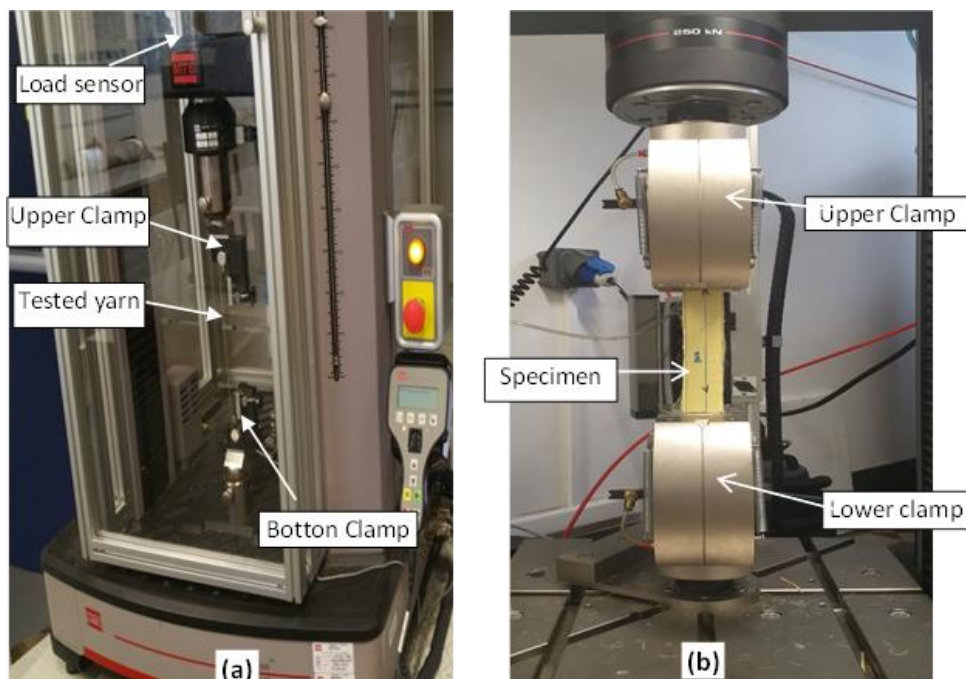
Figure 2.17 Uniaxial tensile testing machine set-up (a) yarn tensile testing device set-up, and (b) Uniaxial fabric tensile testing

The specimen is then firmly mounted between the upper and lower clamps with the bonded size to escape errors in load-displacement reading during testing due to slippage between the specimens and the clamp. For every sample type, three specimens were tested at 100 mm/min both in the weft and warp directions to ensure the repeatability of the investigations. During each testing, the force and its deformation values with time durations were automatically recorded for all tested sample specimens. Moreover, for each test, the tensile machine was checked to avoid sliding between the tested specimen and the clamp to achieve accurate results. The average tensile properties of the different sample during the test in fill and warp directions were then analysed using the extracted data.

2.3.3.3 Fabric flexural rigidity characterizations

Fabric flexural rigidity test - The flexural rigidity of the selected different dry fabrics for ballistic applications was characterized using fabric stiffness testing apparatus following Standard Test Methods for Nonwovens Bending Length (WSP 90.5(05)) under the principle of the Cantilever (fabric stiffness testing apparatus) bending of specimens under its mass. The apparatus was designed and set up with bending curvature based on the fixed angle (41.5°) method (ISO 4604, April 2004) which can adapt the proper specimen. The test carried by manual specimen specific feed using slide scale having 250 gm mass and 350 mm length on low friction platform at a constant rate until the specimen bend by its mass and the leading specimen edge touches the indicator. For all our study, five sample specimens in both directions (weft and warp) were tested for each fabrics type and, its bending length was computed based on the average of the specimens. Before testing, all the specimens were weighed using a digital balance with approximately ±0.001gm precision based on TS 25 and kept at standard atmosphere conditions (RH 65%±2% and temperature - 20° ± 2°) to bring the samples in moisture equilibrium as directed by ERT 60.2-99 or ISO 554. A standard sample of 300×50 mm^2 rectangular stripes of sample specimens both for warp and weft directions were used. **Figure 2.18** shows pictorial and schematic illustrations of fabric stiffness testing apparatus while testing the flexural rigidity properties of preforms.
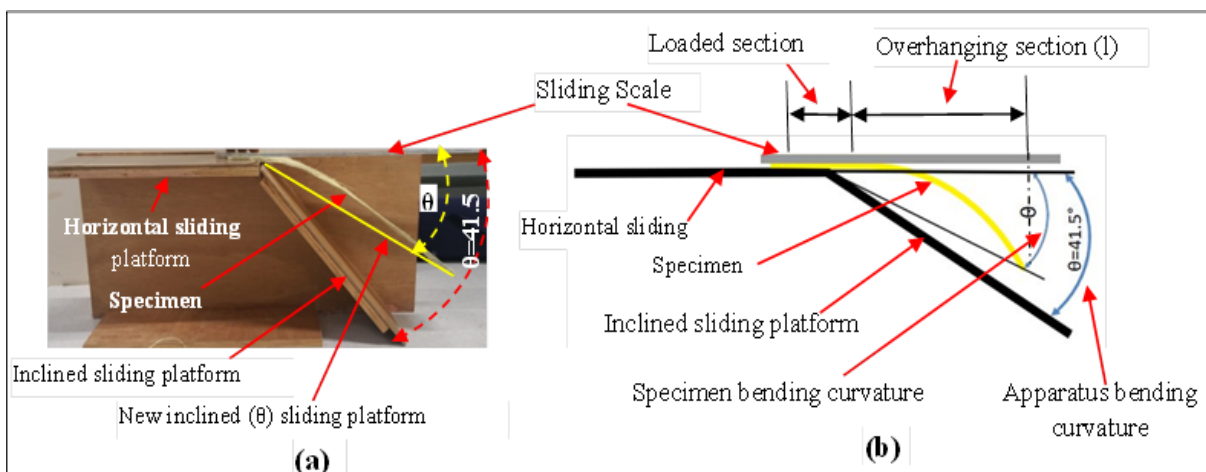
Figure 2.18 Pictorial (a) and schematic (b) flexural rigidity test set-up

While testing, the specimen was properly positioned on the horizontal platform on which one edge is fixed and the other is free to hang on the platform. The sample specimen was allowed to slide on the horizontal sliding platform by pushing gently at regular rate using a regular sliding scale. Depending on the rigidity of the specimen, the experimental investigation could be performed in two ways. First, it is possible to measure both the overhanging specimens (l) and the specimen bending curvature (θ) at any position, if the specimen is enough rigid for unable to touch the edge until the end of bending process. In this case, the flexural rigidity of the fabrics is calculated using **Equation 2.1**.

$$G = \frac{1}{\tan\theta / Cos\frac{\theta}{2}} \cdot \frac{\rho \cdot l^3}{8} \qquad\qquad 2.1$$

Where,

G -is fabric flexural bending rigidity,

ρ –is fabric own weight per unit area (mass per unit area x gravitational acceleration),

l –is the overhanging length and θ - bending curvatures.

Secondly, unlike the 3D warp interlock fabrics and other more rigid fabrics, the overhanging ends of the sample will touch the inclined plane before the other sample end reaches the tip of the horizontal plane. In this case, the testing can be performed until the sample specimen overhangs by its weight and the forefront specimen edges touch the inclined sliding platform (41.5°). Therefore, the fabric flexural bending rigidity could be calculated as **Equation 2.2.**

$$G = \frac{1}{\tan\theta / Cos\frac{\theta}{2}} \cdot \frac{\rho l^3}{8} \text{ , for } \theta = 41.5°, \frac{1}{\tan\theta / \cos\frac{\theta}{2}} = 1$$

$G = 1 \cdot \frac{\rho l^3}{8}$, since l/2 is the bending length and ρ is mass per unit area multiply by the acceleration due to gravity, the fabric flexural bending rigidity could be simplified as follows:

$$G = W \cdot g \cdot c^3 \qquad\qquad 2.2$$

Where,

$G_{specimen}$ is the flexural bending rigidity of the specimen (N m),

W is the specimen unit areal density (g/m^2),

C is the average bending length of the tested specimen (mm),

g is the gravitational acceleration value (m/s^2).

Besides**,** in general, the average bending length of the different samples can be calculated using **Equation 2.3**.

$$C = l/2 \qquad\qquad 2.3$$

Where,

C is the sample bending length

l is the specimen overhanging length while bending test.

For both cases, the flexural rigidity of the different sample specimen was computed based on overhanging length (l), the sample specimen areal weight and its bending curvature (θ).

2.4   Conclusions

Nowadays, 3D warp interlock fabric became a promising structure to develop women body armour not only due to its good forming behaviour but also its noticeable ballistic and mechanical properties. However, it's ballistic and forming performance for different ballistic threats level should be investigated and characterized. This chapter designed, manufactured and presented the different 3D woven fabric solutions for the developments of seamless women body armour development. Besides, the different methods and methodologies employed to measure, investigate, fully understand and improve the ballistic, mechanical and forming capabilities of 3D woven fabric solutions were also outlined. In general, such procedures help to achieve the different aims and objective of the research project. The following are some of the specific conclusions that have been drawn.

➢ Different 3D warp interlock fabrics considering different parameters. Later, the developed ballistic materials should be analysed and characterized by their specific performances.

➢ Different 3D warp interlock fabrics architecture were engineered and manufactured considering different parameter in different production campaign to characterize at quasi-static and dynamic testing. Such characterization would help to improve its performance for the developments of women body armour. In each 3D warp interlock fabric production campaign, comprehensive descriptions and production process of each structure were outlined. Different specific software to design and engineered the intended 3D warp interlock fabrics were discussed. Moreover, Dornier automatic dobby and ARM semi-automatic dobby weaving machines were utilized in a different time to produce the various 3D warp interlock fabrics in different production campaign. Besides, for better comparison, the specification of the corresponding 2D plain-woven fabric which is commonly used for the developments of women body armour was also described.

➢ The ballistic performance, formability and mechanical properties of the different 3D warp interlock and 2D plain fabric were characterized using different testing equipment.

  • The different parameters used while testing the ballistic performances of the different fabric panels' against NIJ (National Institute of Justice) standard–0101.06 Level-IIIA were outlines. Precise measurements of BFS help to compute the energy absorbing capability and trauma values of the panel in the non-perforation analysis methods. Therefore, different equipment, methods and procedures for scanning, modelling and measuring of the Back-Face Signature were explained. For example, handy scanning device and 3D Design concept software were utilized as the non-contact measuring methods to scan the indentation at the backing clay and, to model and measure the depth, diameter and volumes of the BFS respectively. Moreover, post-impact panel failure mechanisms through surface microphotographs, number of panels for stopping the projectile, projectile deformations analysis and panel surface strain from high-speed videos were used to investigate and understand the material ballistic performance.

  • The different forming behaviours of the developed ballistic fabrics were also investigated. An adapted hydraulic-driven stamping bench along with hemispherical punch was utilized to investigate and understand the different formability behaviours of the intended ballistic materials. In this analysis, various formability behaviours of the

materials such as in-plain shear angle and its recovery, material draw-in and its recovery, deformational depth recovery and required stamping forces were analysed using Images analysis. The forming process of the different materials was recorded using camera and surface forming behaviour including drawing-in, shear angle with their recovery were computed and analysed using ImageJ software.

- Moreover, the different quasi-static mechanical testing (such as tensile, crimp, bending) apparatus including tensile, bending, crimp etc., their parameters and testing protocols were discussed. This helps to characterize the mechanical behaviours not only the produced 3D warp interlock fabrics but also to compare with the 2D plain fabric with a similar parameter for the developments of women body armour.

3 Modelling and pattern development system for seamless women frontal body armour

3.1 Introduction

Automatic realistic 3D human body generation is an important research topic in various applications including apparel design. It is even a more crucial process for designing a garment that needs better fitness for functional purposes. This chapter will discuss the modelling, designing and automatically pattern generation systems through an innovative 3D design process for the developments of seamless women soft body armour approaches for better fitness, comfort and ballistic protection. The first sub-topics, unlike other general human body modelling and bra design methods, presents a new virtual reality-based on 3D design approach for developing different volumes of 3D adaptive bust on 3D virtual women body mannequin. Due to very complex 3D women breast geometry, it mainly helps to generate an accurate bust of different sizes on the same women's body size (90B) using specific parameters from its adaptive bust initial value. Considering only bust girth and under bust girths makes the commercial bra sizing system ultimately inappropriate for bra design due to the different volumes of the bust. Therefore, the proposed new designing approach will help to produce a more fit-ensured, comfortable and customized 2D bra patterns. It can also ultimately apply for the developments of customized women soft body armour by incorporating the exact volume of bust derived from the adaptive bust model.

The next sub-topic introduced an innovative 2D-3D-2D pattern designing system based on a direct projection of the exact measurement of 3D body contour directly to the 2D projection grids for developing seamless women body armour front panel. The system uses the 3D virtual adaptive bust mannequin with average bra size (90B) that has been developed in the previous section. Complexity along with better fitness, comfort and better ballistic performance of the women body armour mainly on the bust region was an initiative factor for this study. This new body armour frontal panel pattern development system could greatly help to solve such problems by generating an appropriate 2D block pattern for better fitness and comfort.

The last section of this chapter introduced a design approach for generating multi-layer patterns directly on 3D virtual woman mannequin. In the multi-layer woman soft body armour pattern generation, it is also obvious that the outer fabric layer will have a larger surface area than the lower consecutive fabric layers due to its high surface coverage. This phenomenon needs to be critically considered while pattern generation process to keep the soft body armour panel covering properly the required woman torso surfaces. Moreover, while generating the multi-layer panel pattern, some critical parameters including the thickness of each layer have to be also considered to achieve a good result. However, the pressure applied between layers during stacking was neglected. For sake of validation, only five (05) different layer fabrics were used to observe the evolution of the block pattern rather than considering the level of ballistic protection. However, it is also possible to generate the pattern for a higher or lower number of a layer based on the required level of ballistic protection performance (different NIJ standard levels) and layer thickness using the proposed design method. The approach will be more

important when the soft body armour garment is developed following the contour shape of the body for good ballistic protection performances and better fitness and comfort. Commercial software from Lectra called 3D design concept was used to numerically simulate 3D mesh and pattern generations of multi-layer women soft body armour panels. Therefore, generating soft body armour pattern design directly on the specific 3D virtual adaptive mannequin could give a very good result for both ballistic protection and fitness.

3.2 Adaptive bust modelling and bra pattern generations

Brassier (bra) is one of the intimate women garments with the most complex pieces of the part to support breast soft tissues. Realizing good bra shape is then a must not only support and fit the 3D complex bust contour but also satisfy the consumer's need [281]. The proper and accurate designing method along with proper bra size is mandatory to cater to the required shape and better service. The proper bra size also plays an important role not only in designing bra but also to include different functional features for soft body armour. However, the current commercial 2D bra design method is a lengthy process that also lacks the design creativity, precise pattern-making process and full understanding of materials [280]. Besides, the design system mostly causes uncomfortable and less fitted garments due to lack of standardization within the brands, countries, manufacturers and more a matter of guesswork, trial and error than precise measurements. Generally, in the design and process development of women seamless frontal panels, knowing the exact and good volumes of the bust are the first and very important step for better fit and comfort of the wear. However, the shape, symmetry, size of women's bust can also vary significantly with no correlations to the other body measurements including the heights and girths [321], and even depends on the geographical and ethnic origins [322]. Eventually, the design of bras cannot be independent of the parameters of the woman's body and breasts. Therefore, a new way of designing the 3D women body model based on the 3D-to-2D CAD method, which considers the body contour, seems to be a good solution. This process will certainly make highly representative models to reflect the body features of a specified group of people. Such representative models could then assist in designing customized fitted and comfortable bra that can be accessible to find a technical solution for the different morphology of the body [275].

3.2.1 Bra designing methods

3.2.1.1 Traditional (2D) bra design method

The traditional bra design method is mostly not only a time-consuming process but also demands a combination of design creativity, precise pattern-making skills and detailed material property knowledge [281]. Mostly, the process starts with designing of flat panels of fabric then assembled into a three-dimensional garment to fit the mannequin or a real-life model. At this point, the performance of bra supports concerning fitness and comfort will be checked and adjusted accordingly. Meanwhile, for the last many decades the bra size has been described in terms of the underbust girth along with the difference between the bust girth and under bust girth [323] as shown in **Figure 3.1**.
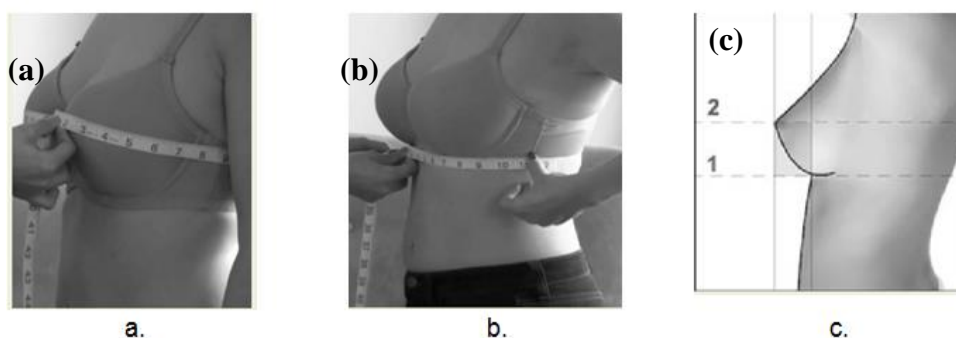
Figure 3.1 Measurements for traditional bra design a) Bust size, b) Band size and c) Cup size

According to the imperial system, the indicative cup size was defined by subtracting the band size from the bust measurement as shown in **Figure 3.1(a), (b) and (c)**. Each difference of inch is said to represent a cup size step [322]. Due to this, the majority of women face to wear the wrong bra size with too small in the cup but too loose around the body or vice-versa. This causes not only poor breast support but also skin irritations and bad posture which sometimes causes the underwire might pinch the delicate breast tissue. Moreover, the bra designing technique through this method is a bit lengthy, which leads to being even inefficient and expensive. However, only a few research studies have worked on developing better bra sizing standard systems considering the breast shapes to fit different groups of the population based on their demographic and anthropometric data [297][298]. This shows that regardless of the design of the bra, using an appropriate sizing system is very critical for the effective support of the breast [299]. This hypothesis has been supported using a comparison between women's bra size as measured by the traditional bra fitting method with their recommended bra size based on professional bra fitting criteria [282]. One of the studies used relatively different breast measurements and propose a new bra sizing system that gives better fitness for Chinese women [283]. The 3D measurement of the human body structure was also used to design the ergonomic brassiere wire that should fit the curve of under breast and thorax [300]. Considering the erroneousness of the traditional breast sizing system on women's who have the same underbust and bust measurement but different body shape, a new system of bra measurement in which band size is still determined by the industry standard of "underbust chest circumference plus 5 inches, but cup size is determined by direct measurement of the bust in proportion to underbust circumference were devised [301]. In general, the traditional bra design process comprises three main steps namely; concept development, pattern making, and grading. **Figure 3.2** shows an example of traditional bra design with the prototyping loops of fit, amending and grades of three sizes. The process involves different parallel and series iterations regarding fit and pattern correction to achieve a well-fitting bra.

According to design and material type, first sample pattern will be designed and then first bra sample will be developed for a fitting test in the life model or standard mannequin. Later, the adjustment might be done on the sample or pass to the next step without alteration. If the pattern maker is satisfied with the fit of the sample garment, the pattern pieces will be graded based on the required size range. If not, it will go back for pattern and sample adjustment for alteration.

Moreover, the graded patterns are also fitted to models for necessary adjustment. If it works on the required criteria, the different sizes of the graded pattern will be sent for approval. Finally, the mass production process will start after all the graded patterns have been approved.
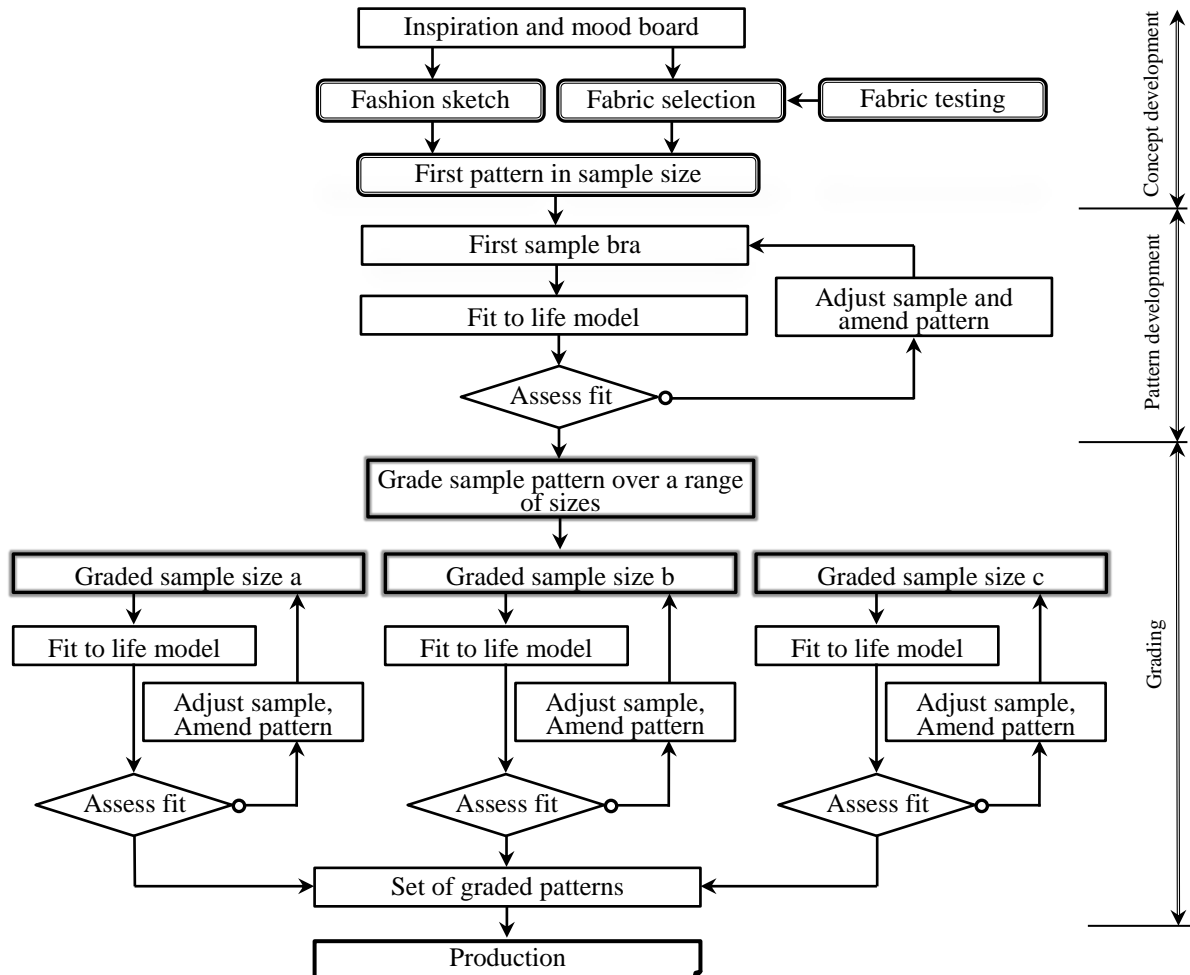
Figure 3.2 Traditional bra design process [18]

3.2.1.2 Bra pattern development through the 3D design process

Today, 3D body scanning and 3D computer-aided design (CAD) methods have been used not only in the apparel industry but also shows a significant role in the lingerie industry [324]. In our design process, both the 3D body scanning and 3D computer-aided design (CAD) methods have been used. The 3D scanning helps to create human models to obtain a sufficient number of body measurements and develop fitted 3D bust shapes. Whereas, 3D CAD methods are responsible for designing and pattern development.

3.2.1.2.1 The 3D design process framework for bra pattern development

The new 3D design process framework aids to generate a highly representative 3D woman model with an adaptive bust. The adaptive bust, which evolves different bust volumes with

specific parametric values, along with the representative 3D model ultimately helps to design an accurate, comfortable and fitted 2D bra pattern for the specific bust volume. This application even extends to develop a pattern for woman frontal soft body armour panel not only for the proper fitness and comfort but also for better ballistic performances. During the process, both the corset and CAD concept was applied to develop the 3D woman adaptive model. The developmental framework of the 3D women adaptive virtual model using the new 3D design process is depicted in **Figure 3.3.**

The design process carried out in different steps.

1st - Both the TC^2 3D body scans and ScanWorX software was used to extract the raw data from the real female body to develop only the front upper torso of the 3D body.

2nd - Rapidform software was utilized to optimize the 3D mesh of the upper torso through closed connection curves during plane and mesh intersection. The software was also used to amend the different defects of the 3D meshed object by filling the holes. This software can execute 3D to 2D pattern unwrapping for clothing product-development purposes using the flattening mechanism [266].

3rd - The 3D Design Concept software from Lectra was used to develop a 3D women adaptive bust model from the 3D surface of the female body shape which is imported from Rapid form software. The bust size of the conceived virtual model was then validated through the standard bra underwire, by aligning the standard scanned underwire bras on the limit contours of the lower bust cup.

4th - Both base and contour of the breast were then defined by cutting marks based on the vertical reference bust plane. During the cutting process, various feature points and lines from the innermost centre of cutting parts were created to define the curve and surface of the adaptive bust volume (in this work 90B) in the form of a wireframe on the bust cup.

5th - The 3D bra pattern can be now developed directly on the model by using the curve and surface of the adaptive bust volume (90B). The flattening method will be then used to create the corresponding 2D pattern from the 3D model.

6th - For comparison, the newly flattened 2D pattern was compared with bra pattern developed with traditional methods with the same size on the Lectra Modaris pattern software.

While matching, some differences due to measurement assumptions during the traditional pattern-making process were observed (it seems to be exaggerated while considering the half of the width of the front is equal to the bust girth divided by 4). Besides, the traditional making process only uses Bust Girth and under-bust, and even other useful measurements were derived from these two measurements while developing bra patterns. This assumption will not be always true and cannot give an accurate value for women's body measurements. For instance, the measurement from side seam to the bust point across the chest would not be 1/4th of the bust circumference due to the existence of 3D bust volumes at the front than the backside. However, the 2D pattern from the 3D model would be more accurate due to the involvement of different measurements taken directly following the body contour.

The next few sections will discuss the different design process steps to develop the customizing 3D bra pattern.

Chapter 3. Modelling and pattern generation system for seamless women frontal body armour
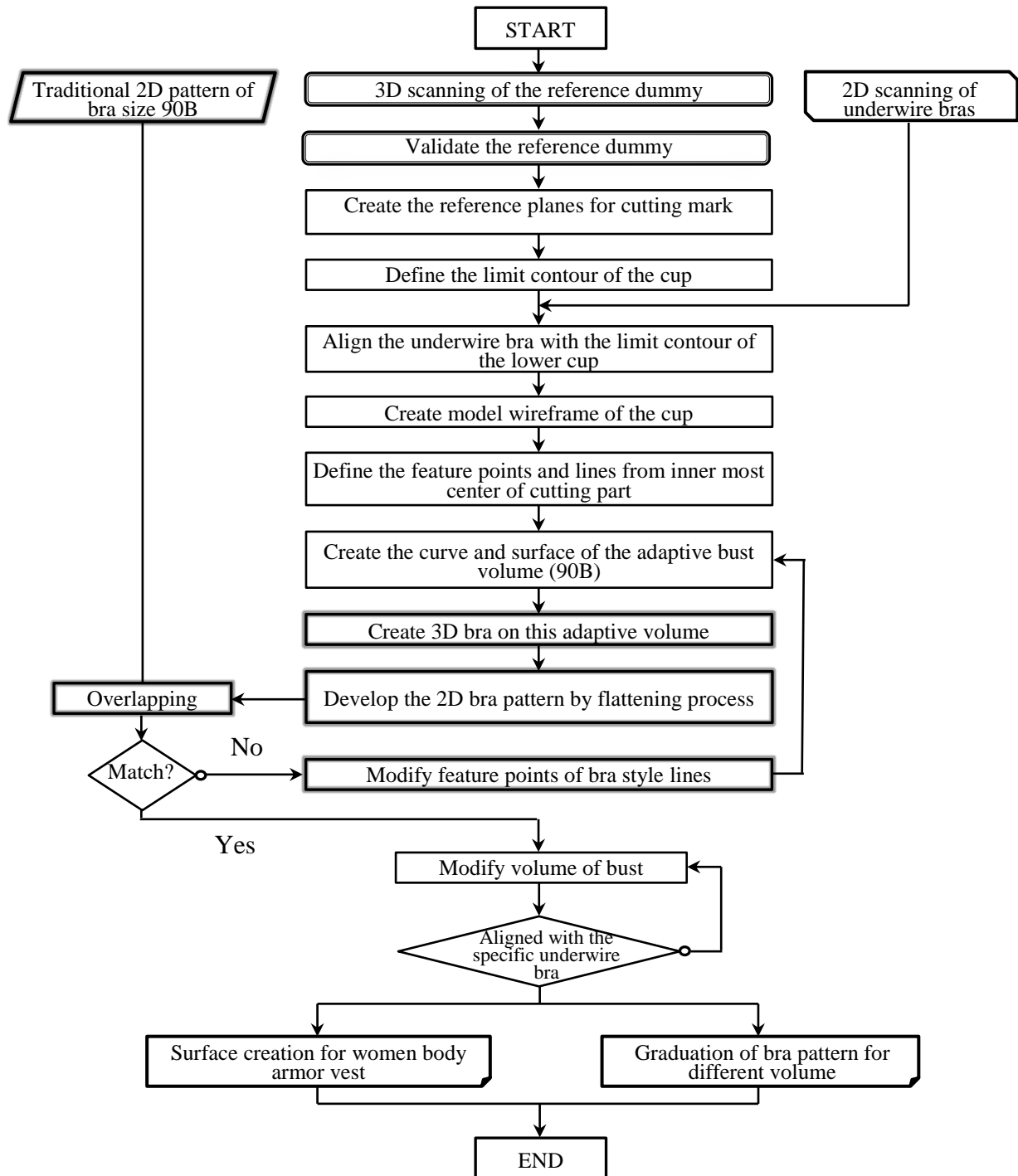
Figure 3.3 General procedures of the proposed 3D virtual design process for developing an adaptive bust and corset pattern for different volumes of the bust

The 3D body scanning provides an accurate body measurement and 3D model of the human body shape with high accuracy. Moreover, it is also very important in the bra designing process to provide accurate breast volume measurements as compared to other classic methods such as nuclear magnetic resonance imaging (MRI), thermoplastic castings, and anthropomorphic measurements [285]. In our 3D design process, both the 3D body scanning and scanWorX software (from the Human Solutions) were used to attain the relevant data on a women's body

shape. Later, Rapid Form software was applied to edit and correct the defects of the imported 3D meshed object (**Figure 3.4 (a)**).The Lectra Company-owned 3D design software known as 3D Design Concept was then used to model the 3D surface of the body shape (**Figure 3.4 (b))**. The operation of 3D scanning permits one to directly obtain the 3D body shape, on which the process is used to analyse and modify the body shape.
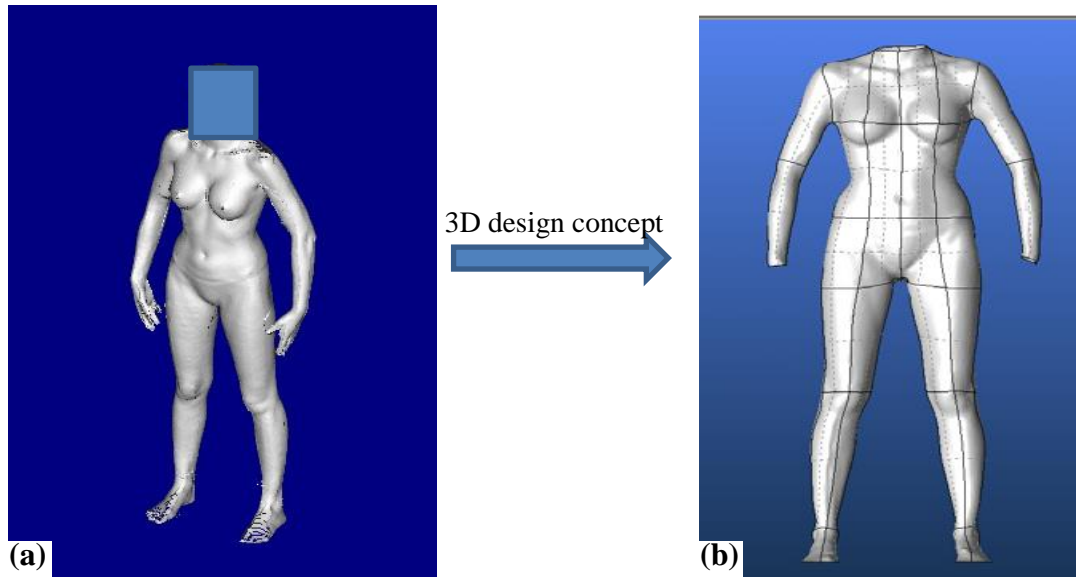
3D design concept

Figure 3.4 (a) The scanned 3D woman body shape (b) the reference 90B bust size 3D woman body model

3.2.1.2.2 3D adaptive bust development through the 3D design process

After receiving the 3D body model with the design concept software and before starting the adaptive bust design process, it is necessary to check and validate the bust volume whether it comes from the standard size 90B morphology or not. This has been checked using the standard size scale of the bra. Based on the result, the morphology and breast volume (90B) having a measurement of the Bust Girth (910mm) and the Under-bust Girth (770mm) were validated.
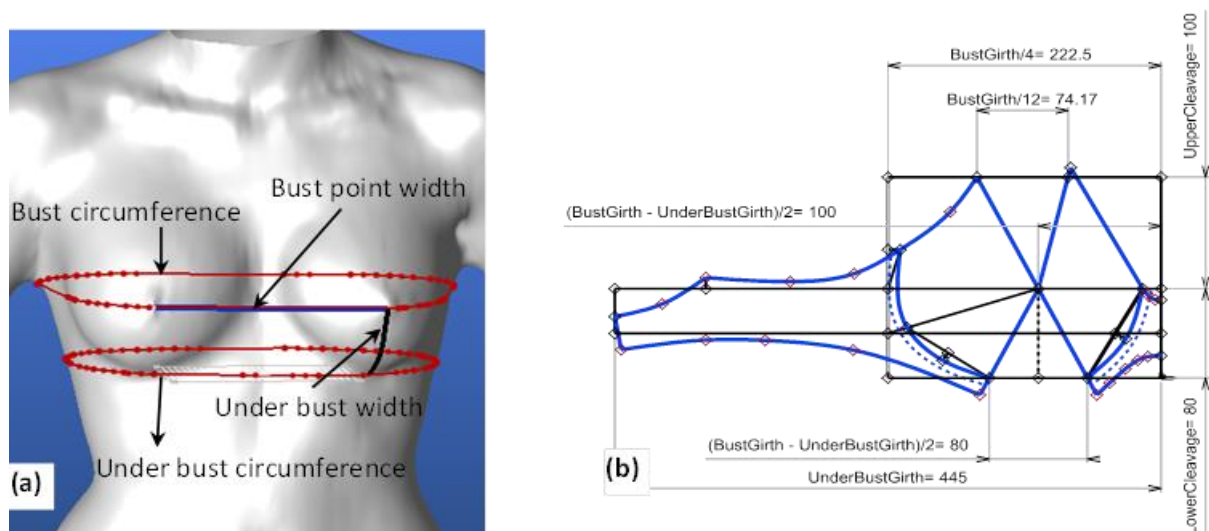
Figure 3.5 (a) measurement on 3D woman model, and (b) 2D bra pattern making [311].

Moreover, the measurements of the bust point width (180mm) and the underbust width (87 mm) were taken to adjust the 2D pattern of the bra (**Figure 3.5 (b)**) [325] and then to validate the 3D pattern of the underwire bra and the bust volume. After validation, the exact position of the centre of the bust (point O with green mark) and bust point (point P with blue mark) was located. Moreover, the different marks around the bust were also used to locate the cutting plane (red plane) along the X and Y axes (2 black markings) (**Figure 3.6 (a)**). The cutting plane mainly helps to define the outer bust contour marked in the black colour (bust circumference). Moreover, the different cutting planes along the X (marked in red colour) and Y (marked in green colour) coordinates oriented in different angles were defined to attain the bust surface volume (ultimately to conceive an adaptive bust) as shown in **Figure 3.6 (b).**
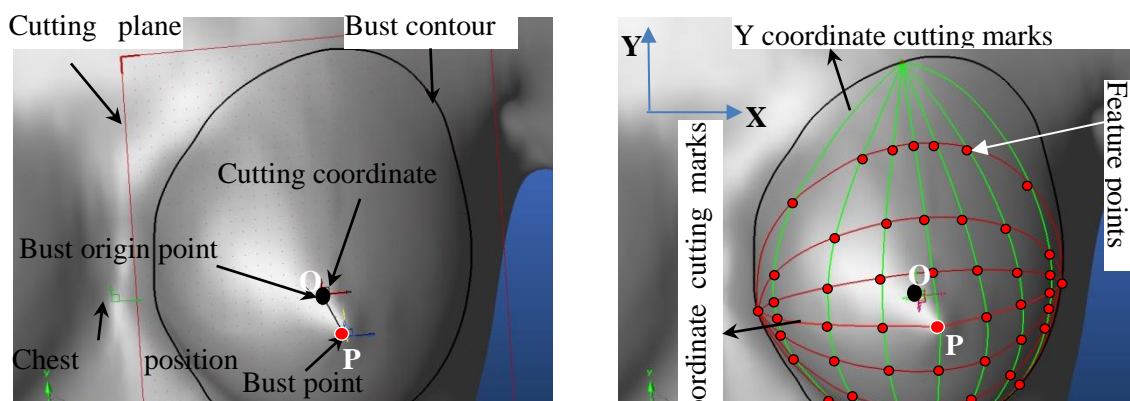
Figure 3.6 (a) Bust with intersection curve of the plane and (b) Feature point extraction and mesh formation on the bust surface.

At this stage of the process, the different key feature points were detected at the intersections of the different cutting and projection planes. Moreover, both planes also help to construct a network of curves (mesh) on the bust surface mainly for determining the volume of the bust.
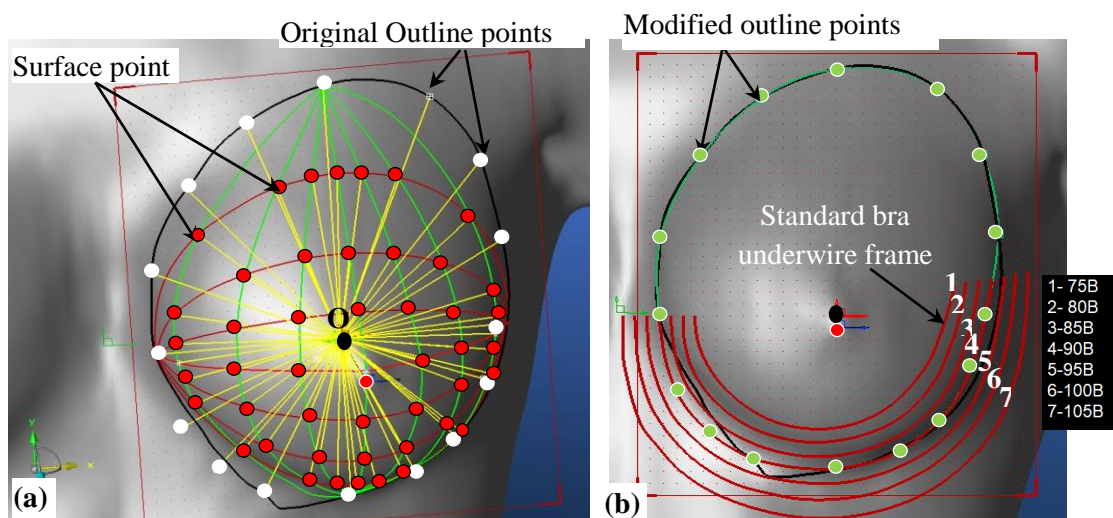
Figure 3.7 (a) projections of line on the bust mesh surface to evolve different bust and, (b) Marking of standard bra underwire frame.

Later, as shown in **Figure 3.7 (a)**, different projection lines in privileged directions (yellow colour line) were projected from bust point origin (point p with a black dot) to different feature points (surface and outline points) to determine the bust volume. In this case, the assumption is that each point on the bust mesh surface (surface points) marked in red dot is directed in its direction (in yellow) toward the cutting mark to determine the bust volume. Whereas, even though the evolution of the outline points (white dots on cutting contour) follows the same hypothesis, it will determine the sizes of the bust. Moreover, to obtain the exact shape of the lower cup of the bra, the standard rigid reinforcements or stan**d**ard bra underwire frame (standards helps to determine the different cups of the bra) were positioned into the model bust as shown in **Figure 3.7(b)**. The cutting bust contour (black circumference) was taken as a reference during the alignment of standard underwire of base volume, size 90B (4) with the bust. Normally, the different standard bra underwire frames are representatives of the different bra lower frames which primarily help to support the bust (support the major weight of the breasts). Moreover, it is also used to amend the bust volume (green curve which connects the modified outline points) at the lower part of the bust cup. Determining accurate representations of the lower bust cup is also very important in comfort aspects.

Finally, a different set of modified surface and outline featured points in the alignment of the yellow directions were created to define the bust with the other sizes. Subsequent, an appropriate network (mesh) on the bust (blue colour) which connects those various feature points has been defined. At this point, this bust surface is responsible to create the other volumes (**Figure 3.8 (a)).** Later, the final shape of the bust has been created (as shown in **Figure 3.8 (b)** with the grey and blue colours) to verify the reconstruction of the volume which conforms to the base volume (90B).
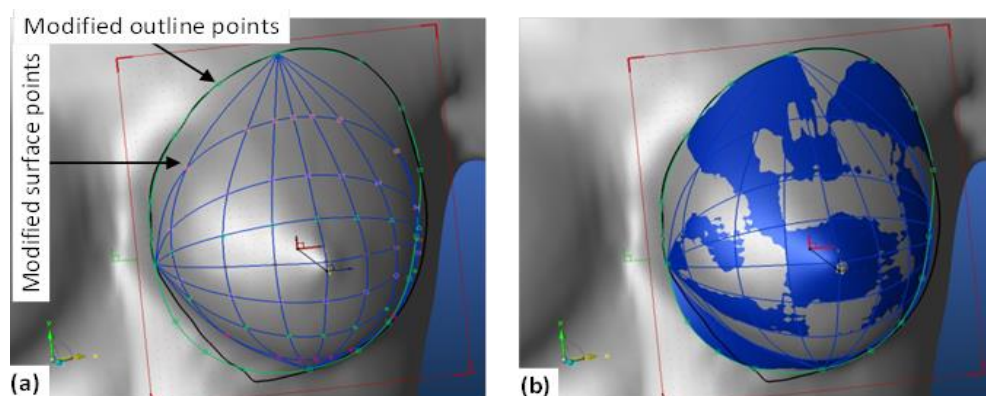
Figure 3.8 (a) the new bust meshes surface and (b) the adjusted bust volume with the base volume (90B).

3.2.1.2.3 The 3D Design process for Bra pattern development (size 90B)

The bra pattern development through the 3D design process starts by defining the different important feature points directly on the developed body model. Due to its importance, the curve of the lower part of the bra has been already defined previously by using the standard bra underwire frames. This lower part of the bra cup is the most important part which is responsible not only to support but also carry the whole weight of the bust. Moreover, the two extreme

outline points which is located in bust contour(green circle marks on left and right) were used to define the two horizontal lines which pass to the centre of the bust as shown in **Figure 3.9 (a)**.
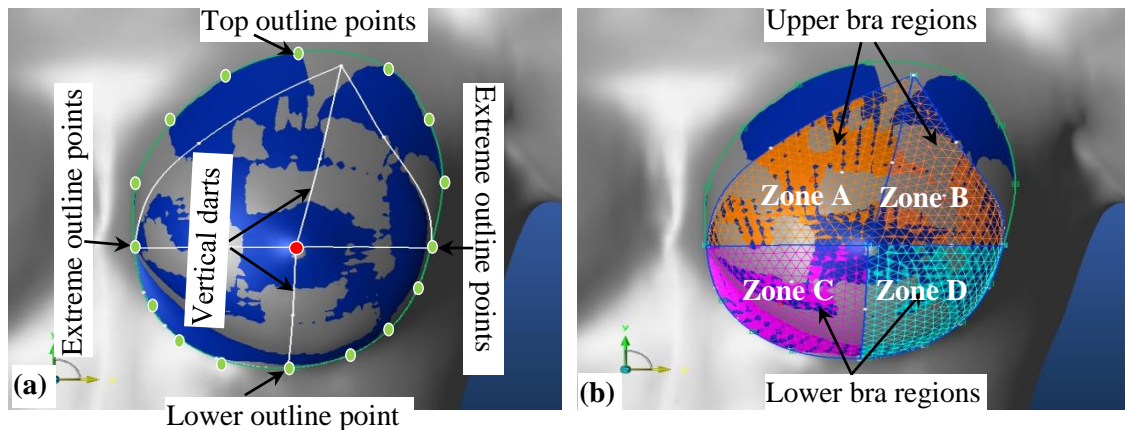
Figure 3.9 (a) Developing the bra region on the 3D and, (b) 3D mesh of different zone of bra

Similarly, the lower vertical lines pass through the centre of the bust (red dot) and connected to the lower outline point in the plane of the lower chest as described in Figure 3.9**(a)**. On contrary, even though the line passes through the bust point, the top vertical line (top vertical dart) is not necessarily connected to the top outline point of the upper cap (upper bra cleavage). Usually, its outer contours will be defined provisionally to cover the upper surface of the bust depending on the style of the bra. Finally, as shown in **Figure 3.9 (b),** the mesh of different zones (Zone A, B, C, and D) has been used to develop different patterns through flattening to represent the basic bodice.

3.2.1.2.4 *Validation of 3D pattern with the traditional 2D pattern*

Further validation has been taken place by overlapping the 2D traditional patterns over the 2D pattern, which was developed from a 3D design process using the 3D-2D flattening process. The adjusted 2D pattern based on the 3D model measurements was found not following the same base as compared to the flattened 2D bra pattern as shown in **Figure 3.10 (a)**. A not exact match between the two patterns was found due to their difference in their accuracy level of measurement and the method they follow. For example, while developing the 2D pattern through the traditional pattern-making process, the body measurements will be taken either from the standard mannequin or standard measurement chart. Besides, this method also considers mostly only the two most common measurements, namely Bust Girth and Under-bust girth for 2D bra pattern development as discussed in details in **Figure 3.5 (b)**. Other important anthropometric measurements used for the design process were derived from these two measurements. For instance, during the traditional pattern-making method, the half-width measurements of the front bust (measurement noted Bust Girth/4) were equal to the bust girth divided by 4. This proposed hypothesis by the method was found a little bit exaggerated and, provide inaccuracy due to the different body shapes of women at the back and fronts of the bust girth. On the contrary, a 2D bra pattern made by the 3D-2D bra pattern-making process took all the necessary body measurements directly on the model without any estimation.
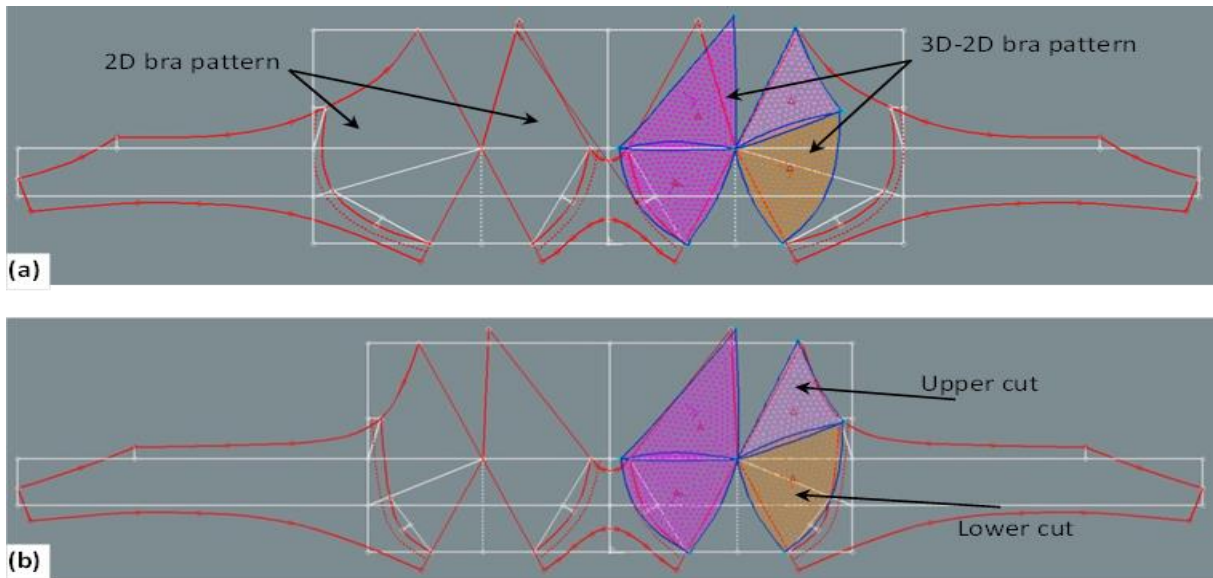
Figure 3.10 (a) Overlapping and comparisons of 3D/2D pattern (Blue border) with traditional 2D pattern (Red) and (b) adjustment of 3D/2D to traditional 2D pattern

Moreover, the pattern was also customized directly on the 3D model following the shape of the bust. This designing process variation, compared to the traditional and 3D-2D flattening, brought a difference between the two patterns while overlapping for the matching process. However, as it is seen in **Figure 3.10 (b)**, an appropriate adjustment leads to the proper results of the pattern. Besides, this modification also took into account a gradual adjustment of the high-cut control points which are extremity points of the dart. The distribution of the two surfaces of the upper bust section was made by adjusting the opening of the uppercut to the value Bust Girth/17 (measurement noted Bust Girth/12 in **Figure 3.5**). Such changes are considered normal since the upper section of the cup is defined mostly by the styles of the chosen model. Given that the method considers only the left and right bra patterns, a new 3D-2D flattening method made it possible to obtain a perfect coincidence of the final results (**Figure 3.11**). Our design process results have the particularity to take into account the shape of the frames that gives this small distinction on the bottom bust cup.
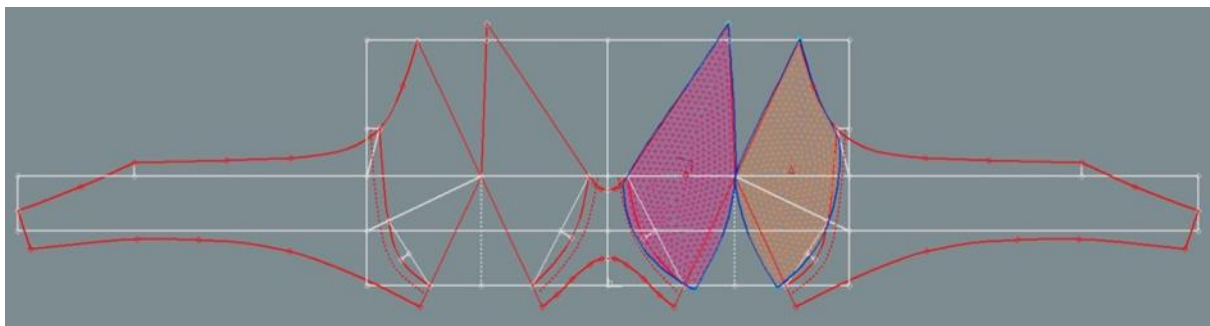
Figure 3.11 Final coincided 3D/2D and traditional 2D pattern

3.2.1.3 Adaptive bust volume and Bra pattern grading for different volumes

The different volumes of bust cup for size 90 are now possible to generate considering the already conceived adaptive bust. The following two most important parameters should be considered while generating the new bust volumes for cup size 90. First, if it is intended to change the sizes of the cup, i.e. 80, 85, 90, 95, 100, etc., the parameters for the outline of the bust (yellow line toward bust contour intersection as shown in **Figure 3.7**) have to be changed. The change has normally defined the cup of the bust size while changing the surface point parameter. Secondly, even if the change of the parameter is relative while conceiving new volumes of the bust, few point parameters may be adjusted to get smooth and accurate surfaces. The additional parameter values to truncate and extend the yellow lines from the original zero value (as shown in **Figure 3.7**) to get the upper (90C, 90D, 90E) and the lower (90A, 90AA, 90AAA) volume of the bust is shown in **Table 3.1**.

Table 3.1 The different parameter values to evolve different upper and lower size bust volume

No.	Upper bust volume		Lower bust volume	
	Parameters (mm)	Bust volume	Parameters (mm)	Bust volume
1.	0	90B	0	90B
2.	-4.55	90A	4.55	90C
3.	-9.1	90AA	12	90D
4.	-15	90AAA	19	90E

Figure 3.12 (a) and (b) has shown the various cup sizes of 90 conceived from the process using the developed adaptive bust (90B). The developed adaptive bust (90B) was normally considered as having a parameter value of zero. The first set of results as shown in **Figure 3.12 (a)** revealed that the evolution of the bust volume for the upper sizes from 90B i.e. 90C, 90D, 90E. Similarly, to display the difference in the volume of the conceived cup, the second set of outcomes represented in **Figure 3.12 (b)** has been designed for the evolution of the bust for the lower sizes from 90B such as 90A, 90AA, optionally 90AAA. The lower part of the bust (which corresponds to the lower cup of the bra) was then aligned with the different standard bra underwire for validations. According to the result, the alignment was found perfect for the corresponding bust cup. This shows that the volumes of the bust obtained through the proposed design process gives a good representation of volumes for each cup size. For our specific model (90), it is possible to generate the grading rules based on the flattened bra pattern from the different volumes.
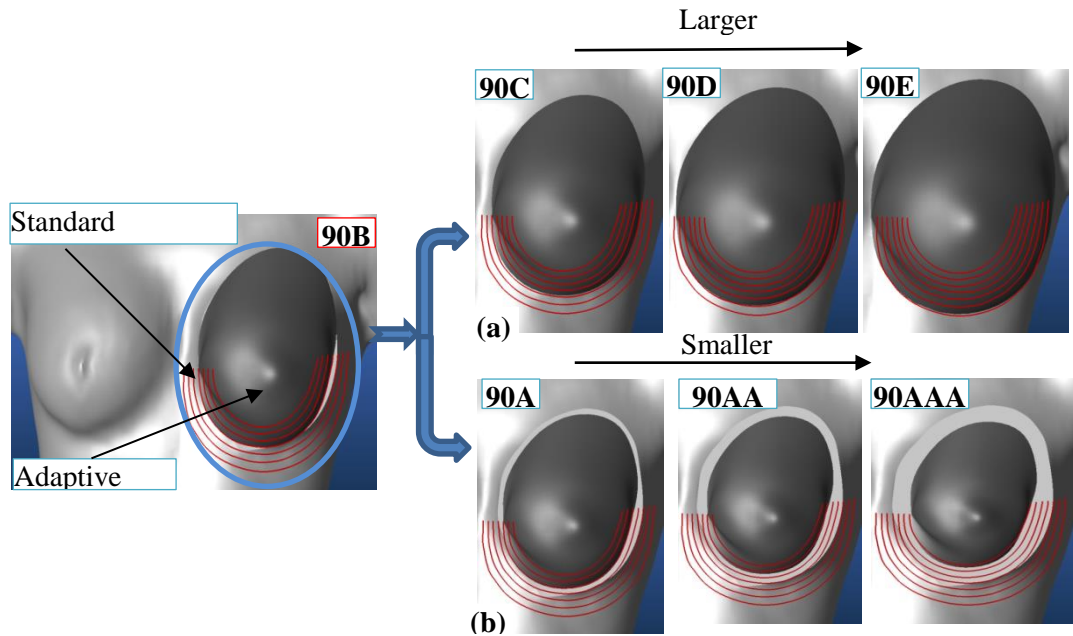
Figure 3.12 (a) Various conceived adaptive bust for the upper sizes and, (b) the lower sizes.

The graded patterns overlapping each other at the centre of the bust are presented in **Figure 3.13**. The evolution laws of the ranking points represent the mean value taken between each size. The regularity of this evolution shows that the obtained cup volumes are also very regular, which is a sign of quality in the corsetry sector.
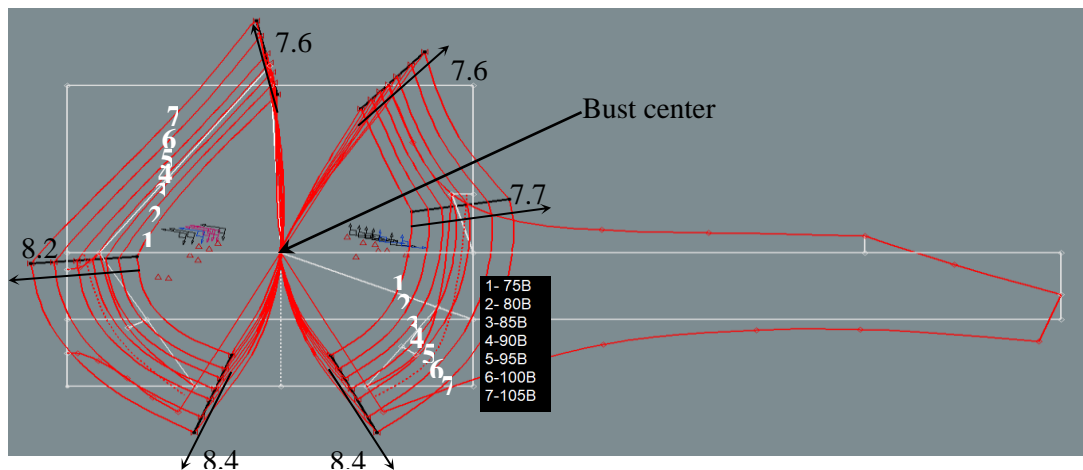
Figure 3.13 Pattern grading for different bra sizes.

3.2.2 Discussion on the bra designing methods

In this chapter, a novel 3D design process on the 3D women model was used to develop an adaptive bust for the specific model (90B). The approach greatly helps to solve the fitting and comfort problems of corsetry in general methods and women's soft body armour development in particular by using the computer-aided design (CAD) knowledge in the morphological evolution of the bust. During the design process, first, the digitalized 3D women body model was developed as reference using 3D scanning technology, and then different feature points were

defined using cutting marks at different angles both in X and Y coordinates located at the most inner centre of the bust. These new planes of coordinate create a form network of curves (mesh) on the bust surface to initiate the creation of different bust volumes. The introduced design process uses a single parameter adjustment for varying the volume of the bust. This parametric change will not only reduce the tedious procedure to change the parameter but also eliminate the trial and error methods to conceive the different bust volumes. Testing of the adaptive corset by changing the parameters for conceiving different volumes of the bust has revealed that using good parameters were all required to get the bust of the correct size. Conceiving the 3D bra patterns on the 3D bust and then comparing it with traditional 2D bra patterns also gave a satisfactory result. The flattening of bra resulting from the different volumes allows us to find a grading rule close to the existing one for this type of model. Moreover, the determination of different volumes of the bust will greatly help for curtailing the current corset problem, i.e. comfort and fitness. This design process will be extended not only to the corset (bra) but also the fitted and comfortable women's soft body armour protection by associating the frontal body part with different cup sizes.

3.3   The design approach of seamless woman soft body armour

As mentioned earlier in the literature review, soft body armour is the most critical piece of protective equipment for law enforcement police officers, personal guards and the civilian subjected to fragments of materials in the working place. It usually composed of the ballistic panel made of flexible material (textile) from a very strong fibre that enables them to absorb the impact energy of the projectile. So far, many serious and potentially fatal injuries have been prevented from criminal conflicts, physical assaults, traffic accidents, and battlefield confrontation by wearing body armour [2]. Nowadays, the involvement of women officers in the field of law enforcement and similar fields has also been significantly increasing across the world [254][255]. However, for the last many decades, they were exposed to hostile environments because of using body armours designed for men. Fitting women with male-based or unisex body armour systems are not acceptable not only for the physiological differences between men and women but also for disproportionate on fitness, comfort, and ballistic protection. Even though significant efforts have been made to improve the performance of women's body armour based on ballistic protection, breathability, cost, fitness and comforts to the wearer in response the customer requirements and experiences, still the majority are primarily concerned for male wearers [326]. As a result, the well-fit women's body armour is in great demand. Currently, there is various body armour design system applied for women users specifically after considering the differences between the male and female body shapes [16][22]. The major designing techniques used are still based on cut-and-sew, fabric folding and stretch-moulding of the conventional fabrics with its drawbacks. The cut-and-sew technique based on the traditional 2D pattern system can form the dome shape to accommodate bust area, but it can also damage the continuity of fibres in the fabric which will reduce the level of protection [35]. Fabric folding is another method to create domes in women's body armour but also affects the wear comfort and personnel mobility due to much allowance for body armour deformation that leads to the panel thicker near the armpit region than other areas. Even using overlapping seams

are much stronger in fabric stitching; however, the small ballistic projectile still can break them directly by penetrating and severing the loop of threads among the seams. Using the above all design system and manufacturing methods for women body armour become even more difficult and encounter problems unlike male body armour due to the curvaceous body shape of females [2]. Developing women body armour especially front panel which properly accommodates the bust area with better impact performance, wearing comfort and considering fitness for different morphological differences among women are very important. Nowadays in order to avoid such problems the most common method to develop the women soft body armour is moulding process. Developing the required shape of women body armour with moulding process not only give proper comfort but also good ballistic protections [24]. However, the moulding techniques require both proper panel design system and ballistic material. This sub-chapter introduced an innovative 2D-3D-2D pattern designing system based on a direct projection of the exact measurement of 3D body contour directly to the 2D projection grids for developing seamless women body armour front panel. The system uses the 3D virtual adaptive bust mannequin with average bra size (90B) that has been developed in the previous section. Such new body armour frontal panel pattern development system could greatly help to solve the problems by generating an appropriate 2D block pattern for better fitness.

3.3.1 Designing methodology and its framework

Nowadays as mentioned in the literature, the most effective method to develop the women's soft body armour panels is moulding process. The techniques help to deform the panel to resemble the shape of the woman's upper torso by leaving all additional finishing operation for better comfort and ballistic protection. Before moulding process, the 3D surface should be converted to a 2D mesh through pattern flattening process. However, due to the compositions of various multiple curved parts in 3D human bodies, it was also found difficulty to convert the 3D human figures into the 2D flat patterns. Moreover, previously the traditional 2D methods with different design elements including darts were used to accommodate those curvy parts by minimising the deformation of the material. However, such involvements of design parts in soft body armour development have also their disadvantage including creating the weakest point on the seams during ballistic penetration and discomforts. To resolve the above problems of developing women's body armour design and speeding up the process of flattening, new reverse engineering approaches have been proposed in these sub-sections. **Figure 3.14** shows the general methodology framework of a new reverse-engineering pattern flattening process for developing women's body armour for the first frontal layer of the panel. This innovative reverse engineering approach has the capability of incorporating direct 3D measurement of the body contour as a means of relieving the strain-stress energy required while producing a 2D flattening pattern from the 3D surface.

The general step is briefly described as follows.

1st - The approach has started by conceiving highly representative adaptive women virtual mannequin with a bust size of 90B. The conceived 3D woman model was mainly responsible for evolving different bust volume with specific parametric values. This particular adaptive virtual

mannequin assists to develop an accurate, comfortable and fitted pattern for soft body armour directly from the model with particular body size and bust volume.

2nd - The developed adapted bust cup (90B) has been then associated with the other frontal upper torso part to determine the precise and complete protection for the specific cup.

3rd - Based on the developed surface, the final protection zone according to the actual needs were defined. Moreover, the developed adaptive bust women mannequin was used to analyse separately the different morphological part of the women front body. The different basic anthropometric feature points (such as shoulder tips, front neck, high neck, the front to the chest, underarm (armpits), side waist, side hip, etc.) on each side of the frontal adaptive mannequin was defined at the beginning of the re-engineering approach. The mentioned feature points help not only to determine the limits of the frontal body size but also guides the different landmarks of various horizontal characteristics line and curves (shoulder, chest, underbust, waist, hip, middle front, etc.) on the frontal body contour.

4th - The vertical (warp) and horizontal (weft) projection grid structure are then outlined in front of the virtual mannequin for projecting the 3D block pattern surface which is developed on the front part of the mannequin. Both grids were then projected to obtain their corresponding 3D grids on the virtual body. Here, both horizontal and vertical grids were associated with specified parameterized values. The use of such grids was to obtain the exact measurement of the body contour while flattening.

 5th - The block pattern of the 3D surface was then flattened by projecting the 3D body contour measurement to the 2D projection grids using the reverse flattening process. This analysis would be interesting to analyse since the material deformation has a great impact on the comfort and ballistic performance of the final product. This material surface deformation has been carried out considering the newly developed female body front panel pattern with the traditional 3D / 2D flattening process.

```
┌─────────────────────┐
│        Start        │
└─────────────────────┘
           │
           ▼
┌─────────────────────────────────────────────────────────┐
│        Obtaining adaptive 3D female mannequin            │
└─────────────────────────────────────────────────────────┘
           │
           ▼
┌─────────────────────────────────────────────────────────┐
│  Marking different anthropometric points on the sides    │
│           of frontal 3D adaptive mannequin               │
└─────────────────────────────────────────────────────────┘
           │
           ▼
┌─────────────────────────────────────────────────────────┐
│  Placing various characteristics line and curves on      │
│  the body refereeing extreme anthropometric reference    │
│                      points                              │
└─────────────────────────────────────────────────────────┘
           │
           ▼
┌─────────────────────────────────────────────────────────┐
│  Outlines of vertical (warp) and horizontal (weft)       │
│           projection grid structure                      │
└─────────────────────────────────────────────────────────┘
           │
           ▼
┌─────────────────────────────────────────────────────────┐
│  Projection of 2D grid to obtain its corresponding 3D    │
│           grids on the virtual body                      │
└─────────────────────────────────────────────────────────┘
           │
           ▼
┌─────────────────────────────────────────────────────────┐
│  Setting of each grids structure on the 3D to extract    │
│           the exact body measurement                     │
└─────────────────────────────────────────────────────────┘
           │
           ▼
┌─────────────────────────────────────────────────────────┐
│   Projection of the 3D body measurement to the 2D grids  │
└─────────────────────────────────────────────────────────┘
           │
           ▼
┌─────────────────────────────────────────────────────────┐
│   Flattening of the 3D surface of the block pattern      │
└─────────────────────────────────────────────────────────┘
           │
           ▼
┌─────────────────────┐
│         End         │
└─────────────────────┘
```

3.3.2 2D block pattern development

Before the development of a 2D block pattern using the new reverse engineering flattening process, the developed woman 3D mannequin with the adaptive bust was introduced. To complete the process, the different bust cups are then associated with the rest of the frontal body part as shown in **Figure 3.15**. The process will greatly help to determine the complete protection cover for the upper torso of the different bust cup with proper fitness. Based on this particular surface, it makes now possible to determine and draw the final protection zone according to the actual needs.
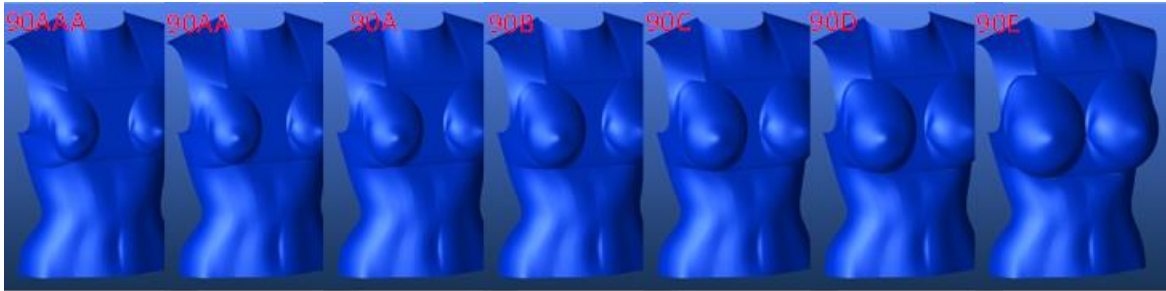
Figure 3.15 Associations of an adaptive bust with other women upper torso

3.3.2.1   Determinations of anthropometric points and 3D block pattern surface

Our research study mainly focused and performed on the frontal part of the woman's adaptive 3D mannequin. The primary advantage of using such mannequin is to analyse the influence of both body morphology and bust volume in the 3D basic bodice pattern creation for woman soft body armour application. As it has been discussed in the literature review, there are different woman soft body armour designing and manufacturing techniques. However, in the design and production of woman body armour front panel using the moulding process (dome formation) to accommodate the bust properly, it is very important to re-organize the 3D structure of the fabric imposed by the lack of elasticity of warp and weft yarns (high-performance fibre). Moreover, in the initial state, the flat shape of the basic bodice pattern must take into account the structural deformation of the fabric to finally obtain a 3D base bodice which perfectly drapes the woman's body. This structural deformation will greatly help not only for the final shape and fitness of the vest product but also for its final ballistic performance. Moreover, an optimal covering of the bust in the greatest respect of the women's morphology is very important for better ballistic performances and comfort due to the sensitivity of the bust. This fundamental situation inspired to develop the front basic bodice directly on a 3D virtual model with 90B bust size (**Figure 3.16 (a)**) then apply a reverse flattening process (2D/3D/2D) to predict the deformation of the material between the 3D and 2D space.
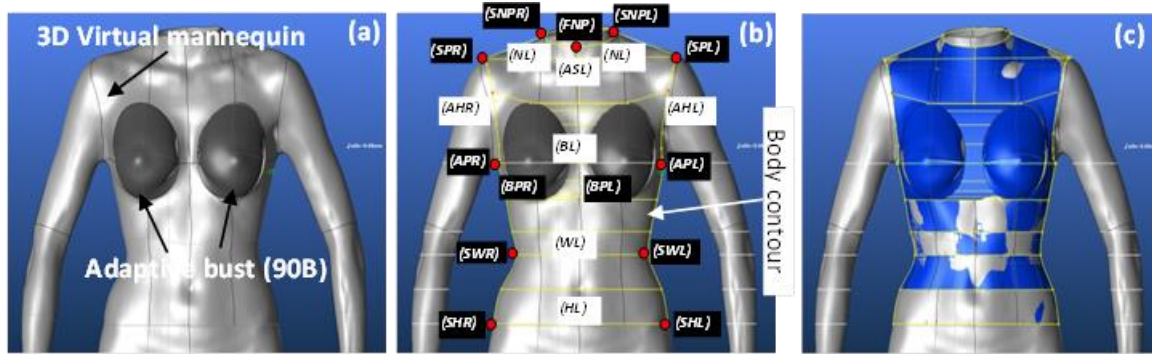
Figure 3.16 (a) Selected 3D virtual mannequin with 90B bust size and (b) Developments of reference point and body border contour on the 3D virtual mannequin, and (c) Creation of the 3D block pattern surface on the wired network

The process of creating the basic bodice begins with the placement of different characteristic lines and curves on the front part of the body (**Figure 3.16 (b)**). For this, first, it was necessary to identify a set of different strategic anthropometric feature points which will be marked manually on the 3D body side contours (such as shoulder tips, front neck, high neck, the front to the chest, underarm (armpits), side waist, side hip etc. as shown in (**Figure 3.16 (b)**: Red points). The detail specifications of anthropometric feature points and landmarks were shown in **Table 3.2.**

Table 3.2 Designations of different anthropometric feature points and landmarks

No.	Anthropometric points	Specification	Feature lines or curves	Specification
1	NPR, NPL	Neck point (right and left)	NL	Neckline curve
2	SPR, SPL	Shoulder point (right and left)	ASL	Across shoulder line
3	APR, APL	Armpit point ((right and left)	BL	Across Bust
4	SWR, SWL	Side waist point (right and left)	WL	Front waistline
5	SHR,SHL	Side hip point (right and left)	HL	Front hip line
6	FNP	Front neck point	AHL, AHR	Armhole curve
7	BPR, BPL	Bust point (right and left)		

With these predefined anthropometric feature points, different feature curves and reference landmark lines with horizontal planes were generated automatically using the geometric method such as front across shoulder lines, across bust lines, bust line, hip line, etc. and curves such as necklines, armholes, etc. contiguous delimiting the outer contour of the pattern. Then, a network of internal curves based on the morphological contours of the body (shoulder, chest, underbust, waist, hip, middle front, etc.) was created within these limits to complete the lines of the creation of the base of the bodice. These curves have the particularity of being hooked to this external contour to create with it a connected 3D wire structure. On this, the structure was created on a 3D surface representing the basic bodice very close to the morphology of the front of the woman's body as shown in **Figure 3.16 (c)**. Moreover, in the ballistic protection point of view, this criterion of proximity is very important since the front panel is shaped based on the

contour of the body which will ultimately give a better blunt trauma signature (BFS) than the panel which is not well fitted to the body.

3.3.2.2 Developments of 2D projection grids and 3D grid structure in 3D body

After obtaining the 3D block pattern surface on the front part of the mannequin, it is time to apply the new reverse 2D / 3D / 2D flattening process. This new pattern design starts with the creation of both horizontal and vertical grid structures positioned in front of the 3D block pattern as illustrated in **Figure 3.17 (a).** This grid has been also designed to represent the common 2D plain weave structure whose pitch is a multiple of the warp and weft yarn density of the final product. This representation will help later to have an idea of the two yarns directions while deformation of the fabric. While developing the grid, great care should be taken and a proper plane coordinate has to be determined to get a better result. This means the horizontal and vertical grid should be perpendicular to each other, parallel within the same line orientation of equal division in the frontal section of the body. The developed weft and warp 2D grid are then projected onto the 3D shape of the block pattern (2D / 3D process) to create a 3D grid on the body. The advantages of generating the 3D grid structure are used to associate with the 3D structure of fabrics in the block pattern (**Figure 3.17 (b)**).
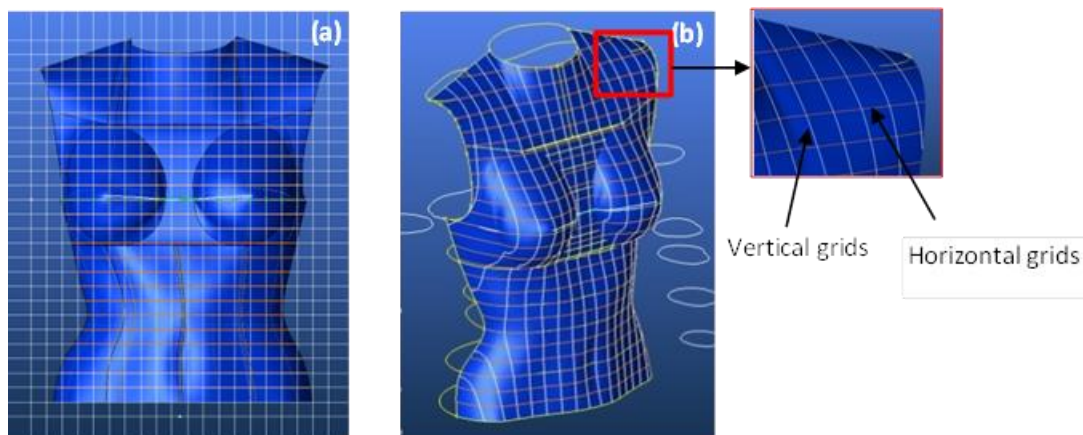
Figure 3.17 (a) 2D grid assimilated to a plain weave structure and (b) 3D grid structure assimilated to a woven architecture of fabrics in 3D body shape

This structure is also then composed of horizontal (weft) (brown curve) and vertical (warp threads) (white curve). Before completing this 3D grid, it was necessary to create a line between the two breast points to know exactly the final position of the tip of the busts. It is from the curves that made it possible to conceive the variable bust that we could generate a curve representing the 3D line of the between-bust (**Figure 3.17 (b)**: green curve). In the design perspective, placing properly the two critical bust points will later use for setting the point at the exact position on the fabric during the dome formation using punching techniques. Proper setting of bust points while dome formation will give the right shape of the deformed panel when it comes to the normal shape after deformation.

3.3.2.3 The projection of 3D grids and 2D/3D/2D pattern flattening process

The next step was to set each vertical (warp) and horizontal (weft) grids in the 3D structure to extract their exact length. Thus, each horizontal (weft yarn) is associated with a parameter H_{ij} (i: number of the horizontal grid (yarn), j: position relative to the chest contour i.e., above (a) or below (b)) defining its 3D length taking into account that the body symmetry makes it possible to measure edge to edge concerning the 3D pattern of the block pattern (**Figure 3.18 (a)**). Similarly, each vertical (warp yarn) is associated with a parameter V_{ijk} (i: number of the vertical grid (yarn), j: position relative to the chest contour i.e., above (a) or below (b) and k: position inside left (l) middle (m) or right (r)) defining its 3D length and taking into account that in this sense the pattern is not symmetrical (**Figure 3.18 (b)**). In the case of vertical measuring, we must separate both the upper measurement from the lower part measurement based on the bust line (j: the relative position to the chest contour i.e. above (a) or below (b)). This division is taking into account the effects of the spread of the structural deformation in the warp direction around the breasts during the punching test. Moreover, some lines, mainly extreme borderline, which projected on the lower part, were also naturally divided into two parts because of the bending on the garment's side (j: intermediate position after division i.e. middle).
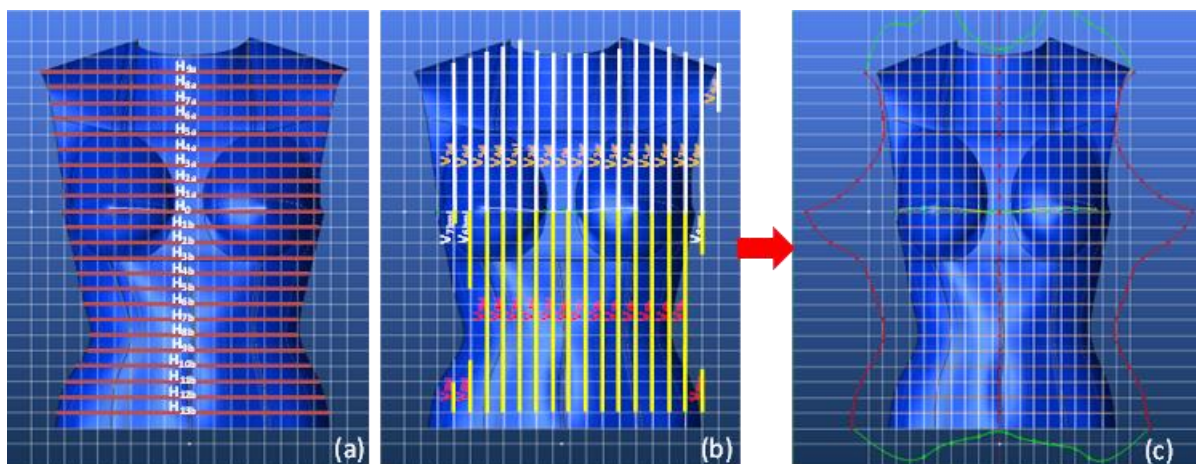
Figure 3.18 Parametrization of the measurement lines of the (a) horizontal (weft), (b) 3D vertical (warp) yarn structure, and (c) 2D/3D/2D flattening process for the block pattern

However, such measurements were not used since it is only intervened on the morphology of the side and generated by the weft threads. **Figure 3.19** shows all the measurements that are performed automatically according to the parameterization to develop previously described pattern blocks. After obtaining the exact measurements of horizontal and vertical strings on the 3D body contour, it is now possible to project the 2D grids for developing the basic block pattern.

Sr no.	Horizontal measurement Designation	Values (mm)
1	H1a	465.14
2	H2a	413.51
3	H3a	374.67
4	H4a	348.26
5	H5a	336.83
6	H6a	338.34
7	H7a	343.29
8	H8a	353.90
9	H9a	390.40
	H0	561.66
1	H1b	537.61
2	H2b	490.21
3	H3b	415.31
4	H4b	384.38
5	H5b	369.67
6	H6b	352.43
7	H7b	338.42
8	H8b	336.36
9	H9b	349.87
10	H10b	376.81
11	H11b	401.80
12	H12b	418.96
13	H13b	427.34

Sr no.	Vertical below measurement Designation	Values (mm)
1	V1br	285.43
2	V2br	292.60
3	V3br	296.17
4	V4br	299.70
5	V5br	302.70
6	V6br	306.31
7	V7br	318.20
8	V8br	95.86
	V0b	284.53
1	V1bl	290.25
2	V2bl	293.88
3	V3bl	298.36
4	V4bl	305.02
5	V5bl	316.65
6	V6bl	116.74
7	V7bl	79.99

Sr no.	Vertical above measurement Designation	Values (mm)
1	V1ar	210.55
2	V2ar	221.19
3	V3ar	234.16
4	V4ar	266.03
5	V5ar	270.61
6	V6ar	257.92
7	V7ar	244.08
8	V8ar	234.49
9	V9ar	93.68
	V0a	210.41
1	V1al	220.75
2	V2al	236.38
3	V3al	273.07
4	V4al	269.08
5	V5al	257.75
6	V6al	241.72
7	V7al	243.15

Sr no.	Vertical middle measurement Designation	Values (mm)
1	V8mr	70.49
2	V6bml	157.75
3	V7bml	19.02

Figure 3.19 Measurement database values for horizontal (weft) and vertical (warp) lines

In the final stage of the new 2D-3D-2D pattern flattening process, we could flatten the 3D surface of the block pattern as shown in **Figure 3.18 (c)**. The illustrated figure shows the front and side view of the flattening elements with the pattern. In our new methods, the principle of flattening mainly deals with using the precise measurement of each vertical (warp) and horizontal (weft) grids to define an exact external frame of the block pattern. In a first step, we use the value of the parameters of the horizontal (weft) grids (H9a, ..., H1a, H0, H1b, ..., H13b) to define a set of points which used for delimiting the pattern of each side (red colour point in **Figure 3.18 (c)**). Later, this value is divided by two to distribute on each side of the body, which is the 3D mannequin is symmetrical to a central axis (red axis of symmetry). This point is our peripheral points to determine the side part of the final block pattern. Then, two spline curves were drawn on each side by connecting these peripheral points to create the red contours. In the same spirit, we use the value of the parameters of the threads of weft (V7al... V1al, V0a, V1ar, ..., V9ar) to define the above part of the pattern (green) and the value of the parameters (V7bl, ..., V1bl, V0b, V1br, ..., V8br) to define the lower part of the pattern (green). In the same condition, the 3D line of the breast was then projected in 2D to locate the tip of each breast on the fabrics before deformation to position the 3D mould of the breasts for the punching test.

3.3.2.4   Material deformation analysis while flattening process

Flattening of 3D surfaces is mostly a challenging problem in the different product design sectors. The triangulated surface methods are the most common flattening with its limitation of existing gaps and overlaps in the resulting meshes. Distortion is also another problem that appeared while obtaining a 2D pattern through deformation. In this regard, different researchers have been conducted various research using different methods and algorithms to solve the flattening process [327][328][329]. For our product development, woman soft body front panel

using the moulding process, it will be interesting to analyse the material deformation of the flattened pattern since it has a great impact on the comfort and ballistic performance of the final product. This material surface deformation has been carried out considering the newly developed woman body front panel pattern with the traditional 3D/2D flattening process. For this, it has been first required to develop the traditional 3D/2D flattened pattern by meshing the 3D surface of the block pattern as shown in **Figure 3.20 (a)**.
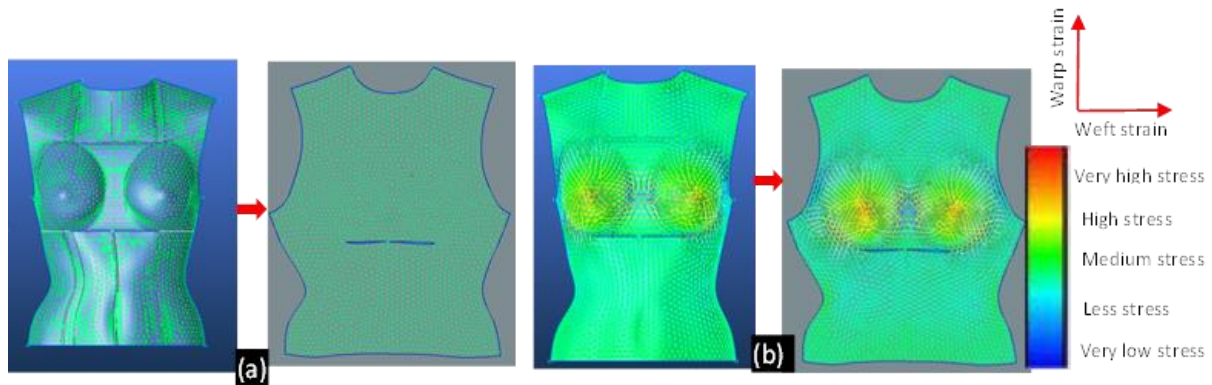
Figure 3.20 (a) 3D and 2D mesh of the block pattern, and (b) mesh deformations of the 3D and 2D in the warp and weft directions

Then, from this mesh, we use the traditional 3D/2D flattening process to obtain the equivalent 2D surface. Usually, the body surface which involved a doubly curved was categorized under a non-developable surface. In this particular surface, material deformation would have a great chance to happen mainly in the bust area while flattening of a 3D surface into an equivalent 2D pattern as shown in **Figure 3.20 (b).** With the traditional 3D-2D flattening methods, to reduce the material deformation and proper accommodation of the bust portion, it would be necessary to use different methods. Among those methods, different designers, researchers and garment developers have usually used various types of darts on the different portion of the body such as waist, shoulder, side etc. to perform a traditional 3D-2D pattern flattening. Based on the above features, in the classical 3D-2D flattened pattern, as shown in **Figure 3.21(a) and (a'),** the deformation of the horizontal (weft) yarns is directed outwards to the side of the bust area.
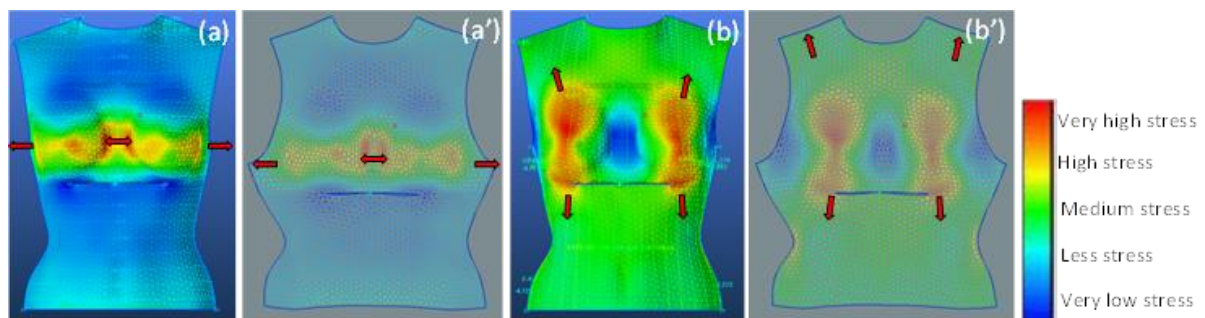
Figure 3.21 a) 3D, (a') 2D weft, and (b) 3D, (b') 2D warp direction deformations of the mesh

However, in the case of our new 2D-3D-2D pattern flattening process, the method already considers and checks how the woven (grid) structures perform during deformation both in the horizontal (weft) and vertical (warp) directions. For this, the post-processing of the flattening

process has the advantage of calculating the deformations in the weft (horizontal) (**Figure 3.21 (a)**) and the warp (vertical) (**Figure 3.21 (b)**) directions. This is one of the most important features which mainly used to compare the results of the two processes due to its critical impact on the woman's body armour comfort and ballistic performance. While flattening patterns using classical methods, the deformation of the material is most significant in the horizontal and vertical directions.

Similarly, as shown in **Figure 3.21 (b) and (b')**, the vertical (warp) deformation is directed up towards the shoulders and down towards the waist of the pattern. This flattening deformation induced in the mentioned direction can be easily observed and maintained by our method with the use of direct measurement from the 3D contour as shown in **Figure 3.22 (c)**. Moreover, **Figure 3.22 (b)** shows the result of both the traditional 2D-3D flattens patterns with our newly designed pattern using a 3D-2D-3D flattening process. The overlapping of the results of the two methods shows that both patterns flattening method has an extending pattern contour. However, as shown from the super-imposed patterns, there are more extended extremes contours in the sides of the bust, which is the nearest pattern contour from the deformation area (bust). Even though the extended extreme contour difference has appeared along the shoulder and waist, it can be easily adjusted without affecting the design and the functional characteristics of the final pattern.
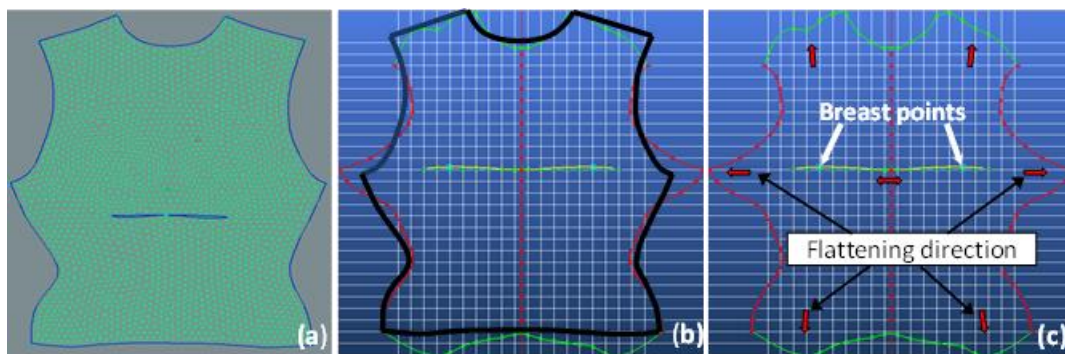
Figure 3.22 Comparison of the new pattern with classical flattened pattern (a) Pattern from classical 3D-to-2D flattening methods with mesh formation (b) Superimposing of 3D-to-2D patterned with the newly pattern and (c) 2D pattern from the new methods

Even though, while comparing the patterns flattening method especially on the sides of the bust, our new 3D-2D-3D flattening process takes into account the actual deformation of the material by propagating it outside the pattern at the desired locations such as shoulders, armpit, and waist. In general, considering the material propagation while pattern flattening process will help to eliminate different drawbacks while material deformation using the moulding method. This drawback may include the unbalanced density of the material in different areas of the panel, high shear deformation, loosing of the required amount of crimp, the unwanted extension of the yarns inside the structure sliding of fibres, and local wrinkles [330]. These unique characteristics have a direct or indirect effect on the final wear comfort, fitness and most importantly ballistic performances.

3.3.3 Discussion on design approach of seamless woman soft body armour

For the last few decades, significant efforts have been made by researchers and developers to improve the overall performance of women's soft body armour. However, designing women's soft body armour which accommodates the bust area for different morphological differences with good comfort, fitness, and better ballistic protection is still in great demand. This sub-chapter introduced an efficient reverse engineering approach (2D-3D-2D pattern generation) for generating appropriate 2D block patterns from 3D woman adaptive virtual mannequin (90B) for woman seamless soft body armour panel. It uniquely involves the process of projecting a 2D pattern measurement on to the 3D body contour and thus the 3D contour wire is flattened to the 2D surface for developing a 2D block pattern. The method was mainly responsible to acquire the bust volume by eliminating the involvements of darts. The process starts by identifying the different strategic anthropometric points on the front body side contours of adaptive mannequin (90B size bust cup). Both horizontal (weft) and vertical (warp) projection grids in front of the virtual mannequin were then marked to generate a 2D block pattern using the necessary body couture measurements. While projection, an accurate measurement using a precise projection system and bust points has been considered. According to the material deformation analysis based on a 3D-to-2D flattened pattern, the generated flattened pattern reveals better shape to accommodate the deformation with low distortion throughout the fabric surface while flattening. This will later greatly helps to keep similar fabric distribution throughout the panel and give better ballistic protection, fit-ensured and good comfort for the wearer. Moreover, the proposed approach also used to generate a 2D block pattern for women's body armour front panel with different bust volumes automatically by manipulating only the body contour measurement on the 3D virtual mannequin.

3.4 Automatic pattern generation for seamless women's multi-layer body armour

In the last few decades, light weighted and flexible soft body armour along with good ballistic performances has been greatly increased considering different parameters. Still, efforts have been continued by researchers to develop better ballistic protective soft body armour with a much-reduced weight with better fitness and comfort. Developing women's body armour front panel which properly accommodates the bust area with better impact performance, comfort and fitness for different women morphology without the need of cutting, stitching, stretch folding or folding is also very imperative. Nowadays, moulding becomes the most commonly used designing technique which helps to develop seamless front panel by mimicking the bust area without the need of cut-and-stitch or any other finishing methods for better fitness and efficient protection. Our previous section has developed the pattern for the 1st layers of seamless frontal women body armour panel using a reverse engineering approach. Such methods could improve the problems of obtaining accurate surface data for women's bust due to its ambiguous borderline with the skin surface, and helps to create the required 3D shape through dome-formation. Besides, it is known that woman soft body armour should be adaptive to the required human body morphology to ensure the effectiveness of ballistic protection. As the body armour

resemble the required body shape, the better the fitness and efficient protection will be achieved. However, since women soft body armour panel is composed of successive ballistic layers, it is imperative to develop the proper pattern for all successive panel layers to achieve better fitness and protection after moulding process. This section introduced new and novel methods based on 3D design approach through parametrization process for generating a pattern for multiple layers of woman soft body armour panel directly on the 3D virtual mannequin. The method utilises a previously developed single layer women soft body armour block pattern with an average bra size (90B). Dome-formation techniques were then applied for customizing seamless frontal woman body armour panel through newly developed adapted moulding bench by applying the right and left bust-shaped punch on the 3D warp interlock-aramid fabrics.

3.4.1 Adaptive bust and first layer body armour block pattern generation

Before we proceed to generate the successive patterns for multi-layer (full package) body armour panel, a basic block pattern for the single layer of female soft body armour panel was conceived from our previous subsection 3.2. The entire pattern generation system has been applied to the 3D adaptive bust female mannequin (with a cup size of 90B). As discussed in our previous sub-section 3.1, developing a good bra design with accurate bra sizing system has been played an important role in the development of seamless women's soft body armour. Due to the inaccurate traditional bra sizing system to precisely determine the complex three dimensional (3D) breast volumes, introducing a new way of the 3D design process on 3D virtual women body model using 3D-to-2D CAD method is a good solution for developing seamless woman front armour.

In our previous section, different bust cup sizes were conceived for the 3D virtual woman mannequin of size (90) through new 3D designing approaches based on parametrization [332][333]. This approach solved previous design problems by using the computer-aided design (CAD) knowledge in the morphological evolution of the bust and introduced into a 3D design process for comfortable and well fitted 3D bra design. Moreover, developing such adapting busts with the possible variation of the cup will momentously help not only to design a comfortable and customized bra pattern but also seamless woman soft body armour development. Based on the developed bust volumes (90B) on the 3D women virtual mannequin, the frontal armour panel pattern associating with the specific bust has been developed through reverse engineering (2D-3D-2D) pattern flattening approaches. This method helps to develop the first single-layer frontal pattern from the selected adaptive woman 3D virtual mannequin of specified bust size (90B). Such a process involved the developments of a basic bodice directly on a 3D virtual model (90B bust size) with a reverse process of 2D/3D/2D flattening method.

Since the body armour is multi-layer, an appropriate technique to design the whole multi-layer body armour panel, considering the fabric thickness along with its pattern projection, is required. To solve this issue the current sub-chapter will propose a new and systematic 3D design approach through the parametrization process to generate block patterns for the manufacturing successive panel layer.

3.4.2 A methodological framework for multi-layer panel pattern generations

In general, the soft body armour panels are usually manufactured by layering up various high-performance materials depending on the type of threat, protection level, type of material, body type, etc. Meanwhile, the ballistic protection vest should be developed in such a way that the material has to have better resistance to projectile penetration, lightweight and comfortable. Adding many protective layers in the panel might offer greater ballistic protection, but it also adds undesirable weight and inflexibility of the vests. To balance the above contradictory parameters and develop well-being multi-layer soft body armour, not only selecting proper multi-layer material but also precise garment designing process and pattern making techniques play an important role. Due to the curvilinear body shape, designing and pattern making techniques even become more difficult to obtain accurate surface data along the precise pattern making process while designing women's soft body armour. To generate such patterns for the different layers a precise and systematic 3D design approach working directly on the 3D virtual mannequin will be very effective. **Figure 3.23** shows the methodological framework for the new design approach to develop the intended patterns for each layer of multi-layer women's soft body armour panel.

The general steps and designing framework is briefly described as follows.

1st **-** The design starts with by conceiving an already generated basic block pattern of the first layer of the armour panel on the 3D adaptive bust virtual mannequin (90B bust size).

2nd - Based on the conceived block patterns of the first fabric layer the appropriate surface mesh on the front surface of a 3D virtual mannequin will be then generated. This will greatly help to limit the body contour for shifting the mesh with appropriate values.

3rd - The different shifting values of the mesh will be properly defined to start developing the various layers. Here, the thickness of corresponding material layers was considered as the parameter values for shifting the meshes.

4th - Later, using the good parameter values and appropriate coordinate points, the reference meshes have been shifted for new surface mesh generations, and can be observed in the superimposed multi-layer mesh on the 3D virtual mannequin for verification.

5th -The multi-layer mesh could be then flattened using traditional flattening techniques (3D-to-2D) to generate different block patterns.

6th - Further, the multi-layer pattern then checked in the real fabrics by developing the multi-layer panels and draping on the real body/mannequin with the same size for validations.

START

Pattern generation process for first layer panel

Conceive 90B bust size 3D adaptive bust mannequin

Validity of the block pattern

Generating a basic block pattern for a single layer

Summary of sub-chapter 3.1 and 3.2

Developing of surface mesh on the 3D virtual body using basic block patterns

Define the limit contour of the surface mesh on the 3D virtual body

Defining the different parameter to be consider for pattern increment, i.e. layer thickness

Modelling and moulding of the bust for punching

Pattern generation process for multi-layer panel

Creating the proper coordinate on the 3D virtual mannequin

Parametrization of the values to generate the consecutive layer pattern

Adapted Punching Bench

Shifting of the surface mesh using the corresponding layer thickness values

Checking of the 3D multi-layer pattern on the adaptive mannequin

Develop the corresponding each 2D layer pattern by flattening process

Continue for the other bust size for prototyping

Yes

Checking on real body/dummy?

Developing the panel on the real fabrics through moulding with appropriate bust-shaped punch

No

Analysis of the fitness and other problems

Manufacturing of multi-layer frontal panel with moulding process

Problem identification and correction

Developments of seamless female soft body armour panel

Generation of multi-layer panel pattern for other bust volume

END

Figure 3.23 A 3D design approach methodological framework for multi-layer patterns generation and manufacturing of woman soft body armour panel using a dome-formation process

3.4.3 Developing surface mesh on the 3D virtual woman body

Creating the mesh surface (cream colour body mesh in **Figure 3.24**) on the surface of a 3D virtual mannequin (with the value of zero) is the first step to develop the woman front multi-layer panel patterns through a 3D designing process. **Figure 3.24** shows the associated surface mesh with the 3D virtual mannequin and the generation of the first layer on the surface mesh. This particular 3D surface mesh is essential and will be a reference for the developments of different surfaces based on the corresponding thickness of the fabric layer. The surface mesh is generally the associated surface layer on the body mannequin with limiting the outer border of the 3D body. To generate the mesh surface, the first block pattern with zero fabric thickness values has been used. Besides, the appropriate 3D coordinates have been critically described for devising the surface mesh for realizing the good results. The developed surfaces mesh directly on the 3D female virtual mannequin with zero fabric thickness values will later use as a reference to generate the patterns for different successive layers of the multi-layer panel. The different successive layers will be achieved using defined fabric layer values through shifting outwards.
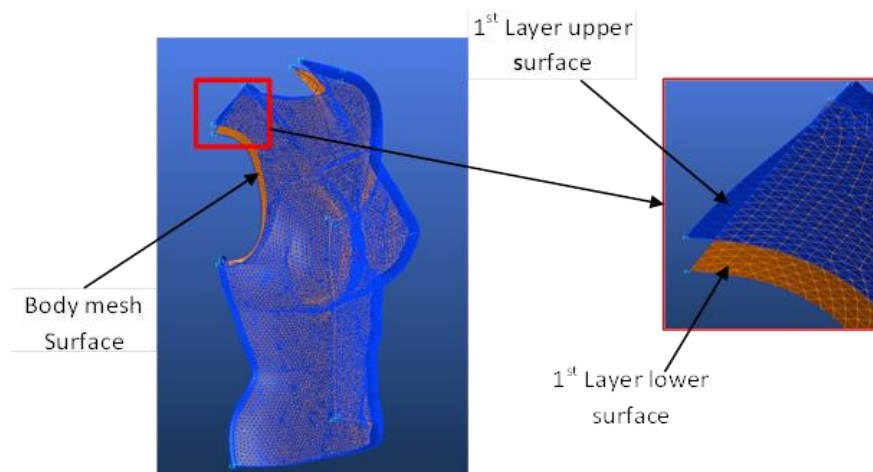
Figure 3.24 3D body mesh creation and generation of 1st layer surface mesh on the front virtual adaptive female body

3.4.4 Multi-layer pattern generation process for woman soft body armour panel

In the multi-layer woman soft body armour development process, generating an appropriate and accurate pattern for each successive layer is very crucial not only to achieve good ballistic protection but also better comfort and fitness. Besides as discussed earlier, the protective body armour panel must be adapted to the human morphology to ensure efficient ballistic protection. It is also obvious that generations of pattern for body armour panel directly on the 3D virtual mannequin will provide better-fitted products on the body and optimizations of raw materials during production [334][335]. However, the currently available 3D CAD software for garment design is not always effective in maximizing the fitness. Considering this, as discussed in subsection 3.2, the pattern for the base layer of woman soft body armour were generated

through an innovative reverse engineering approaches [158]. This approach ultimately helps to see in details how the different garment parts orient itself in free space around the body. Consequently, the more fitted and closer body armour clothing toward the body will provide better ballistic protection due to tight configuration and uniform distribution of impact throughout the surface. This helps to optimize equally the level of protection for the expected energy absorption behaviour of the different parts of the body.

This section will discuss the newly proposed design approach for generating multi-layer patterns directly on 3D virtual woman mannequin. In the multi-layer woman soft body armour pattern generation, it is also obvious that the outer fabric layer will have a larger surface area than the lower consecutive fabric layers due to its high surface coverage. This phenomenon needs to be critically considered while pattern generation process to keep the soft body armour panel covering properly the required woman torso surfaces. Moreover, while generating the multi-layer panel pattern, some critical parameters including the thickness of each layer have to be also considered to achieve a good result. However, the pressure applied between layers during stacking was neglected. For the sake of validation, only five different layer fabrics were used to observe the evolution of the block pattern rather than considering the level of ballistic protection. However, it is also possible to generate the pattern for a higher or lower number of a layer based on the required level of ballistic protection performance (different NIJ standard levels) and layer thickness using the proposed design method. The approach will be more important when the soft body armour garment is developed following the contour shape of the body for good ballistic protection performances and better fitness and comfort.
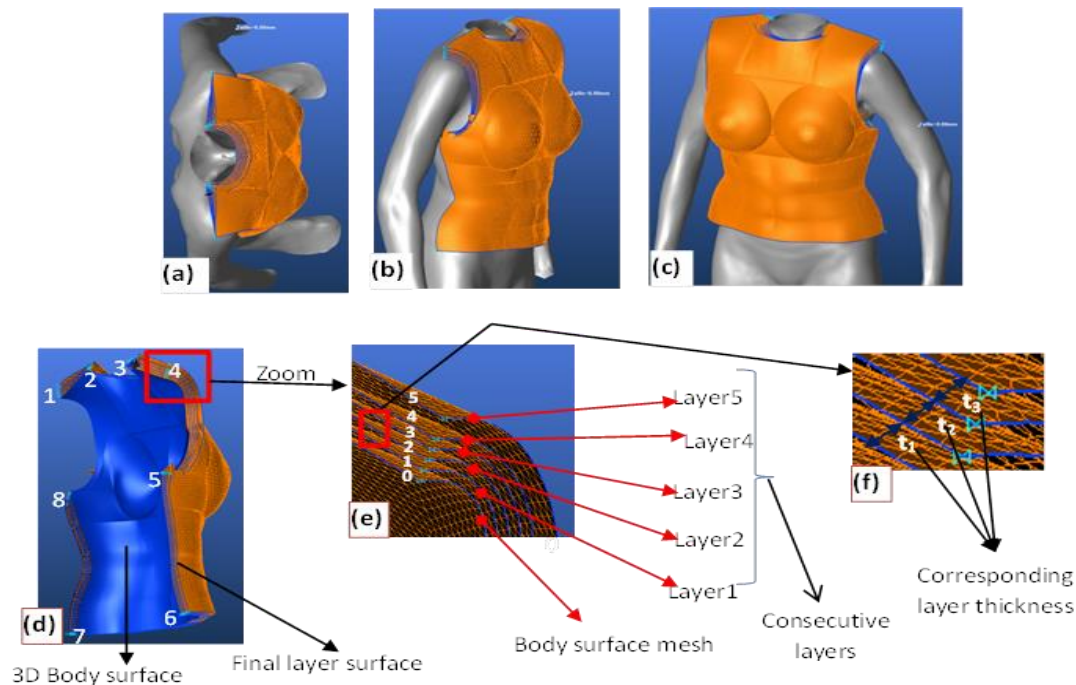
Figure 3.25 Multi-layer seamless soft armour mesh on virtual adaptive women body (a) top, (b) side, (c) Front view, (d) multi-layer meshes on body (e) 5 layers mesh zoomed views of corresponding (5 layers), and (f) each successive layers thickness (t1, t2, t3... tn).

Commercial software from Lectra called 3D design concept was used to numerically simulate 3D mesh and pattern generations of multi-layer women soft body armour panels. Therefore, generating soft body armour pattern design directly on the specific 3D virtual adaptive mannequin could give a very good result for both ballistic protection and fitness. The 3D design process for multi-layer soft body armour pattern generation starts from conceiving an appropriate block pattern for the specific size of the first layer which is close to the body. The surface mesh on the frontal 3D virtual mannequin was generated as described in previous sub-sections. The first surface mesh was generated and defined in a plane parallel to the 3D virtual front mannequin with zero thickness values of the layer (close to the body). The various thickness of the successive fabric layers such as t_1, t_2, t_3… t_n, was coded in the 3D design software which helps to shift the next successive layer mesh in all directions (x, y, and z) with proper coordinate as shown in **Figure 3.25**. Moreover, thanks to such 3D designing software, it is also possible to automatically count the value of gradation for each of the specified measurements at the pre-defined reference (gradation) points to attain each successive layer mesh based on the input values (thickness of the fabric layer). Consequently, the next layer mesh will be generated simply by shifting the values at the already defined coordinate points depending on the space gap of each consecutive layer. The developed meshed for the soft body armour front panel block surface can be then undergone to the flattening operation to generate the corresponding 2D pattern. The generation of flattened 2D patterns also strictly follows the principle of the classical 2D pattern design knowledge (**Figure 3.26 (a) and (b)).** The different successive flattened block patterns for the panel are shown in **Figure 3.26 (c).**
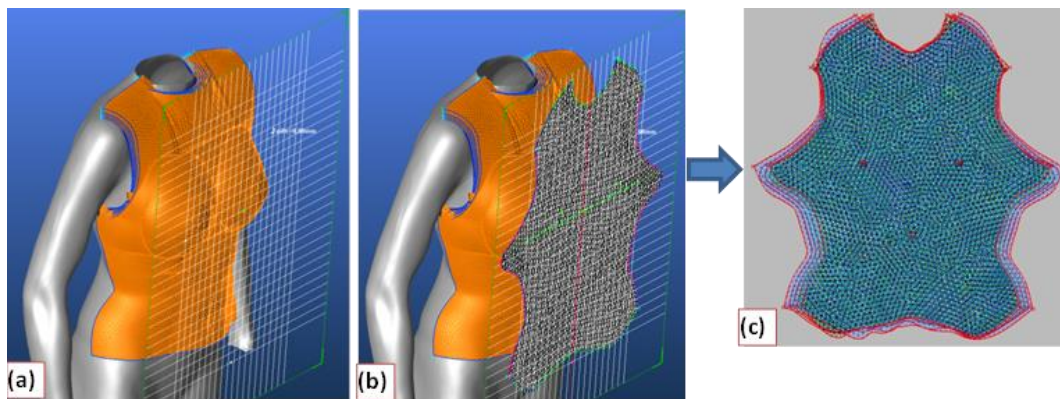
Figure 3.26 Multi-layer pattern flattening (a) projection grids (b) pattern block projection for multi-layer through flattening (c) flattened multi-layer soft body armour panel pattern

3.4.5 Validations of the generated multi-layer pattern

This section will try to evaluate and validate the developed pattern for the multi-layer panel by producing the customized seamless woman front body armour through dome-creation. For better evaluation, textile materials that could possess good bending and flexible (moulding) properties without affecting its ballistic protection performance to achieve better breathability and movement of the wearer are preferred. Besides, bending and moulding properties of the materials become even more important while developing the woman's soft body armour to accommodate easily the curvy body shapes including the bust [166]. This would also avoid

various defects such as wrinkles (around the contact edges of the deformed regions) and excessive shear deformation, throughout intended material zones during the dome-formation (moulding) process. Moreover, unless a better material is used, the density of the materials will never possess the same throughout the area which also leads to different fabric behaviour under force and consequently while moulding. So, to achieve the above advantage and deliver better deep drawing capability, the materials should be manufactured with appropriate and accurate specifications. For this purpose, a fabric having excellent moulding ability properties, 3D warp interlock fabrics made of high-performance p-aramid yarn, were designed and manufactured in GEMTEX, ENSAIT laboratory using automatic dobby weaving machine.

3.4.6 Bust-shaped punch and punching bench for dome-formation

Moulding is one of the most widely used methods to create the required dome-shaped fabric to produce different technical products using either an appropriate pattern design or a moulded model of the final product. Nowadays, it also becomes one of the appropriate methods to create the required woman soft body armour front panel to accommodate the bust area and resembles the shape of the torso without the involvement of darts. This armour design process does not only give the fit and comfort but also eradicates the weakest parts towards the seams while ballistic treats. For the generated pattern validation purpose, the specific right and left bust volume (90B) were virtually obtained using SolidWorks software's from the 3D virtual mannequin (**Figure 3.27 (a)**) and then moulded both in single (**Figure 3.27 (b)**) and double-curved (**Figure 3.27 (c)**) surface bust-shape by the help of 3D printing machine and specialized solid moulding machine respectively.
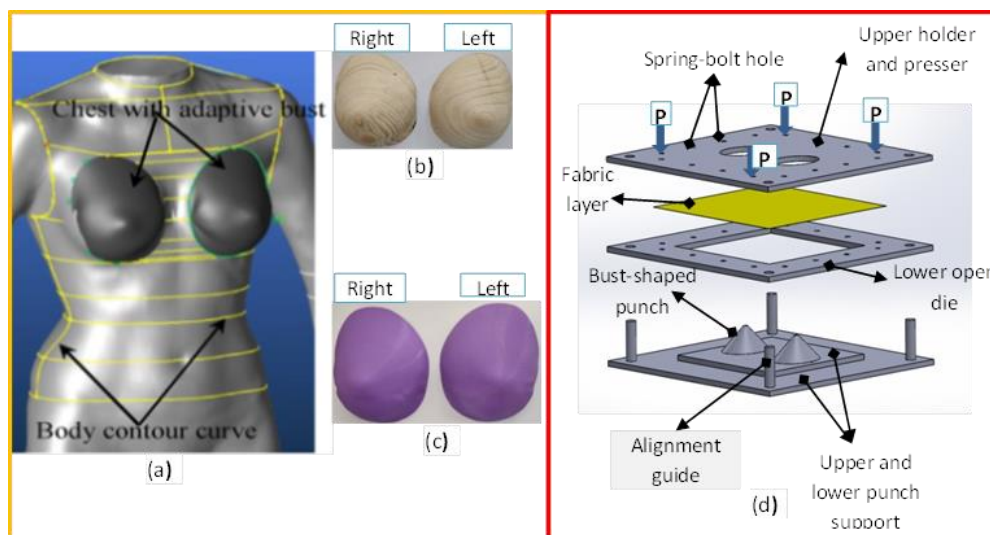
Figure 3.27 90B bust size cup moulding and the punching bench (a) women body with adaptive bust (90B) (b) single-curved (solid) (c) double- curved (surface) paired bust-shaped punch, and (d) schematic view of adapted forming bench set up

The single-curved (solid moulded) bust-shaped was made from wood materials which are mainly used as a punch during the forming process. Whereas, the moulded double-curved (surface moulded) bust was responsible for draping the produced soft body armour on the

mannequin and later for moulding of the plastillina while ballistic testing. Moreover, the specific and adapted punching bench with an appropriate blank holder and open die has been also designed and prepared for the dome-formation of multi-layer soft body panel materials. **Figure 3.27 (d)** shows the schematic diagrams of the non-symmetrical bust-shaped punch forming bench device and it's forming setup. The moulding bench generally composed of a dedicated lower and top static punch support, upper and lower open dies for forming the specimen and apply the pressure for better deformability and bust shaped-punch. The upper holder and the open die were fixed together by spring bolt to sandwich and firmly grip the panel layers while moulding. While dome-formation, the guide on the static punch which supports the lower base was used for proper alignment with the upper-pressure holder and presser plates. Both the right and left single-curved bust-shaped punch was mounted on the lower static punch support to form the required domed shapes on woman soft body armour panels.

3.4.7 Developing process and validations of woman body armour panel

The seamless woman soft body armour front panel has been produced through the moulding process on the produced 3D warp interlock fabrics (5 layers) using the adapted punching bench. **Figure 3.28** shows the dome-formation process of 3D warp interlock fabrics while producing the woman multi-layer soft body armour front prototype. While manufacturing, it is very imperative to consider and indicate the exact positions of the two bust points on each fabric layer to align properly with the punch for better fabric drawing-in values in all directions to achieve the good final frontal armour panel shape as shown in **Figure 3.28 (a).** While moulding process, it is also noticed that applying proper pressure is very critical and should be well considered during compressing the different fabric layers between the upper holder and lower open dies to avoid various fabric layer defects including wrinkling, buckling, high shear on the final panels. After or before the dome-formation process, applications of some kind of fixation between the 3D warp interlock fabric layers especially on the domed bust surface might be good to achieve even more stable shaped panels.

Based on the corresponding thickness of the fabric layers and their surface coverage difference, each consecutive panel layers (the 1st, 2nd, 3rd... n^{th} layers) revealed different patterns sizes as discussed in **section 3.3.5** based on **Figure 3.25.** Obtaining the different sizes of the pattern for each consecutive panel layers helps to align and fit the body at the same contour while moulding**.** Moreover, it is also very important to check and evaluate the alignments of the final shapes the outer contour of each consecutive layer after moulding not only for fitness purposes but also to achieve better ballistic protection by proper coverages.

To evaluate this, after the shaping process of each consecutive layer, the different borderline (contour) of the shaped panel layer were aligned together to check whether the final borderline was on the same line position (**Figure 3.28 (b)).** The alignment of the different consecutive layers of the panel in the borderline (especially on waist and sideline (contour)) after moulding was demonstrated by detaching and observing whether they are aligned or not at one corner of the upper panel layer and a half of the under panel layer as shown in **Figure 3.28 (c).**
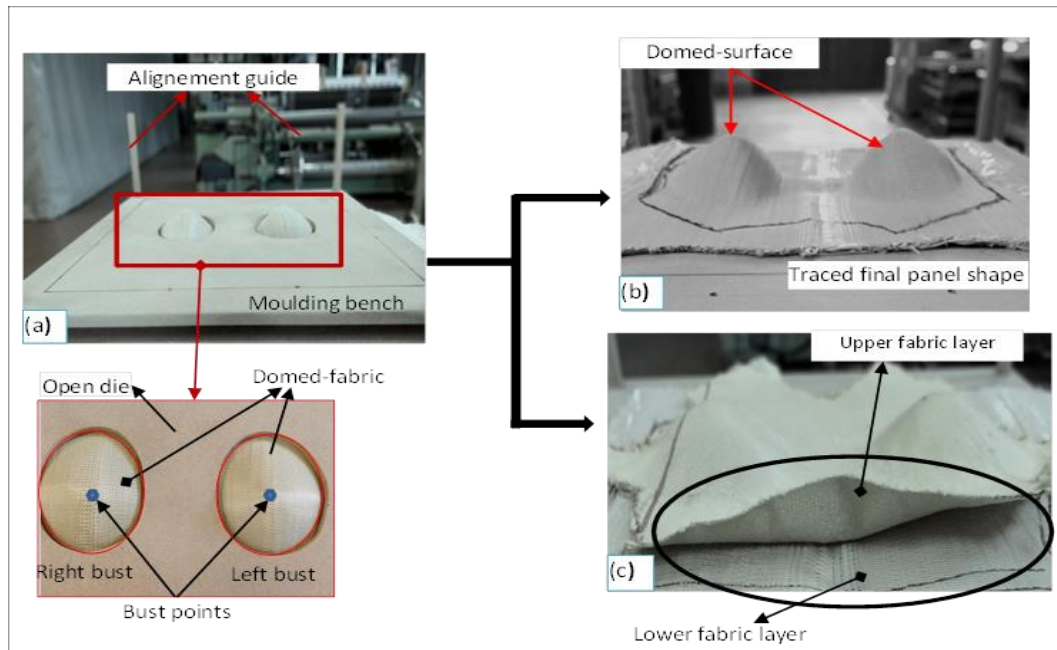
Figure 3.28 Dome-formation and validation of woman seamless soft body armour (a)
Moulding bench set-up and forming of the layer, (b) final domed-shape frontal panel, and
(c) Panel's contour line alignment verification of the different layers after dome-formations

The result revealed that the borderlines of the consecutive layers in the panels found well aligned. Later, the frontal woman body armour panel was also draped on the physical mannequin of a similar body and bust size (90B) for visual observation and validation. **Figure 3.29 (a) and (b)** show the draped woman soft body armour panels from the top and front views respectively. According to the visual observation, the shaped panels were draped well both on the flat and bust area of the respective mannequin.
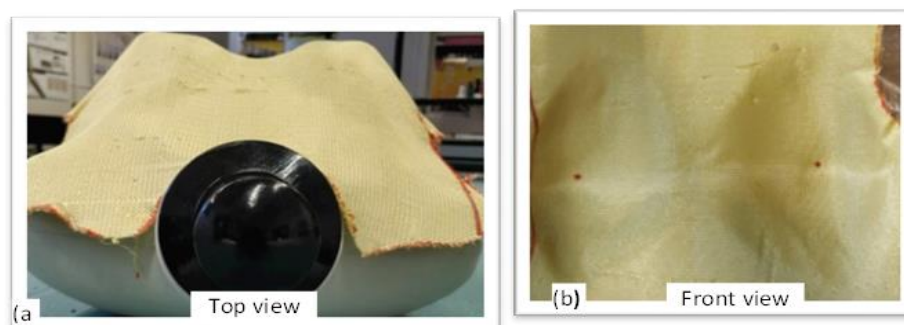
Figure 3.29 Draping of the developed seamless woman soft body armour panels on the physical
mannequin with the right bust volume for fitness observation

With this design and manufacturing process, we have been able to develop a pattern generation method that is also very promising to develop women ballistic vests that are form-fitting without any darting or rigid inserts, such as Shield@ materials. Plies in the vest require no cutting in construction about the same as a male vest.

3.5 Conclusions

For the last few decades, significant efforts have been made by researchers and developers to improve the overall performance of women's soft body armour. However, designing women's soft body armour which accommodates the bust area for different morphological differences with good comfort, fitness, and better ballistic protection is still in great demand. In this chapter, 3D designing process on the virtual mannequins of woman body (90B sizes) was applied to generate the pattern systems for multi-layer seamless soft body armour developments. To achieve this, the current chapter comprises three different sub-chapter and the following conclusions are drawn:

➢ In the first sub-chapter, a novel 3D design process on the 3D women model was introduced to develop an adaptive bust for the specific model (90B). The approach greatly helps to solve the fitting problems of corsetry in general, and specifically women's soft body armour development by using the CAD knowledge in the morphological evolution of the bust. During the design process, first, the digitalized 3D women body model was developed as reference using 3D scanning technology, and then different feature points were defined using cutting marks at different angles both in X and Y coordinates centred at the most inner centre of the bust. These new planes of coordinate create a form network of curves (mesh) on the bust surface to initiate the creation of different bust volumes. The introduced design process uses a single parameter adjustment for varying the volume of the bust. This parametric change will not only reduce the tedious procedure to change the parameter but also eliminate the trial and error methods to conceive the different bust volumes. Testing of the adaptive corset by changing the parameters for conceiving different volumes of bust revealed that using good parameters were all required to get the bust of the correct size. Conceiving the 3D bra patterns on the 3D bust and then comparing it with traditional 2D bra patterns also gave a satisfactory result. The flattening of bra resulting from the different volumes allows us to find a grading rule close to the existing one for this type of model. Moreover, the determination of different volumes of the bust will greatly help for curtailing the current corset problem, i.e. comfort and fitness. This design process will be extended to design not only the corset (bra) but also the fitted and comfortable women's soft body armor protection by associating the frontal body part with different cup sizes.

➢ The second sub-chapter introduced an efficient reverse engineering approach (2D-3D-2D pattern generation) for generating appropriate 2D block patterns from 3D woman adaptive virtual mannequin (90B) for woman seamless soft body armour panel. It uniquely involves the process of projecting a 2D pattern measurement on to the 3D body contour and thus the 3D contour wire is flattened to the 2D surface for developing a 2D block pattern. The method was mainly responsible to acquire the bust volume by eliminating the involvements of darts. The process starts by identifying the different strategic anthropometric points on the front body side contours of adaptive mannequin (90B size bust cup). Both horizontal (weft) and vertical (warp) projection grids in front of the virtual mannequin were then marked to generate a 2D block pattern using the necessary body couture measurements. While projection, an accurate measurement using a precise projection system and bust points has been considered. According to the material deformation analysis based on a 3D-to-2D

flattened pattern, the generated flattened pattern reveals better shape to accommodate the deformation with low distortion throughout the fabric surface while flattening. This will later greatly helps to keep similar fabric distribution throughout the panel and give better ballistic protection, fit-ensured and good comfort for the wearer. Moreover, the proposed approach also used to generate a 2D block pattern for women's body armour front panel with different bust volumes automatically by manipulating only the body contour measurement on the 3D virtual mannequin.

➢ The last sub-section presented and discussed a novel method using a systematic 3D design approach through the parametrization process based on the conceived 3D virtual adaptive woman mannequin to generate block patterns for consecutive layers in the woman body armour front panel. The system uses a previously developed block pattern through a reverse (2D-3D-2D flattening) engineering method for the first layer in the woman body armour panel (**subsection 3.2**) as a base. Parametrization process based on the base layer position (zero value) and the thickness of each layer in the 3D design process database was applied for automatic shifting and generating of each consecutive outer mesh on the 3D virtual mannequin with appropriate coordinates. The different layers of mesh developed on the 3D virtual adaptive woman mannequin were then flattened for the front panel of each successive layer to make a multi-layer pattern design. Even though the modelling and simulation of the mesh have become close to the shape of virtual mannequin body, the frontal soft body armour panel was developed using 3D warp interlock fabrics through moulding process on the adapted bust-shaped punching bench to validate the system. The result shows that the new 3D design approach was found good to generate multi-layer panels block pattern for better shape and fitness of the final garment. Even though the new design approach for multi-layer woman body armour panel layer offers better pattern block projection, an improvement in the manufacturing process in terms of making scientific dome-formation process is required.

4 Quasi-static characterizations of 3D warp interlock p-aramid fabrics

4.1 Introduction

The current research trend in a most textile technical application is to familiarise low-cost manufacturing techniques for advanced material without compromising the overall performances. For the past many years, 2D textile fabrics have been utilised in different technical applications [336][337][25][157]. However, recently 3D woven fabrics were also developed in advanced textile weaving techniques to extensively substitute 2D fabrics. Among the 3D woven fabrics, 3D warp interlock fabrics provide various advantages in most applications. It is involved in ballistic protection [147] due to the enhanced mechanical properties through the thickness direction [304][305] and lightweight [46] as compared to the 2D fabric structure. It can also be efficiently draped with better surface quality and forms a complex shape along with good moulding capability while forming [165]. However, various factors could affect the mechanical and moulding properties of the 3D warp interlock fabrics. Various research studies have investigated the influences of different parameters that affect the mechanical and moulding properties of 3D woven fabrics [338]. Yarn type, yarn properties, weft density, fibre architecture, woven fabric structure, number of layers, weaving process, etc., are among the different parameters which could affect the mechanical and moulding properties of the 3D woven fabrics [339][340][341][342]. For example, the mechanical performances of 2D, UD and 3D woven structures were compared and the result shows that except the tensile strength, the 3D woven fabrics showed higher mechanical properties compared to 2D fabrics [343]. Moreover, the effect of different weft density on tensile strength behaviour of 3D angle interlock woven fabric was studied, and fabric with higher weft density showed better tensile strength performances [344]. Another study also shows the influences of the 3D woven structure (3D orthogonal, 3D throughout angle interlocking and 3D layered angle interlocking) on the fabrics' mechanical properties, especially on bending and tensile properties. In the study, the maximum and minimum bending and tensile modulus of elasticity (MOE) values were recorded for 3D O-L structure and 3D A-T structure respectively, whereas, 3D A-T and 3D A-L structure fabrics show better and lower tensile elongation values respectively [345]. The weft, warp and binder warp yarn have also shown an effect on the tensile property of the 3D woven structures both in warp and weft directions [346]. In the developments of seamless women's body armour, the good forming capability of the textile fabric material avoids the need for cutting and sewing [347] of fabrics not only to properly mimic the upper women's torso shape but also minimize the direct production cost. This finally provides better comfort, fitness and ballistic protection for the wearer. However, unless proper material with good moulding ability used, moulding of the frontal woman armour might create shear deformation, panel thickness variations, and wrinkles on the material which will affect the mentioned performances.

The current chapter investigates and discussed the influences of fabric density on mechanical (bending, tensile and moulding) behaviours of 3D warp interlocks fabrics. The fabric production process, experimental techniques, and approach are designated in the material part. The

outcomes of this chapter help to consider the fabric density while using 3D warp interlock fabrics for different technical applications including women body armour.

4.2 Experimental

The two variants of 3D orthogonal layer-to-layer interlock fabric structure having 5 and 7 weft layers (developed in the production campaign one) based on different yarn density were considered. A rectangular 300 mm X 50 mm samples from each variant are prepared for bending property tests. Besides, the same dimension of samples but adhesively bonded on both ends with an extension of 50 mm are prepared for tensile tests. This would help to avoid errors in load-cell reading of displacements and strains due to the possibility of slippage of the specimens in the machine grip. Besides, the produced 3D warp interlock fabrics and the purchased 2D plain weave fabrics (CT -709) from the Teijin Company made of similar yarn with specific warp and weft densities of the same layers with dimensions of 250 mm X 250 mm were considered for formability test. Specimens for the bending, tensile and formability property test are shown in **Figure 4.1(a), (b) and (c)** respectively.
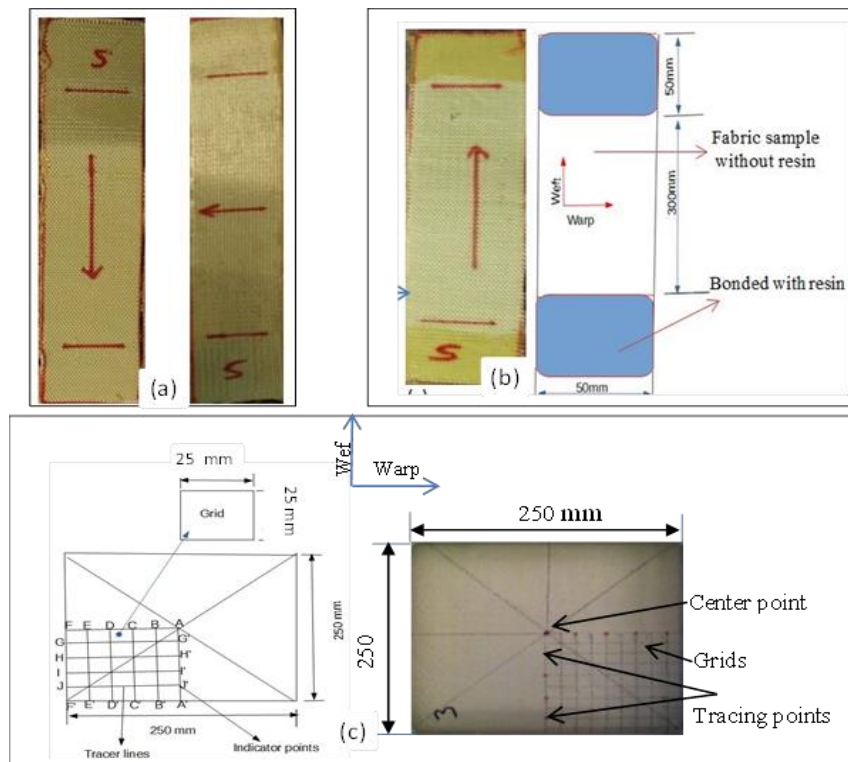
Figure 4.1 Sample specimen preparation for (a) bending rigidity test (b) Tensile property test (c) Forming property test

For better result analysis, all the tests were performed with five replicas of the same specimen both for the warp and weft directions. For the forming test, a tracking mark line and points have been used on warp (AF, G'G, H'H, I'I, J'J and A'F') and weft (AA', BB', CC', DD', EE' and FF') direction with equal distance for better following up, understanding and monitoring of different local deformational during and after forming process. The different indicator marks were plotted on 1/4th part of the specimens with 25 X 25 mm square area each. All the bending,

tensile and forming properties of the mention samples were tested according to the principle and protocol as explained in the methodology section.

4.3 Results and discussions

4.3.1 Effect of fabric density on bending rigidity of 3D warp interlock fabric

 The bending rigidities of the different preforms both in warp and weft directions were computed based on the average bending length, unit areal weight and bending curvature angle using either Equation 2.1 or 2.2 (section 3.3.1.) depending on the testing conditions**.** In general, the bending length of textile materials depends on specific yarn density and the moving ability of weft and warp yarns within the fabrics. For instance, as the weft yarn density increases, the average bending length of the fabric in the warp direction will increase. This is since, as the fabric possesses higher yarn density, the relative mobility of fibres in the yarn or/and yarns in the fabric become restricted. This will result in an increment in the bending lengths of the tested samples [348]. **Figure 4.2** shows the average bending length values of tested 3D warp interlock fabric samples both in the warp and weft directions. Based on the result, there was no clear relationship between the bending length and fabric density as a whole**.** However**,** the yarn density in its particular direction also showed an effect on the fabric bending length values**.** For example, $3DS_1$ has shown approximately the same bending length values both in the warp (11.95 mm) and weft (12.05 mm) direction due to their similar weft and warp yarn density (30 yarns/cm). On the contrary, $3DS_2$ shows higher bending length in the warp (14.65 mm) and lower in weft (11.75 mm) direction due to their respective higher weft (49 yarns/cm) and lower warp (32 yarns/cm) yarn densities. Moreover, due to higher warp (64 yarns/cm) and low weft (35 yarns/cm) yarn densities, $3DS_4$ possesses more bending length in the weft (14.67 mm) than warp (12.65 mm) direction.
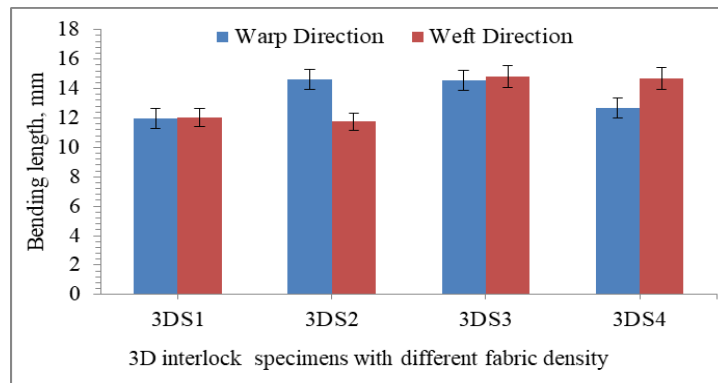
Figure 4.2 Average bending length of 3D warp interlock fabrics in warp and weft directions

Moreover, the $3DS_3$ and $3DS_2$ also possess the maximum (14.8 mm) and minimum (11.75 mm) bending length due to the respective higher and lower yarn densities in the weft direction. **Figure 4.3** shows the relationships between the yarn density and fabric areal density with the fabric bending rigidity of the 3D warp interlock fabrics in warp and weft directions. In general, 2D fabrics having higher yarn density with lower yarn floating shows better fabrics bending rigidity [338]. This due to the increment of yarn density brought higher frictional and

geometrical restraints within and between yarns of the fabric. The bending rigidity of 3D warp interlock fabrics also shows a similar trend with the multi-layer 2D fabrics. Fabric with higher areal density brings better rigidity than with low areal density. According to our investigation, regardless of the variation in the weft or warp densities, the bending rigidity of 3D warp interlock fabrics also depends on the overall fabrics' areal density. For example, $3DS_3$ shows the same bending rigidity in both directions due to its similar yarn density in warp and weft directions (30 yarns/cm). On the contrary, $3DS_2$ revealed lower warp density and fabric areal densities as compared to $3DS_3$. However, the bending rigidity of $3DS_3$ was found higher in weft direction (144.4 µN m) as compared to $3DS_2$ (72 µN m) due to its overall fabric density. Similarly, $3DS_3$ also showed higher bending rigidity in weft (144.47 µN.m) as compared to warp (137.27 µN.m) direction due to its higher warp density (42 yarns/ cm) and weft density (38 yarns/cm) respectively. In a similar trend, the bending rigidity of sample $3DS_4$ is found higher in weft than warp direction due to its higher warp density.
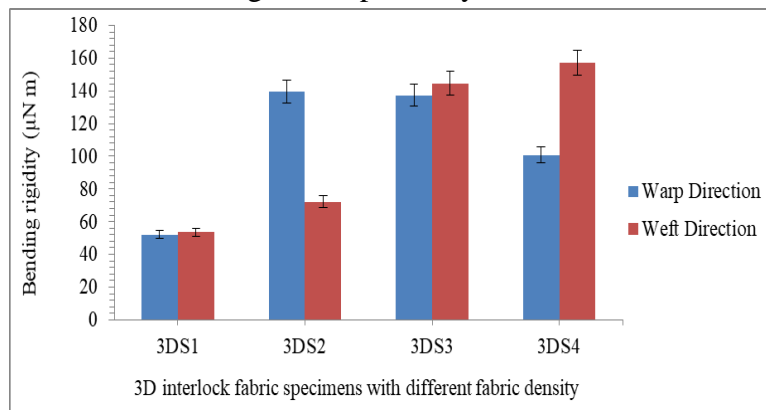
Figure 4.3 Bending rigidity of 3D warp interlock fabric with different areal density in warp and weft directions

From a general point of view, the experimental results clearly show that, besides the effect of overall fabrics areal density, yarn densities in both directions greatly influence the bending rigidity of 3D warp interlock fabrics. The bending rigidity in the warp and weft directions were higher in fabrics having higher weft and warp yarns densities respectively. The bending rigidity ratio of 3D warp interlock fabric in warp and weft directions and its relation to yarn density ratio within the sample specimen is illustrated in **Table 4.1**.

Table 4.1 Bending rigidity and yarn density ratios in warp and weft direction

No.	Samples	Bending rigidity ratio (Warp/Weft)	Yarn density ratio (Warp/Weft)	Fabric areal weight (g/m^2)
1	$3DS_1$	0.975	1	3,115
2	$3DS_2$	1.94	0.65	4,526
3	$3DS_3$	0.95	1.105	4,543
4	$3DS_4$	0.64	1.83	5,074

The results indicate that varying only on the total fabric density does not have a significant effect on the flexural behaviours of the 3D woven fabrics. Homogenous flexural behaviour in both yarn directions was achieved when only both directions' yarn density was found similar. Similarly, the same bending rigidity ratio (Warp/Weft) was achieved for preforms having

similar warp and weft yarn density (having yarn density ratio 1). Higher preforms bending rigidity was observed for those having lower yarn density ratio and vice versa. For instance, $3DS_4$ and $3DS_2$ show lower (0.64) and higher bending ratio (1.94) due to their respective higher (1.83) and lower yarn density ration (0.65). The result suggests that the bending stiffness is directly related to the fabric surface density. Moreover, the fabric bending rigidity was also directly influenced by the yarn density.

4.3.2 Effect of density on the tensile property of 3D warp interlock fabric

All the tensile preforms were tested both in the machine (warp, MD) and cross (weft, CD) orientations until it reaches the maximum deformation states (fracture). During testing, the force and the deformational values of all preforms were measured and recorded.
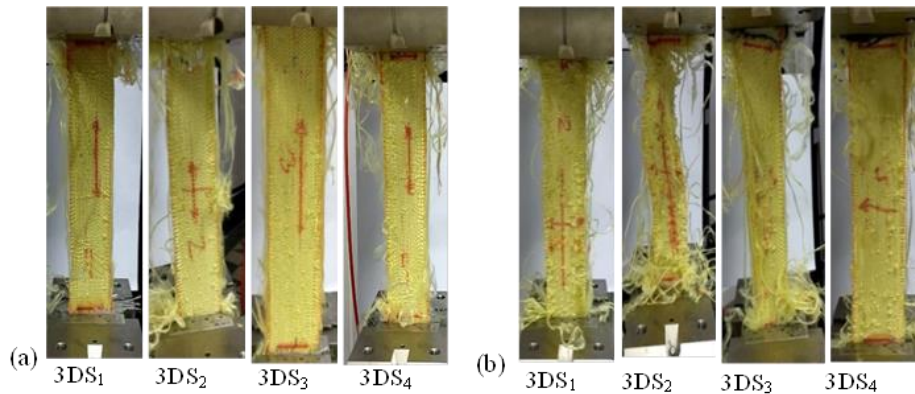
Figure 4.4 Different deformed specimen in (a) Warp direction (MD) (b) Weft direction (CD) at maximum tensile load

Figure 4.4 shows the preforms at its fracture state both in the warp and weft direction. The tensile machine was checked after each test to avoid sliding between the preform and the grip for attaining good values. **Figure 4.5 (a)** and **(b)** show the tensile load (N) vs. strain (%) curves of the average value of the five preforms for each 3D warp interlock fabrics in the warp and warp directions. The tensile loading response was found more or less similar for all tested specimens of each 3D warp interlock fabric preforms in both directions. Based on these graphs, both curves have shown very similar progression as the tensile load increases with higher strain values. In general, the strain vs strain curves can be divided into two parts. The 1st part of the non-linear curve revealed smaller load vs. strain values due to mainly the alignments of the yarn inside the fabric took sometime before real deformation in the specific load direction. Besides, the strain values start to increases with small increments of tensile loads. On the contrary, the 2nd part of the curve has shown a linear progression where real straightening of yarn inside the fabric with the rapid growth of tensile loads. The tensile load has been increased until the preform reaches its breaking point. $3DS_2$ shows a higher maximum tensile load with a higher strain in the weft direction. However, samples $3DS_1$ and $3DS_4$ present weaker maximum tensile load at higher strain than sample $3DS_2$ and $3DS_3$. This indicated that yarn density in the specific direction shows a great influence on the tensile behaviours of the 3D warp interlock fabrics. Moreover, as shown in **Figure 4.5 (b)**, similar to weft direction, the maximum tensile loads with the strain in the warp direction depend on the yarn density. Samples $3DS_4$ and $3DS_3$ shows

higher maximum tensile load with the higher strain in the warp direction as compared to sample $3DS_1$ and $3DS_2$ due to their respective yarn density. In conclusion, higher yarn density in the respective warp or/and weft direction increases the maximum tensile load with maximum strain while deformation.
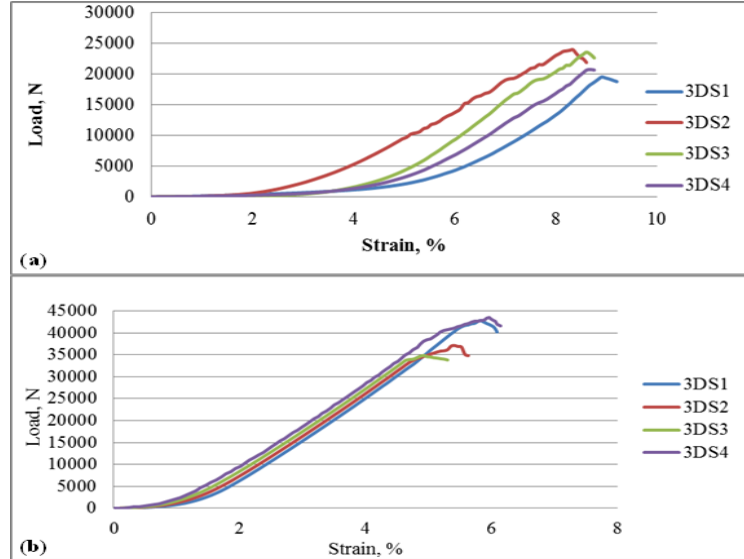
Figure 4.5 Tensile load (N) vs. strain (%) curves of 3D warp interlock fabrics in the weft (a) and warp (b) directions

4.3.3 Effect of fabric density on forming property

The effect of yarn density on the forming and its recovery properties of 3D warp interlock and 2D plain weave para-aramid fabrics have been analysed and discussed in these sections. Different important parameters including blank holder pressure and velocity of the punch have to be properly considered throughout the forming process for better deformability results [318]. Based on the preliminary test result, the suitable pressure to give the required mould for the sample without creating either folding or yarn breakage was found 2 bars (0.2MPa) of blank-holder pressure. For better analysis, our study considered 2 bars (0.2MPa) for blank-holder pressure for all the samples while clamping.

All the samples were also tested with a constant stamping velocity of 45 mm/s and a stamping punch of 100 mm diameter. The Maximum forming deformation depths for all specimens were specified at 65 mm. The local and global moulding behaviour at different positions was studied using a non-contact measurement method (as discussed in methods and material section 3.3) by capturing a picture using a digital camera located on the top of the forming bench**.** Finally, the formed sample (**Figure 4.6**) was removed gently for analysis of different formability properties such as material draw-in, the in-plane shear angle, deformation recovery etc. For this study, the analysis was made considering material while deformation (a) and after full recovery (b).
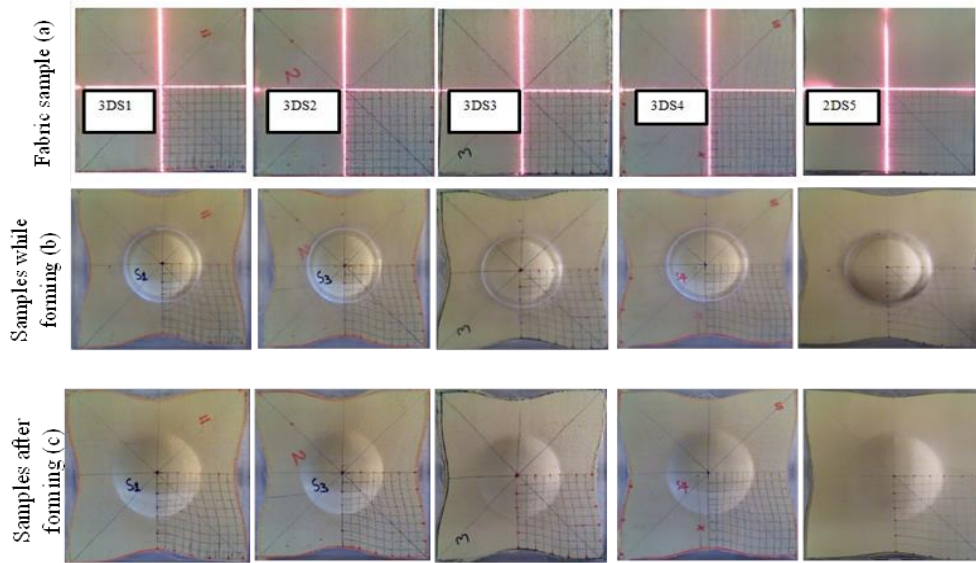
Figure 4.6 (a) Different 3D warp interlock and2D weave fabric samples (b) sample while deformation and (c) after recovery

4.3.3.1 Punching force vs. time and displacement while forming process

In the forming process, constant load by a hemispherical punch which is controlled by an electric jack with sensors were applied for measuring the applied force, control and measure its position and speed. Applying proper punching force is vital not only to deform the preform properly but also to avoid unnecessary preform slippage and wrinkling. During forming, the punching load along with its corresponding average punching time was automatically recorded. **Figure 4.7** shows both load vs displacement and load vs. time curves while forming different 3D warp interlock preforms.
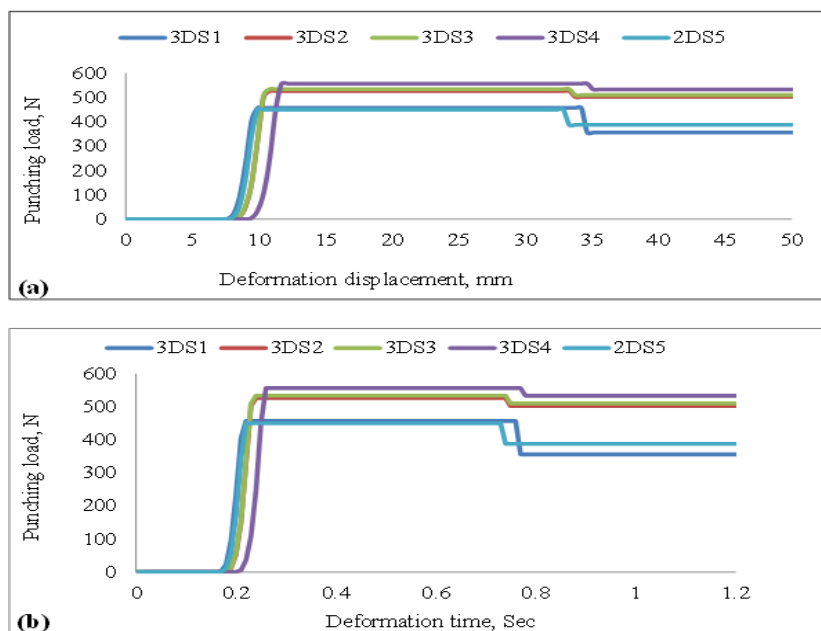
Figure 4.7 Stamping force vs. moulding time relationship while deformation of different preforms

All the external and internal parameters were kept constant while stamping the different preform for better comparisons. Based on the curve, all the 3D warp interlock preforms show similar trends of load vs. time curve evolution with various categories. For example, the punching force shows insignificant load amount at the beginning of the curve and later rapidly increased through time while deforming the preform until maximum deformational height has been achieved.

When the deformed preform reached the maximum deformational height, the loads become constant due to the inertia effects to keep the final deformed shapes as shown in the load-time graphs. Besides, the result clearly shows that sample with higher fabric density, $3DS_4$, possesses higher punching load with time to attain the maximum deformational shape. Meanwhile, the sample with lower fabrics density, $3DS_1$, faces lower stamping load as compared to other 3D warp interlock preforms. Moreover, both $3DS_2$ and $3DS_3$ show a similar curve trend and quasi-equal punching loads throughout the curve due to their very close fabric density. On the contrary, $2DS_5$ also shows higher stamping load vs. time as compared to 3D warp interlock preform with similar fabric density ($3DS_1$). Similarly, since the deformation is directly related to the load, $3DS_4$ and $3DS_1$ demonstrate maximum load vs displacement and minimum load vs. displacement respectively. Moreover, fabric density is directly proportional to the punching force for moulding the different preforms to achieve the predefined maximum deformation. This is because the sample with high fabric density is more rigid and consequently needs high punching loads than smaller fabric density preform.

4.3.3.2 Material drawing-in value while forming

In the hemispherical punch moulding process, the length of the preform both in warp and weft directions were mostly deformed and consumed toward the centre of the preform. The consumed length also called material draw-in depends not only on external factors such as blank holding pressure, punching force, punching velocity, punching diameter and depth but also on the material factors including the type of material used, number of layers, fabric density, fabric architecture etc. Usually, the values are observed and analysed through capture images during the forming process. In the quasi-symmetric hemispherical moulding process, the drawing-in values were assumed to be similar in the preform four-quadrants (**Figure 4.8**).
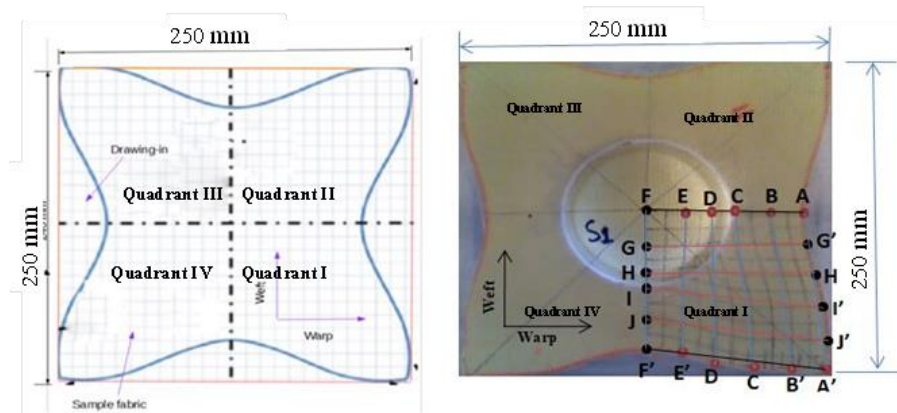
Figure 4.8 The photographic and schematic diagram of sample material drawing-in while deformation

For this study, the right side below the position of the quadrant (Quadrant I) drawing-in values were studied considering it could represent the other quadrants (Quadrant II, III, and IV). Three specimens for each 2D plain weave and 3D warp interlock fabric types were tested and the average value was represented. For better comparison and understanding of the influences of warp and weft yarn densities on the material drawing-in values, all other internal and external factors were considered constant. **Figure 4.9** shows the effects of yarn density on the drawing-in values of 3D warp interlock fabrics and compared with the sample made with corresponding 2D plain weave fabric. Based on the result, even if the fabric density has an impact on formability, the material drawing-in values were specifically affected by the weft and warp yarn densities in its respective directions. For example, $3DS_1$ demonstrates the higher drawing-in value in most of its parts than other preforms both in the warp and weft directions.

On the contrary, $3DS_4$ revealed very less drawing-in values as compared to the other 3D warp interlock samples in the warp direction. Besides, $3DS_4$ shows better drawing-in value in the weft direction compared to 3D warp interlock fabric preforms. However, as described in the **material section**, $3DS_4$ has higher overall fabric density in comparison with other preforms. This is also supported by sample $3DS_2$, where it has shown higher drawing-in value as compared to $3DS_3$ and $3DS_4$ in warp direction than weft direction. Moreover, the highest drawing-in values for all preforms were achieved at the central points of the four sides around the top ply (point FF' and point AF in weft and warp directions respectively). The lowermost values were achieved at the corner edges of the preform (point AA' and point A'F' in weft and warp directions respectively). The values were found inversely proportional to the yarn density in their respective directions. For example, $3DS_1$ which has less warp yarn density displays maximum central drawing-in values in warp direction (point AF) as compared to other preforms. Whereas, $3DS_4$ which has higher warp density and less weft density as compared to the other 3D warp interlock fabrics demonstrates minimum and maximum drawing-in value in the warp (Point AF) and weft (point FF') directions respectively.
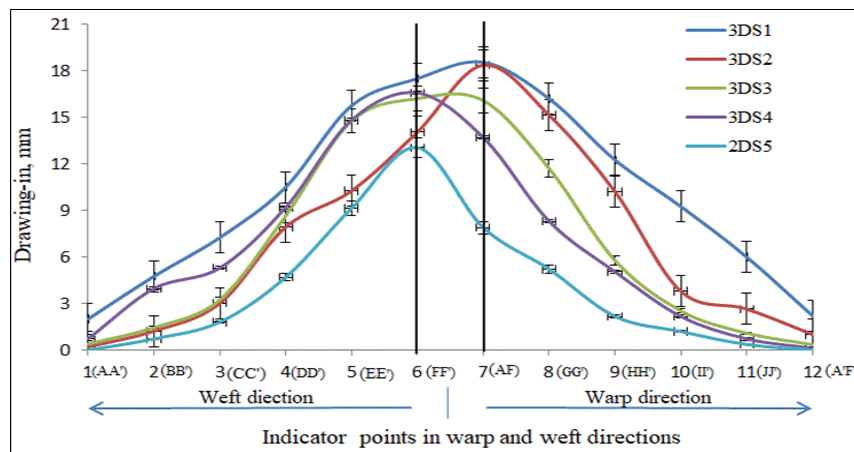
Figure 4.9 Drawing-in values at different selected points in warp and weft directions for preforms

The weave diagram of the 3D warp interlock preform has also an effect on the drawing-in values. For example, $2DS_1$ shows lower drawing-in values in maximum central points as well as other indicator points as compared to all other 3D warp interlock fabric preforms both in warp and weft directions. This is due to the stiffer property of 2D plain weave fabric that provides less

formability as compared to the respective 3D warp interlock fabric preforms. In conclusion, regardless of the fabric's areal density, both warp and weft yarn densities greatly influence the preform drawing-in values in their respective directions. As the yarn density increases, the drawing-value decreases in its respective direction. This is because, as the yarn density increases, the fabrics become more compact, stiff and dense not only to resist the deformation but also exhibit higher frictional coefficient among yarns to absorb the punching force.

4.3.3.3   In-plane surface shear angle while deformation

During moulding, the textile materials will undergo a huge deformational process to adapt various complex shapes, i.e., hemispherical punch. In multi-layers fabrics, inter-ply and intra-ply shears are the most common phenomenon which existed while forming. The phenomenon determines how the fabric will behave when subjected to a wide variety of complex deformations. Even though a small and limited degree of stretchability in the yarn directions may occur in woven fabric forming due to non-crimping of the yarns, intra-ply shear is a must to allow a textile preform to conform to a formed curvature. Besides, such type of deformation is characterized by a change of fibre orientation, due to rotation of the yarns at their crossover points. The amount of in-plane shear is indicated by a shear angle μ, which is defined as the complement of the enclosed angle, (α and β), between the warp and the weft yarns as indicated in **Figure 4.10 (c)**. The in-plane shear angle can also bring the most common and global phenomenon which causes unexpected failures depending on force and strain components of moulding called wrinkling [349][350]. The inbuilt camera was used to capture the in-plane shear angle then and measure using ImageJ software as demonstrated in **the method section.**
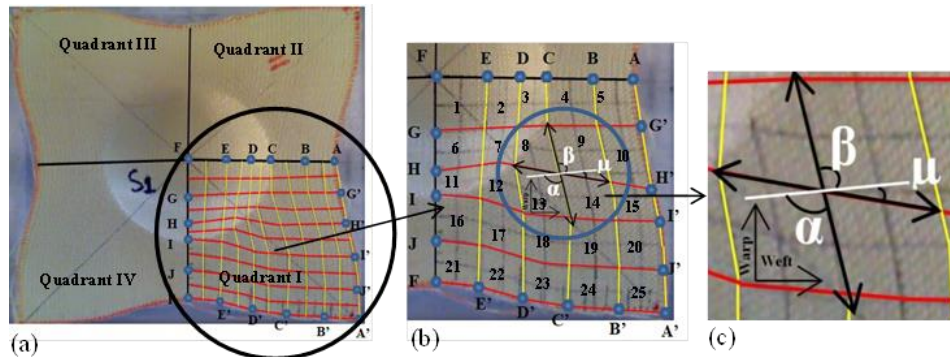
Figure 4.10 (a) Preformed sample, (b) Quadrant section for shear angle measurement, and (c) Surface shear angles measurement

The in-plane shear was considered in the area where less or no wrinkling effect is found. The wrinkling surface might cause exaggerated shear angles and will not give better result among the preforms. Similar to material drawing-in value measurement, due to quasi-symmetric moulding by hemispherical punching, the average in-plane shear angle values of one quadrant (Quadrant I) moulded surface were considered. This deformed surface average shear angle values for each sub-divided region (region 1, 2, 3 …25) were assumed to possess similar values as of the other three quadrants (Quadrant I, II and III). As discussed earlier, angles α and β show the angle between warp and weft yarns at the initial position before deformations. Whereas, shear angle (μ) is the difference between the extended angles measured while deformation from the initial position. **Figure 4.11** shows the in-plane shear angle measurement of different

preform after moulding process. For better understanding and analysis, we have segregated the different angle measurements and designated them with different colours in the diagram's sub-region as shown in **Table 4.2**.

As shown in **Figure 4.11**, even though there was no very clear relation, $3DS_1$ and $3DS_4$ show higher and lower in-plane shear angle values as compared to the other preforms in majority or all sub-regions respectively. The increments of fabric density have revealed a decrease in the in-plane shear angle values of the sub-region. This might be due to the increments of yarn density which brings the yarns closer and compress each other in the specific sub-region. Consequently, the compressed yarns can increase the shear angle value which later has a probability of reaching the shear locking point.
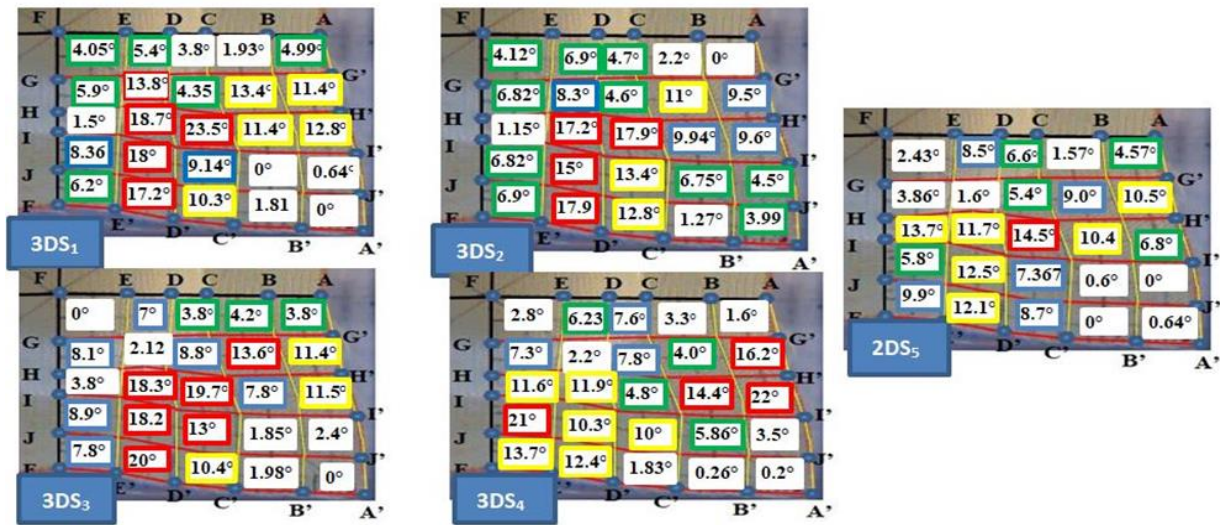
Figure 4.11 In-plane surface shear angle of different sample preforms at different regions

Besides, the maximum shear angles in the sub-region were observed around the neck of the deformed region (22, 17, and 13) for most of the preforms. Whereas, sub-regions around the edge end of the preform possess lower shear angle values while deformation for most preforms. Sub-region 1, 5, 19, 20 and 25 with the shear angle of 0° and region 13 with a shear angle of 23.5° were recorded as minimum and maximum shear angle values respectively.

Table 4.2 In-plane shear angle segregation in sub-regions

No.	Range of shear angle	Designated colour for region
1.	0 – 3.99	White
2.	4 – 6.99	Green
3.	7 – 9.99	Blue
4.	10 – 13.99	Yellow
5.	≥ 13	Red

4.3.4 Effect of density on forming recovery performances

Forming recovery can be expressed as the ability of the material to resist the permanent deformation through a time when faces with the predefined forces. Like other material, textile fabrics used in the different technical applications have a probability of retraining to its initial

position after forming with a specific amount of load. Moreover, a dry 3D woven fabric also faces these time-dependent moulding recovery behaviours to a significant extent as compared to most composite materials. In this particular section, the different forming recovery behaviours of 3D warp interlock fabric samples with various fabric densities by maintaining other internal and external parameters will be discussed. **Figure 4.12** shows the schematic and photographic descriptions of formability recovery of drawing-in values (ΔL), punching displacement at maximum height (ΔH) and in-plane shear angle values after deformation (Δμ) of 3D warp interlock fabrics. For comparison, dry multi-layers 2D plain weave having similar fabric density and number of layers were also investigated. All the preforms before and after the process were kept in the standard atmospheric conditions (20°C at 65% RH) for 48 hours to avoid the effects of different external parameters during and after the process. Each preform was also gently taken out after forming process and kept into a flat position for better-recovered values measurements at different positions.
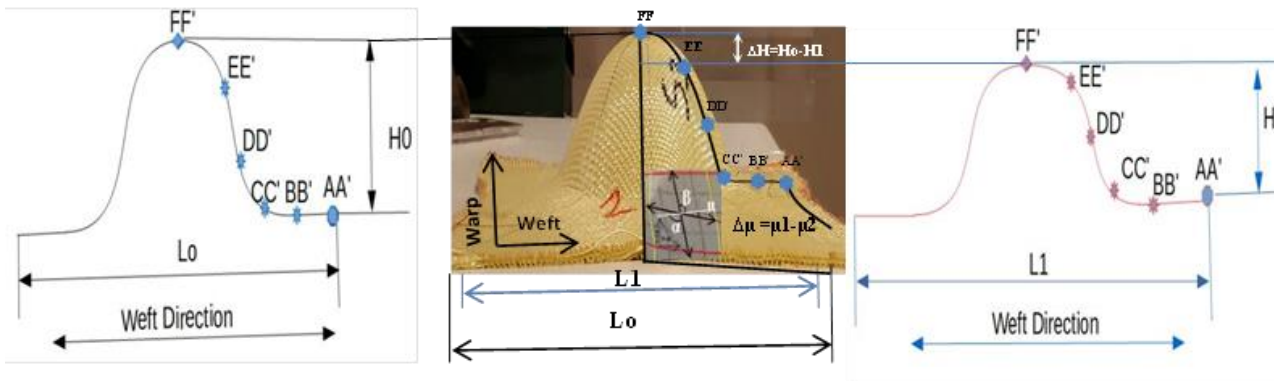
Figure 4.12 Moulding recovery of draw-in, maximum height, and shear angle after deformation

Even though a full understanding of textile moulding recovery behaviours from imposed strain is complex due to its structural element interaction of textile mechanics [351], the study tried to use some quantitative measurement for better analysis and understanding.

4.3.4.1 Forming recovery at maximum height displacement

The maximum height is the point where maximum deformation takes place in the punching direction. The forming recovery of different 3D warp interlock fabrics made with different fabric density at the pick height ('indicator' point FF') has been measured and analysed.
The maximum deformation recovery displacement (ΔH) was given as follows;

$$\Delta H = H0 - H1 \tag{4.1}$$

Where,

ΔH - is maximum height recovery at the centre,

H_0 - is the displacement of deformation when moulding,

H_1 - is deformation after moulding within 48 hours in standard conditions.

The percentage of recovery after deformation has been calculated by the following formula;

$$\%\Delta H = \left(\frac{\Delta H}{H0}\right) \times 100 \tag{4.2}$$

Where, %ΔH is recovery percentage

In the hemispherical forming process the preform was deformed till the fixed maximum deformation height (H_0 = 65 mm) at the centre of the preform. **Figure 4.13** shows the maximum height deformational recovery of different 3D warp interlock fabrics with various fabric densities and 2D plain weave fabrics. 3D warp interlock fabrics with higher fabric density possess a lower deformational recovery percentage as compared to the fabric with lower fabric density. $3DS_1$ having a fabric density of 3.115 kg/m^2 demonstrated a higher deformational recovery percentage in height position as compared to $3DS_2$ (fabric density of 4.526 kg/m^2), $3DS_3$ (fabric density of 5.543 kg/m^2 and $3DS_4$ (fabric density of 5.074 kg/m^2). In these investigations, $3DS_1$ and $3DS_4$ noted maximum (9.23%) and minimum (3.08%) deformational recovery percentage respectively.
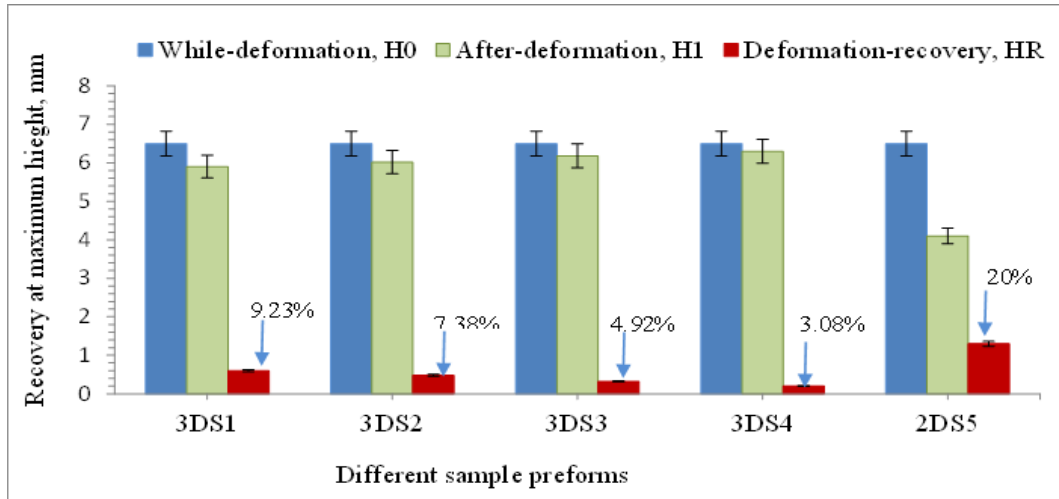
Figure 4.13 Maximum height recovery for moulded 2D and 3D warp interlock fabric preforms

This might be due to 3D warp interlock fabric having less fabric density and then faces lack of additional force to lock the yarn, which resulted to low binding force within the yarns to recover from the initial dimension. On the contrary, when the fabric density increases, the inter-layer strength and mechanical connection within the layers will increase. This leads to higher inter-yarns friction (restrict the free-flowing of yarns) and increases the resistance of the fabric to recover easily after releasing the applied punching load. Besides, as shown in **Figure 4.13,** $2DS_5$ has also demonstrated better height deformational recovery (20%) as compared to its counterpart $3DS_1$ (9.23%). In general, fabrics density was found one of the factors which affect the maximum height deformational recovery of dry 3D warp interlock fabric preforms.

4.3.4.2 Drawing-in recovery after deformation

3D warp interlock fabrics are also undergone a drawing-in recovery after the punching load is removed. The drawing-in recovery value (ΔL) is usually computed by subtracting the initial drawing-in value (L_0) from the relaxation values (L_1) which were measured after releasing the load in 24 hours as shown in **(Equation 4.3)**. As discussed earlier, the average values of a quadrant (Quadrant I) region were selected as representatives of the other three quadrants due to their quasi-symmetric moulding behaviours. Different tracer points were systematically plotted in weft and warp edges of the preforms to investigate the drawing-in recovery values of 2D plain and 3D warp interlock fabrics in both directions. In general, the material drawing-in recovery at different points are computed as follows:

$$\Delta L = (Lo - L1)/2 \tag{4.3}$$

Where,

ΔL = material drawing-in recovery,

L_0 = drawing-in values at immediate forming,

L_1 = drawing-in values after relaxation for 24 hours. **Figure 4.14 (a) and (b)** shows the material drawing-in recovery of 3D warp interlock fabrics having different fabric density and 2D plain weave fabrics in warp and weft directions. As illustrated in **Figure 4.15 (a)),** besides the fabric density the yarn density influences the drawing-in recovery of 3D warp interlocks fabrics in the corresponding direction. For example, $3DS_1$ reveals higher drawing-in recovery in weft direction than $3DS_2, 3DS_3, 3DS_4$ and $2DS_5.$ Whereas, $3DS_2$ shows the minimum drawing-in recovery in the weft direction as compared to other 3D warp interlock preforms. Like the drawing-in value, its recoveries were affected by the respective yarn densities. For example, as the preforms yarn density in the measured drawing-in direction increases, the drawing-in recovery tends to reduce. In comparison, $2DS_5$ recorded higher drawing-in recovery values than its corresponding sample made of 3D warp interlock fabric with similar fabric density ($3DS_2$) in both directions **Figure 4.15 (b)** shows the draw-in recovery value of 3D warp interlock fabrics and 2D plain weave fabric preform in the warp direction. $3DS_4$ and $3DS_1$ show the minimum and maximum draw-in recovery in the warp direction respectively. Whereas, $3DS_2$ shows better recovery than $3DS_3$ in the warp direction in majority tracer points. Moreover, it is observed that the recovery was higher around the centre with higher drawing-in values and minimum around the corner edges of the preform for both warp and weft directions.
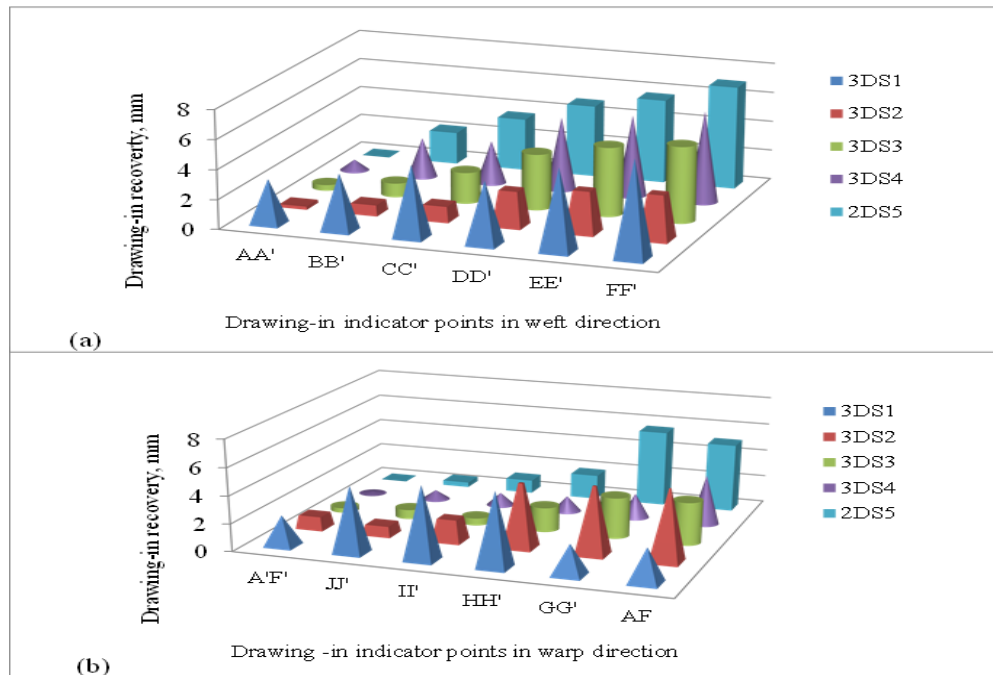
Figure 4.14 Material drawing-in recovery of 2D and 3D warp interlock preform at different indicator points in weft (a) and warp(b) direction

4.3.4.3 In-plane surface shear angle recovery analysis

In-plane shear is one of the most important deformational modes especially in woven fabric moulding deformed by the double-curvature punch. Like other moulding characteristics, woven fabrics have also undergone in-plane surface shear angle recovery after the load is released. It is defined as the angle difference ($\Delta\mu$) between the in-plane shear while deformation ($\mu1$) and the measured shear angle ($\mu2$) after the loads are removed. Due to quasi-symmetric moulding behaviour, here the average values of one quadrant (Quadrant I) were also used for discussion as representatives of the other quadrants. The quadrant was systematically divided using different sub-regions of the sample preforms. **Table 4.3** shows the in-plane shear angle recovery within the sub-region which is categorized with a range of 2° using predefined colour for better understanding and analysing of the different shear angle in the given sub-regions.

The in-plane shear angle recovery at different sub-regions is computed as follows:

$$\Delta\mu = |\mu1 - \mu2| \qquad\qquad\qquad (4.4)$$

Where,

$\Delta\mu$ - is in-plane shear angle recovery,

$\mu1$ - is in-plane shear angle measurement immediately after deformation,

$\mu2$ - is the in-plane shear angle of preform after 24 hours since deformation.

Figure 4.15 illustrated the different in-plane shear angle recoveries of preforms made of 3D warp interlock and 2D plain weave fabric preforms for the selected quadrant (Quadrant I). Based on the result, a clear relationship was not found among the in-plane shear recovery and 3D warp interlock fabric densities. However, fabrics with higher fabric density show very less recovery as compared to fabric with lesser density.

Table 4.3 In-plane shear angle recovery designation

No.	Range of shear angle recovery	Designated colour for region
1.	0 – 1.99	White
2.	2 – 3.99	Green
3.	4 –5.99	Blue
4.	5 – 6.99	Yellow
5.	7 – 8.99	Red

For example, $3DS_1$ shows more shear angle recovery in most of the selected sub-regions as compared to sample $3DS_2$, $3DS_3$ and $3DS_4$. Whereas, $3DS_4$ demonstrates the minimum shear angle recovery than the rest 3D warp interlock preforms in most sub-regions.
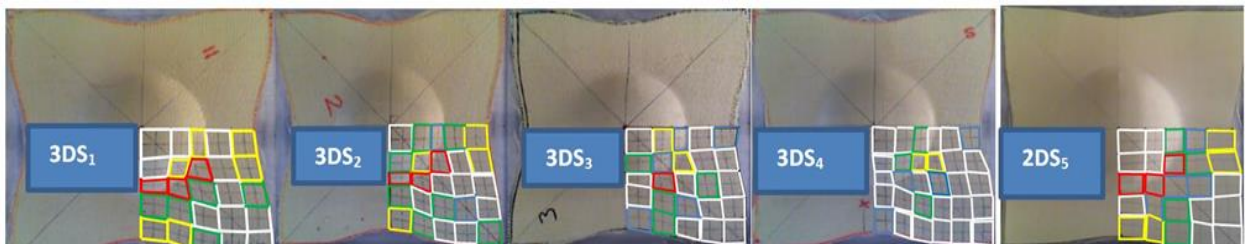
Figure 4.15 In-plane shear recovery of 2D plain weave and 3D warp interlock fabric preforms

As the fabric density increases, the fabric will be more rigid with high inter-yarns frictional resistance to recover from the deformed positions. $2DS_5$ also shows more shear angle recovery not only compared to 3D warp interlock preform with similar fabric density but also all 3D fabric preforms in a majority of sub-regions. Besides, higher shear recovery was observed mostly around the neck (sub-region 7, 8, 11, 12) and centres (sub-region 5, 10, 21, 22) than the edges (sub-region 15, 20, 24, 25) of the deformed samples.

4.4 Conclusions

This sub-chapter comprehensively investigates the influences of fabric density on the tensile, bending and moulding behaviours of 3D orthogonal warp interlock fabrics. The produced four 3D woven fabrics made of 168Tex p-aramid Kevlar yarn with different fabric density were considered (material section). 2D plain weave fabric with specific fabric density was also considered for comparison. Based on the result, the following conclusions were outlines:

➢ The bending rigidity of 3D warp interlock fabrics with higher fabric areal density shows higher values than low areal density. For example, even though $3DS_2$ shows higher weft density since it has lower areal density than $3DS_{3,}$ it possesses lower bending rigidity in the weft direction. Besides, the average bending curvature of the preform showed sharp bending curve with a reduced angle as the density of the yarn increases in the same bending direction. Moreover, the fabric becomes very stiff and faces resistance to bend in the higher yarn density direction.

➢ The tensile strength of 3D warp interlock fabric was also influenced by the yarn densities in the respective directions. As the yarn density in their respective warp or/and weft directions increases, the maximum tensile load with maximum strain also increases in specific directions. For example, $3DS_4$ and $3DS_2$ show maximum tensile load and maximum strain in the warp and weft directions respectively.

➢ Higher punching load vs. time to attain the maximum deformational shape was observed in the 3D warp interlock preform with higher fabric density. This is because preforms with high fabric density are more rigid and consequently need high punching loads than the smaller fabric density preform. On the contrary, $2DS_5$ showed higher punching load vs. time and displacement as compared to sample $3DS_1$ with similar fabric density.

➢ Even though the overall fabric density showed an effect on the deformability, the drawing-in values in specific directions were mainly influenced by the respective yarn densities. For instance, $3DS_1$ and $3DS_4$ demonstrate higher and lower drawing-in in a majority of edge indicator points as compared to other preforms in the warp direction. Whereas, $3DS_4$ shows better draw-in in the weft direction due to its lower yarn density in the same direction.

➢ Besides, even though there was no clear relationship between the in-plane shear and its recovery values with the fabric density; in general, the higher the fabric density reduced the in-plane shear angle and its recovery of the sub-region. For example, $3DS_4$ and $3DS_1$ show a higher and lower shear angle as compared to the other preforms. This might be as the yarn density increases; the yarn comes closer and compresses each other to create a more rigid fabric with high frictional resistance between them. This helps to resist the shear angle formation and recovery from the deformed positions.

5 Effects of internal structures of 3D warp interlock p-aramid fabric on its mechanical and forming behaviours

5.1 Introduction

Textile materials nowadays have been widely used in more advanced applications including composite reinforcement for military, aerospace, transport, etc. applications. However, unlike conventional applications such as clothing and home furnishing, fabrics involved in advanced applications should possess various outstanding mechanical and moulding performances. For the last many decades, 2D woven fabrics in the form of plain, twill and satin and UD fabric structures were more commonly used and well-discussed regarding their mechanical and moulding performances under different loading conditions [352]. Different research studies have also studied and used 2D, UD fabric structure to develop various soft body armour panels [90, 353, 354]. Apart from 2D and UD fabrics, recently 3D woven fabric also becomes the most promising material to be used in many applications including woman soft body armour development as protective solutions [2, 33, 34, 262], fibrous reinforcement for composite as well as other technical applications. The fabric provides good mechanical and an improved capacity to absorb energy by higher intra-ply resistance to delamination [355][143][356][24, 132, 148]. Besides, while developing women soft body armour, not only the ballistic performances but also good bending and moulding properties without affecting the final performances of the product become even very crucial. Various studies have also studied on the formability behaviour and agree on its capabilities on low shear rigidity and excellent formability behaviours [33][166][332][357][33][163][34][358] for 3D shape solutions. This is mainly due to the linking of different yarns through various weave diagrams at the required thickness to substitute the traditional (2D and UD) fabrics. It becomes more important when the women soft body armour is designed and developed through moulding of the textile materials to form properly the intended three-dimensional women frontal torso without involving any kind of stitching system [36][37][25, 88, 219]. The involvement of different internal structures inside the fabric help to provides good mechanical properties and delivers good ballistic performance for the 3D woven fabrics. Achieving all those performances in the textile fabric is one of the most important steps. However, the mechanical and moulding properties of 3D woven fabric are much different from the conventional 2D and UD fabric due to their complex structure. This makes it very interesting to understand the overall mechanical and moulding behaviours of a 3D woven fabric before recommending to the particular applications.

Based on this fact, different researches have been intensively studied to understand not only the mechanical and moulding behaviour under static or dynamic loading but also the influence of various factors on the final performances of 3D woven fabrics at dry and composites reinforcement stages [359][360]. For example, the fabric weave type and geometry of the fabric were found one of the most important factors which greatly affect the mechanical properties of the 3D warp interlock fabrics and composites [342, 361–365]. Besides, fabric structure has shown a great effect not only on the tensile strength but also on its dimensional stability of the

3D textile woven composites [362][342]. Raw material types (fibre and yarn), warp yarn shrinkage inside the woven structure and their corresponding combinations (hybridization) have also been studied and shown a great effect on the mechanical behaviours of both the dry 3D warp interlock fabrics and its composites [366–369]. Yarn densities and weave diagrams are also playing an important role in the mechanical properties of the 3D woven fabrics [340, 370]. Yarn density inside the dry 3D warp interlock fabric also brings a great effect on the tensile, bending and forming behaviours of the final fabric both in the warp and weft directions [166]. Moreover, the weaving process and its different parameters including the positions of stuffer, fibre volume fractions and linking warp yarns inside the 3D warp orthogonal and warp interlock woven fabrics structure have also shown an influence on their mechanical properties [371, 372]. The Z-yarn in the geometry and an interlocking pattern is also another factor that affects the final mechanical performance of the three-dimensional composites [373][374]. The angles when arranging the different yarn (off-axis angles of yarns) while developing the 3D woven fabrics also showed an influence on the different mechanical properties of the materials [375, 376].

Even though the 3D warp interlock fabric gives better mechanical and forming capability, still selecting an appropriate fabric structure and different influent parameters should be more exploited for better understand, characterise and achieve the combined behaviours for the specific applications. Besides, the warp yarn interchange ratios inside the structure also play a great role in the mechanical and moulding performances of the 3D warp interlock fabrics. For example, the types of warp yarns, binding warp yarn, greatly helps to disintegrate loads in different directions and keep the yarns by stabilizing the integrity of the entire structure [377]. The location of a binding warp yarn [378] also ensures better mechanical properties both in the thickness of the 3D warp interlock structure as compared to stacked 2D fabrics. Therefore, such investigations could lead us to find the optimized 3D warp interlock fabric with the specific warp yarn interchange ratio for the developments of woman body armour with better ballistic protection and moulding ability. To fill this gap and give an in-depth understanding, the current chapter intensively investigates and discusses the influences of the warp yarn interchange ratio on the mechanical and forming characteristics of the 3D warp interlock fabrics for women body armour applications.

5.2 Experimental Procedure

The involvement, movement and deformational behaviours of different warp (stuffer and binding) and weft yarns could affect the overall properties of the fabrics. The stuffer and binding warp yarns could also delineate the longitudinal and through-the- thickness properties of the final fabric respectively [148]. Whereas, weft yarns help not only to describe the number of the layer but also determine the transverse properties of the fabric. **Figure 5.1** shows the general interlacing structures of the different yarns inside the 3D woven fabrics. A total of four different variants of 3D warp interlock p- aramid orthogonal layer to layer (O-L) fabrics based on different binding and stuffer warp yarns interchange ratios, namely 3D-8W-0S, 3D-8W-4S, 3D-8W-8S, 3D-4W-8S were designed and manufactured to investigate and understand its effect on the final fabrics mechanical and moulding behaviours. All the specifications and production

parameters of the produced 3D warp interlock fabrics are discussed in the material section (production campaign 3).
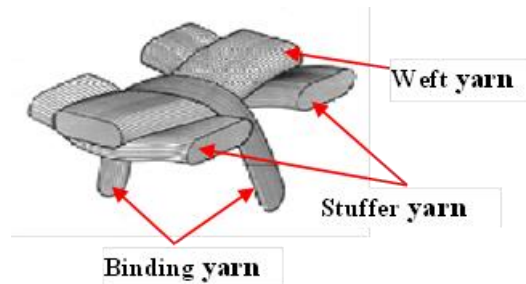
Figure 5.1 General schematic diagrams of deformations of binder, stuffer and weft yarns inside 3D woven fabrics [359]

Figure 5.2 also shows the cross-sectional and top views of the different 3D warp interlock P-aramid fabrics. Besides, the general testing methodologies and procedures for the different mechanical testing including uniaxial tensile tests for yarn and textile fabrics, flexural rigidity test and formability behaviour have been also discussed in methodology sections
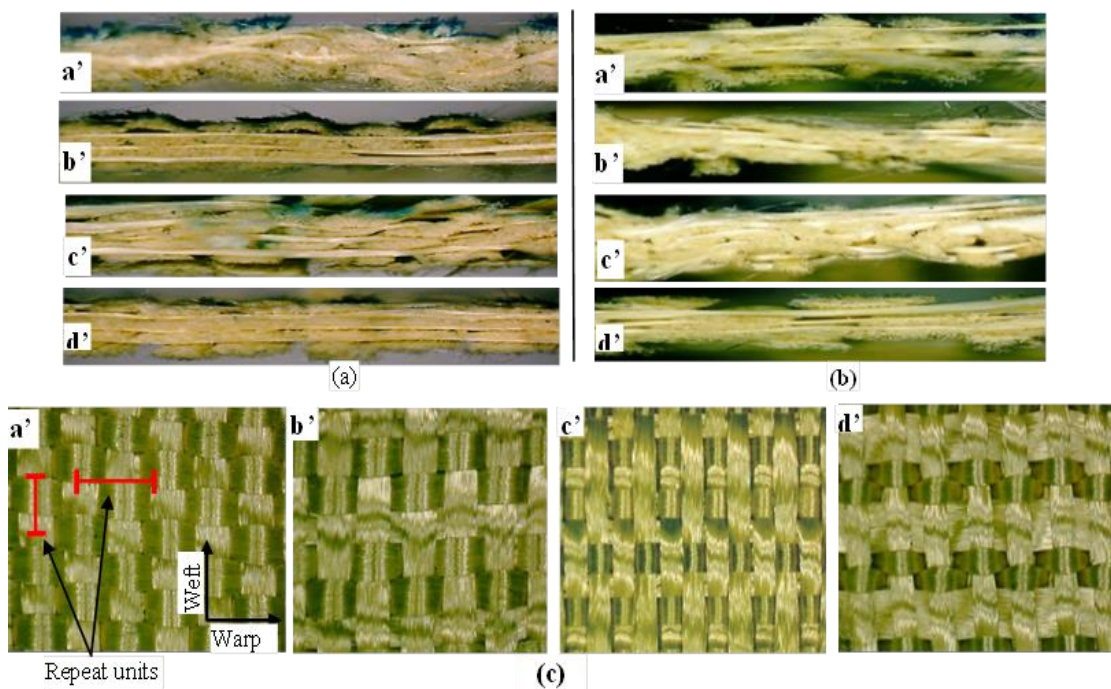
Figure 5.2 Microscopic pictures of the different 3D warp interlock fabrics (a) and (b) - Cross-sectional views of the weft yarn and warp direction respectively, and (c) Top views of the different 3D warp interlock fabrics

In this chapter, different mechanical tests on different types of yarn inside the fabric, flexural rigidity test, and uniaxial fabric tensile test will be performed to characterize and understand the effects of the binder: stuffer yarn interchange ratio on the mechanical property of 3D warp interlock high-performance p-aramid fabrics. Various fabrics properties including the fabric crimp (%), actual fabric thickness (mm) and actual fabric density (g/m^2) were also computed. Besides, the fabrics were tested against their formability behaviour using a pneumatic based

punching bench with hemispherical shape punches. For the formability test, squared samples of each fabric with the dimensions of 250 mm x 250 mm but having different fabric thickness due to the binding effects of the warp yarn in each fabric types were prepared as illustrated in **Figure 5.3.**
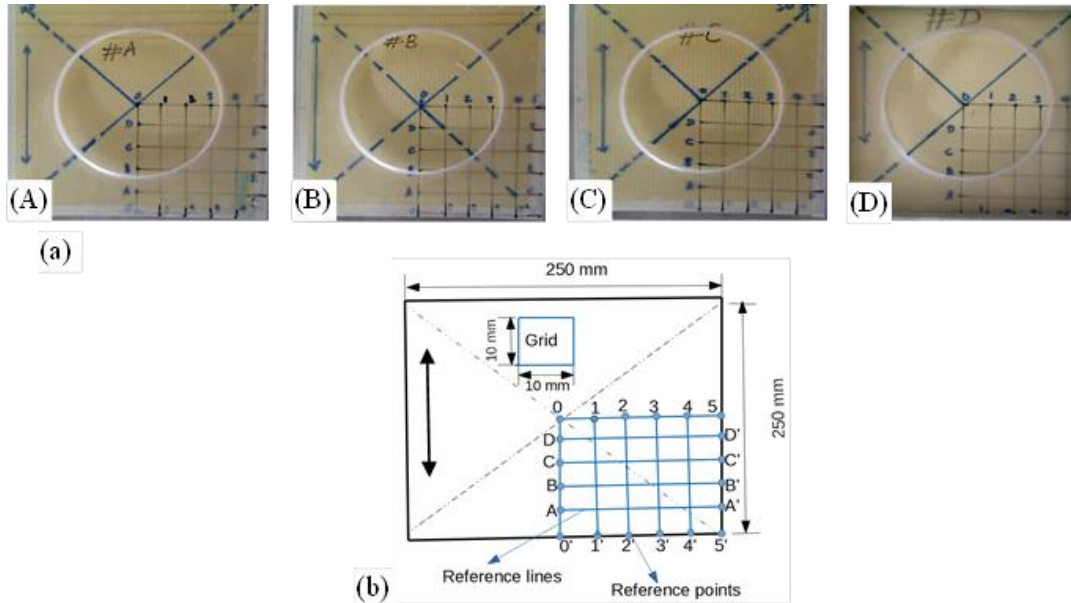
Figure 5.3 (a) Different 3D warp interlock fabrics for formability test and (b) Pictorial examples of positions of reference point and line on the top surfaces of preform

For better tracking, monitoring, and analysis of the different important forming characteristics, a defined reference tracer lines by joining the specific indicator points were carefully drawn on the surface of the preforms. Six surface reference lines each were drawn both in the machine (warp) and cross (weft direction) with equal distance and amounts. The different reference lines are designated as 0-0', 1-1', 3-3', 4-4' and 5-5' in the machine (warp) direction and 0-5, D-D', C-C', B-B', A-A' and 0'-5' in the cross (weft) directions. Normally, such reference tracer lines were drawn only on the quarter regions (1/4th) of the active preform regions to investigate the different formability characteristics. This is since the application of double-curvature shape forming using the hemispherical punching test on the centre of the sample would give a uniform distribution of the forming behaviour in all of the preform regions. This means that analysing different forming characteristics on one quadrant (1/4th) is assumed to give more probably uniform and similar forming behaviour results for the rest of other sub-regions due to the quasi-symmetric of hemispherical punching. In these investigations, the produced different fabric were designated as 3D-8W-0S, 3D-8W-4S, 3D-8W-8S, and 3D-8W-0S to represent 100% binding warp yarns, 66.7% binding & 33.3% stuffer warp yarns, 50% binding & 50% stuffer warp yarns and lastly 33.3% binding & 66.7% stuffer warp yarns interchange ratios inside the 3D warp interlock preforms respectively. As discussed on the methodological part, an adapted forming machine was used at conditioned room temperature to investigate the formability process. The forming process events of each preform were recorded through an installed digital camera. The specific parameters considered while investigating the forming behaviours of the different preforms during this study are listed in **Table 5.1**

147

Table 5.1 The different forming parameter used during formability testing

Forming parameters	Parameter values
Punch shape	Hemispherical
Punch diameter	150 mm
Stamping velocity	45 mm/s
Blank-holder pressure	4 bars
Max. Punching depth	65 mm

Moreover, three specimens test was repeated with similar forming conditions for each 3D warp interlock preforms to extract better measurement data along with satisfactory reproducibility. However, to give good results and achieve better comparisons, all other internal and external parameters were kept constant throughout the moulding process of the different preforms.

5.3 Results and Discussions

In this section, the mechanical behaviour of the various 3D warp interlock fabrics made with different binding/stuffer warp yarn compositions was discussed. Moreover, the different yarns inside the 3D fabric structure were investigated and discussed. The fabric and its corresponding yarn tensile behaviours were carried out based on the load-strain response curve as well as the average maximum tensile load (N) and strain (%) values at the fracture point. Moreover, the rigidity behaviours of the different fabrics were also assessed based on flexural bending rigidity (Nm) and fabric bending length. Finally, the effects of warp yarn compositions on the waviness of the yarn inside the 3D warp interlock fabrics in both directions were explained in terms of the crimp percentages.

5.3.1 Yarn uniaxial tensile properties

When the textile material is intended to apply in the technical application where better mechanical behaviour is in great demand i.e. ballistic impact, investigating its mechanical properties at the yarn level is very important. Moreover, testing and analysing the mechanical behaviours at the yarn level would greatly help to understand the different yarn mechanics during applications at dry fabric and composite stages. For such experimental investigations, 10 yarns from each 3D warp interlock fabrics in both warp (stuffer and binder) and weft (at different weft layers) directions were drawn carefully without damaging the fibres/filaments. The uniaxial tensile tests help to attain the different parameters including Load-time, Load-strain relations, Elastic modulus (E), maximum load (σmax) and maximum strain (εmax) in the yarn longitudinal direction both Machine (warp) and cross (weft) directions. The yarn uniaxial tensile tests were conducted. All the yarn tests were performed at ten replicas for each specimen both in the warp and weft directions using INSTRON 8516 universal testing machine with a 5 KN load cell at a velocity of 50 mm/min to guarantee the results repeatability as it can see in **Figure 5.4** (the load-displacement curves). Each yarn specimen were prepared with 250 mm total length but firmly fixed in both ends at 200 mm distance
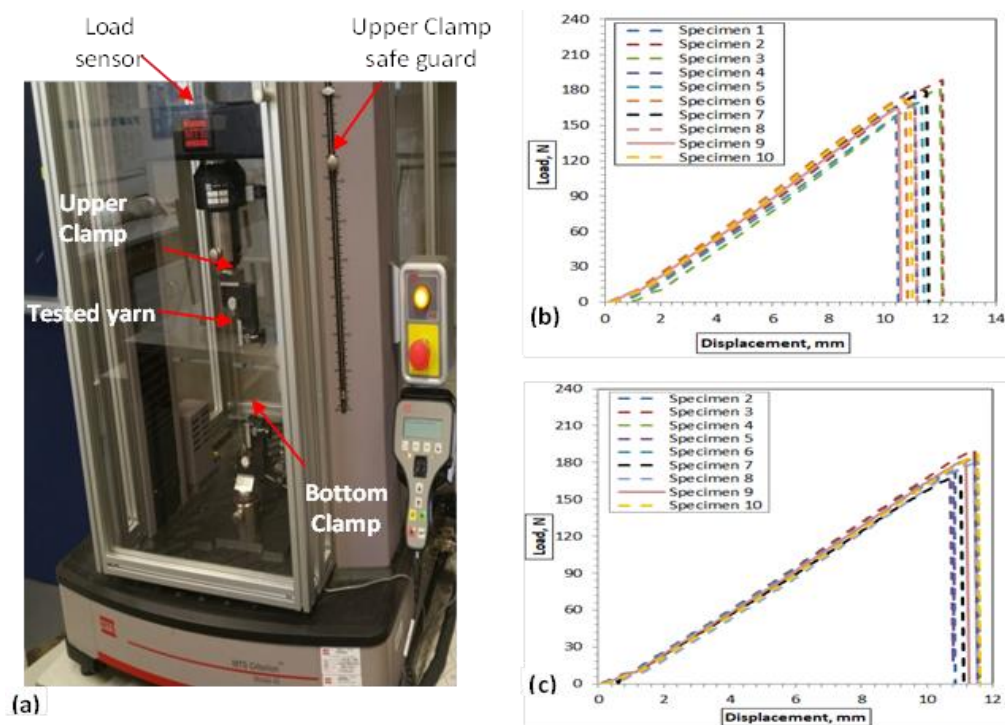
Figure 5.4 Uniaxial yarn tensile testing (a) Yarn tensile testing device set-up; (b) Uniaxial warp-binder and (c) Warp-stuffer yarn tensile test results of different specimens for sample fabric 3D-4W-8S in the machine direction (MD)

5.3.1.1 Stuffer and binding warp yarn testing

but also consists of another type of warp yarns in the thickness of the structure [148]. This benefits the 3D warp interlock fabric to be reinforced in the three directions, each group of yarns providing a specific function within the structure. The compositions of one or more different types of warp yarn mainly depending on the final applications. Moreover, the 3D warp interlock fabric can be represented with different weft layers of fabrics interlaced through the fabric thickness direction by using with binding warp yarns. Due to the yarn of different interlacement and binding positions, it could present different mechanical behaviours. **Figure 5.5 (a) and (b)** shows the average load vs strain curves for binder and stuffer warp yarn for each 3D warp interlock fabric. From such load–strain curves, it is also possible to analyse the mechanical properties of each yarn in the fabric. The tensile load–strain curve shows similar trends for the binder and stuffer yarn inside the different fabrics. As it is observed in **Figure 5.5,** except for 3D-8W-8S**,** the higher the proportions of binder warp yarn in the fabrics, the lower its tensile modulus (E) in the warp directions**.** The average tensile modulus (E) of binding warp yarn for 3D-4W-8S were found higher than the other samples. Sample C revealed the lowest tensile modulus (E) followed by 3D-8W-4S and 3D-4W-8S respectively. A very similar tensile modulus (E) of the stuffer yarn was observed for all the fabrics. However, the tensile modulus (E) of the stuffer yarn was found a little bit higher for samples having less proportion of stuffer yarn and vice versa. 3D-8W-4S shows the better tensile modulus (E), whereas 3D-4W-8S recorded the least.
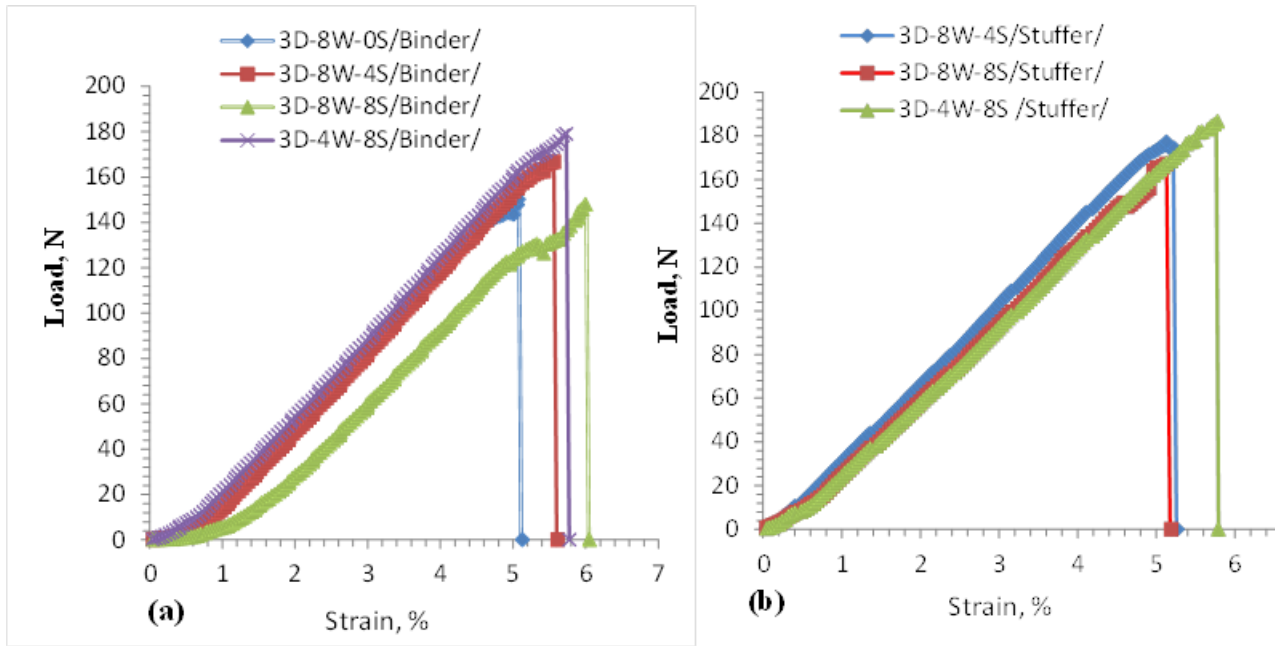
Figure 5.5 Load-strain curves of warp-binder yarn (a) and warp-stuffer yarn (b) for different 3D warp interlock fabric architecture

Moreover, **Figure 5.6 (a) and (b)** also shows the maximum load at failure (σmax) and tensile failure strain (εmax) for the respective warp yarns. The maximum stresses are higher in the case of fill yarns; however, the failure strains are quite similar in both directions. The average maximum load and tensile strain at failure for binder warp yarn of 3D-WS-0S revealed lower values than other fabric type binder yarns. The maximum tensile failure of binder warp yarn was obtained for 3D-8S-8S followed by 3D-4W-8S. Whereas the maximum load at failure of binder warp yarn was achieved in 3D-4W-8S.
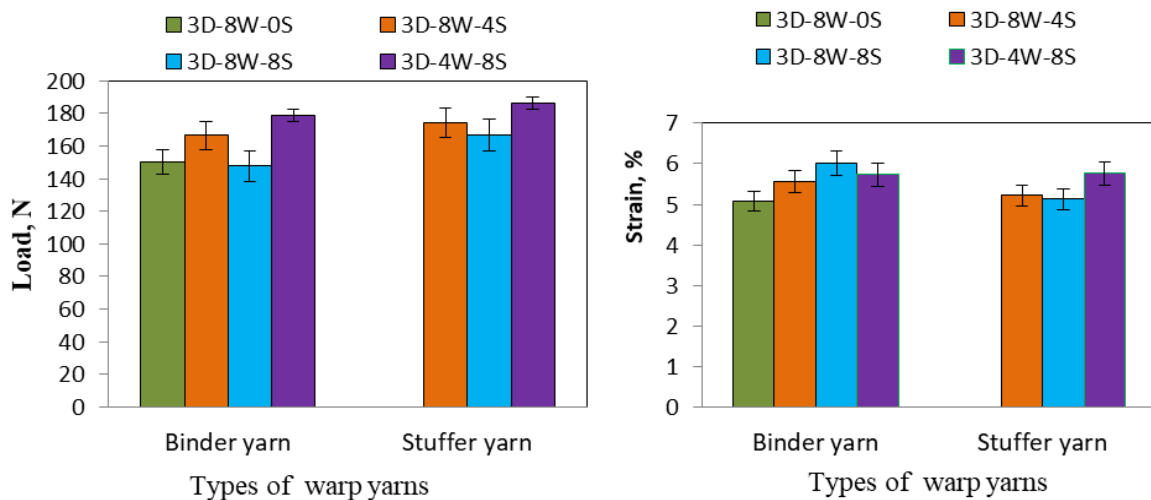
Figure 5.6 a) Maximum Load (a) and failure strain (b) graphs of the tested sample for both binding and stuffer warp yarns for different fabrics

The elongation failure of binding warp yarns mainly depends on both the crimp of the binding warps inside the fabric and the tensile failure of the stuffer warp yarns. Unlike the binding yarn, the maximum load and tensile strain at failure of stuffer yarn show a similar trend in all samples. Both load and strain at failure were higher for 3D-4W-8S followed by 3D-8W-4S and 3D-8W-8S.

5.3.1.2 Weft layer yarn testing

The tensile behaviours of weft yarn in the 3D warp interlock fabrics may be influenced by various parameters. shows the tensile load-strain curves of different weft yarns in the different layer of 3D warp interlock fabrics. In general, the load-strain curves of the different weft yarns inside the different layers of the respective fabric show a similar trend. However, both binders: stuffer of warp yarn interchange ratio and location of weft yarn in the weft layer could influence on the tensile properties of the corresponding weft yarn. The fabric with the highest or minimal binding warp yarn proportion exhibited no effect on the final weft yarn tensile properties. For example, 3D-8W-0S and 3D-4W-8S had shown approximately similar tensile modulus (E) of weft yarn within the respective layers than 3D-8W-8S and 3D-8W-4S.
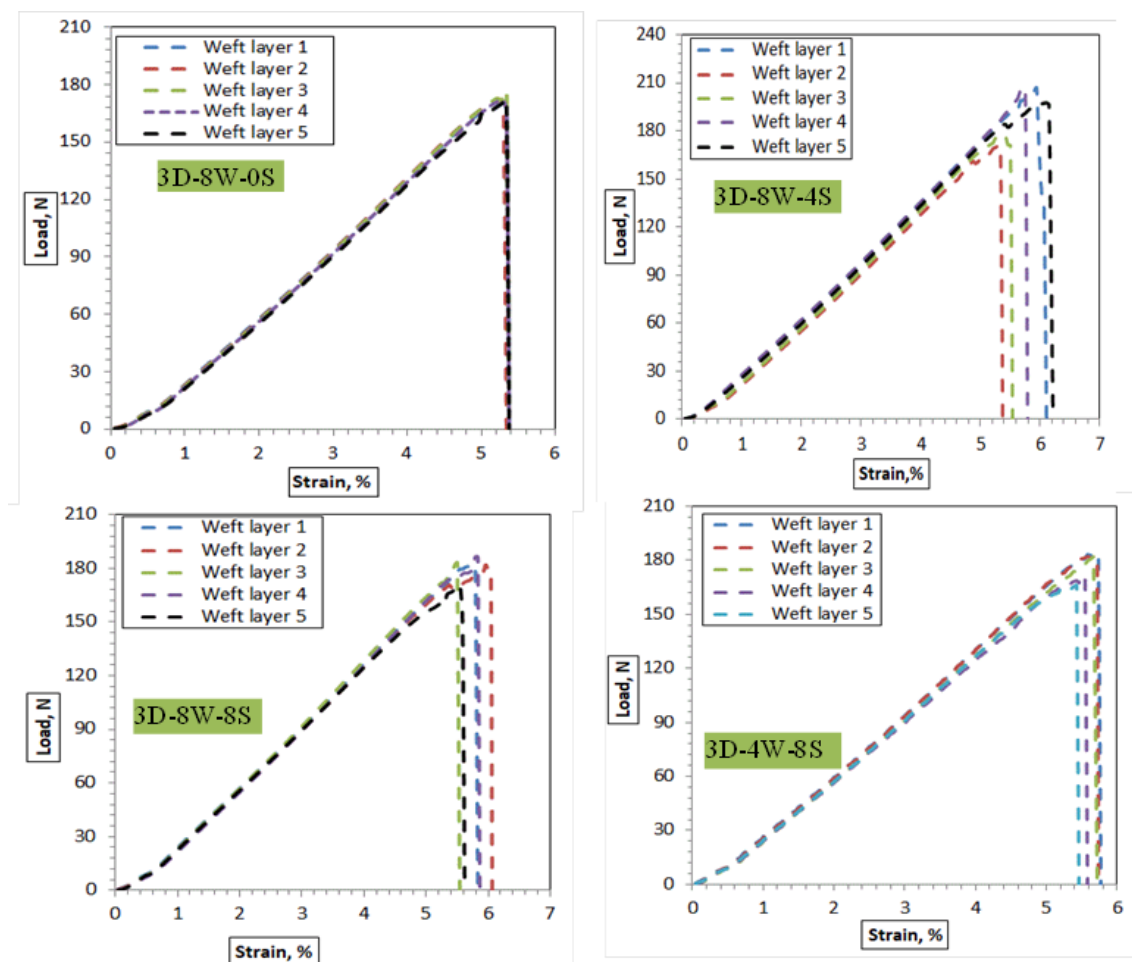
Figure 5.7 Load -Strain curves of different layers (1st, 2nd, 3rd, 4th and 5th layer) fill yarn for the different 3D warp interlock fabric architecture

Moreover, even though the positions of weft yarn in the respective fabric layer affects its tensile properties, clear trends were not observed in the different fabrics. Moreover, based on the load-strain curves, the mechanical properties of the different 3D warp interlock fabric samples were also characterized based on their unique tensile behaviour of strength (N) and corresponding strain (%) at the breaking point. **Figure 5.8 (a) and (b)** shows the average maximum load/ strength (N) and strain (%) values at fracture point respectively for the different samples in the weft directions. The average maximum Load (N) and maximum tensile strain (%) of weft yarn for layers were found more or less similar in 3D-8W-0S and 3D-4S-8S D than 3D-8W-4S and 3D-8W-8S. Weft yarn in the 1st layers shows maximum load and tensile strain (%) in 3D-8S-4S compared to the majority weft layers. Whereas, except 3D-8W-4S, weft yarn in Layer 5 shows lower maximum tensile strain (%) than other weft layers.
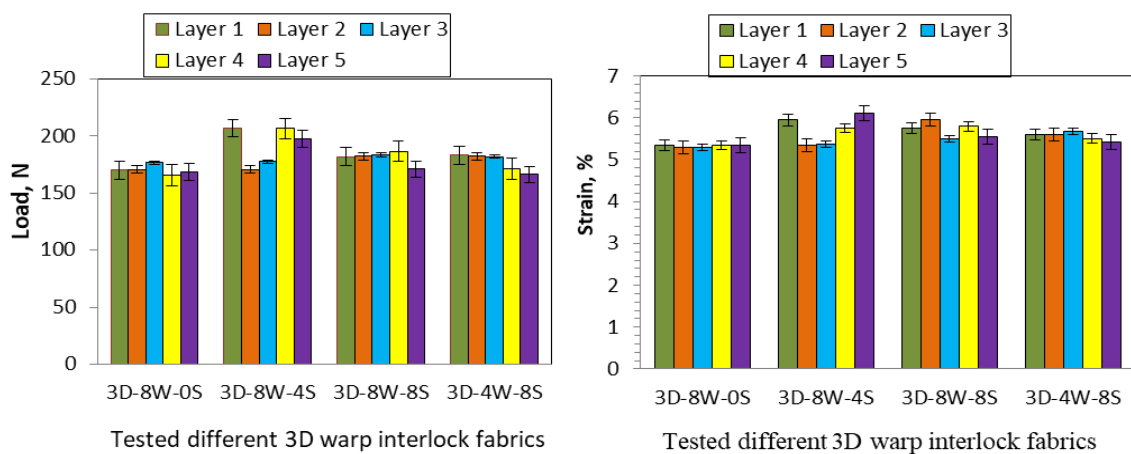
Figure 5.8 Maximum Load (a) and maximum tensile failure strain (b) graphs of the tested sample for weft yarns in different layers of the sample

5.3.2 Fabric uniaxial tensile property

The different specimen's tensile behaviour was performed on the INSTRON 5900 tensile testing machine with a 250 KN load cell according to standard EN ISO 13 934-1[312] as discussed in the methodology section. A rectangular 300 mm × 50 mm specimen adhesively bonded with resin on both ends with an extension of 50 mm to avoid slippage between the specimens and the clamp was prepared. Before every test, the two jaws (the top clamp is movable the lower one is fixed) of the uniaxial testing machine were set with 200 mm apart. For every sample type, three specimens were tested at 100 mm/min both in the weft and warp directions to ensure the repeatability of the investigations. **Figure 5.9** shows the uniaxial fabric tensile machine experimental set-up with the clamped specimen in its initial state and representative uniaxial tensile tests of different specimens for sample fabric A in the warp and weft direction. The uniaxial tensile load to the tensile strain of the 3D warp interlock orthogonal layer to layer fabrics made with different warp yarn compositions were experimentally examined both in the warp and weft directions. In this sub-section, the uniaxial tensile test results of the different tested 3D warp interlock orthogonal layer to layer fabrics are discussed. The average load (N) vs. strain (%) curves of the three different tensile tests for each 3D warp interlock fabric

specimens is described in **Figure 5.10 (a) and (b)**. The test was performed until the tested sample reaches the maximum deformation states and fails. In general, the load-strain curve of the different sample specimens has indicated a similar progression in which the values of the tensile load higher as the strain value increase. The load-strain curve mainly comprises three main parts, the first section shows a non-linear curve (crimp area), and the second section with higher loads vs strain values (elongation area) and the last sections have shown declining of loads with strain values.
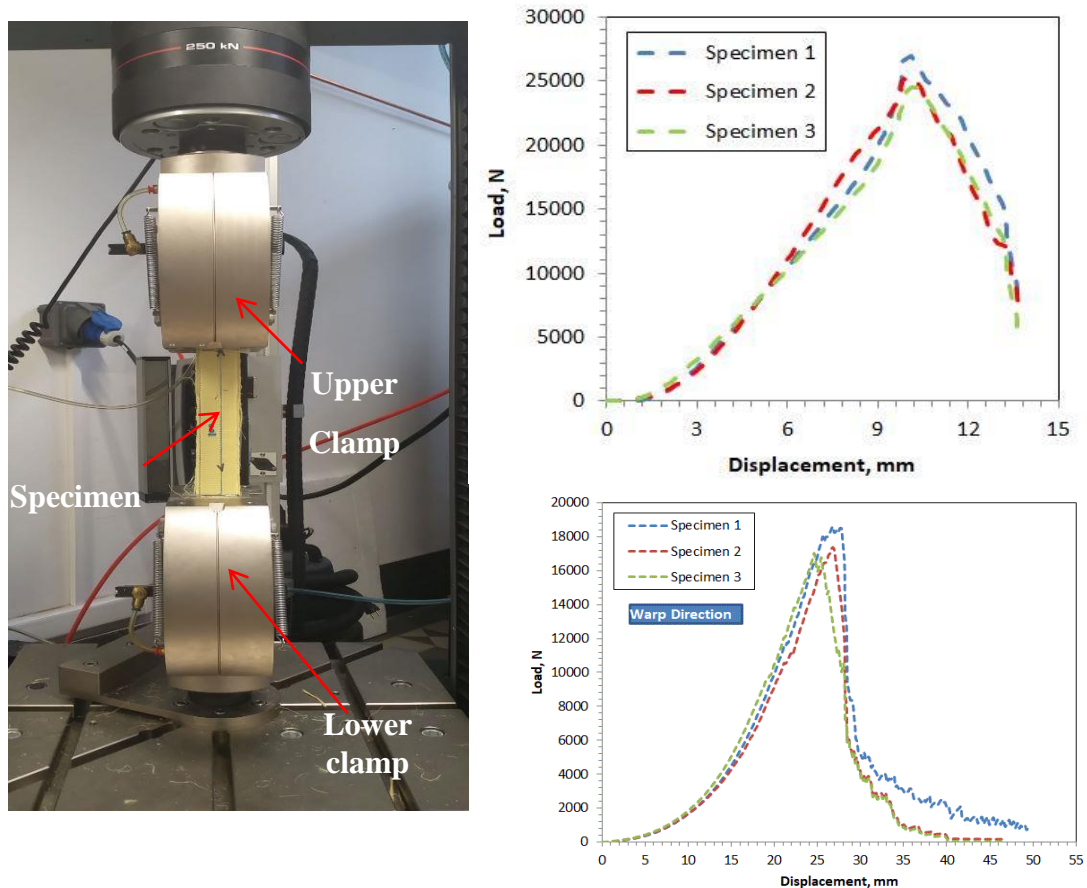
Figure 5.9 Uniaxial fabric tensile testing (a) Fabric tensile testing device set-up; (b) and (c) Uniaxial fabric tensile test results of different specimens in a cross (weft) and machine (warp) direction respectively, for sample fabric A

In the first section, crimp area, which is observed at the beginning of the load-strain curve shows almost negligible values for both the load in the applied loading direction and deformation in the displacement direction at the beginning, and then gradually increases. This is mainly due to the straightening of yarn within the fabric before real deformation occurs along the load direction. When it is closely observed, the crimp area (marked with a black circle) was found similar for all the sample specimens for the weft direction. However, due to the different warp yarn (the binding and stuffer yarn) compositions inside the various fabrics; all the samples show different crimp areas in the warp direction (black and red colour). For example, 3D-8W-0S shows more straightening area (marked with a red circle), as compared to the other samples in the warp direction. Whereas, 3D-4W-8S show higher crimp area followed by 3D-8W-4S and 3D-8W-8S. The maximum strain approximately 1.13% and 1.72% was a maximum strain which is absorbed

in the crimp area for weft and warp directions respectively. In the second section of the load-strain curve, as shown in **Figure 5.10 (a) and (b),** different linear progression with the rapid growth of tensile loads and strain until the sample specimen reaches its breaking point both in warp and weft directions were observed. The tensile load and strain curve was exhibited more or less a similar trend for all the sample specimens in the weft directions due to the balanced weft yarn compositions inside all the fabrics. Even though the curve is linearly progressive, the different warp yarn compositions system inside the 3D warp interlock fabrics leads to diverse tensile load and strain relationships in the warp directions. Most obviously, due to the balanced proportions of stuffer and binding warp yarns inside the fabric, 3D-8W-8S typical load-strain curve display two main peak points (**Figure 5.10 (a)**) during a tensile test in the warp direction. The dominant first and second failure peaks were due to the failure of stuffer and binding warp yarns respectively. Such condition arises mainly from the actual length difference between the stuffer and binding warp yarns in the fabrics while loading.
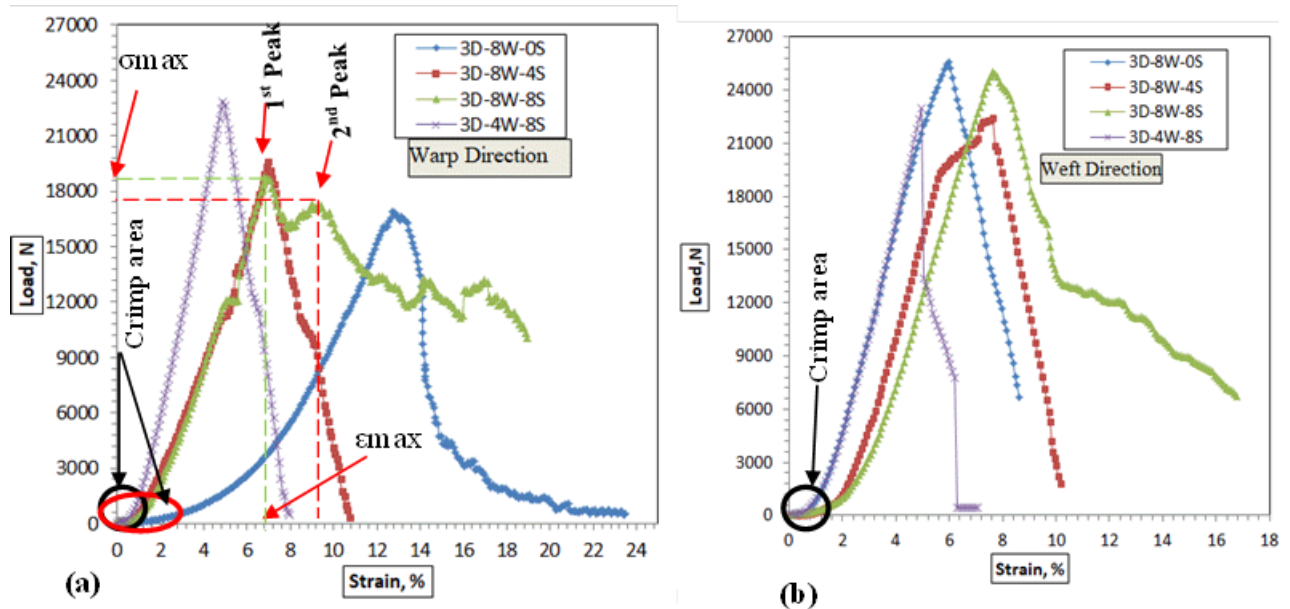
Figure 5.10 Load-strain curves of different 3D warp interlock fabric architecture in warp (machine) direction (a) and, Weft (cross) directions (b)

On the contrary, different peak points were not visible in the other samples either having the same or one dominated warp yarn (stuffer or binder) systems in the warp directions. For instance, 3D-8S-0S (100% binding warp yarn) revealed a gentler progressive slope and single tensile failure peak with the lower tensile modulus (E) in the warp direction as shown in **Figure 5.10 (a)**. Whereas, 3D-4W-8S (66.7% stuffer warp yarn) demonstrates a steeper, single peak linear progressive curve with the higher tensile modulus (E). The higher tensile modulus (E) value of 3D-4W-8S is due to its higher stiffness behaviour which comes from comprising higher proportions of stuffer warp yarn inside the fabrics in the warp directions. Whereas, the lower value of 3D-8W-0S is due to the higher waviness of the binding warp yarn inside the fabrics which needs more load to deform the specimen. 3D-8W-4S and 3D-8W-8S were lying between

and show similar linear progressive slope with the approximately equal tensile modulus (E) till the breaking peak points in warp directions (**Figure 5.10 (a)**).

Unlike the warp directions, the load-strain curve of the different fabric samples in the weft direction performed almost as a linear and elastic progressive curve with approximately similar trends (**Figure 5.10 (b)**). This might be due to possessing the same weft yarn compositions and yarn density among all the fabrics in the weft directions. However, while interlacing, due to a very stressing of different warp yarn compositions on the weft; the load vs strain curve slope and its tensile strength values might be affected. 3D-8W-0S and 3D-4W-8S have shown almost equal tensile modulus strength ((E) with a higher value as compared to 3D-8W-4S and 3D-8W-8S. This is due to the presence of higher weft yarn undulations in 3D-8W-0S and 3D-4W-8S, which could absorb more exerting forces in the loading directions. 3D-8W-4S also recorded better tensile modulus (E) as compared to the 3D-8W-8S. Even though the various 3D warp interlock fabric has the same structure and areal density, it possesses different maximum tensile strain (εmax) and load (σmax) at failures. **Figure 5.11** shows the different fabric specimens tensile strain and strength at failure both in warp and weft directions.

While considering the weft direction, all the fabric samples did not show a significant difference among their maximum tensile strain (εmax) and load (σmax) at failures as shown in **Figure 5.11 (a) and (b)** respectively. This is because of possessing the same weft yarn compositions inside their 3D fabrics architectures. Their slight differences could come are from the stressing effects of warp yarn while interlacing to form the fabrics. For example, 3D-8W-0S and 3D-8W-4S were failed at the tensile strain values of approximately around 5.88% and 7.8% while the load is applied along with the weft directions.
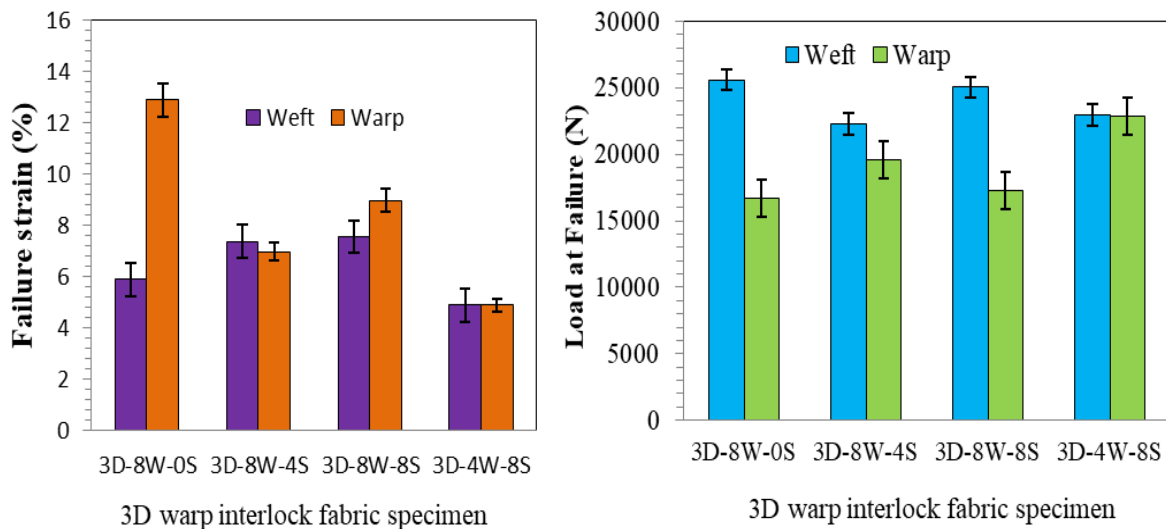
Figure 5.11 Maximum tensile strain (εmax) and tensile strength (σmax) at failure for different 3D warp interlock fabric specimens in the warp and weft directions

Whereas, 3D-8W-8S and 3D-4W-8S failed at the strain values of 7.55% and 4.8%. However, due to the different warp yarn proportions inside the fabric architecture, the maximum tensile strain (εmax) and load (σmax) at failure were found different in the warp direction among the different 3D warp interlock fabric specimens.

For example, 3D-8W-0S (100% binding warp yarn) possesses higher tensile strain at failure in the warp direction (12.88%) than weft directions (5.88%) due to higher undulating properties of binder warp yarn inside the fabrics architecture. On the contrary, 3D-4W-8S (66.7% stuffer and 33.3% binding warp yarn) shows nearly equal tensile strain at failure both in the warp and weft direction (4.88%). This is because both directions have approximately equal undulation of warp and weft yarns inside the fabric structures. Similarly, the tensile strength at failure for the different fabric samples was also affected by the different warp yarn compositions systems inside the fabric structure. For example, the tensile responses of 3D-4W-8S were found equal both in the warp and weft direction due to approximately similar undulations behaviours of yarns in both directions. Whereas, 3D-8W-0S, 3D-8W-4S and 3D-8W-8S own different tensile strength at failures in warp and weft directions due to the involvements of various binding warp yarn compositions inside the architectures (**Figure 5.11 (b))**.

Besides, different tensile fabric damage on the different samples after each test was also observed and analysed. **Figure 5.12** shows the pictures for after test specimens of different 3D warp interlock fabrics sample at its tensile failure state both in the warp and weft direction. The damages mechanisms of the fabrics were observed at tensile deformational failure states based on macroscopic levels. The tensile fabric damage of all samples in the weft direction shows a similar trend and majorly from crooking of weft yarns as shown in **Figure 5.12 (a)**. However, the fabric tensile failure mechanism in the warp directions was different due to the different warp yarn systems inside each fabric.
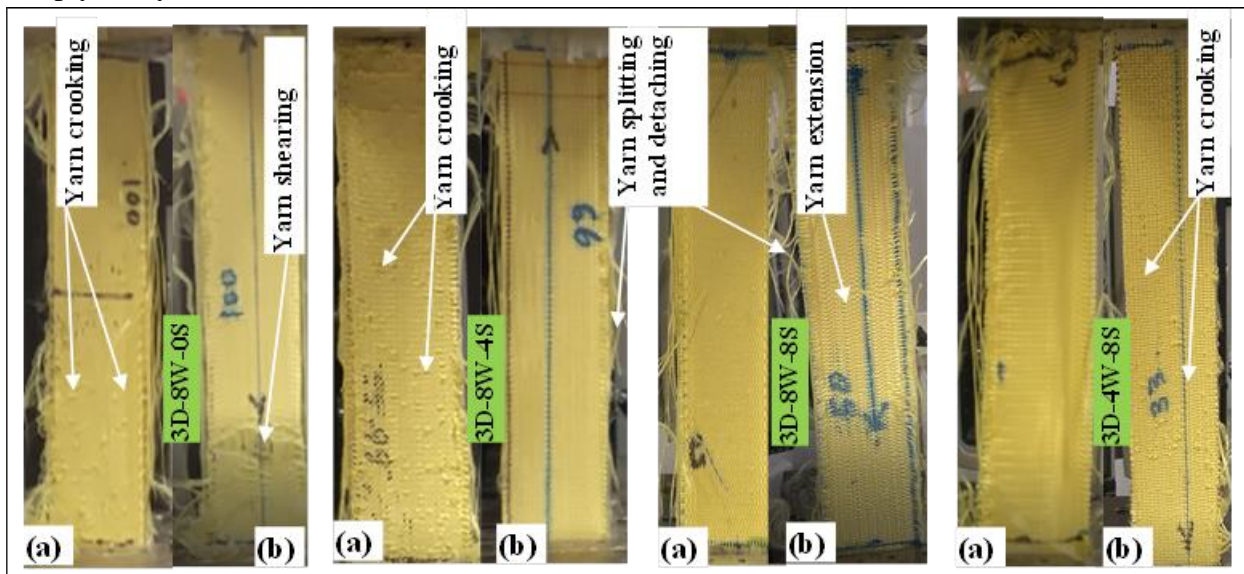
Figure 5.12 Pictures of different 3D warp interlock fabrics at tensile failure in the weft (a) and the warp (b) directions

For example, 3D-8S-0S exhibited shearing of yarns throughout the specimen width just near to the gripping end until failure. Sample 3D-8W-4S and 3D-8W-8S show similar fabric tensile failures with yarn straightening and extension and in the warp directions. However, 3D-4W-8S possesses similar tensile fabric damage as tensile fabric damage of all samples in the weft direction. This is since 3D-4W-8S fabric architecture composes more stuffer than binding warp yarn in the warp direction which brings similar yarn orientation inside the fabric as weft yarn.

Regardless of warp yarn ratios in the fabrics and testing directions (warp and weft), all the specimens face some yarn splitting from the edges followed by separation along the fabric length. Moreover, higher weft yarn undulation due to involvements of more binding warp yarns inside the fabric enhances the tensile strength at failures in the respective direction. The yarn undulation while interlacing of yarn inside the fabric could bring extra inter-yarn friction between the yarns and enhance the tensile load at failures. For instance, the tensile strength of 3D-8W-0S (25.6KN) and 3D-WS-8S (22.9KN) was found higher as compared to all other remaining fabric samples in the weft and warp direction respectively. Whereas 3D-WS-4S (19.6KN, 22.3KN) and 3D-WS-8S (17.3KN, 25.04KN) own different tensile strength at failures in warp and weft directions respectively due to the involvements of higher binding warp yarn compositions inside the architectures (**Figure 5.12 (b)).** Based on the observation, warp yarn compositions in the warp directions could influence not only 3D warp interlock fabric's maximum tensile strength and strains in the warp direction but also has an impact in the weft direction. For example, 3D-4W-8S made with more stuffer warp yarn possesses approximately the same maximum tensile strength at failure both in the weft and warp direction. 3D-8W-0S with higher binding warp yarn (100%) shows a great difference both for the maximum tensile strength and strains both in the warp and weft directions.

5.3.3 Fabric flexural rigidity behaviour

Apart from tensile and other mechanical properties of the fabrics, it's flexibility properties which could determine the drape comfort, and handling of the fabrics textile materials in the developments of soft body armour material is also equally important to be investigated. As explained earlier, various factors could affect the fabric bending behaviours such as material types, fabric structure, areal density, fabric size, etc. In this section, the effects of the stuffer: binding warp yarn interchange ratios on the flexural rigidity properties of the 3D warp interlock fabrics are investigated and discussed. A bending rigidity test apparatus, testing parameter, testing procedures and its sample specifications were discussed in methodology sections. Besides, the flexural bending rigidity (N.m) which is used to characterize the bending behaviour of different specimens were computed based on Equation 2.1 or Equation 2.2 as mentioned in methodology sections. While investigating, due to their higher fabric flexural rigidity properties, except 3D-8W-0S in the warp direction, all other sample specimens were considered their bending curvature angle (θ) at their specific bending length (C). Based on the newly obtained bending angle and bending length(C), it is possible to compute the flexural rigidity of each specimen using Equation 2.1. **Figure 5.13 (a)** shows the values of average flexural rigidity of different 3D warp interlock fabrics concerning the warp yarn type ratios both in the warp and weft directions.

It is worth to observe that, fabrics which comprise more stuffer warp yarn compositions possess the highest flexural rigidity as compared to fabrics with low or no stuffer warp yarns in the warp direction. For example, fabrics made with higher stuffer warp yarn compositions, 3D-4W-8S has the highest specific flexural rigidity followed by 3D-8W-8S and 3D-8W-0S. Whereas, fabrics which only comprise binding warp yarn (3D-8W-0S) shows the lowest flexural rigidity. Here two things have been observed and outlined. First, the presence of higher interchange ratio of stuffer yarn greatly affects the bending stiffness of the fabrics in the longitudinal directions.
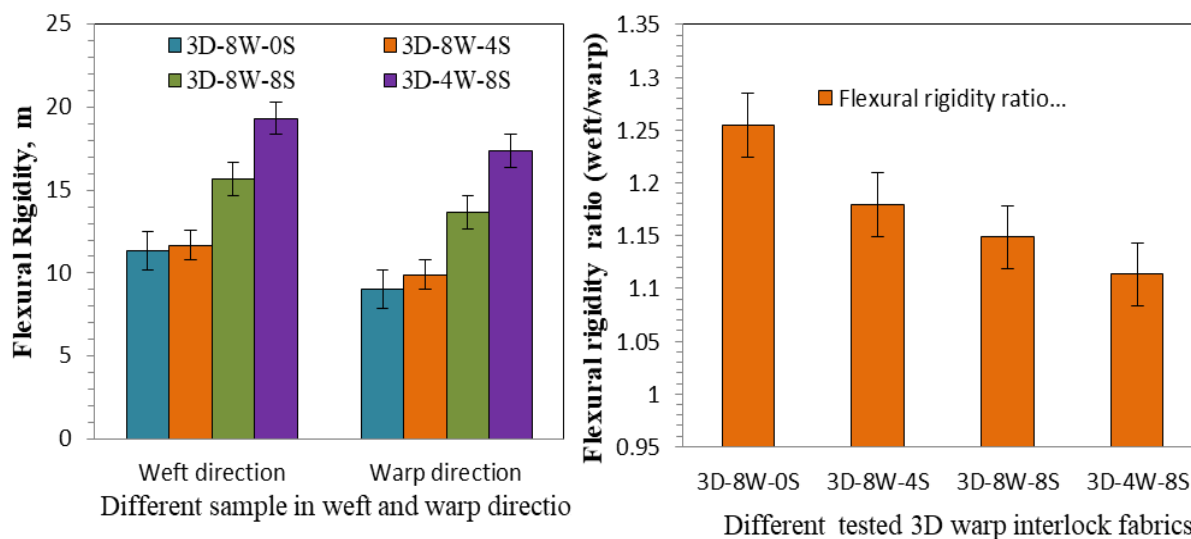
Figure 5.13 (a) Flexural rigidity value of different 3D warp interlock fabric sample both in the weft and warp directions and (b) flexural rigidity ratio (weft/warp)

For example, it is clearly shown that the fabric sample with 66.7% stuffer yarn is about twice as stiff as the ones with no stuffer yarn in warp directions. It can be expected that this trend is significant and will be reduced for fabrics with a lower amount of stuffer yarn in their warp compositions. Hence, if ballistic materials require lower bending stiffness, structure with appropriate warp yarn compositions should be used for better flexibility and ballistic performances. Second, the flexural rigidity in the weft direction has been also slightly influenced by the warp yarn compositions. Even though all the weft density and compositions were the same for all fabric structure, the weft directions were found slightly higher than that of warp direction. This is because weft yarns are more or less straight than warp yarns which make a significant difference in bending stiffness. **Figure 5.13 (b)** shows the flexural rigidity ratio of each fabric in the weft to warp direction. For example, the flexural rigidity of 3D-4W-8S in the weft direction was found higher than the warp directions. It is seen that even further reducing the proportions of stuffer yarn in warp direction helps to lower some stiffness and brings as much lower stiffness as weft directions. For example, 3D-8W-0S, with no stuffer yarn fabric shows much less stiffness in warp direction compared to weft directions. Without considering other mechanical properties, an increase in the proportions of stuffer yarn in the warp yarn compositions of 3D warp interlock fabrics is an effective way of obtaining higher bending stiffness properties in both warp and weft directions.

It is a great interest to compare the two 3D warp interlock fabrics, one with null stuffer yarn and other with 66.7% stuffer warp yarn compositions. Ideally, the bending stiffness for both zero-stuffer and 66.7% stuffer warp yarn fabric structures should be the same in the weft direction. This is due to the same type of yarn, yarn density, and yarn arrangements. However, the difference is due to the orthogonal characteristics of warp yarn composition which influences the arrangement of weft yarn. Thus, fabrics with more stuffer warp yarn proportions have less stress on the weft yarn which sustains its bending stiffness ability.

5.3.4 Fabric crimp

It is the measure of the waviness of the yarn inside the fabrics. The relationship between the geometry of the fabric structure, crimp, and its physical behaviour is complex. The waviness (crimp) behaviours of the yarn inside the fabric affect the mechanical properties of the final materials. It is very important to understand the waviness of yarn with different parameters before applications. It is usually expressed in percentage and defined as the mean difference between the straightened thread length and curved thread length while in the fabrics using the following formula (**Eq. 4.1**).

$$Cp = \left((Co - Cr)/Cr \right) \cdot 100 \qquad (4.1)$$

Where;

      Cp = Crimp percentage of the material,

      Co = Un-crimped length,

      Cr = Crimped length.

Table 5.2 shows the values of the crimp percentage for different warp yarn (stuffer and binder) as well as weft yarns in the 3D warp interlock fabrics.

Table 5.2 Crimp percentage of different warp and weft yarn inside the 3D warp interlock fabrics

Yarns	Yarn types	Crimp percentage			
		3D-8W-0S	3D-8W-4S	3D-8W-8S	3D-4W-8S
Warp yarn	Binding-yarn	17.22	9.75	10.5	24.75
	Stuffer-yarn	-	1.166	1	1
Weft yarn	Weft yarn	2.666667	1.055	0.78	0.6

Figure 5.14 also shows the amount of crimp in the load-bearing for different 3D warp interlock fabrics with different warp yarn compositions. 3D warp interlock fabrics with either higher or lower binding warp yarn proportions revealed a higher crimp percentage for the binding warp yarn. For example, 3D-4W-8S shows better bending warp yarn crimp percentage followed by 3D-8W-0S. Whereas, 3D-8W-4S and 3D-8W-8S show almost similar crimp percentages. However, the crimp percentages of the stuffer yarn were directly proportional to the warp yarn compositions.
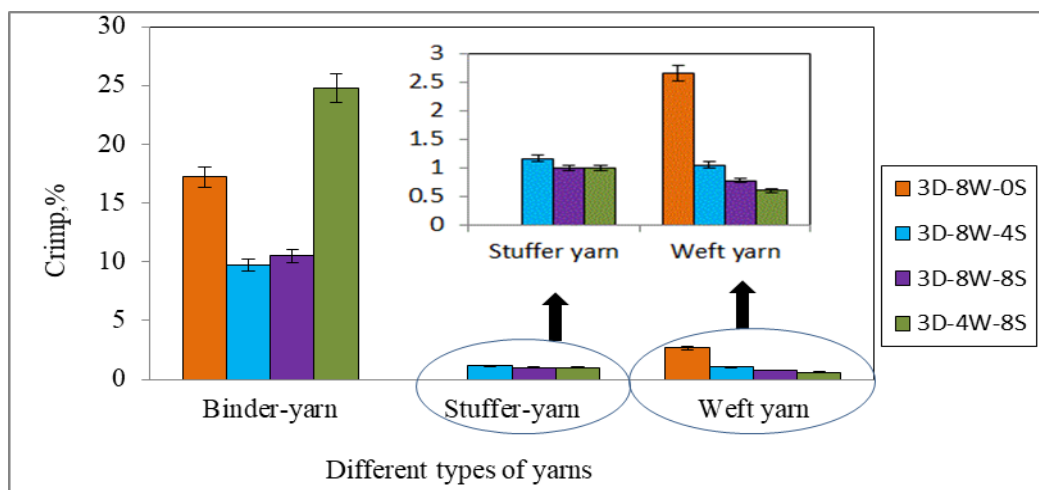
Figure 5.14 Crimp percentage (%) of the different yarns in both warp and weft directions of various 3D warp interlock p-aramid fabrics

As the proportion of stuffer yarn inside the fabric increases, its crimp percentages were found minimal. This is since there is no or minimal binding warp yarn, there would not much load to be applied on the stuffer yarn to bend inside the fabrics. Fabrics with minimum proportions of binding warp yarn, 3D-4W-8S, show lesser stuffer yarn crimp percentage than other fabrics with higher binding warp yarn compositions, 3D-8W-4S and 3D-8W-8S. It may be also important to mention that the compositions of warp yarn in the 3D fabric show its effect on the crimp percentages of the fabric in the weft directions. The more the binding warp yarn on the fabric the higher stress brings on the weft yarn while binding by moving throughout the fabric thickness. Even though the difference of the crimp percentages of the fabrics was not much significant, as the binding warp yarn composition increases, the fabric crimp percentage was found higher in the weft directions. It is highest for the sample with higher warp yarn compositions, 3D-8W-0S, followed by 3D-8W-4S, 3D-8W-8S, and sample 3D-4W-8S consecutively. Moreover, the crimp per cent is almost similar and insignificant in the sample with higher stuffer yarn compositions, 3D-8S-8S and 3D-4S-8S. For example, the weft yarn crimps percentage for 3D-8W-0S, 3D-8W-4S, 3D-8W-8S and 3D-4W-8S were recorded as 2.67, 1.06, 0.78 and 0.61 respectively. Except warp yarn stress effect to bend, the approximately equal amount of crimp percentage of the fabrics in the weft directions may be attributed due to its same yarn orientation inside the structure and similar weft yarn composition throughout the fabrics. The weft yarn and stuffer warp yarn were shown more or less similar crimp percentages and used to stabilize the fabric after the fabric productions.

5.3.5 Formability characteristics of the 3D warp interlock fabrics

Generally, textile material involves different fine and flexible yarns which are arranged in different geometrical ways. Those yarns are usually arranged in bent, twisted configurations and contacting the neighbouring yarns inside the fabrics. During the forming process, the different yarn starts to move relatively and bring lots of forming behaviours on the deformed fabrics [351]. The section will investigate the influences of the warp yarn interchange ratio on the

forming characteristics of 3D warp interlock fabrics. **Figure 5.15** shows the pictures of the deformed preforms of the different tested 3D warp interlock fabrics by the hemispherical punch at the same testing conditions. Normally, due to the hemispherical punch shape, all the preform exhibited symmetric and similar deformed shapes. However, the 3D warp interlock fabrics might reveal different important forming and recovery behaviours due to warp yarn interchange ratio differences. This section will discuss those important forming characteristics of the different preforms for a better understanding of 3D warp interlock fabrics and its influence by the warp yarn interchange ratio.

(a) 3D-8W-0S (b) 3D-8W-4S
(c) 3D-8W-8S (d) 3D-4W-8S
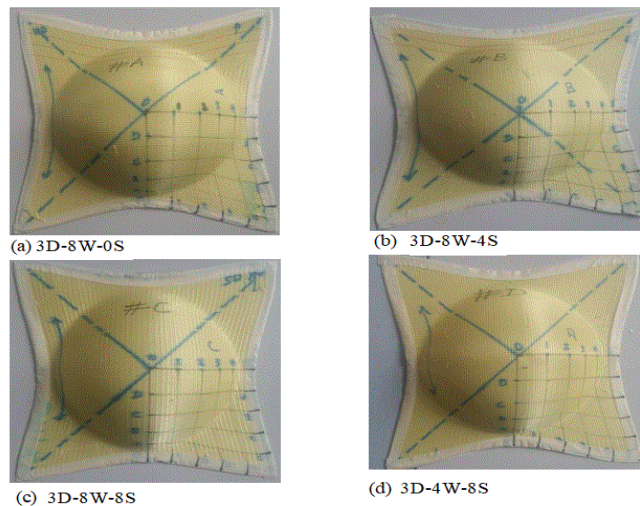
Figure 5.15 The different 3D warp interlock preforms after performing

5.3.5.1 Influence of warp yarn system on the punch force of 3D warp interlock fabric

To obtain the final deformed shape of the preform, a vertical force was constantly applied from the bottom with the help of an electric jack along with sensors. The sensors under the electric jack were designed to measure the amount of the force applied. Regulating the amount of force then helps to properly stamp the well-firmed preforms by the hemispherical punch (Fig.4) for a better forming process and to avoid process defects. Thanks to the sensor and its display, the different parameters including deformation time, displacement, peak loads, etc. will be were automatically recorded after the forming process. In this section, we tried to analyses the relations between the stamping forces with the deformation times for different preforms. **Figure 5.16(a)** shows the punching load vs deformation curves of the different preforms during forming test. The result reveals similar trend evolutions of load vs deformation curves for all 3D warp interlock preforms. The load vs deformation curve was started with insignificant loads for around three seconds until the punch tip-off the preforms. Then, the load drastically starts to increase through time during stamping the preform. The load has continuously increased until the preform reached the maximum deformation displacement (65 mm). Finally, the force applied by the punch on the preform becomes constant through time after maximum deformational height has been achieved. Moreover, the maximum punching load which required deforming and maintaining the final shape of the deformed preform of the different 3D warp interlock preform has been illustrated in **Figure 5.16 (b).** Based on the investigations, the

maximum punching loads were influenced by the binder and stuffer warp yarn interchange ratio inside 3D war interlock fabrics.
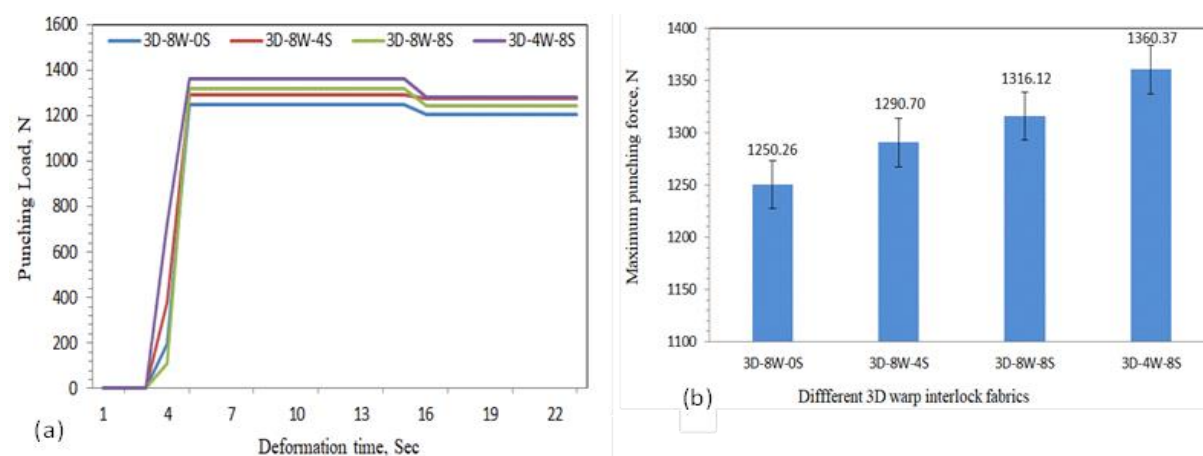
Figure 5.16 (a) The punching forces vs. Deformation time curves and (b) its maximum punching forces of different 3D warp interlock preforms

Normally, higher compositions of binder yarn inside the fabric bring higher rigidity of the fabric. The study noticeably revealed that the stuffer yarn ratio shows an impact and directly proportional to the punching force while forming the different 3D warp interlock preforms. This is due to the fact the samples with higher stuffer yarn ration possess less yarn undulation in the warp direction which in turn needs a higher amount of punching loads to deform the preforms to the maximum deformational depth. Sample 3D-8W-0S and 3D-4W-8S revealed the minimum and maximum punching loads of 1250.26 and 1360.37 N respectively. Moreover, Sample 3D-8W-8S and 3D-8W-4S recorded 1290.7 and 1316.13 N respectively to deform the preform to maximum depth.

5.3.5.2 Influence of warp yarn system on the in-plane shear angle

The inter-ply and intra-ply shearing are among the most common deformational modes of the textile preform that might exist during the formability process. The forming of multi-layer fabric preforms generally involves significant amounts of both intra-ply shearing and inter–ply sliding effect while the fabrics undergo the deformation process. However, unlike multi-layered fabric preforms, 3D woven fabric forming faces considerable amounts of intra-ply shearing than inter-ply sliding due to the better linking of the different weft layers through-out the thickness by the binder warp yarns. Moreover, in textile material deformation, the intra-ply shearing effect is mainly associated with the in-plane shear angle. The intra-ply shear angle is an angle mostly measured between the orthogonal complement of warp and weft yarn at the crossover which is used to measure the amount of fabric shear deformation. It is also analyses based on the fibre orientation on the top surface of the preforms. However, to better analyse and compare the different preforms' in-plane shear angles, it should be measured on the deformed preform surface where there are lower or insignificant amounts of wrinkles. This because wrinkling is one of the forming defects which makes difficult the shearing angle measurements and might

not give better result analysis of surface shear angle between the different deformed preforms. **Figure 5.17** indicated the pictorial and its schematic representations of in-plane shear and its recovery angles for the selected sub-regions of the preform.
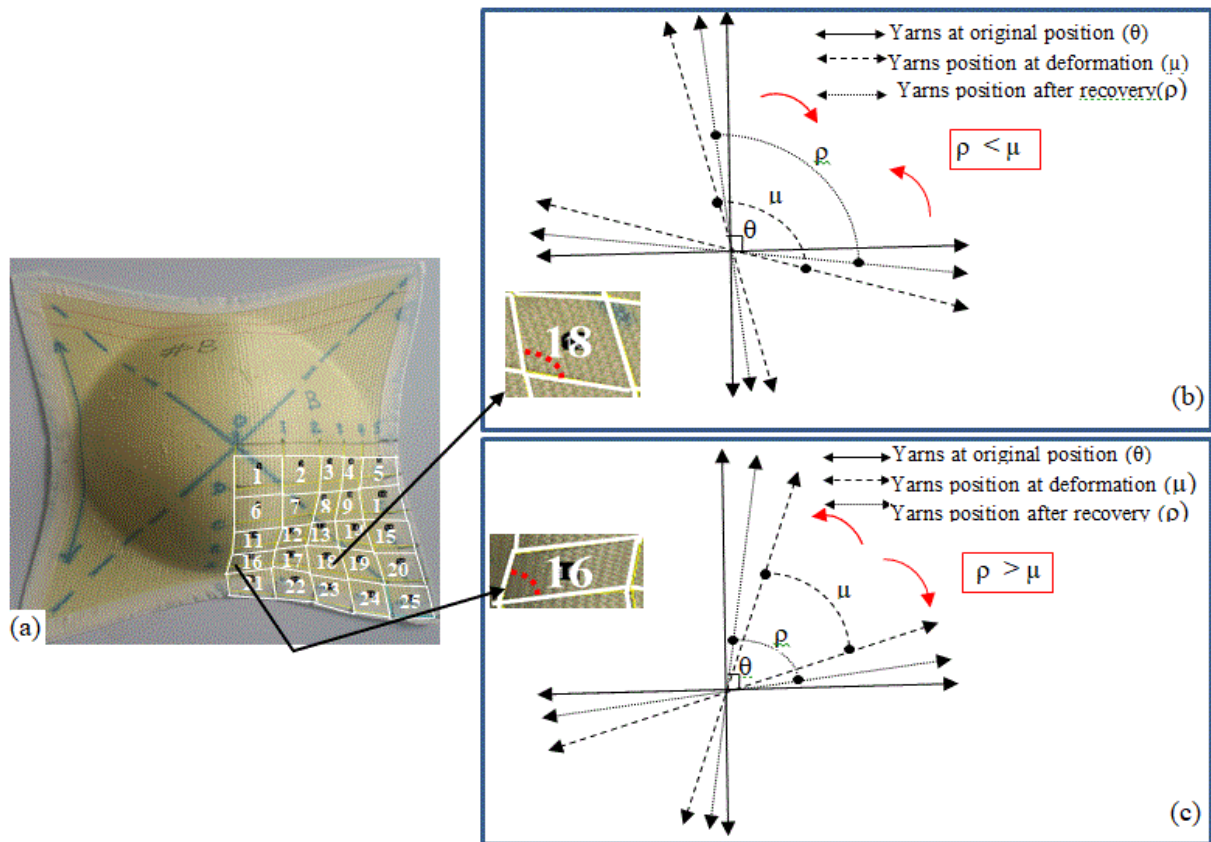
Figure 5.17 (a) The deformed preform and its different measurement angles on the surfaces of the deformed preform to determine for in-plan shear angle values and its recovery (b, c)

As shown in **Figure 5.17**, θ is the perpendicular angle between the warp and weft yarns at initial/ positions before forming a test and measured mostly on the preform surface. The deformation by the de-crimping of the interlaced yarn to conform to the intended compound curvature creates the in-plane shear angle, δ, which was developed between the weft and warp yarns at the crossover. So, the shear angle between the yarns on the preform surface has been measured and computed as follows:

$$\delta = |\theta - \mu| \tag{5.1}$$

Where;

    δ – is the in-plane shear angle,

    θ – is the measured initial angle between the yarns (mostly 90°),

    μ - is the angle measured between the weft and warp yarns after immediate deformation. Normally, the orientations of the fibre/yarn tend to return to the original position after releasing the punching load on the deformed preforms. However, depending on the positions of shear on the preform surface, the initial angle measurement values inside the sub-region could be higher when negatively deviate or lower with positive deviation as compared to the recovery angle. For example, as shown in **Figure 5.17 (b)** of sub-region 18, the measured angle at immediate

deformation (μ) was negatively deviated and found higher than the measured angle after recovery (ρ) measurement, (μ>ρ). On the contrary, in **Figure 5.17 (c)** of sub-region 16, illustrated that the immediate angle measurement after deformation (μ) was found lower than the angle after recovery (ρ) measurement (μ<ρ). This is because through time the orientations of yarn tend to return to its original angle orientation (θ). As it is also discussed in the experimental section, like other forming characteristics, the different angles were efficiently captured by the inbuilt digital camera and extracted with the help of ImageJ software for better analysis. **Figure 5.18** shows the in-plane shear angle and its measurements of the different 3D warp interlock preforms in the selected one quadrant sub-regions. For quick and better observation and comparisons, the different sub-regions of the preforms were further clustered into three regions namely: Low, Medium and High in-plane shear angle regions.
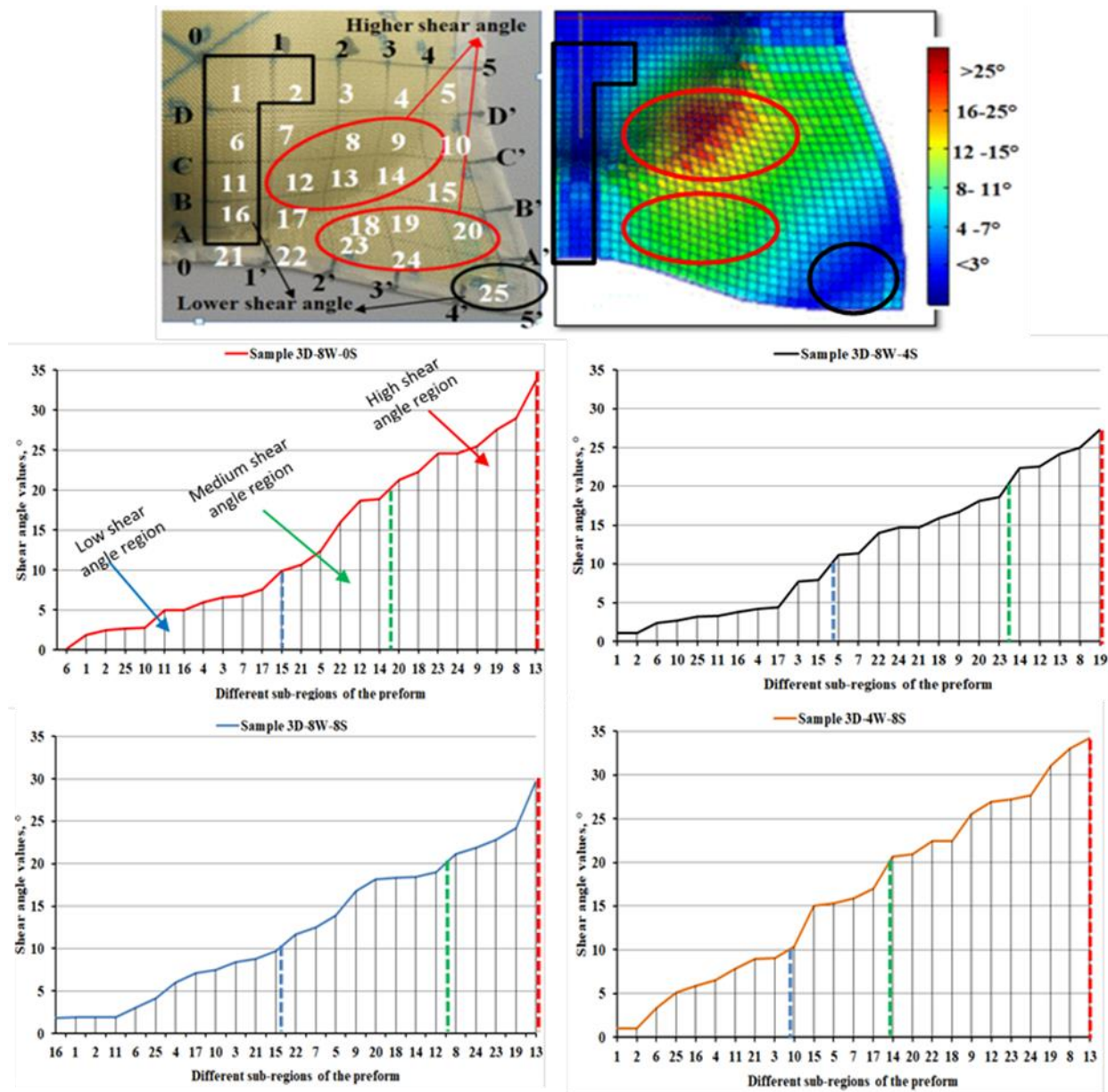
Figure 5.18 General in-plane shear angle diagram representations for the selected sub-regions and its measurement values for the different 3D warp interlock preforms

Based on the analysis, in general, all preform shows a similar trend of in-plane shear angle values in different clustered regions. A high in-plane shear angle values were more observed and accumulated both around the neck and corner-end near the neck regions of the deformed preforms. For example, both the deformed preforms around the neck area of sub-region 8, 9, 12, 13 and 14 and the majority of the flat surfaces near the neck of sub-regions 19, 20 23 and 24 were laid on the high in-plane shear angle clustered regions as compared to the other sub-regions. On the contrary, the centre top deformed preform of sub-region 1, 2, 3, 4, 6, 10, 11, 16 and 25, and the peripheral edges of the preforms sub-region 5, 15, 21 and 25 were located at low in-plane shear angle cluster region. However, according to the observation, all the preforms do not have similar sub-regions that could locate on the medium in-plane shear angle regions. Moreover, the in-plane shear angle values of the 3D warp interlock fabrics were also greatly affected by the interchange ratio of binding and stuffer yarns in the warp direction. According to these observations, as the compositions of the stuffer warp yarns inside the 3D warp interlock fabric structure increases, the in-plane shear angles were observed higher in a majority of the region. Samples 3D-4W-8S and 3D-8W-0S show higher in-plane shear angles whereas samples 3D-8W-4S and 3D-8W-8S revealed relatively lower or nearly equivalent in-plane shear angle values in most of the sub-regions. This is because the presence of an unbalanced warp yarns interchange ratio could reduce the stability of the preforms and might increase the deformation shearing effect on the preforms. Therefore, yarns in such preform which is made of unbalanced warp yarns ratio would be then easily disturbed and create a higher shear while forming easily. The maximum and minimum shear angles of samples 3D-8W-0S and 3D-4W-8S recorded a shear angle of 34° and 28° and 1.042° and 0.142 respectively. Besides, according to the numerical simulations obtained by using the commercially available software (Abacus FEA), it can be also seen that the predicted final shape and the different local shear angle of different sub-regions in one-quarter of the preformed dry fabric have shown a good agreement with the experimental result.

5.3.5.3 Influence of warp yarn system in material drawing-in values

When the dry fabric preform undergoes the forming process, some of the preform lengths have been consumed due to deformations. The consumptions of the length could be different at various preform positions depending on the shape of the punch. For example, in the single-curved hemispherical punch, the positions with higher deformation depth possess the maximum consumed length toward the centre of deformation. However, not only the punching shape (diameter and depth) but also various factors would also contribute to the drawing-in values. Base on researches, the preform binding pressure, stamping load, preform thickness, material types and fabric architectures were also some of the factors which greatly affect the drawing-in values [29][45][46]. Like shear angle measurements, the image from the inbuilt camera on the top of the forming machine was extracted by the ImageJ software to compute the different drawing-in values at different positions. **Figure 5.19 (a), (b) and (c)** show the flat, deformed and flat-deformed super-imposed preform representations to compute the material drawing-in values at designated different positions. As discussed in experimental methods, only 1/4th regions of the preforms were considered for analysis due to its quasi-symmetric forming

properties. The average values of the three tested preforms with the same testing conditions were presented.
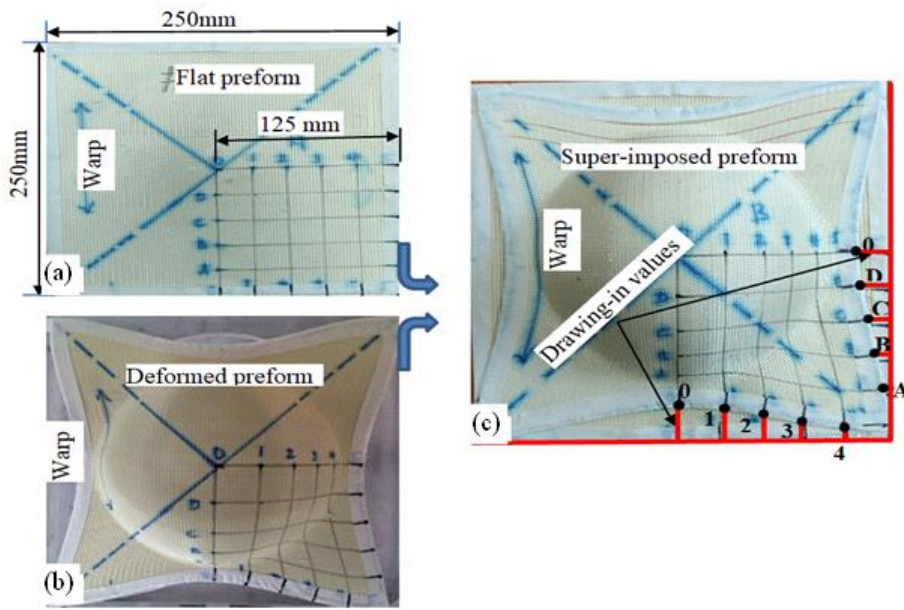
Figure 5.19 (a) Flat, (b) deformed and (c) Flat and deformed preform super-imposing to compute the drawing-in values of 3D warp interlock preforms at different positions

Figure 5.20 (a) and (b) show the representation of the drawing-in values at different positions both in the weft and warp directions respectively. As per the general observations, the involvements of different proportions of binding and stuffer warp yarns greatly influence the material drawing-in values of 3D warp interlock preforms at different positions both in machines (warp, MD) and cross (weft, CD) directions. The involvements of stuffer warp yarn directly proportional to the preforms' drawing-in values.
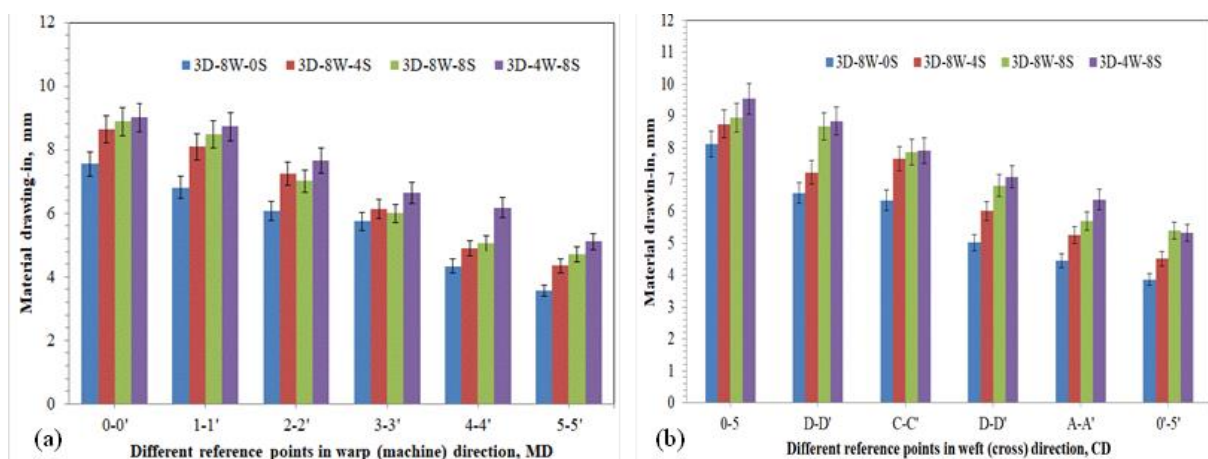
Figure 5.20 Influences of warp yarn system on the drawing-in values of 3D warp interlock preform at different points in the machine (a) and cross (b) direction

As shown in **Figure 5.20 (a),** as the stuffer warp yarn interchange ratio inside the fabric structure increases, the drawing-in values were found higher in all defined positions. Samples having a higher stuffer warp yarns ratio inside the structure, for example, sample 3D-4W-8S, revealed higher drawing-in values. On the contrary, preform with no stuffer yarn, sample 3D-4W-8S, exhibited the minimum drawing-in values among all the preforms at all reference positions. Moreover, preform 3D-8W-8S revealed higher drawing-in values in the majority of measured positions as compared to its counterpart preform, sample 3D-8W-4S. The main reason for this is that, as the involvements of binding warp yarn inside the fabric increases, due to its higher yarn undulations/waviness property, the preforms will not be quickly draws-in toward the centre of the punching region until all the undulated yarns are fully straightened. **Figure 5.21** represents the waviness structure of both the stuffer and binder yarn which is taken from the preform 3D-8W-8S. As the punching process proceeds, only after the straightening of the yarn completed, then the preform started to draw-in. This delay of draw-in due to the straightening of the waviness of the yarn inside the fabrics has shown a negative effect on the final draw-in values of the preform.
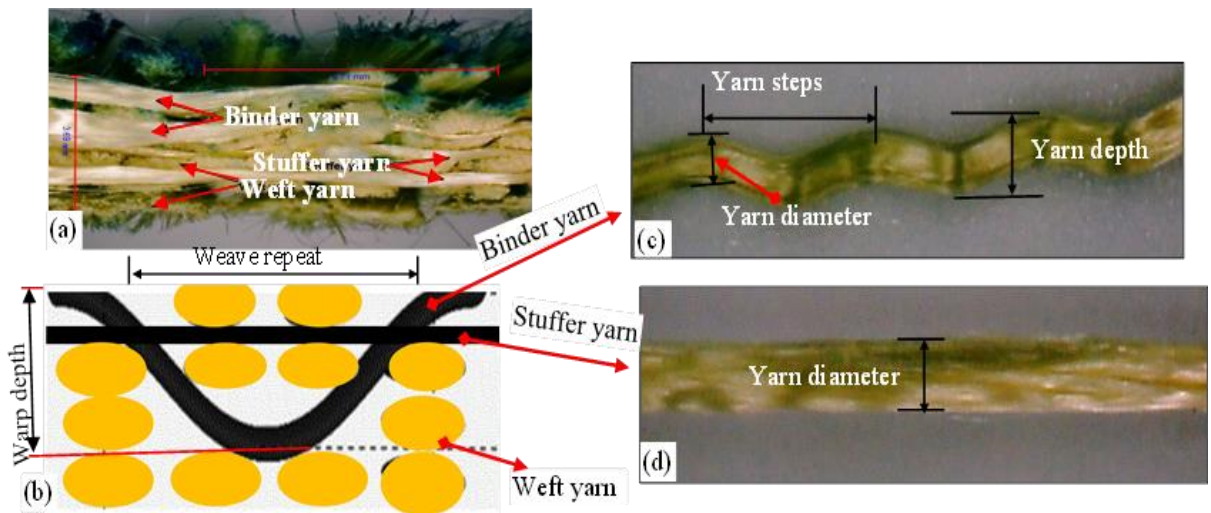
Figure 5.21 (a) and (b) microscopic and models of fabric cross-sectional view respectively, and (c)binder and (d) stuffer warp yarn waviness inside the 3D warp interlock fabric structure

On the contrary, fabric with more stuffer warp yarn, for example, 3D-4W-8S, will start drawing-in toward the centre of the punch due to very low undulations of the yarn inside the fabric as the punching load starts to apply. This means that as the punching load applied, the fabric directly starts to drawing-in toward the centre without the straightening process of the yarn inside the fabrics. As shown in **Figure 5.20 (b),** the interchange ratio of the warp yarn in the machine direction was also affected by the drawing-in values of the preform in the cross-direction. Considering all the parameters in the cross (weft) direction are similar, as the interchange ratio of binding warp yarns in the machine direction increase, the drawing-values in the cross direction were also recorded lower and vice-versa. This is because the presence of different warp yarns system in the fabrics will also impose different compression loads on the weft yarns. However, still, the result revealed a lowered drawing-in values in the cross (weft) direction as compared to its corresponding machine (warp) direction at similar reference measured positions. This is because of the involvement of higher yarn waviness in machine directions to absorb

some of the punching load before the drawing-in phenomenon takes place. Moreover, the maximum and minimum draw-in values of different 3D warp interlock preform forming both in machine and cross direction at various reference positions are presented in **Figure 5.22 (a) and (b)**. In general, the maximum and minimum drawing-in values were achieved at the centre top (MD (0-0') & CD (0-5)) and far corner peripheral edges (MD (5-5') & CD (0-5')) of the preform respectively for all fabric types.
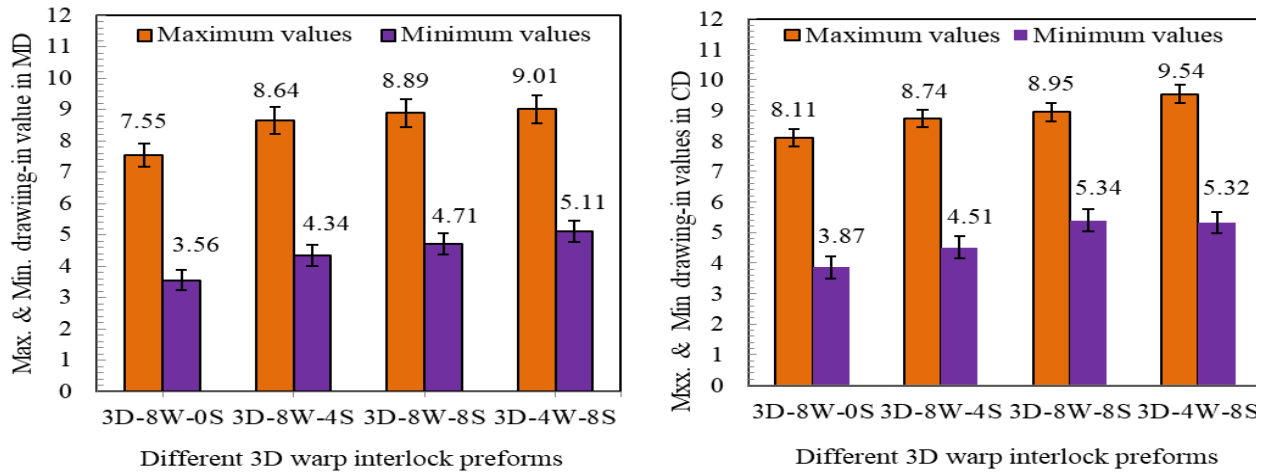
Figure 5.22 The maximum and minimum drawing-in values of 3D warp interlock preforms in Machine (MD) (a) and Cross (CD) (b) direction

3D-4S-8W and 3D-8WS-0S preform possess the highest and lowest drawing-in values both in the machine and cross direction among other preforms as shown in **Figure 5.22 (a) and (b)**. 3D-4S-8W achieved a 1.46 mm (16.2 %) and 1.43 mm (14.99 %) higher drawing-in values than sample 3D-8W-0S in the machine (0-0') and cross (0-5) directions of maximum drawing-in positions respectively. Similarly, a 1.55 mm (30%) and 1.45 mm (27.25 %) increments were observed at the minimum machine (5-5') and cross (0-5') reference position of 3D-4S-8W than sample 3D-8W-0S. Besides, both samples 3D-8W-8S and 3D-8W-4S have also exhibited higher and lower drawing-in values than 3D-8W-0S and 3D-4W-8S respectively both in machine and cross directions. For example, sample 3D-8W-4S noted lower drawing-values by 0.8 mm (8.3 %) in the cross (weft) and 0.37 mm (4%) in the machine (warp) maximum positions. Similarly, sample 3D-8W-8S were also revealed lower drawing values by 0.59 mm (6%) in the cross (weft) and 0.12 (1.3%) in the machine (warp) maximum positions. Furthermore, for all the preforms, the maximum and minimum drawing-in values were recorded slightly higher values in cross direction as compared to the machine direction. For instance, sample 3D-4W-8S shows a 0.53 mm (5%) and 0.21 mm (3%) increment at maximum and minimum draw-in positions respectively in the cross direction than machine direction. In the same way, 3D-8W-8S also revealed an increment of 0.06 mm (0.06%) at maximum and 0.63 (1.1%) in minimum draw-in positions of values in cross direction than machine direction. From this, it can be also concluded that within the same preforms the interchange warp ratio in warp direction has played a great role in lowering the material draw-in in the machine direction.

5.3.6 Forming recovery characteristics

After releasing the specific punching loads which are used for deformation, the different forming behaviours of the textile material start to recover from its deformational state (formed initial dimension) through time to the original position mainly in three dimensions (height, length, and thickness). Due to the complexity of textile mechanics, even though it is very difficult to fully understand the recovery behaviour of the material, however, it is also possible to use some quantitative analysis to compute its recovery behaviour. Understanding of such behaviours would help to define the suitability of an engineered material for particular applications. While using forming as manufacturing techniques, besides determining how much the textile material resists the forming loads and sustain its maximum loads, it is also very important to understand how the material behaves in the recovery of the deformed positions while removing the forming load [351]. The recovery properties of the textile material after forming might be either important (where an aesthetic requirement is predominant, such as most apparel or furnishing uses) or demerit in some industrial applications (soft body armour, composite parts, flat-spotting of tires, etc.). Normally, such recovery performance of the textile material is mainly dependent on the different parameters which are involved during the forming process. In this section, we tried to discuss the influences of the warp yarn interchange ratio on the different 3D warp interlock preform recovery behaviours after releasing the deformational loads by hemispherical punches. This includes the drawing-in recovery, maximum deformed depth recovery and in-plane shear angle recovery of 3D warp interlocks fabrics. The deformed preforms were kept in the standard atmospheric conditions (20 °C at 65% RH) for 48 hours before recovery measurements.

5.3.6.1 Influence of warp yarn system on maximum deformed height recovery

Deformational recovery at maximum depths of the preform in the punching directions is also one of the forming characteristics that have to be considered while moulding. This would help to consider the recovery parameters while applying for the specific technical application including soft body armour design and deformable composite parts. In this section, the effects of warp interchange ratios on the maximum height deformational recovery of dry 3D warp interlock preforms in the forming process have been investigated. **Figure 5.23** shows the pictorial side and sectional representations while deformation and after recovery at the maximum depth positions. The deformational depth (H_o) is the measured highest deformation value while forming in the stamping direction.
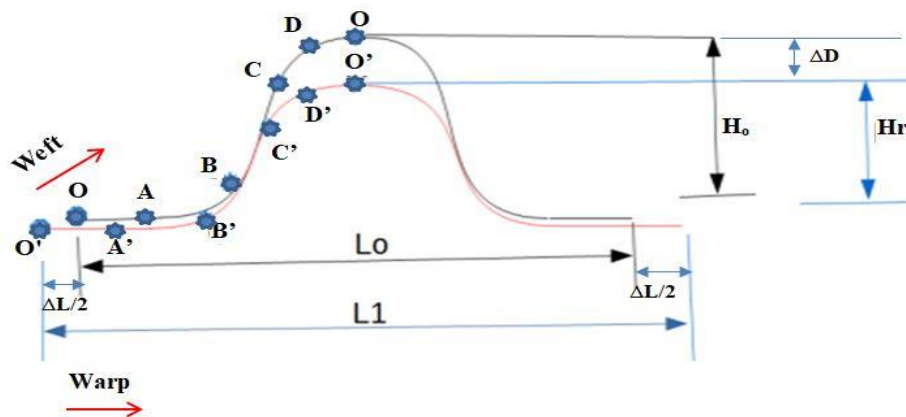
Figure 5.23 Schematic diagrams of the preform in front view at maximum deformation (Ho) and after recovery (H$_r$)

The deformational depth (H$_o$) is the measured highest deformation value while forming in the stamping direction. This measured deformation height value is the first deformational height which is constant throughout all the preforms (65 mm). Whereas, deformational depth (H$_r$) is the deformational depth of the preform measured after the recovery. Both the deformational depth while and after forming was measured using a height measuring scale having 0.01mm precision. The deformational recovery percentage (ΔD) at the highest deformational displacement is given as:

$$\Delta D = \left((Ho - Hr) / Ho \right) * 100 \qquad\qquad (5.2)$$

Where,

ΔD- is the deformational recovery in percentage at maximum central depth toward the punching load,

H$_0$ – is deformational recovery at maximum central depth while forming;

H$_r$ - is deformational recovery at maximum central depth after recovery

Figure 5.24 illustrates the deformational recovery at the maximum depth for different 3D warp interlock fabrics preforms. The result depicts that, the warp yarn interchange ratio revealed an influence on the deformational depth recovery of 3D warp interlock fabric during forming. In general, the involvements of higher stuffer warp yarn interchange ratio inside the 3D warp interlock preform possesses a higher maximum depth deformational recovery percentage as compared to the fabric with lower stuffer warp yarn interchange ratio. Preform 3D-8W-0S (100% binder yarn) and 3D-4W-8S (33.3% binder and 66.7% stuffer warp yarn) revealed a lower and higher deformational height recovery percentage respectively compared to all other preforms.

170
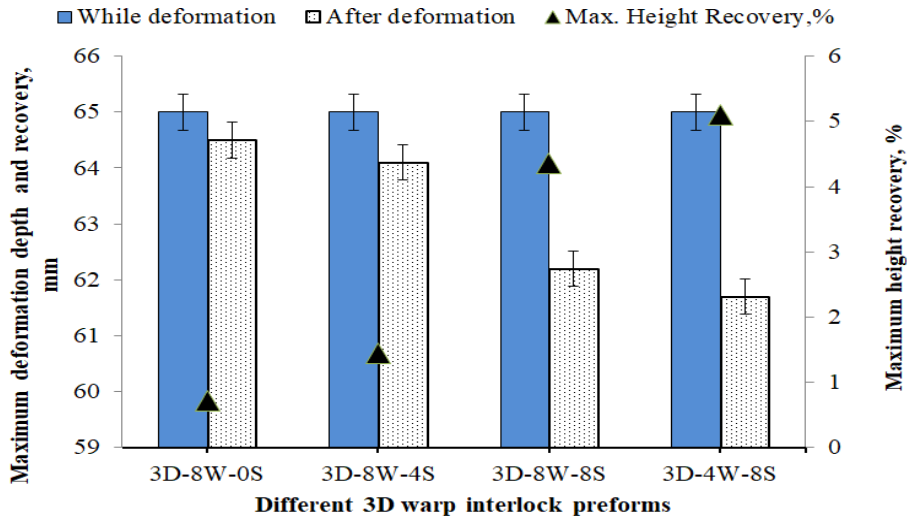
Figure 5.24 Forming recovery at maximum depths of the different preform

Sample 3D-4W-8S exhibited a maximum deformational height recovery percentage of, whereas 3D-8W-0S recorded only 0.72%. Moreover, samples 3D-8W-4S and 3D-8W-8S revealed 1.45% and 4.35% recovery percentages toward the deformational height at maximum position. Such performances are not only due to the involvement of higher yarn waviness, but 3D warp interlock fabrics with more binding warp yarns also give a tendency of good linking of the different layers of yarn throughout the weft layers. Performing such good interlacing of yarns could produce a higher binding force within the yarns inside the fabric and finally helps to enhance the stability of the preforms and resist to the recovery after deformations. In general, the investigation revealed that the warp yarns interchange ratio affects the deformational recovery of dry 3D warp interlock fabric preforms at maximum positions.

5.3.6.2 Influence of warp yarn system on drawing-in recovery

As mentioned previously, the textile material will undergo recovery from deformation after removing the punching force. The regaining of the material plane dimension both in warp and warp directions is one of the more important among the different recovered parameters. Such regaining of textile materials is referred to as drawing-in recovery values. For the sake of better measurement and comparisons, the recovery measurements were followed the reference points for all the preforms. **Figure 5.25** shows the representations of drawing-in value at initial and after to compute the recovery from forming. The recovery of the dimensions was computed in both directions of the 1/4th sub-regions by measuring the drawing-in values during forming and after keeping the deformed preform for 48 hours in atmospheric conditions. ImageJ software was utilized to measure both the drawing-in values during and after the deformations.
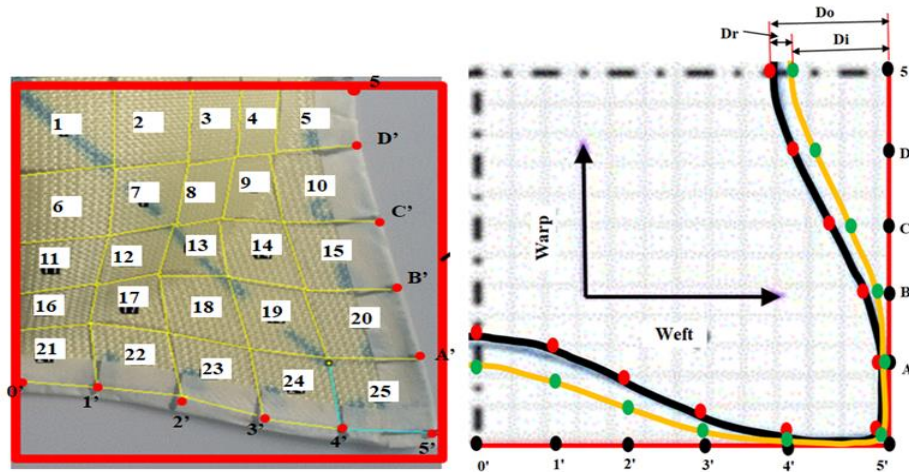
Figure 5.25 Pictorial and schematic representations of deformed preforms of the quadrant sub-region for drawing-in recovery representation

The drawing-in recovery of each preform was computed as:

$$Dr = (Do - Di \tag{5.3}$$

Where,

D_o - is drawing-in values at the initial,

D_i - drawing-in values after recovery,

D_r - the recovered drawing-in values after removing the load and waiting 48 hours.

To better understand the recovery performance and effects of the warp yarn system on the different 3D warp interlock preforms, the recovery percentage of the preform for the selected reference positions were computed. **Figure 5.26** shows the material drawing-in recovery
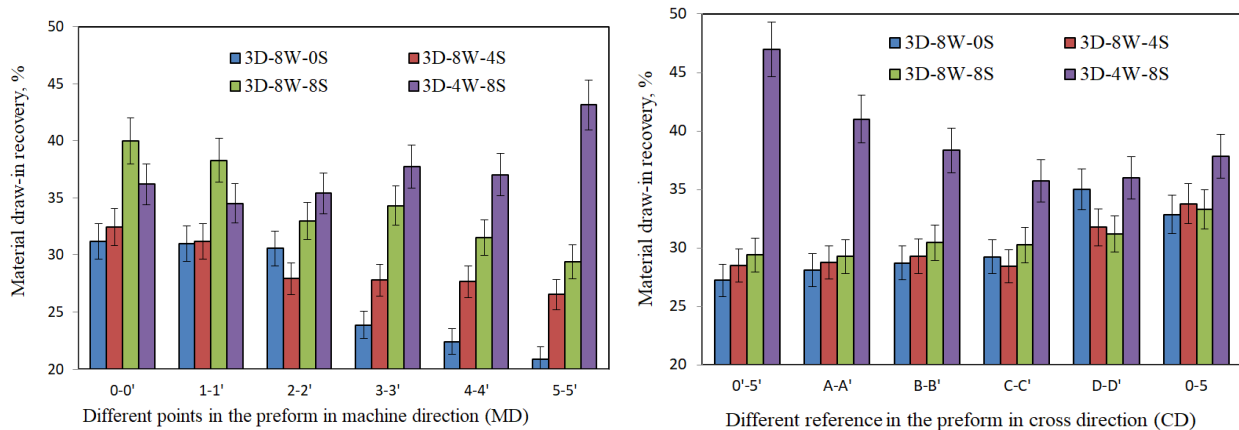
Figure 5.26 Influences of warp yarn inter-change ratio on the drawing-in recovery percentages of 3D warp interlock preforms at different points.

percentages values of the different 3D warp interlock preforms with different warp yarn system.

Based on the results, the involvements of the warp yarns interchange ratio on the drawing-in recovery were playing a great role both in the machine and cross directions. In general, the drawing-in recovery percentages of the preforms were found higher at the top centre of the preforms and decrease as it goes toward the peripheral edges of the preform. However, sample

172

3D-4W-8S revealed higher drawing-in recovery percentages values around the far peripheral edges of the preform. The 3D warp interlock preform with a higher interchange ratio of stuffer warp yarns revealed higher drawing-in recovery percentage both in the warp and weft directions. However, 3D warp interlock fabrics with higher binding warp yarn interchange ratio face lower drawing-in recovery percentage to retain its original material position. For instance, 3D-4W-8S preform with higher stuffer warp yarns interchange ratio, and 3D-8W-0S preform with lower stuffer warp yarns interchange ratio, recorded higher and lower material drawing-in recovery percentage respectively in the majority of sub-region both in machine and cross directions compared to other preforms. Moreover, samples 3D-8W-8S and 3D-8W-4S both show a higher drawing-in recovery percentage than samples 3D-4W-8S. The yarns inside the 3D warp interlock fabrics made with higher binding warp yarn interchange ratios were not highly stressed during the forming process. This is due to the presence of extra yarn length/waviness during fabric production. This extra length of yarn/waviness then helps to relieve higher stress during forming by the punching loads which in turn gives lower yarn recovery. Moreover, the recovery percentage of the different preforms was also found higher in the machine (warp) than cross (weft) direction at the same reference positions. This is due to the weft yarn faces higher stress by the punching load due to its interlacing structure than the warp yarn. **Figure 5.27 (a) and (b)** also show the maximum and minimum drawing-in recovery percentage values of different 3D warp interlock preforms in a machine and cross directions respectively. Sample 3D-4W-8S revealed the maximum drawing-in recovery percentage values of 43.13% and 46.98% in the machine and cross direction respectively around the preform peripheral edges. On the contrary, samples with higher binding warp yarns as sample 3D-8W-0S show the maximum drawing-in recovery percentages values of 31.21 % and 34.99% in machine and cross direction respectively. Sample 3D-8W-8S retains its maximum drawing-in recovery percentage in machine directions more compared to 3D-8W-4S than in cross directions.
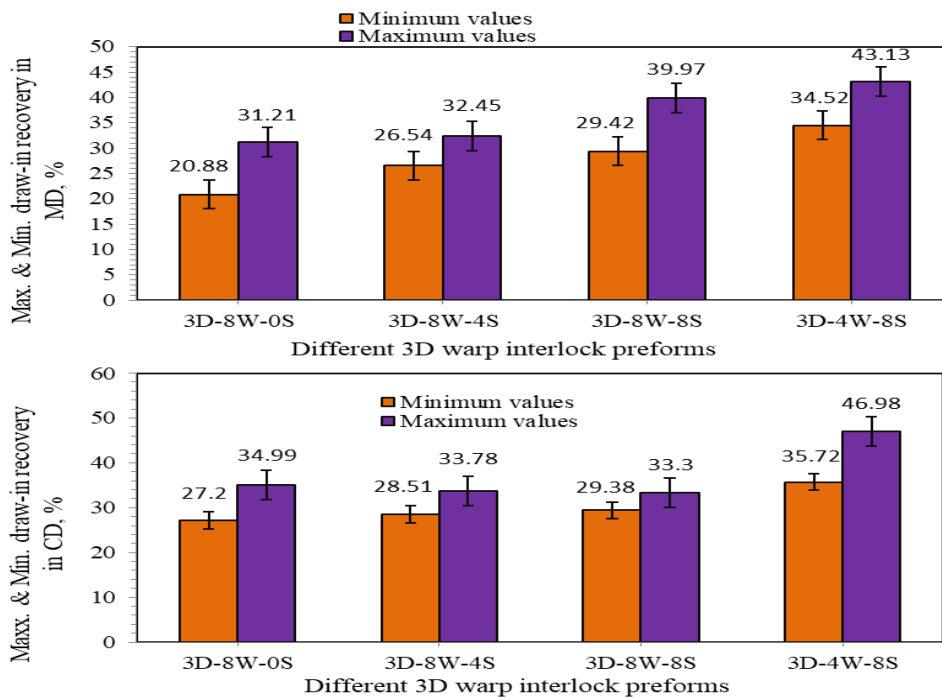
Figure 5.27 The maximum and minimum drawing-in recovery values of 3D warp interlock preforms after forming

5.3.6.3   Influence of warp yarn system on In-plane shear angle recovery

Like the drawing-in values, the in-plane shear angles of textile materials also tend to recover to its original positions after releasing the punching loads during the forming process. The recovery angles of the deformed preform ($|\rho-\mu|$) could be determined by measuring the different angles between the warp and weft yarns. As discussed earlier, the angle at initial deformation (ρ) was measured while deformation whereas, the final angle μ is measured after releasing the punching loads and keeping the preforms for another 48 hours at atmospheric conditions. **Figure 5.28** shows the in-plane shear angle recovery values of the different 3D warp interlock preforms for the selected sub-regions. Like the in-plane shear angle, the recovery also was clustered into three main regions, High, medium and low in-plain shear angle recovery regions for brief and better understanding. Based on the result analysis, regardless of the inter-change ratios of the warp yarn insides the fabric structure, nearly all the deformed preforms possess a higher amount of shear angle recovery around the neck of sub-region 8, 9, 12, 13, 14, 19, 23 and 24. This due to mainly the involvement of higher status of deformation in the specified regions. Whereas, the lower shear angle recovery was observed on the top and peripheral edges of preform sub-regions of 1, 2, 4, 6 11, 16 and 25. On the contrary, sub-region 3, 15, 17, 20, 22, 19, 18 shows medium values of in-plane shear angle recovery for all the preforms. Besides, 3D warp interlock preform having more stuffer warp yarns interchange ratio inside the structure revealed higher shear angle recovery in the majority of the sub-regions as compared to preforms with lower stuffer warp yarns.
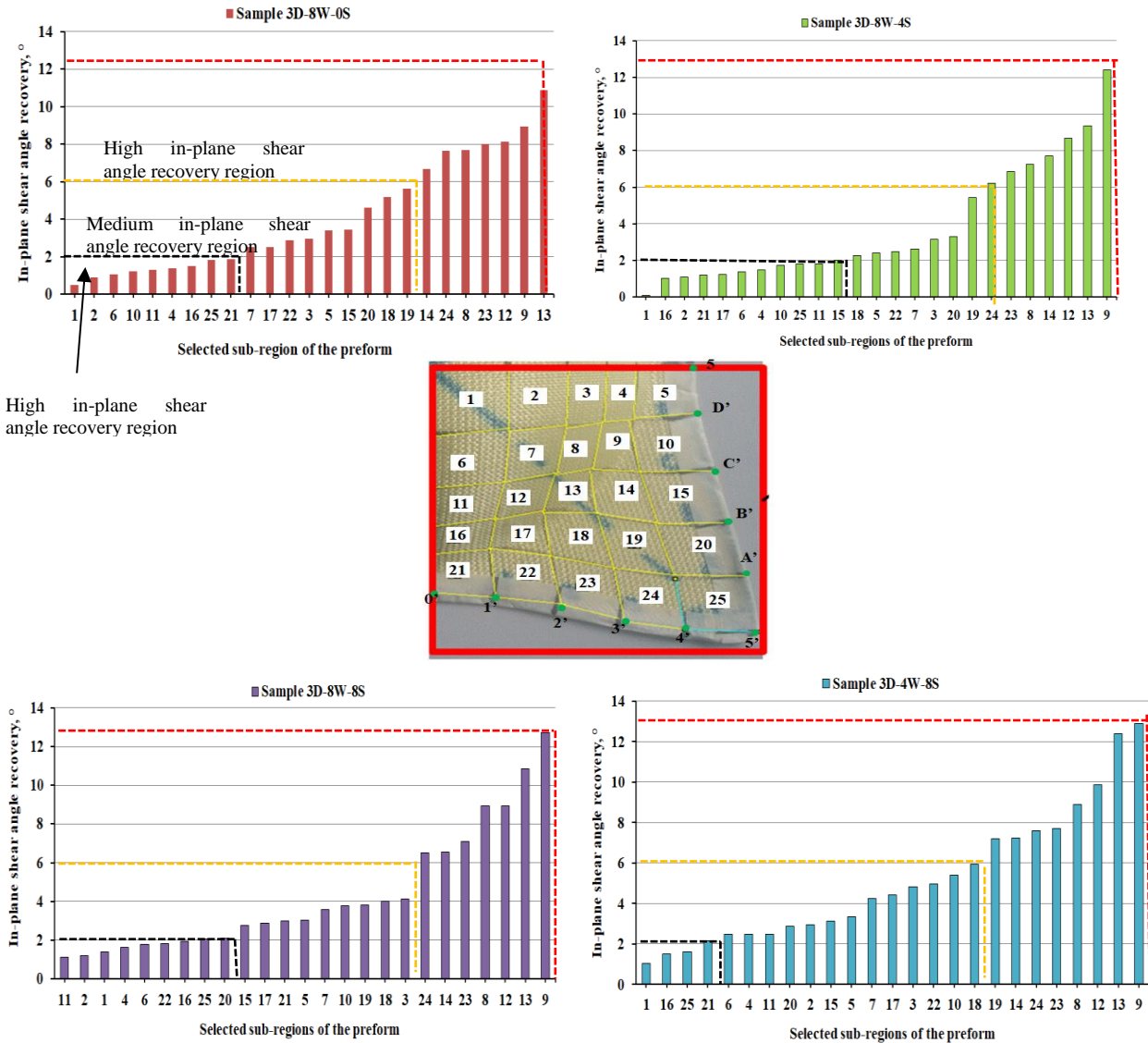
Figure 5.28 In-plane shear angle recoveries for the selected sub-regions of the different 3D warp interlock preforms in ascending order

Preforms 3D-4W-8S and 3D-8W-0S revealed higher and lower in-plane shear angle recovery respectively in majority sub-regions as compared to other types of the preform. The maximum in-plane shear angle recovery for 3D-4W-8S was 12% higher than preform 3D-4W-8S in the same positions. Whereas, preform 3D-8W-4S and 3D-8W-8S preforms show comparable in-plane shear angle recovery in most of the measured preform sub-region positions. Finally, the higher in-plane shear angle recovery for all 3D warp interlock fabrics was observed for the preforms which have higher shear angle values during deformations.

5.4 Conclusions

Technical application including soft body armour material should mainly possess not only good mechanical performance but also better light-weight and formability. Recently, introducing 3D warp interlock fabrics to substitute the traditional fabrics for the development of women's body armour to accommodate the bust for better protection and comfort had shown a great promise. However, understanding the critical factors affecting their mechanical and mechanical behaviours for better performance is very crucial. This chapter has investigated and discussed the effects of the warp yarn interchange ratios on mechanical and forming behaviours of 3D warp interlock p-aramid architectures. 3D warp interlock variants with the same structural characteristics but different binding: stuffer warp yarn ratios were manufactured (and as described in material sections) and some quasi-static mechanical and pneumatic based forming tests were carried out (described in the methodology section). Based on the result, the following conclusions were drawn:

➢ The warp yarn interchange ratios showed a significant influence on the tensile properties of the 3D warp interlock fabrics. Fabrics with higher stuffer warp yarn (3D-4W-8S) revealed higher tensile modulus (E) than fabrics with lower stuffer yarn proportion due to the improved stiffness and less waviness behaviour. Besides, fabrics with balanced proportions of stuffer and binding warp yarn (3D-8W-8S) exhibited two tensile peak points at failures because of the actual length difference between the two warp yarns during weaving. Unlike the warp directions, the different fabric load-strain curve in weft direction performed almost as a linear and progressive curve with approximately similar trends. This is due to possessing the same weft yarn compositions and yarn density among all the fabrics. The fabrics with higher binding warp yarn possess higher tensile strain at failure due to higher undulating properties of binding warp yarn inside the fabric architecture. 3D-8W-0S possesses higher tensile strain at failure in warp direction (12.88%) than in weft directions (5.88%), whereas, 3D-4W-8S records approximately equal tensile strain at failure both in the warp and weft directions (4.88%) due to having similar undulation of warp and weft yarns inside the fabrics structures. Unlike warp directions, the maximum tensile strain (εmax) and load (σmax) at failures in weft directions were slightly affected by the warp yarn even it possesses the same weft yarn compositions inside 3D fabrics architecture. 3D-8W-0S and 3D-8W-4S were failed at the tensile strain values of approximately around 5.88% and 7.8% and Sample C and D failed at the strain values of 7.55% and 4.8%.

➢ 3D warp interlock fabrics which comprise more stuffer warp yarn also possess the highest flexural rigidity as compared to fabrics with low or no stuffer warp yarns in the warp direction. Whereas, fabrics that only involved binding warp yarn (3D-8W-0S) revealed the lowest flexural rigidity. Moreover, the flexural rigidity in the weft direction has been also slightly influenced by the warp yarn compositions and found higher than the respective warp direction due to its less waviness and straight properties than warp yarns.

➢ The 3D warp interlock fabrics with either higher or lower binding warp yarns also revealed a higher crimp percentage for the binding warp yarn. 3D-4W-8S shows better-bending warp yarn crimp percentage followed by 3D-8W-0S whereas, sample 3D-8W-4S and 3D-8W-8S show almost similar crimp percentages. The crimp percentages of the stuffer yarn

were also influenced by the warp yarn compositions. As the proportion of stuffer yarn inside the fabric increases, its crimp percentages were found minimal since there was not much load applied on the stuffer yarn to bend inside the fabrics.

➤ The different forming characteristics of 3D warp interlock fabrics were greatly influenced by the warp yarn interchange ratio. For example, the increments of the stuffer warp yarn interchange ratio exhibit an impact and directly proportional to the stamping force while forming. Sample with higher stuffer warp yarns ratio possesses less yarn undulation in the warp direction which in turn needs a higher amount of punching loads to deform the preforms to the maximum deformational depth.

➤ Besides, in-plane shear angles were observed higher in the majority of the region for warp interlock fabric with lower binder yarn ratio. Furthermore, fabric structure with a higher stuffer warp yarn ratio also revealed higher drawing-in values than no or less stuffer warp yarn.

➤ The warp yarns interchange ratio also showed a great influence on the forming recovery properties of the 3D warp interlock fabric. The involvement of a higher stuffer warp yarns interchange ratio possesses a better deformational recovery percentage at maximum depth than fabric with a lower stuffer warp yarn interchange ratio. For example, preform 3D-8W-0S exhibited a maximum deformational height recovery percentage of 5.1%, whereas 3D-4W-8S recorded only 0.72%. Moreover, preform 3D-8W-4S and 3D-8W-8S revealed 1.45% and 4.35% recovery percentages toward the deformational height at maximum position. The drawing-in recovery percentages of the preforms were found higher at the centre top of the preforms and decrease as it goes toward the peripheral edges of the preform. Specifically, 3D-4S-8W revealed the maximum drawing-in recovery percentage of 43.13% and 46.98% in the machine (warp) and cross (weft) direction respectively around the preform peripheral edges. On the contrary, samples with higher binding warp yarns; 3D-8W-0S show the maximum drawing-in recovery percentages values of 31.21 % and 34.99% in the machine (warp) and cross (weft) directions respectively. In general, this chapter would give useful information and to further improve the overall understanding of the influences of the warp yarn interchange ratio on the formability behaviours of 3D warp interlock preforms.

6 Ballistic performance of 3D warp interlock p-aramid fabrics for women soft body armour

6.1 Introduction

Both the development of high-speed projectiles and explosive materials have reconstructed the dynamics of the battlefield, which further advocated the growth of advanced ballistic protection system with low cost, lightweight and comfortable to wear along with efficient energy absorbing capacity [42]. The ballistic impact is a very complex mechanical process when a low-mass high-velocity projectile propelled by a source onto a target which mainly effects near impact areas. Both energy absorption before it gains access to the body and energy distribution among the ballistic materials are the two aspects that help to understand the principle and effect of energy transfer from projectile [336]. For the last many decades, various materials including fabrics felt, metals and composite materials have been used in the development of body armour systems [303]. Generally, the effectiveness of the soft body armour related to ballistic impact performance, fitness and comfort depend on the type of ballistic material, material finishing, garment designing techniques, etc. Regarding the material, individual fibre types [40], yarn properties [8], material areal density [48], plies numbers [50], etc. show a great effect on the material ballistic performances. Besides, fabric construction and its type (2D, UD, 3D fabrics) are also one of the most important factors which influence the ballistic performances of the material[43][44][45]. Mostly 2D woven and UD laminates made from high-strength fibres are widely used in soft body armour due to their excellent mechanical properties and better fatigue life [304][305]. The high-performance fibres, such Twaron®, Kevlar®, Dyneema® and Spectra® are the well-known fibres extensively used in flexible personnel ballistic protection due to their high resistance-to-impact damage [50][79][80], high strength, high tenacity, good chemical resistance and lightweight characteristics [44][81]. Research studies have investigated the ballistic performances of various layers of different 2D fabrics and UD laminates made of high-performance fibres while developing soft body armour [93][380][381]. Unlike the male body armour, developing women's soft body armour with the required domed shape (moulding techniques) needs not only good ballistic materials but also proper material which could accommodate a unique body shape with adequate protection, fit and comfort [24, 158, 357]. However, to apply such designing techniques using a proper material which can both have the capacity toward both proper moulding capabilities without compromising the ballistic protection is very important. Today, 3D woven fabrics are also enormously involved in various ballistic protection including women soft body armor due to their enhanced mechanical properties in the thickness direction [304][305]. Besides, researchers have also claim 3D warp interlock structures shows not less ballistic protection performance and display excellent moulding ability and lightweight as compared to its counterpart 2D structures [46][147].

In our previous chapter (Chapter 3), patterns for single and multi-layers panels of seamless soft women body armour were developed using a reverse engineering and new pattern generation system. Besides, 3D warp interlock fabrics were also moulded using an adapted punch based on

the generated pattern and tested its fitness by draping on the physical mannequin [333][332][158][357]. However, besides testing it's forming ability and fitness for the design, testing the ballistic protection performances of 3D warp interlock fabrics in the current form are also a very critical parameter that should be considered. The current sub-chapter investigates and discusses the ballistic impact performances of 3D warp interlock fabrics (developed in the second campaign of the material section) and compared with its counterpart 2D plain fabrics for developing seamless women soft body protective armor.

6.2 Experimental

Two different kinds of fabric structures, 3D warp interlock O-L (orthogonal layer by layer) and 2D plain weave (Twaron- CT 716), made with same p-aramid yarns (Twaron®) were manufactured and prepared for the ballistic test against NIJ standard-Level IIIA for women body armour application. The 3D warp interlock fabric was designed and manufactured in GEMTEX, ENSAIT laboratory using an automatic Dornier dobby weaving machine. The corresponding 2D plain para-aramid fabric structure (Twaron-CT-709) which are mainly recommended for women soft body armour manufacturing due to its good ballistic protection performance combined with a high level of forming capability was purchased and delivered by Teijin® Aramid Company. The design, manufacturing process and the different parameters of the mentioned 3D warp interlock fabric (production campaign 2), and the specifications of 2D plain weave (CT-709) are discussed in the material sections.

6.2.1.1 Panels preparation for ballistic test

Five different panel targets were prepared for the specified ballistic test as described in **Table 6.1**. Among all the targets, three were made with 30, 35 and 40 layers of 2D plain weave fabric and the other two panels with 30 (6 panels) and 40 (8 panels) layers of 3D warp interlock fabric layers. All the panels were cut and arranged with 50 cm x 50 cm dimensions. The fabrics were cut by using ROBUSO SOLINGEN (Germany) based electro-powered shear delicately designed to cut multi-layered p-aramid and other heavyweight materials without any problem.

Table 6.1 Samples made of 2D plain and 3D warp interlock fabrics for ballistic test

Fabric type	Shooting panel system	No of layers	Total target areal density (g/m^2)	Target Weight (g)	Total target thickness (mm)
2D plain weave fabric	2D-40	40	8000	2000	12
	2D-35	35	7000	1750	10.5
	2D-30	30	6000	1500	9
3D warp interlock fabric	3D-40	40	8000	2000	14.4
	3D-30	30	6000	1500	10.8

The different layers in the target were prepared in a 90/90° ply arrangement system without any kind of assembling such as resin matrix or stitches. Rather each target was firmly attached at the edge using scotch tapes to avoid fibre unravelling and preventing the layers slippage from their

original positions. All the panels were kept in the black plastic bags to protect from degradation by different environmental effect including UV light. Each target panel was moulded at two pre-defined bust points using adapted moulding bench to resemble the women's frontal upper torso with 90B bust size before the test as shown in **Figure 6.1.** The design, working protocols and general principles of the adapted moulding bench for preparing ballistic samples are discussed in the methodology section. The samples were tested against ballistic impact according to NIJ 0101.06 Standard Level-IIIA [319]. Such standard level would give the highest level of ballistic protection among the soft body armour category. The ballistic testing apparatus along with the general testing procedures and different parameters considered were discussed in detail in the **methodology section.**
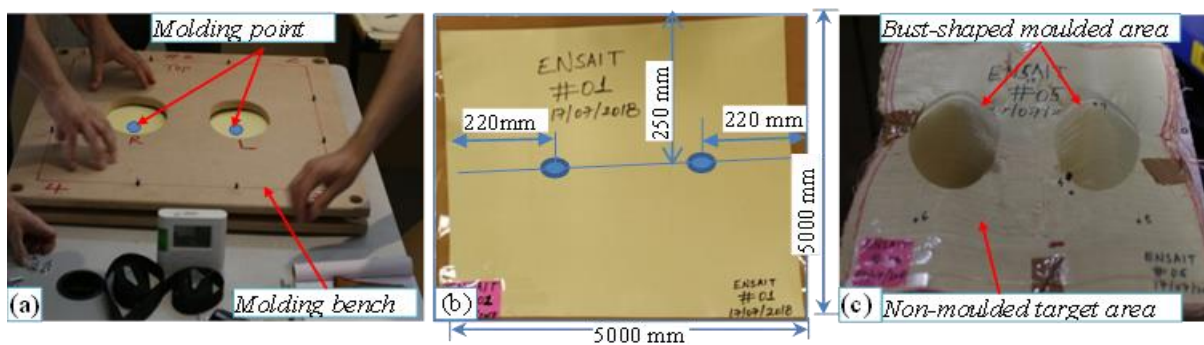
Figure 6.1 Sample preparation process for the ballistic test (a) Moulding of panels on adapted moulding bench, (b) Target before moulding, and (c) Moulded target panel

As discussed in the material and methods sections, Our investigation considers not only the non-perforation ballistic test approach which considered BFS values on the backing clay but also the surface failure mechanisms through microphotographs for assessing the ballistic impact performances of the different panels. Each panel was tested with three shots (shot 1, 2 and 4) at the moulded (d) area and another three shots (shot 3, 5 and 6) at the non-moulded (f) area of the panels considering the NIJ standard. The panel was properly mounted on the backing clay box using narrow fabrics with Velcro tape with uniform clamping pressure and tested as shown in **Figure 6.2**. The general scanning, modelling and measuring process of the BFS values were explained in the methodology section.
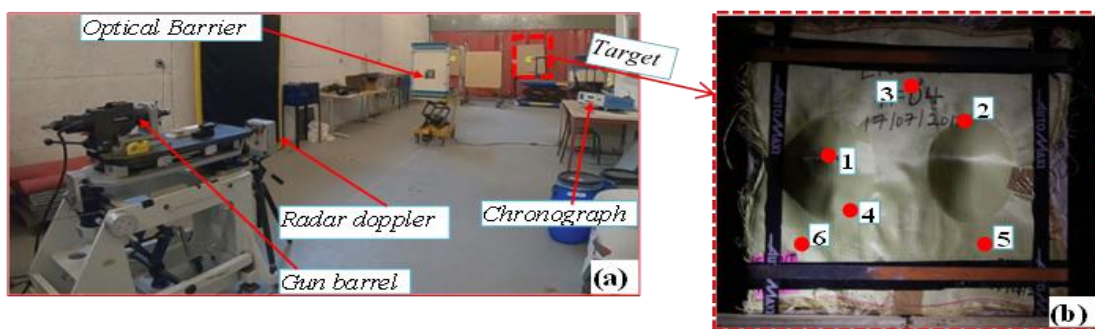
Figure 6.2 Ballistic impact testing (a) - Photograph of the ballistic testing apparatus and (b) mounted Panel with different shot points

6.3 Results and discussion

The measured BFS values were used to analyse and discuss the energy transmitted and absorbed values by the different panels**.** Besides, the ballistic impact performance mechanisms were also interpreted in terms of panel surface damage and post-mortem analysis of projectile deformation.

6.3.1 Analysis of the BFS depth and diameters of the tested panels

In this section, the effects of fabric types (3D warp interlock and 2D plain weave p-aramid fabrics), number of panel layers and shot points on the ballistic impact response of soft body armor panels are analysed and discussed using the measured BFS values. **Figure 6.3 (a) and (b)** show the BFS depth and diameter values of panels made of 3D warp interlock and 2D plain weave p-aramid fabrics respectively. Among the different factors, fabric type shows significant effects on the BFS values of panels made with a similar number of layers at the same shot points. For example, except in target shot point 4, the 40 layers of 2D plain weave fabric panel shows lower BFS depth as compared to its counterpart panel made with the same number of 3D warp interlock fabric layers (**Figure 6.3 (a)**). Similar results were also recorded for panels made with 30 layers of both woven fabric types. Besides, the number of layers involved in the panels also became one of the factors that affect the BFS measurements. Based on the result, considering similar fabric type, panels with a higher number of layers tend to decline the BFS depth in most of the shot points. For instance, the panels with 40 layers of 2D plain weave fabrics revealed very low BFS depth values in most of the target points compared to the corresponding panels with 30 and 35 layers with similar fabric type. This is since the higher number of the layer in the panel helps to lower BFS value through propagating higher energy into a larger panel area. For example, the average BFS depth for the 30, 35 and 40 fabric layers at moulded target shot 1 recorded 29 mm, 17 mm and 16 mm respectively. Panels with a similar number of fabric layers at the non-moulded shot point 6 were 22 mm, 21 mm and 13 mm respectively. Besides, panels with 40 layers show 47% and 39% BFS depth reduction at a moulded shot point 1 and non-moulded shot point 6 respectively as compared to panels of similar fabric type made with 30 layers. However, unlike BFS depth reduction, panels with a higher number of layers might also bring a negative effect on flexibility and comfort of the final panel while applying in soft body armour. So, the final panels should be maximized considering the weight, comfort and ballistic performances. Similarly, the moulded and non-moulded shot points have also shown an effect on BFS depth. According to the investigations, the target shot on the moulded area of the panel's revealed higher BFS depth as compared to the non-moulded target areas.

For example, panels with 40 layers of 3D warp interlock fabric and 2D plain weave fabric shown 29 mm and 16 mm in the moulded shot point 1 whereas, 23 mm and 13 mm for non-moulded shot point 6 respectively. Such increments of BFS depth in the moulded target areas might be due to various reasons. For instance, the thickness of the material in the moulded area could be reduced due to stretching and compacting of yarns around the area while panel forming. Such stretching of yarns will be then highly tensioned and could face fibre undulations

and different yarn defects. This phenomenon reduces the ballistic performances and increased the BFS depths of the final panels at the specified target points. The effects of the above parameters were also analysed in terms of average BFS diameter as shown in **Figure 6.3 (b)**. Like the BFS depth, the mentioned target parameters have also affected directly or indirectly the BFS diameter.
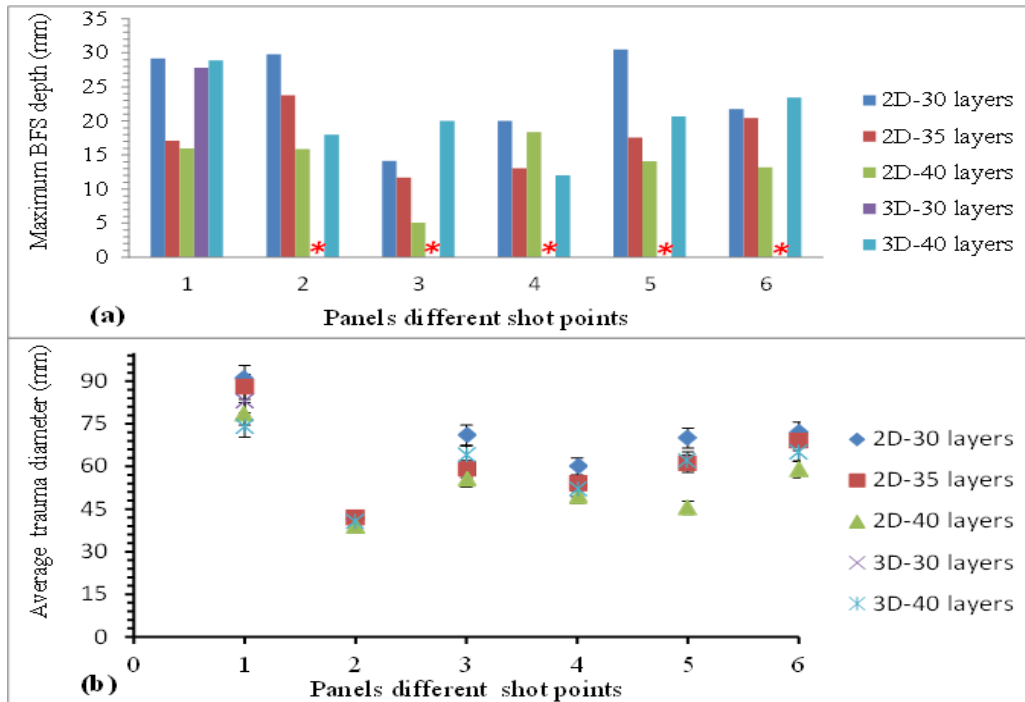
Figure 6.3 BFS analysis of the panels (a) The maximum BFS depth and (b) the averaged BFS diameters for panels made of 2D and 3D warp interlock p-aramid fabrics. *(*Except target shoot location 1, all target points of the panel made with 3D-30 layers were penetrated and BFS values were not considered at those points.)*

The panel targets made with a higher number of layers display lower BFS diameter considering the same fabric type and target shoot conditions. The type of fabric constructions has also exhibited an effect on the average BFS diameter of the final panel target

6.3.2 Energy absorption capability of 3D and 2D p-aramid fabric panels

In general, when the fabric panel is impacted by the high-speed bullet, the energy exerted by the projectile will be converted mainly into kinetic energy. Some portion of this kinetic energy is absorbed by each layer of the panels whereas; the remaining portions will be transmitted to the back of the target to create an indentation on the backing materials. The amount of energy absorbed by the target mainly depends on various internal and external ballistic performance factors. While ballistic impact, the energy generates shock wave propagations on the surface of the fabric which in turn damages the filaments, fibres, and yarns. The energy might also ultimately distorts the fabric layer in the longitudinal direction. Investigating the energy absorbed by the target panels and the transmitted energy to the backing material would help to understand such ballistic impact phenomenon. In this study, all panels were undergoing

deformation in order to resist the propagating energy exerted by the projectiles. The different projectile impact velocity, impact energy, and target panels with their corresponding absorbed and transmitted energy were computed. The kinetic energy generated on the target might be different from one to another shot due to the projectile speed difference even using the same projectile mass throughout the test. The following sub-section will discuss the energy absorption by the different panels of 2D and 3D warp interlock O-L fabrics based on the shooting target, target areas (deformed and flat) and type of fabric structures (2D and 3D fabrics) with nearly similar fabric layers and panel areal densities.

6.3.2.1   Effect of shot point condition on the energy absorption capabilities of panels

The kinetic energy of a bullet is the energy applied and affecting the panel targets during ballistic impact tests. Such kinetic energy generated by the projectile mainly depends on the projectile speed considering other factors constant including the mass and shape of the bullet throughout the test. This energy should be fully absorbed in the least by the final panel target before perforation and created some damages on the vital organs of the human body. Besides, the energy absorption capabilities of the panel will be influenced by different parameters including material properties, type of fabric structure, layers arrangement, panel finishing, panel thickness (areal density), projectile geometries, etc.

In this section, the energy absorption capabilities of panels made of 3D and 2D fabrics considering different target systems and shot points (moulded and non-moulded) will be discussed. However, the percentage of the absorbed and transmitted energy will give a better comparison than the computed absorbed and transmitted energy values. For example, different impact energy values could be generated at different shot points of the same panel due to the different impact bullet velocity. Owing to such circumstances, it is not possible solely to compare the energy absorption capabilities of each shot using directly the numerical energy (Joule) values. For instance, a panel made with 40 layers of 3D warp interlock fabrics absorbed 639.88, 656.78, 627.16, 669.53, 679.12 and 662.43 J of energy in shot points T1 (d), T2 (d), T3 (f), T4 (d), T5 (f) and T6 (f) respectively. However, the percentages of energy absorption of T 1(d), T2 (d), T3 (f), T4 (d), T5 (f) and T6 (f) were found 94.98%, 97.74%, 97.89%, 97.51%, 99.54% and 98.69% respectively. In this case, T2 (d) seems to absorb higher energy values than T3 (d), however, in normalization (percentage), the reverse is true. This indicated that energy percentage values will give a better room for comparisons of different shot points within the same panel than specific energy values (J). **Figure 6.4 (a), (b) and (c)** show the absorbed and transmitted energy percentage (%) values of 40, 35 and 30 layers of 2D plain p-aramid fabric respectively at moulded (d) and non-moulded (f) shot points. A significant energy absorption difference was found between the non-moulded (f) and moulded (d) target points of panels made with 40 layers of 2D plain weave fabric. The moulded (d) target points (T1 (d), T2 (d) and T4 (d)) show a less percentage of energy absorption capability than non-moulded (f) target points (T3 (d) and T6 (f)). For example, the absorbed energy percentages of T1 (d), T2 (d) and T4 (d) recorded as 96.93%, 97.74%, and 97.76%, whereas for T3 (f), T5 (f) and T6 (f) are 99.14%, 99.03% and 99.73%. This lower energy absorbing capabilities of the moulded area of 2D fabric panel might arise from various moulding defects which could hinder the ballistic protection

performances of those particular areas. The absorbed and transmitted energy percentage (%) of the target made with 35 layers of 2D fabric at different shooting points is also shown in **Figure 6.4 (b)**. Based on the observations, the targets at the moulded areas revealed a much higher energy transmitted percentage than the non-moulded target areas. The energy transmitted percentage beyond the panels at shots target area T1 (d), T2 (d), T4(d) are 4.99%, 4.63% and 3.02%, whereas shots at the target areas T3 (f), T5 (f) and T6 (f) were recorded 1.8%, 0.74%, 1.38%.
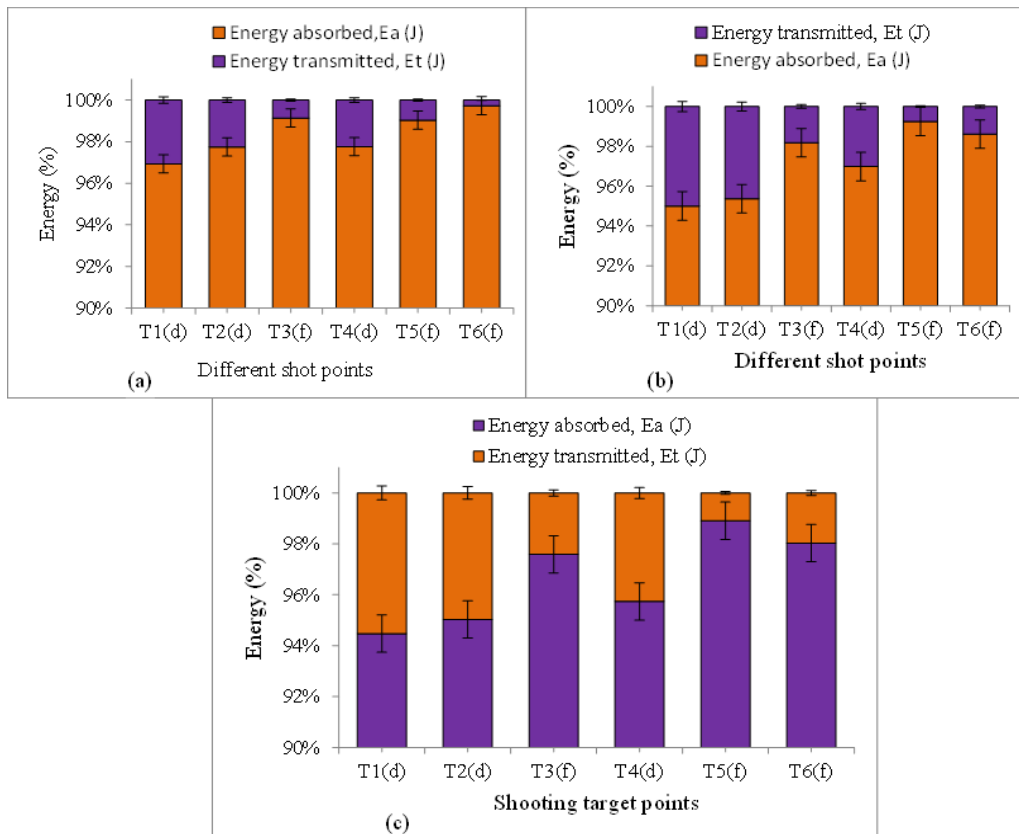
Figure 6.4 Percentages (%) of absorbed and transmitted energy of (a) 2D-40, (b) 2D-35 and (c) 2D-30 at different shooting areas (moulded (d) and non-moulded (f) area)

In general, it was found 4.25% value differences in the transmitted energy between the highest value (4.99%) at T1 (d) and lowest value (0.74%) of T5 (f). Similarly, the energy absorption and transmitted percentage (%) values for 30 layers of 2D plain fabric at different shot points show a similar trend as discussed in the previous panels. Its energy absorption and transmitted percentage (%) values are shown in **Figure 6.4 (c)**. The energy percentage of absorbed by moulded (d) target area of T1 (d), T2 (d) and T4 (d) were recorded as 94.45%, 95.03%, and 95.74%. Whereas, the percentage of the energy absorbed for non-moulded (f) target points T3 (f), T5 (f) and T6 (f) show 97.58%, 98.9%, and 98.03%. The panel has also revealed maximum and minimum energy absorption percentage capabilities in target points of T5 (f) (non-moulded (f)) and target points of T1 (d) (moulded (d) respectively. Moreover, the energy absorption capabilities of the 30 layer panel show smaller values as compared to the 35 and 40 layers both

in the moulded (d) and non-moulded (f) target points. In general, the result indicated that the energy absorbed and transmitted energy of the 2D fabric made panels was affected by the number of fabric layers and specific target point conditions. More energy was absorbed in the non-moulded shot points as compared to shot point at the moulded for all the panels regardless of the number of their layers.

The energy absorption and transmitted percentage (%) values of the two samples, 3D-40 and 3D-30, made of 3D warp interlock fabric at the moulded and non-moulded target points were discussed as shown in **Figure 6.5 (a) and (b).** Unlike 2D fabric panel targets, the energy absorbed and transmitted values of 3D warp interlock fabric exhibit differently. As shown in **Figure 6.5 (a)** except the two extreme higher (99.54%) and lower (94.98%) percentage values at target point T5 (f) and T1 (d) respectively, other shot points show a similar trend. Target point T1(d), T2(d), T3(f), T4(d), T5(f), and T6(f) of panels possess 5.02%, 2.26%, 2.1%, 2.48%, 0.46% and 1.31% of energy transmitted values. The increase in the transmitted energy almost corresponds to the decrease in the absorbed energy.
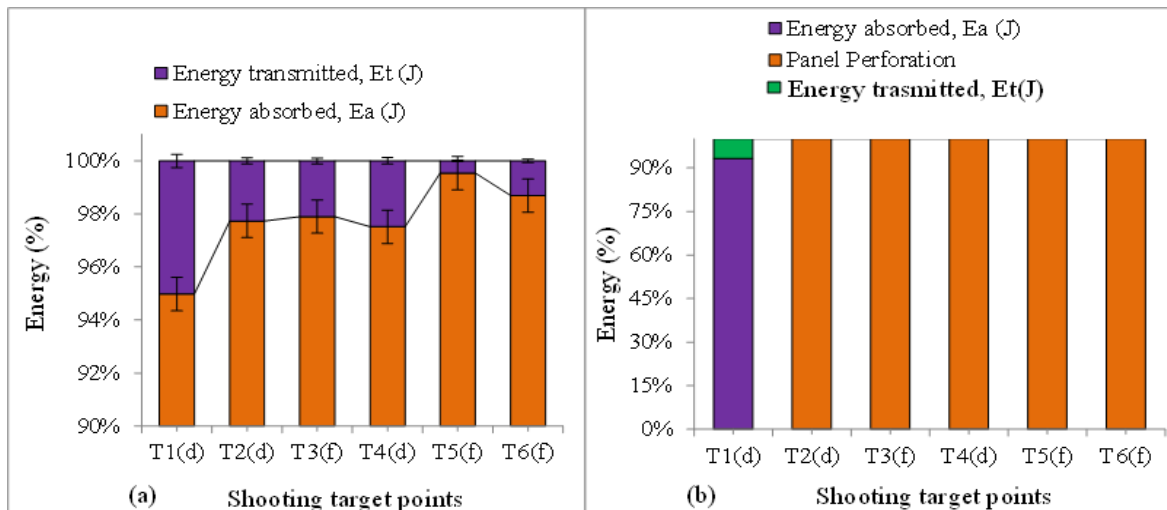
Figure 6.5 Percentages (%) of absorbed and transmitted energy of (a) 3D-40, (b) 3D-30 at moulded and non-moulded shot points)

The moulding process did not significantly affect the ballistic performances of the 3D fabric panel while shaping the panel to make the intended target form. **Figure 6.5 (b)** shows the energy absorbed and transmitted energy percentage (%) values of sample 3D-30 at different moulded (d) and non-moulded (f) points. The energy absorbed by the panel was calculated only when the panel is not penetrated. In this panel, except for T1 (d), all the shot points were unable to resist the ballistic impact from penetration and not considered for further analysis. Besides, panels made with 30 and 40 layers of 3D warp interlock fabrics recorded 93.28% and 94.98% of energy absorption values respectively at shot point T1 (d). This indicated that not only the shot point conditions (moulded and non-moulded) but also the number of layers involved in the panels contributed to energy absorption capacities. Moreover, the shot point conditions (moulded and non-moulded) were also more or less affected by the energy-absorbing

capabilities of all the 2D plain fabrics panels. However, unlike the 2D plain fabrics panels, panels made of 3D warp interlock fabric shows limited outcomes on the energy absorption and transmitted values in the moulded target points. This indicates that shots on moulded (d) and non-moulded (f) of panels made with 3D warp interlock fabric shows nearly similar energy absorbed percentages as compared to panels made of its counterpart 2D plain weave fabrics at similar shot points and fabric density. This is since 3D warp interlock fabric shows good forming ability without affecting the mechanical performances of the final products. The panel rigidity could also increase with the compactness of the respected fabric type. Such behaviour, in turn, brings a positive upshot on the energy-absorbing performances of the target.

6.3.2.2   Effect of fabric layers on energy absorption capabilities of 2D plain weave and 3D warp interlock fabrics panels

During the design of the ballistic protection panel, the panel weight is taken into consideration as much as ballistic performance is considered. As discussed above, the number of fabric layers in the panel system has a direct relation to its energy-absorbing capabilities. The more the fabric layers in the panel system, the higher the energy will be absorbed by the panel. However, a higher number of layers lowered the flexibility and increase the rigidity of the ballistic panel. Rigid ballistic panels also not only limit the movement of the user but also create difficulty in the body armour design and production process. This contradiction makes it very difficult to achieve the body armour entailing both light-weighted along with better ballistic protection performance. Various materials that encompass the above parameter have been investigated for the optimization of the final ballistic panel.

This section thoroughly discussed the energy absorption capabilities of panels composing 2D plain weave and 3D warp interlock fabric layers. **Figure 6.6 (a) and (b)** show the average energy absorption and transmission percentage (%) values of 2D fabric with different layers at non-moulded (f) and moulded (d) shot points respectively. Based on that result, in general, the energy absorption capacity of the panel significantly increased as the number of ply fabric increases. For example, the average percentages (%) of energy transmitted by panels made with 30, 35 and 40-layers of 2D fabric were also computed as 1.82%, 1.31% and 0.70% at the non-moulded shot points. This clearly shows that panels made with 40-plies 2D fabrics transmitted 1.11% and 0.6% fewer energy values as compared to panels with 30 and 35-layers of 2D fabrics respectively. Besides, the result also clearly shows the energy absorbed has been increasing when the layers have been increased from 30 to 35 and from 35 to 40. Besides, as shown in **Figure 6.6 (b),** at the moulded (d) target points, the panel of the sample with 2D-30, 2D-35, and 2D-40 absorb the average percentage (%) of 95.08%, 95.8% and 97.48% of the total projectile kinetic energy. This indicated that 2D-40 absorbed an average 2.4% more energy as compared to sample 2D-30 at the moulded (d) target points. However, sample 2D-35 absorbs almost equal average energy as compared to sample 2D-30. This clearly shows that as the number of layers in the panel increases, the energy absorbing capability difference between samples made of 3D warp interlock and 2D plain weave fabric becomes insignificant.
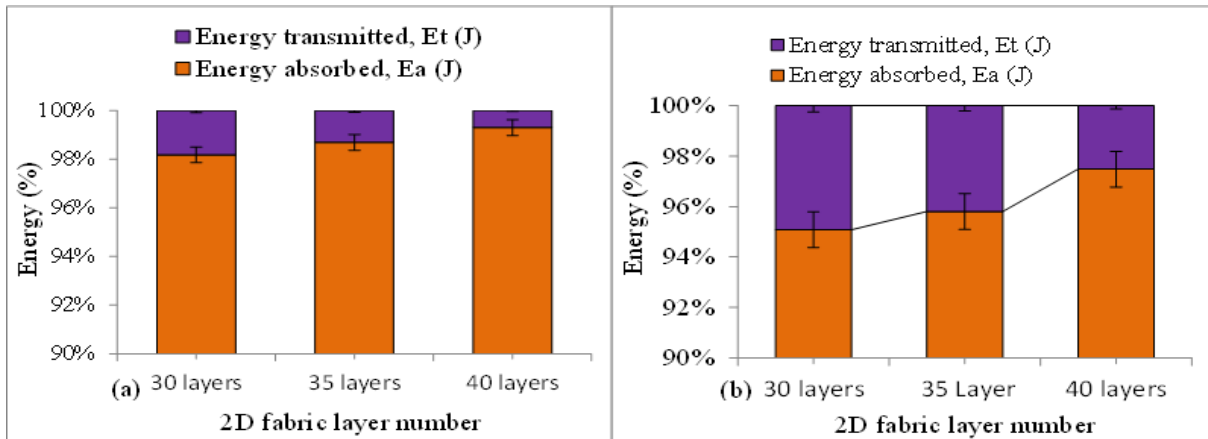
Figure 6.6 Average energy absorption and transmission (%) values of 2D fabric with different layers at (a) non-moulded (f) (shot 3, 5 and 6) and (b) moulded (d) (shot 1, 2 and 4) areas

6.3.2.3 Effect of fabric type on energy absorption capabilities at different shot points

Nowadays high-strength woven fabrics made of polymeric yarns are widely used for ballistic materials due to their low density and high toughness. Those materials give good resistance to high-speed loading, particularly during ballistic impact. Though, their response to impact is complex because of the final material fabric architecture, target conditions and rate-dependent behaviours of their constituent yarns. Different researches have been studied on the different influential factors of the ballistic performances of materials. Fabric type was found one of the key factors which affect the ballistic performance of fabrics.

This section compares the ballistic impact performances and energy absorption capabilities of the final target made of 2D plain weave and 3D warp interlock fabrics of the same fabric density. Moreover, the comparison has been also considered not only the type of fabric type but also the impact point condition (moulded (d) and non-moulded (f)) of the fabric panels. **Figure 6.7** illustrated the average energy absorption by the panel and transmitted to the backing material of percentage (%) values of 2D plain weave and 3D warp interlock fabrics. For a better analysis, the same numbers of layers (40 layers) with similar fabric densities for both fabric structures at similar target points were considered. The energy absorbed by the moulded (d) target panel of 2D plain and 3D warp interlock p-aramid fabric panels were found 650.79J and 655.4J. Whereas its energy transmitted energy to the backing material is recorded with 16.82J and 22.03J. However, due to the different initial impact energy which emanates from impact projectile velocity, the energy absorbed and transmitted energy values might be different. Considering this it is necessary and efficient to analyses the intended panel energy absorption capabilities in terms of fraction or percentages (%) as shown in **Figure 6.7 (a).** Based on this analysis, 40 layers of panels made with a 2D plain weave and 3D warp interlock p-aramid fabrics at the moulded target points possess 97.48% and 96.75% energy absorption respectively. Whereas the energy transmitted values beyond the 40 layer panel of 2D plain weave and 3D warp interlock p-aramid fabrics were recorded as 2.51% and 3.25% respectively. This primarily indicated that the energy absorbed by the 2D fabrics at the moulded target points shows 0.74%

increment and 0.74 % decrement of energy absorption and transmitted energy values respectively compared to 3D warp interlock fabrics. In the other direction, the amount of absorbed and transmitted energy by the 2D plain weave and 3D warp interlock p-aramid fabrics considering the average values at the non-moulded (f) target points was analysed. The average energy absorption and transmission percentage values for 40 layers of 2D plain weave and 3D warp interlock fabric panels at non-moulded (f) target area has been also discussed. For better analysis, other than the numerical values, it is also imperative to discuss more on the percentage values of the absorbed and transmitted energy both in the 2D plain weave and 3D warp interlock fabrics panel at non-moulded (f) target. Based on the ballistic test, the total ballistic impact energy exerted was found 659.79J and 664.71J on the 40 layers of 2D plain and 3D warp interlock fabric panels at the non-moulded (f) target respectively. Among the total energy, 659.79J and 664.71J were recorded as average absorbed energy by the panels. However, 4.63J and 8.47J energy were transmitted beyond the intended panels of 2D plain weave and 3D warp interlock fabrics respectively. The percentage (%) values of the absorbed and transmitted energy by the intended panels (40 layers) of 2D plain weave and 3D warp interlock fabrics at non-moulded (f) target points were also highlighted as shown on **Figure 6.7 (b).**
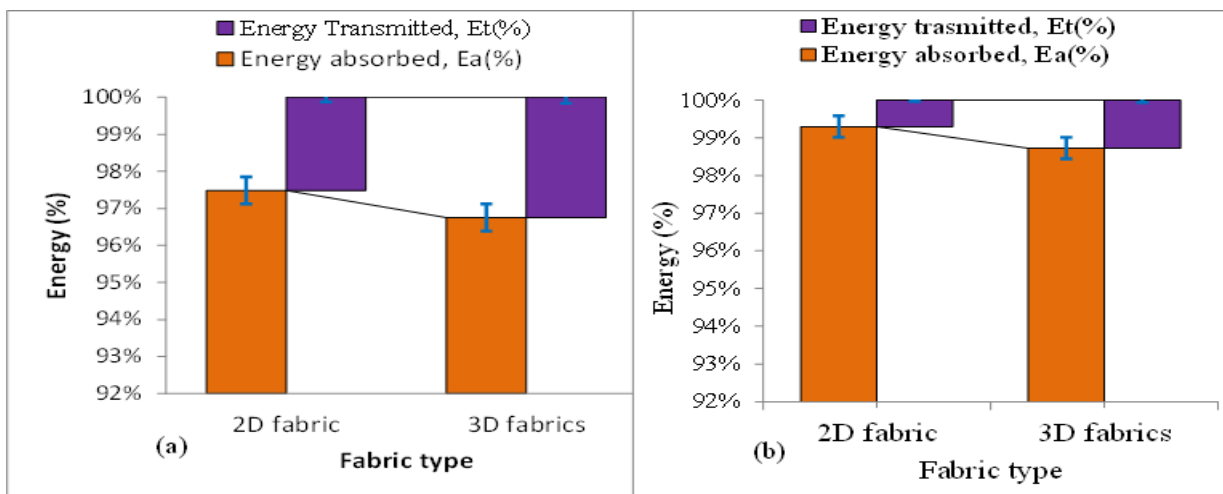
Figure 6.7 Average energy absorption and transmission percentage of 2D-40 and 3D-40 at (a) Moulded (d) area (average values of shot 1, 2 and 4), and (b) non-moulded (f) area (average values of shot 3, 5 and 6)

Based on these investigations, their respective initial total impact energies, 99.29%, and 98.72% were absorbed by the panels, whereas 0.7% and 1.27% of energy were transmitted beyond the panels of 2D plain weave and 3D warp interlock fabrics respectively. Unlike in the moulded target areas, the absorbed energy of the 2D plain weave panels shows 0.67% of increment as compared to 3D warp interlocks panels. On the contrary, the energy transmitted to the backing material by the 2D plain panel shows 0.57% of decrement as compared to 3D warp interlock panels. This small difference does not show by itself as a significant effect in the energy-absorbing capabilities of the panels. 2D and 3D warp interlock fabrics with the same number of layers show almost similar energy absorbing capabilities during ballistic impacts. Moreover, the

conditions of target areas within the same number of fabrics type also show almost smaller difference both in the energy absorption capabilities of the panel and its transmitted energy to the backing materials. As shown in **Figure 6.8,** the average energy absorption and transmission values and its percentage of both 35 layers of 2D fabric and 40 layers of 3D fabric both at non-moulded (f) and moulded (d) target points were also investigated. The average percentage (%) energy absorbed and transmitted at the non-moulded (f) points of 35 layers of 2D fabrics panels was recorded as 98.68% and 1.31%. Whereas 98.7% and 1.27% values were observed in the non-moulded (f) points of target panels made with 40-layers 3D warp interlock fabric. On the contrary, the average percentage (%) energy absorbed and transmitted at the moulded (d) target points with 35 layers of 2D fabric panels was recorded 95.8 % and 4.19%. 96.75% and 3.25% values plotted for 40-layers of 3D warp interlock fabric panels in the moulded (d) target points. Besides, the average percentage of energy absorbed and transmitted while impacting 35 layers of 2D fabrics panel at deformed target area reveals almost similar values as for 40 layers of 3D fabrics panel compared to at the non-moulded points. As per the general observations, the energy absorption of the 3D warp interlock fabric panel shows better capabilities in the moulded (d) target points than non-moulded (f) points as compared to 2D plain weave fabric panels.
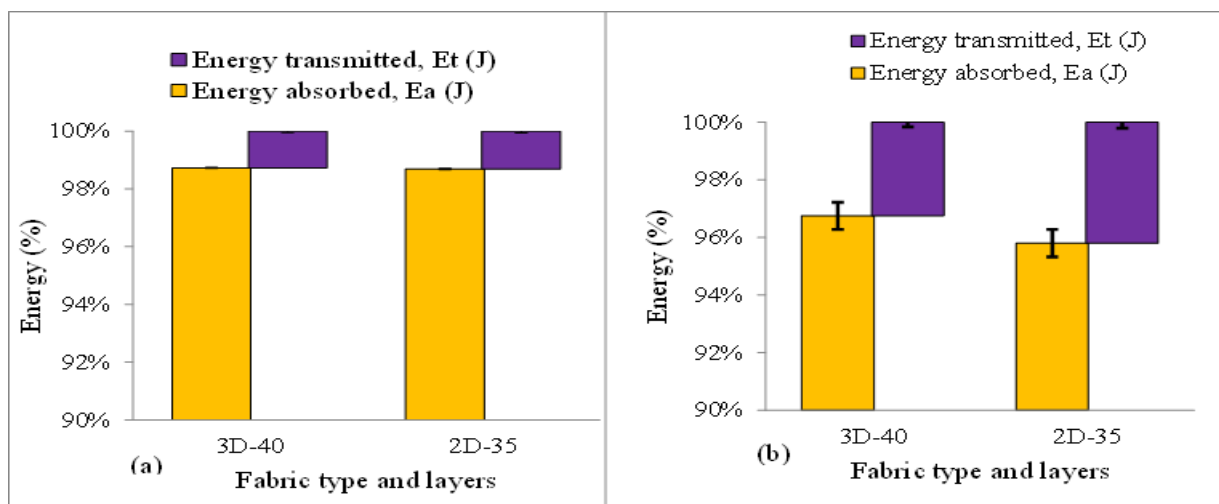
Figure 6.8 Average energy absorption and transmission values and its percentage of 2D-35 and 3D-40 at (a) non-moulded (f) shooting area (average values of shot 3, 5 and 6) and (b) Moulded (d) shooting area (average values of shot 1, 2 and 4)

This indicated that 3D warp interlock fabrics in the moulded condition show better capabilities due to its extra forming ability without affecting the mechanical performances of the materials. However, the energy absorbed percentage panels made of 2D fabric possesses better values in the non-moulded (f) shot points as compared to the 3D warp interlock fabrics. This might be due to the stiffness property of 2D plain weave fabrics which gives better ballistic protection. Other than the average energy absorption and transmitted percentage (%) values, each shot points of sample 3D-40 and 2D-40 were analysed as shown in **Figure 6.9.** Taking into account both fabric types, the energy absorbed by the panel was found higher in the non-moulded (d) shot points than its counterpart moulded (d) areas. However, in a specific comparison between 2D plain weave and 3D warp interlock fabrics, the non-moulded (f) target points of 2D plain weave

panel show better energy absorption capabilities in most points compared to 3D warp interlock fabrics. For example, non-moulded target areas T1 (d) and T6 (f) show 1% and 1.1% higher energy absorption than the 3D warp interlock fabrics with similar target areas as shown in **Figure 6.9 (b)**. Similarly, the energy absorption capabilities of 2D plain weave fabric panels still show higher values in the moulded (d) target areas compared to the 3D warp interlock fabric panels. If we see the energy absorption capabilities of target areas as a whole, the values for moulded (d) target were found lower than the non-moulded target area for both types of the fabric structure.
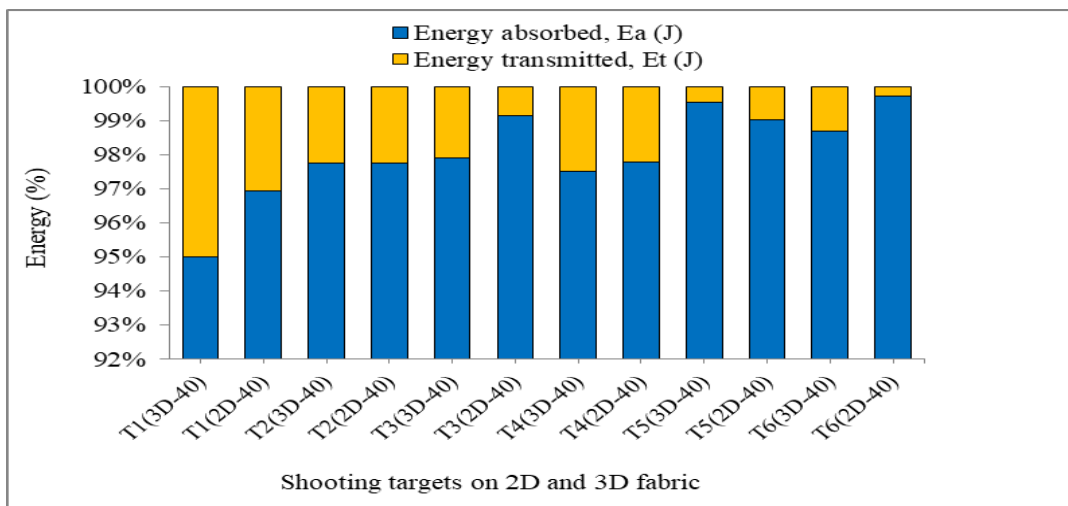
Figure 6.9 Energy absorption and transmission percentage values (%) of 2D-40 and 3D-40 at non-moulded (f) and moulded (d) shot points

The moulded (d) target area T1 (d), T2 (d) and T4 (d) had 94.98%, 97.74% and 97.52% for the 3D warp interlock fabric, whereas 96.93%, 97.74% and 97.76% of the 2D plain weave fabric. Similarly, the non-moulded (f) target area T3 (f), T5 (f) and T6 (f) revealed 97.9%, 99.54% and 98.69% for the 3D warp interlock fabrics and 99.14%, 99.03% and 99.73% for the 2D plain weave fabrics of energy absorption from the total impact energy.

6.3.2.4 Fabric panel surface failure mechanism

A shock wave due to projectile kinetic energy during ballistic is exerted on the target panel and the panel made of textile in return generates resistance against the projectile penetration. While impact test, some of this kinetic energy is absorbed by the panel and the rest energy will be transmitted to the backing material. In the case of a non-penetrated target, the projectile impact kinetic energy is supposed to be absorbed fully by the target through various kinds of target surface damage and energy-absorbing mechanisms. The projectile impact energy will be transferred to the target, and as a result, the speed of the projectile starts to decline and finally stops before penetrating the panels. In such a phenomenon, the propagated shock energy wave on the panels will cause various local and global damages including target compression below the projectile and around the impacted zone, cone formation on the back panel, primary yarn failure due to stretching and tensile, secondary yarn failure due to tensile deformation. Moreover, bowing of yarn, friction between the projectile and the target, matrix cracking and

delamination were also occurred depending on various parameters. In this section, different panel surface damages after the ballistic impact will be investigated and discussed at the micro-scale with the help of an optical microscope and a digital camera. First, the global and local damages of the different fabric panels made of different woven construction at the specified layer will be investigated. Later, the front and backside failure views of both top and projectile arrested layers for each pane will be considered for investigation and interpretation.

6.3.3 Global and localized damages of the impacted panels targets

The ballistic impact that led to perforation and failure mechanisms of the fabric panels depends on various factors including projectile mass, speed, and shapes, material and fabric weave types, target conditions, panel areal density, etc. The predominant textile fabric panel failure mechanisms that occur during ballistic impact include rupturing of yarns, yarn tensioning, fibrillation or splitting of fibre, cone formations, friction and yarn bowing [53]. For better analysis and comparisons, the impact-induced failure mechanism of different panels has been studied by taking macroscopic images. During ballistic impact, panels could be either fully penetrated or exhibited partial penetration with panel surface failures. In our study, different panels were impacted with nearly equivalent incident energy, and different intensity of global and local panel failures was itemized due to various parameters including type of woven construction used, panel layer numbers and target point conditions. **Figure 6.10** and **Figure 6.11** show the effect of woven construction (2D plain weave and 3D warp interlock fabric) on surface failure mechanisms of the panel comprising a similar number of layers (40 layers) at different impact locations. Even though each panel possesses different energy absorbing and surface failure mechanisms, two kinds of damages namely, local damage (damages concentrated at the specific target shoot area) and global surface damage (damages through the larger panel surface) were commonly noticed after the ballistic impact. **Figure 6.10** shows the global and local surface damages at the top (1st) and projectile arresting (15th) layers of panels made with 40 layers of 2D plain weave fabrics. For example, unlike localized damages, the top (1st) layer of the 2D plain weave fabrics panels exhibited less global damages at the surface as observed in **Figure 6.10** *(a)*. However, the bullet arresting layers of this panel was faced more global and less local damages as indicated in **Figure 6.10** *(b).* This might indicate only a small portion of the top layers (usually primary yarns) was involved in the energy absorption and surface failure mechanism during ballistic impact. On the contrary, a higher panel surface was involved in absorbing impact energy for bullet arresting (15th) layer as compared to the top panel layer. Such a correlation could help not only for more energy dissipation but also reducing the number of layers while arresting projectile arresting. Unlike panels made of 2D plain weave fabric, 3D warp interlock fabric layer panels revealed a smaller global deformation in the case of no-perforation situations for both top (1st) and projectile arresting layers as shown in **Figure 6.11**. The 3D warp interlock fabric layer panel damages were concentrated mainly in the local areas, a place where the panel layer and the projectile are contacted. The concentration of impact load could increasingly weaken the inter-phase bonding between the fibres and brought fewer layers of deformation during the impact.
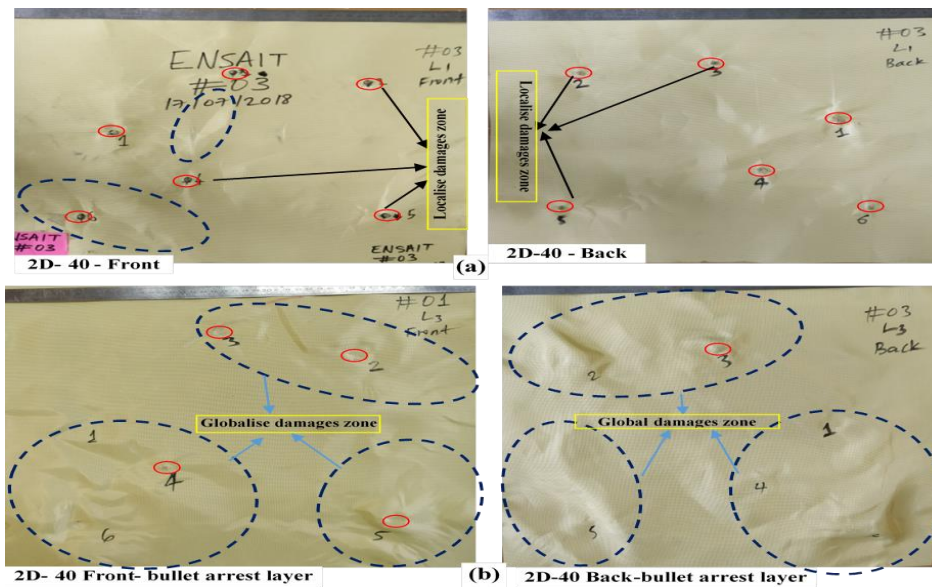
Figure 6.10 Ballistic failure modes of the front and back surfaces for (a) -top layer and, (b) bullet arresting layers of sample 2D-40

Such impacting conditions on the smaller portion of the panel could involve lesser panel surface and upshots a very less impact energy absorptions. As a result, an increased number of layers might be required by the panels not only to absorb the projectile impact energy but also to slow down and trap the projectile from complete penetrations.
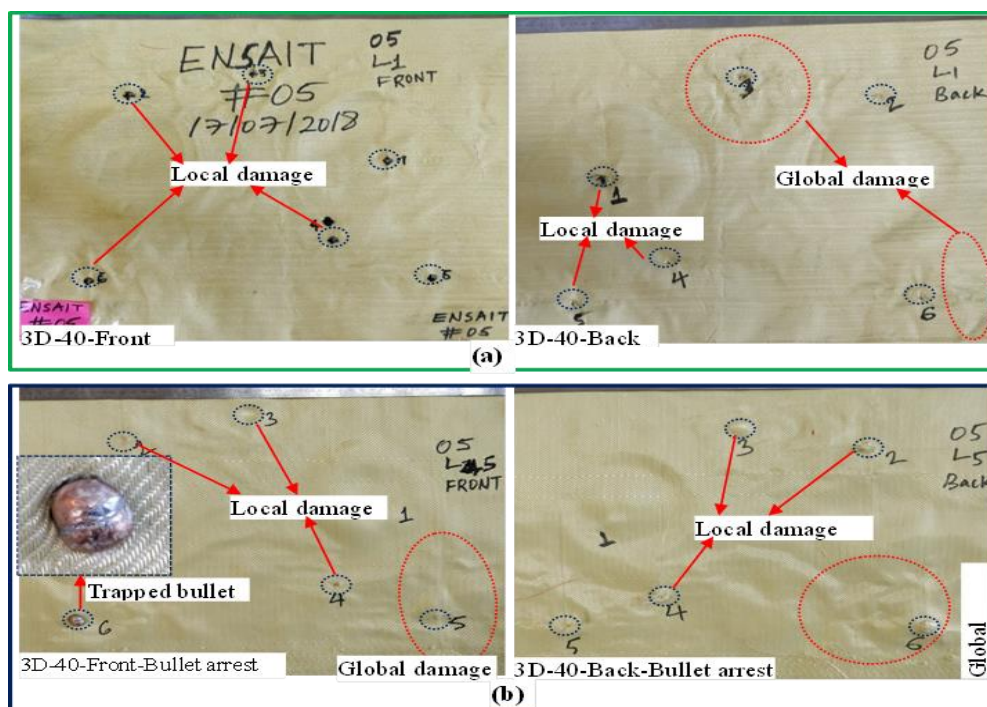
Figure 6.11Ballistic failure modes of the front and back surfaces (a) top panel layer and, (b bullet arresting panel layers of sample 3D-40

6.3.3.1 The local panels surface failures modes of the different fabrics panels

When the projectile penetrates through the dry panel target, strain waves propagate until the yarn fails. However, if the corresponding yarns do not fail, the propagation and reflections of strain waves exist during the whole impact event. In such a phenomenon, various damages mechanisms have occurred on the local surface until the projectile stopped. In this section, the commonly observed local damages in the different panels will be identified and discussed for a better understanding of the influences of woven construction, layer amount and impact conditions toward panels' damage mechanisms. **Figure 6.12** to **Figure 6.19** detail the different commonly occurred panel layer surface damage at the impact point for tested panels.

Yarn breakages and its damage volumes

Upon ballistic impact, the yarn within the fabrics becomes stretch in the longitudinal direction to absorb the ballistic impact energy. However, if the fibre strain reached and exceeded at its failure point, the corresponding primary yarn on the impact regions tends to break. Moreover, the yarn breakage by the projectile in the damage zone was also dependent on various parameters. **Figure 6.12** shows the average yarn damage diameters of different panels of 3D warp interlock and 2D plain weave fabrics for visual observation and discussion at various impact locations.
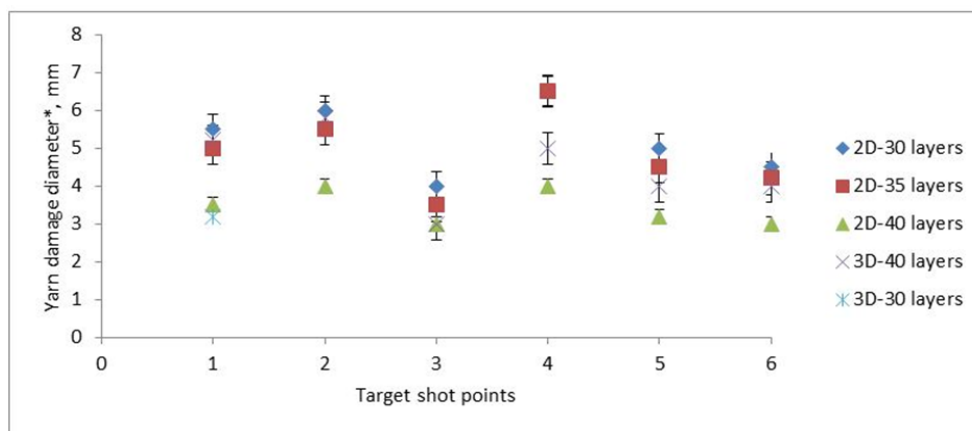
Figure 6.12 Yarn damage diameters of the different panels at different target locations
*(*Except target shoot location 1, all target points of the panel made with 3D-30 layers were penetrated and trauma diameters were not considered at those points.)*

Figure 6.13 (a) and (b) indicate the volumes of yarn damages regions in the localized damaged zone for 2D plain weave and 3D warp interlock fabric panels against ballistic impact respectively. The damages or severed volumes of the yarns involve the breaking of either the primary or covalent bonds of the fibre chains around the impacted region. However, both panels show a relative yarn failure volume at different levels. As shown in **Figure 6.13 (a)** the average yarn damages diameter for the panels made with the 2D plain weave fabrics appear higher than the panels made of 3D warp interlock fabrics with the same number of fabrics layer (40 layers) and shooting point conditions. This means that, in the 2D plain fabrics panels, the primary yarns

were found more involved to resist the projectile impact energy than the panels made of 3D warp interlock fabrics. However, the panels of the 3D warp interlock fabric damage zone are mostly concentrated on the specific zones where the smaller primary yarn is involved. Moreover, further close observation of the tested unperforated panels revealed that a small number of yarns breakage was also observed in the periphery of the penetrating regions for 3D warp interlock fabrics. On the contrary, the involvement of the principal yarns involved in the penetration process was found higher in the case of 2D plain weave fabric panels. For example, the damaged regions of target panels made of 2D plain weave fabric consisted of approximately on the average **18 × 18** yarns in warp and weft directions**.** Whereas, a damaged region of the panels made with 3D warp interlock dry fabric recorded **11 × 05** warp and weft yarns in the layer. The values confirmed our visual observations of a higher number of involved principal yarns in the 2D plain weave fabric panels.
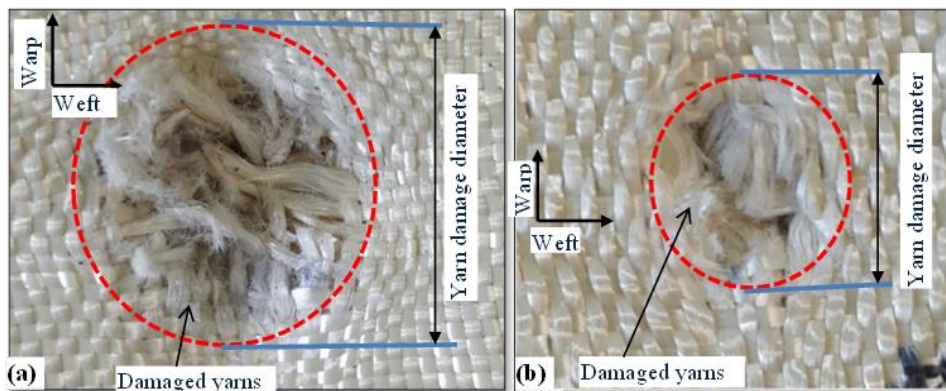
Figure 6.13 Yarn damage diameter in the localized shoot regions for (a) 2D plain weave and, (b) 3D warp interlock fabric panel

This might indicate that the 2D plain weave fabrics due to its stiffed weave structure will fail/penetrate at much higher impact energy compared to 3D warp interlock fabric panels. This is due to the fact the projectile would require more impacting force to break many involved primary yarns simultaneously. Therefore, woven fabric construction would be one of the parameters that affect the failure process of panels made of dry fabrics.

Conical deformation at the back face of target panels

When the projectile suddenly impacted the multi-layer panel target, at first only the upper few layers tends to fail. This is due to the occurrence of shear failures since the shear wave propagates along the thickness direction. Then, when the impact went further, the undamaged lower layer tried to absorb the remaining residual kinetic energy of the projectile through creating a cone-shaped deformation. This phenomenon happens when the shear wave reaches the back face of the target. The cone formation at the back face of the panels made with both the 3D warp interlock and 2D plain weave fabrics were observed. **Figure 6.14** indicated the conical deformation in the back and front views of both panels made with 40 layers of 3D warp interlock and 2D plain weave fabrics. However, the formations of such kinds of deformation at the back of the panels were more distinctive on the target that absorbed higher energy than

panels with less energy-absorbing capabilities. While observing the cone deformations of both panels at their corresponding bullet arresting layers, panels made of 2D plain weave fabrics show wider with 'wedge through' effects on the primary yarns. However, the 3D warp interlock fabric panels had a narrower cone deformation with higher primary yarn damages on the front view. This mainly shows that the earlier panels tend to absorb more energy in the larger surface area than the later panel. In the 3D warp interlock fabrics, cone-shape formation and trauma were mainly formed by un-crimping and elongation of the primary binding yarns. Imposing higher strain on such few primary yarns will then craft narrower and deeper cone shape deformation at the back face of the panel layers indicated the conical deformation in the back and front views of both panels made with 40 layers of 3D warp interlock and 2D plain weave fabrics.
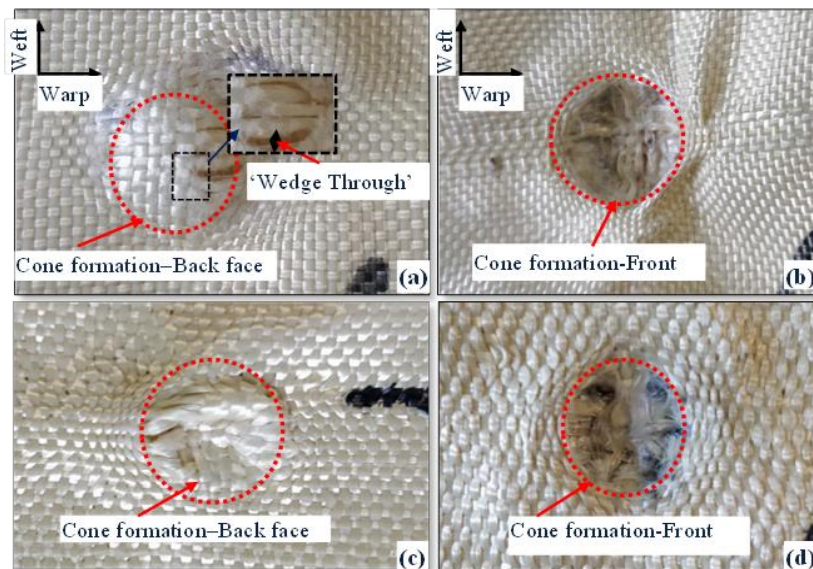
Figure 6.14 The conical deformation for back and front view for (a) and (b) 2D plain weave fabric and, (c) and (d) for 3D warp interlock fabric panel respectively

However, the formation of such kinds of deformation at the back of the panels was more distinctive on the targets that absorbed higher energy, than panels with less energy-absorbing capabilities. While observing the cone deformations of both panels at their corresponding bullet arresting layers, panels made of 2D plain weave fabrics show wider with 'wedge through' effects on the primary yarns. However, the 3D warp interlock fabric panels had a narrower cone deformation with higher primary yarn damages on the front view. This mainly shows that the earlier panels tend to absorb more energy in the larger surface area than the later panel. In the 3D warp interlock fabrics, cone-shape formation and trauma were mainly formed by un-crimping and elongation of the primary binding yarns. Imposing higher strain on such few primary yarns will then craft narrower and deeper cone shape deformation at the back face of the panel layers. On the contrary, target layers made of 2D plain weave fabrics were deformed mostly through elongations of the primary yarns. The low crimp and stiff weave structures of the 2D plain fabrics did not give a tendency to deep cone deformation easily as of 3D warp interlock fabrics.

Surface failures due to tension in the primary yarns and secondary yarn

Primary yarns are the prominent yarns to resist the direct projectile impact force into the target. This led the yarn to face the higher strain and also provides the force to resist the penetration of the projectile into the target. The tension created on such primary yarn would help to absorb and dissipate the majority of the projectile impact energy. In general, during the ballistic impact, the primary yarns tend to fail when the induced tensile strain of these yarns by the impact exceeds the ultimate strain. Sometimes, besides primary yarns, the deformation of secondary yarns (yarn other than the primary yarn) would also help to absorb some of the impact energy. Mostly such kinds of yarn absorb energy based on their strain distribution within the yarns and highest values are found near the top face of the deformed cone. **Figure 6.15** *(a) and (b)* show the different damage mechanisms caused on the primary and secondary yarns of target made of 2D plain weave para-aramid fabric. As it is clearly illustrated, after ballistic impact and yarn fracturing in the damage zones, the primary yarn was highly tensioned toward the impacted points. Besides, tensioning of the primary yarns also, as a result, creates fabrics wrinkles on the surface of the fabrics not only in the primary zone but also in the secondary zones (**Figure 6.15** *(b)*).

The un-crimping and tensioning of this yarn after fracture and wrinkle formation on the fabric surface, in turn, help to dissipate more impact energy before the projectile penetrates the target panels. Moreover, high compression of the target directly below the projectile was also observed due to a transverse shear wave propagating in the in-plane directions. On the contrary, target panels made of 3D warp interlock para-aramid fabrics exhibited a very less tensioning of primary yarns and no wrinkle formation on the surface of the fabric as shown in **Figure 6.15** *(c)*.
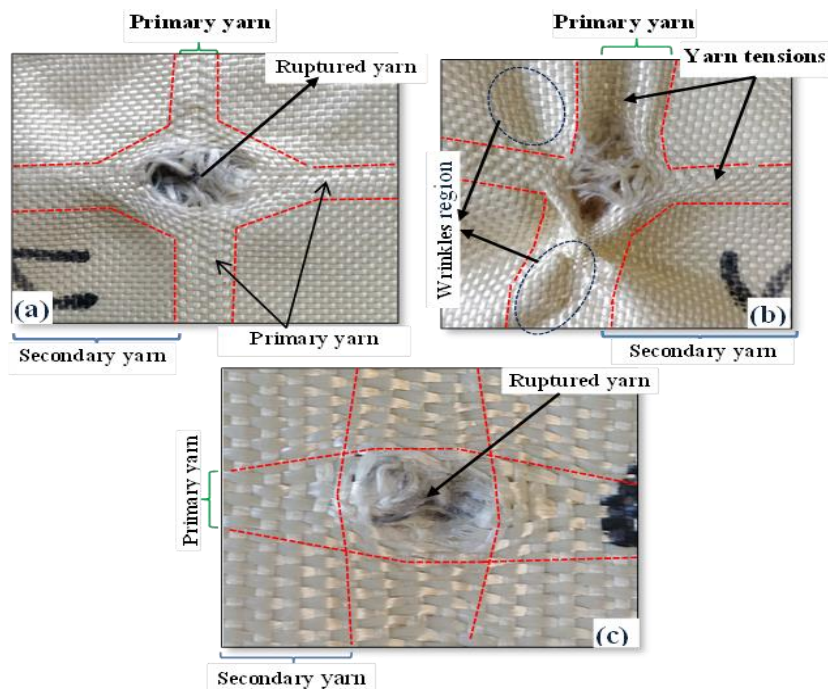
Figure 6.15 primary yarns tensioning during impact for (a) & (b) 2D plain weave fabric, and (c) 3D warp interlock fabric panel

This indicates that more yarn slippage occurred during ballistic impacts of the target made of 3D warp interlock fabrics, which in turn results from a very less impact energy absorption by the yarn. This phenomenon mostly appeared when the woven fabric structure is loose and have higher yarn mobility at the cross point. This allows the projectile to easily penetrate the specified primary yarns without any tensioning or wrinkle formations. Such conditions existed since the yarns in the 3D warp interlock fabrics were not constrained enough each other at the cross-point to lock the movement of each yarn. In conclusion, considering other external and internal parameters that affect the impact mechanisms, the failure of primary and secondary yarns and related damages mechanisms of both targets made of 2D plain weave and 3D warp interlock fabrics exhibit different events

Transverse deformation (Bowing) of yarn in the fabric

Bowing, also known as 'transverse fabric deformation', is another commonly observed failure mechanisms on fabric surface during ballistic impact. It is a phenomenon where the warp and weft yarns become non-orthogonal or away from each other around the projectile impact zone. It is formed either by directly pushing the yarns aside by the projectile while passing through the fabric or by creating a displaced yarn from crossover points, due to the stress wave propagation away from impact points. The bowing effects of the target panels made with 2D plain weave and 3D warp interlock fabrics are presented in **Figure 6.16 *(a) and (b)*** respectively. Based on the observations, the bowing effect at the specific target point was substantially observed in the panels made of 3D warp interlock fabric than 2D plain weave fabrics. This might be due to the stiff and close yarn weave structure of 2D plain weave fabrics than 3D fabrics. In the penetration process fabric having such fabric behaviours, the projectile forced to penetrate the fabrics through shearing of the primary yarns instead of sliding or pushing aside the surrounded primary yarn. On the contrary, transverse fabric deformation will be higher where there is enough space available between the neighbouring yarns at the time of impact. This phenomenon occurred when there projectile stress on the target and such sudden yarns stress causes pushing aside effect which results in more transverse fabric deformation. In general, bowing in the 3D warp interlock as shown in **Figure 6.16 *(b)*** were mainly performed due to thrusting aside of the surrounded yarns as the projectile penetrates with less stress on the primary yarns. However, in the case of 2D plain weave fabric panels, bowing was existed due to creating a displaced yarn from crossover points by the stress wave propagation away from impact points. Moreover, a very close examination of the unperforated target on the 2D fabrics target in **Figure 6.16 *(a)*** revealed that the projectile sheared the fabric at the edges of its contact surface.
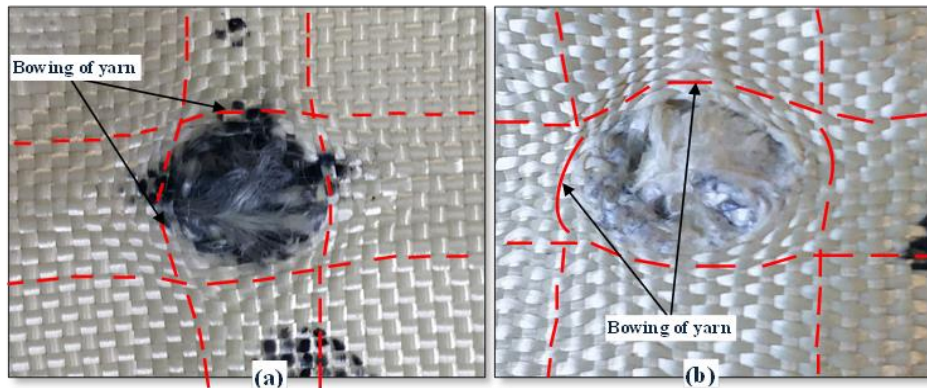
Figure 6.16 Bowing of yarn at the shot region for (a) 2D plain weave and (b) 3D warp interlock fabric layers

6.3.4 Panels layers responsible for arresting the ballistic projectile

In this section, the number of layers responsible for arresting the ballistic projectile based on woven construction, the number of layers used in the panels and target conditions (moulded and non-moulded) will be discussed. Such investigation will be carried out to interpret the ballistic behaviour of the individual target considering solely panel layers involved in the projectile capturing process at different shooting points. Ideally, one of the three different situations may happen during ballistic impacts depending on the various parameters such as material properties, target conditions, projectile parameters, etc. First, complete penetrations might occur when the impact energy gets either higher or same (ballistic limit) values with the material energy-absorbing capability. However, if the material shows higher energy absorbing capabilities than the projectile impact energy, the projectile will either rebound back or stacked inside the ballistic material. Unlike complete perforation, scrutinizing and identifying the number of layers required to capture the projectile during partial penetrations at the different shoot is very important for further armour panel design improvements. **Figure 6.17** *(a) and (b)* denote the scenario of the arrested projectile by the responsible number of layers at different target point conditions in different layers of 3D warp interlock and 2D plain weave fabric respectively. According to the result, the 2D weave fabrics revealed more precise and relative values for panels having a different number of layers and different shoot target as shown in **Figure 6.17 (a)**. More or less a majority of the number of layers responsible for arresting the projectile were concentrated in the black dot oval regions.

The 12, 8 and 7 layers were recorded as the minimum and 16, 14 and 13 layers were the maximum required number layers to arrest the projectile for 30, 35 and 40 layers of 2D fabric panels respectively This clearly shows that 2D plain weave target panels made with high numbers of layers publicized lesser number of layer penetration as compared to panels with less number of layers of the same fabric type. This might be since panels with higher layer numbers possess a larger area to dissipate and absorb more impact energy. Moreover, other than the panel layer number, the targets shoot conditions (moulded and non-moulded) have also shown an effect on the effective layer number to capture the projectile.
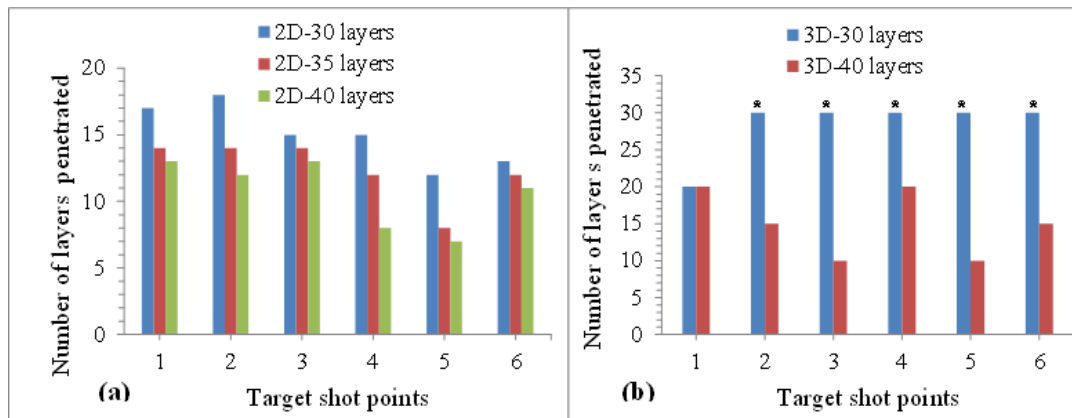
Figure 6.17 Number of layers penetrated for (a) 2D plain weave and (b) 3D warp interlock fabric (*Except target shoot location 1, all target points of the panel made with 3D-30 layers were penetrated (P*))

In the 2D woven fabric, the effect of different target shoot conditions brought some differences in the number of layers required to arrest the projectile. For example, the target regions at the moulded region (target regions 1, 2 and 4) required relatively higher layer number as compared to non-moulded target regions (target regions 3, 5 and 6) to arrest the projectile. This is due to the reduction of the areal density of the fabric at the specified moulded region while punching the fabric. Moreover, the fewer performances of the moulded region might also come from not only straightening and higher yarn tension but also some failure modes at the punched area by the punching force. Usually straightening and higher yarn tension causes the opening of the crimp and then the projectile will be easily penetrated the fabric panel. This clearly showed that not only the configuration of the fabric but also the target shoot area also influenced the capability of the sample to stop the projectile at the specific number of layers. **Figure 6.17 (b)** shows the number of penetrated layers of different 3D warps interlock panels in respective shoot points. In general, the number of layers required to capture the bullet in the case of 3D warp interlock fabrics was found different from 2D plain weave fabrics. Unlike the 2D plain weave fabrics, the number of projectiles arresting layers of 3D warp interlock fabrics panels at the different target points was found scattered at a wider range Moreover, the 30 layers panels of 3D warp interlock fabrics, except shoot targets 1, the complete penetration (p) were recorded for all shots. On the other hand, the bullet shot on the 40 layers of 3D warp interlock aramid fabrics panels were captured at the minimum and maximum layer of 10 and 20 layers respectively. Moreover, unlike the 2D plain weave fabrics, the number of penetrated layers was affected by the target shot points. Target shot points on the moulded area need a higher number of layers to capture the projectile as compared to the non-moulded. This is because, even though less panel's surface damage occurs due to its good moulding, however, its less recovery ability will also reduce the areal density and increased the tension and straightening of the yarn. As discussed earlier those phenomena during the moulding process may affect both the mechanical and ballistic performances of the materials.

The effects of fabric type on capturing the projectile before it perforates were also investigated by considering sample 3D-40 and 2D-40 with the different shot points (**Figure 6.18**). According

to the result, the type of fabric has shown a significant effect on the number of layers required to arrest the projectile. 2D plain weave fabrics enjoyed the somewhat better ballistic performance with a minimum number of layers requirement compared to the 3D warp interlock aramid fabrics. As illustrated in **Figure 6.18, t**he maximum and a minimum number of layers required for arresting the bullet was recorded 20 and 15 for sample 3D-40 whereas, 10 and 7 layers for sample 2D-40. Moreover, except in shot point 3, sample 2D-40 benefited required a low number of layers as compared to sample 3D-40 in all other shot points. In general, sample 2D-40 possessed an average of 30 to 35% reduction of layer than the layer used in sample 3D-40 to halt the projectile. Based on the above discussions, it is seen that the configuration of the fabric, number of layers in the panels and target shoot area conditions could influence the capability of the sample to halt the projectile at the specific number of layers. This could help to understand and design a better 3D warp interlock fabric structure to develop and design women's soft-body armor with less number of ply and weight for better protection and comfort.
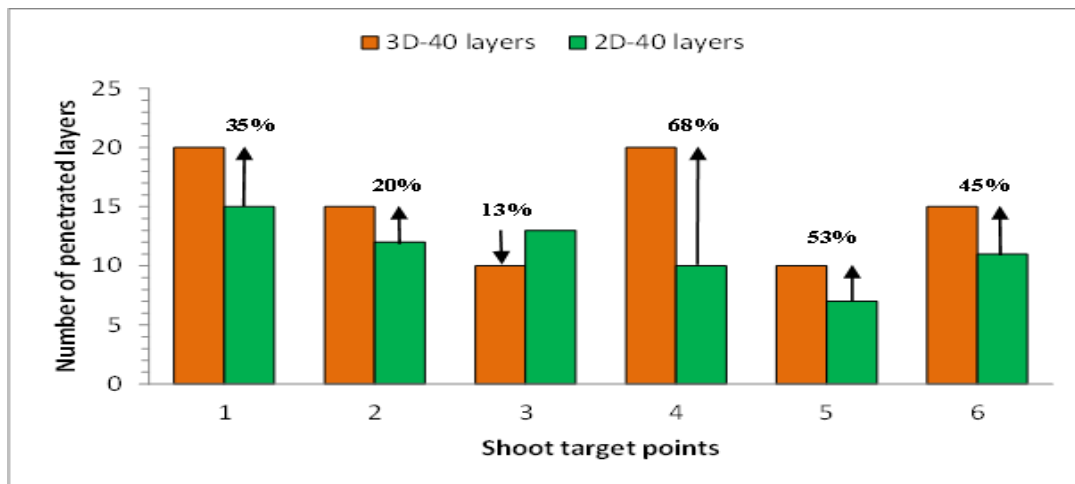
Figure 6.18 Graph of 3D-40 and 2D-40 layers to arrest the projectile at different shot points

6.3.5 Projectile deformation analysis

This section discusses the debris dimensional deformation and its percentage values which are trapped by different 2D plain weave and 3D warp interlock fabric panel. A total of 30 shots, 6 shots for each 5 target panels, were considered. Among the 30 projectiles, 4 projectiles which impacted the 30 layers of 2D plain weave fabric panel were not trapped. All the projectiles were precisely measured before and after the ballistic test Vernier scale. Besides, the deformational percentage of each projectile debris was also calculated as:

$$P_d(\%) = \frac{P_i - P_0}{P_i} \; x \; 100 \tag{5.1}$$

Where;

P_d - is deformed debris percentage in length and diameter (%),

P_i - is the initial projectile measurement (mm),

P_o - is the final deformed debris values (mm).

As observed in **Figure 6.19 (a),** the maximum and minimum debris measurement was recorded as 4.2 mm and 13 mm respectively. The higher debris measurement values publicized the lesser tendency of deformation while ballistic impact. For better comparison, the deformational percentages of the post-impact debris against the original length measurement values were computed using Equation. 5.1**. Figure 6.19 (b)** shows the deformational projectile debris percentage values for various target panels made of 3D warp interlock and 2D plain weave fabrics at different shot locations. Based on the result, the maximum and minimum length deformational percentage of the projectile were found 31.58 % and 77.9 % respectively.
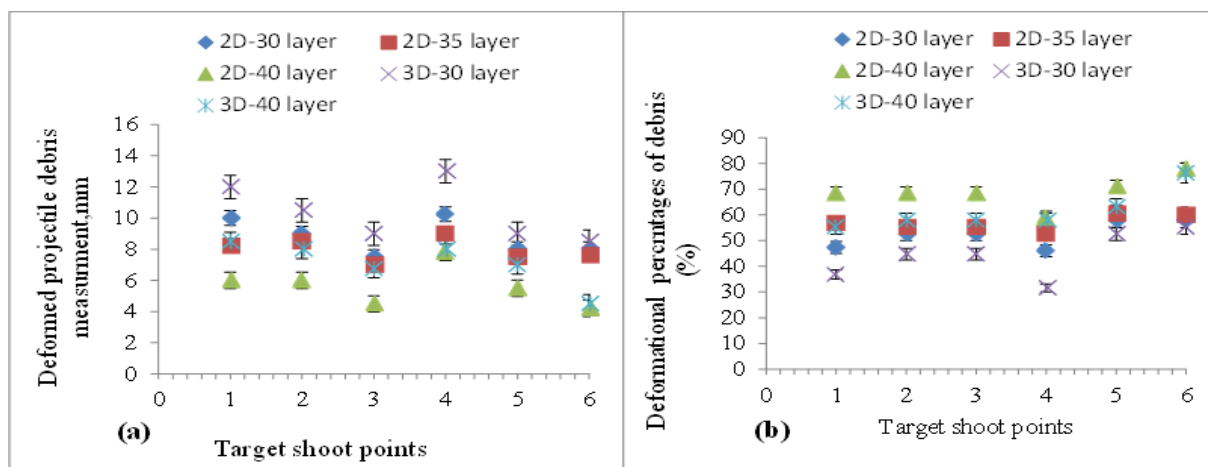
Figure 6.19 (a) Debris deformation measurement and (b) deformational percentages for different panels

The effect of woven construction, the number of layers in the panels and conditions of the shoot location on the projectile deformation were also investigated. Based on these results, the projectile impacted onto the target panels made of 2D plain weave fabrics faced much higher deformation than those panel targets developed from the 3D warp interlock fabrics considering both similar numbers of layers and shoot locations. This might be due to its high stiffness with strain energy capabilities as compared to the counterpart 3D warp interlock fabrics. For example, target panels with 40 layers of 2D plain weave exhibit higher projectile deformation at shoot locations point 1, 2, 3 and 5 than its 3D warp interlock fabric panels' counterparts with a similar number of layers. However, at target points 4 and 6, 40 layers panel made of both fabric types recorded the same level of projectile deformations. Similarly, 30 layers of 2D plain weave fabric panel possessed higher projectile deformation values in most target locations as compared to its counterpart 3D warp interlock fabrics panel. The numbers of layers involved in the design of the panels were also found another profound factor that affects the projectile deformation. For such comparisons, panels made with a different number of layers made of similar woven construction along with the specific target locations were considered for projectile post-deformation investigations. According to the investigations, as the number of pane layers increases, the higher projectile deformation has been achieved for both types of woven construction. The effects number of layers on projectile deformational percentages was found

substantial in 3D warp interlock fabrics panels as compared to the 2D plain weave fabrics panels. Besides, impact location has also revealed an effect on the post-impact projectile deformations. In the majority of panel target made of both 2D and 3D fabrics, shooting at the non-moulded target locations (target 3, 5 and 6) displays high post-impact projectile deformational percentages than the moulded target locations (target 1, 2 and 4). Moreover, 2D plain weave fabric panels made with a higher number of layers and shot at the non-moulded target location shows the maximum post-impact projectile deformation percentage than the other panel targets.

6.4 Conclusions

In this chapter the ballistic performances of 3D warp interlock and 2D plain weave p-aramid fabrics made of similar high-performance yarn (Twaron®) for seamless women, ballistic vest application was discussed. Thus, different panels made of various layers of those fabrics were arranged and moulded to resemble the frontal women's body shape before ballistic impact test against NIJ-Level IIIA. The non-perforation methods using BFS measurement (depth and volume) and surface failure mechanisms were used to discuss the ballistic performance and energy-absorbing capabilities of the different panels. Based on the result, in general, the type of fabric (2D/3D), number of layers involved and conditions of shot points (moulded/flat) greatly affect the BFS measurement values and surface failure mechanisms of the final panels during the ballistic test. For example, panels made with 2D plain weave fabrics show lower BFS measurement values and required a lower number of layers to halt the projectile as compared to 3D warp interlocks aramid fabrics. Panel with 40 layers of 2D fabric shows 47% and 39% BFS depth reduction as compared to panels with 30 layers of fabric in moulded shot point 1 and non-moulded shot point 6 respectively. Besides, the ballistic protection capabilities of 3D warp interlock fabric show no significant difference as compared to 2D plain woven fabrics with similar fabric density while using a higher number of layers. However, due to its structural compactness and rigidity, 2D plain p-aramid fabrics possess good ballistic performance with the minimum number of layers as compared to 3D warp interlock fabrics. For example, 40-layers of 2D plain weave and its corresponding 3D warp interlock fabric panels show similar deformation and energy absorption capability. However, 30 layers of 2D plain fabric have still shown good ballistic performance as compared to its counterpart 3D warp interlock fabric. Moreover, even though it is not much significant, the energy absorption capabilities of the panel at the non-moulded shot point revealed better values than the moulded shot points. This is because, while moulding the panel, the compactness and rigidity of the panel in the specified area has been compromised and ultimately gives lower mechanical and ballistic performances. On the contrary, the 3D warp interlock fabric displays better shaping ability according to the women contour while designing the body armor than its counterpart 2D plain weave p-aramid fabric.

The different tested panels were also captured with a digital camera and microphotographs to discuss on the surface failure mechanisms. 2D plain weave fabric panel shows a higher level of local surface damages than 3D warp interlock fabric panels at a similar number of layers and shooting points due to the involvement of many primary yarns to resist the projectile impact

energy. The cone deformations at the back of 2D plain weave fabrics panels were found wider with 'wedge through' effects on the primary yarns than 3D warp interlock fabric panels. Due to the stiff and close yarns weave structure, bowing of yarn was substantially observed more in the 3D warp interlock fabric panels than 2D plain weave fabrics panels.

Since fabrics type along with rigidity property were found a significant factor for designing women seamless women body armor, improving the ballistic performance along good moulding properties of 3D warp interlock fabric structure is important. The next sub-chapter will discuss on the ballistic performances of the improved 3D warp interlock fabric structure considering different warp yarn interchange ratios.

7   Enhancing ballistic impact performances of 3D warp interlock p-aramid fabric

7.1 Introduction

While developing soft body armour, it should possess not only good ballistic performance toward projectile penetration but also be reasonably light in weight, flexible, and comfortable [42]. To achieve such kinds of soft body armour, apart from the vest design technique, its ballistic performance and comfort depend on the material characteristics. As discussed in the literature review, the ballistic performances of soft body armour ballistic textile materials influenced by various internal factors including fibre types, yarn properties, material areal density, target plies numbers, target ply sequence, fabric constructions (woven/nonwoven, 2D/3D fabrics), etc. The high-performance fibres, such as Twaron®, Kevlar®, Dyneema®, and Spectra® are among the well-known textile materials extensively used in flexible ballistic protection due to their high resistance-to-impact damage [50, 79, 80], high strength, high tenacity, good chemical resistance and lightweight characteristics [44, 81]. Besides, as it is mentioned in the previous chapter, 2D woven and unidirectional laminates made from high-strength fibres were widely used in soft body armour development due to their excellent mechanical properties and better fatigue life. Moreover, due to the various limitations to be used in different ballistic protection applications, developments of improved materials or alternative approaches are very necessary for more protective and lighter ballistic materials. For example, hybrid panels with different textile materials and arrangements were used and studied by different researchers to develop protection body armour for better ballistic performance [382–384]. Moreover, unlike the male, women personnel working in the various sectors need body armour not only with better ballistic protection but also needs to fit properly their unique curvilinear body shape. Therefore, it is very necessary to design and manufacture women's soft body armor with special attention both in designing and material selection. While developing, the material should have a capability to accommodate the curvilinear shape of the women's body including the bust according to the armour design for better fitness, comfort and ballistic performance. 3D angle interlock fabric architecture is the most promising fabrics which are using in various technical applications due to its excellent moulding capability [148, 166, 385]. Besides, our few previous chapters have investigated both the forming behaviour and the ballistic performances of the designed and manufactured 3D warp angle-interlock fabrics, and compared with its counterpart of the commonly used 2D plain weave fabrics with similar materials and areal densities. Even though 3D warp angle-interlock fabrics possessed an excellent forming property, but it shows less ballistic performance as compared to its counterpart 2D structures [353, 354]. However, further research was essential to enhance its ballistic impact performance considering various factors without affecting its good forming behaviours before applying to the specific body armour.

Based on our ballistic performance result on 3D warp interlock fabrics, the current chapter tried to enhance its performances considering the involvements of different warp yarn compositions inside the structures. For this, different 3D warp interlock fabrics based on different binding:

stuffer warp yarn interchange ratios inside the structure as explained in the material section were designed, engineered and manufactured. The produced four different architectures were also investigated against their ballistic impact performances according to NIJ Standard-0101.06, Level IIIA. Different approaches were used to study and optimise the appropriate warp yarn orientation and interchange ratio inside the fabrics for better ballistic performances.

7.2 Experimental

The 3D warp interlock O-L fabric which was engineered and produced based on different binder: stuffer warp yarn interchange ratio such as 8:0 (100% binder and 0% stuffer), 8:4 (66.7% binder and 33.5% stuffer), 8:8 (50% binder and 50% stuffer) and 4:8 (33.3% binder and 66.7% stuffer were used. The structural design, developing parameter, material used and its manufacturing process was discussed in detail in the material section (Chapter 2). As discussed in the previous chapters, the warp yarn interchange ratio inside the fabric structure was found one of the main factors which affect not only the forming behaviour but also quasi-static mechanical behaviour (Chapter 5). The current chapter also investigates the effect of binding: stuffer warp yarn interchange ratios on the dynamic (ballistic impact performance) behaviours of 3D warp interlock O-L fabric structures. The campaign comprises four target panels made of different 3D warp interlock O-L structure, and another one target panel made from 2D plain weave p-aramid fabrics (CT-709). Every target of 3D warps interlock fabrics were arranged with 8 panels (or 40 weft layers) and that of 2D plain weave fabric comprises 35 layers. The panels were arranged in the aligned fabrics panel's orientations, by which each of the fabric layers and panels was arranged one on the top of the other in the same yarn direction. No lamination, stitching or other joining methods were used to bind the different layers during panel preparation. However, the final target panel was firmly taped together at the four edge using scotch tapes to avoid the fibre unravelling and the layers slippage from original positions as done in the previous ballistic test (Chapter 6). For a better recording of the ballistic phenomenon with a high-speed camera, a very dense and random speckle pattern on the specified regions of the shooting points (10 cm X 10 cm) was systematically drawn on the strike faces of the panel as shown **Figure 7.1 (a, b and c)**.

Before each ballistic test, all the panels were also moulded at the two pre-defined bust points to mimic the frontal contour of the specific women's body. The bust shaped punch, adapted forming bench and its procedure to mould each panel for the desired shapes were explained in the methodology section. Besides, the ballistic test was carried out based on NIJ Standard-0101.06 Level IIIA using ballistic test apparatus as discussed in the methodology part. Unlike the first ballistic test campaign, shot 1 and 4 were performed on the edges of moulded bust shapes, whereas shot 5 were tested on the centre of the moulded surface. Moreover, shot 6 and 2 were carried out on the upper centre and lower right corner parts of non-moulded panels whereas; shot 3 were carried out on the centre of the two moulded bust shapes. Such proper distributions of the different shots at various parts of the panels help for better understanding and assessing of its ballistic performances. Also, two high-speed cameras at the front (its descriptions are given in method section) were installed to properly capture the stereoscopic ballistic phenomenon during the test. **Figure 7.2** shows the ballistic test set up and shot point position while testing.
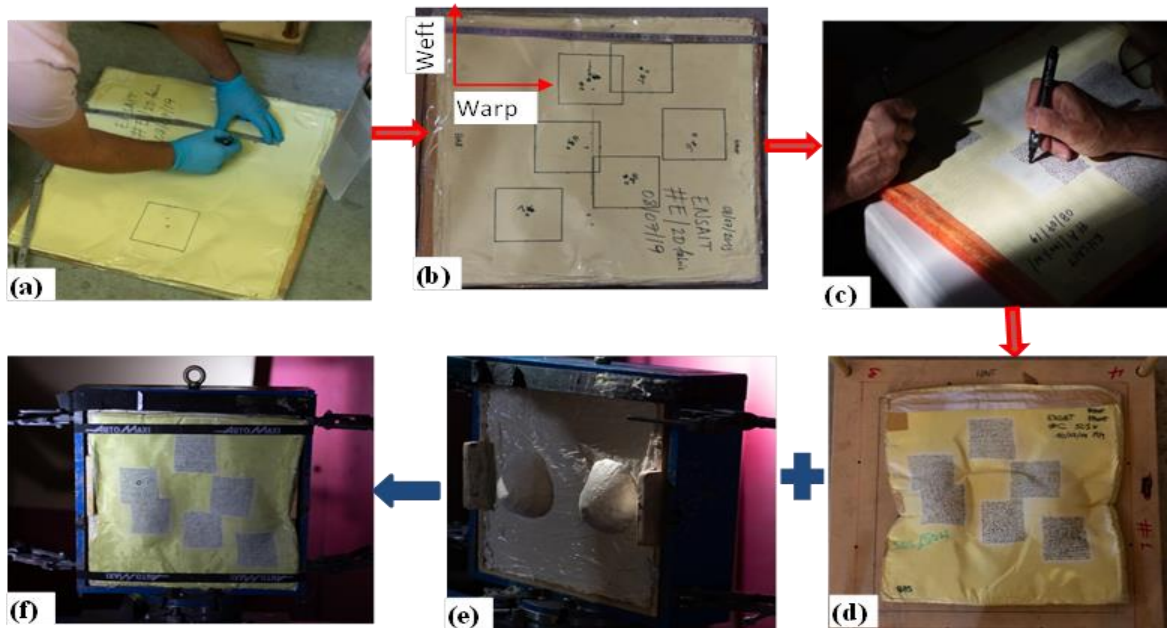
Figure 7.1 Sample preparations (a) Preparing shot locations (b) and (c) Regions for speckle patterns and its drawing, (d) Moulding of panel on adapted moulding bench (e) Prepared plastilina (f) Panel for test

In the current study, besides the non-penetration test evaluation approach for determining the panels' ballistic performances and energy absorption capabilities, the post-mortem analysis of panel surface failure and bullet deformations using the high-speed camera captured images and post-impact debris measurement respectively were analysed and discussed.
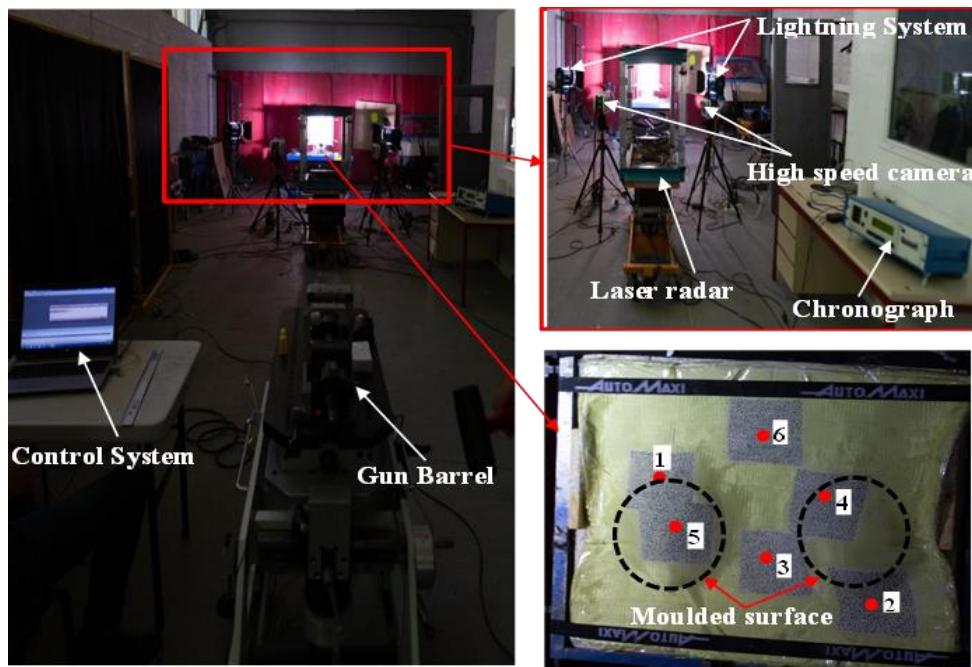
Figure 7.2 Ballistic testing set-up and backing material

Table 7.1 shows the parameters of the tested panels and their designations.

Table 7.1 Tested panels parameter and testing conditions

Samples designation	Fabric description	Layer No.	Areal density [g/m²]		Plastilina Temp. at 1ˢᵗ and 6ᵗʰ shot [°C]
			Actual	Theoretical	
2D-35	2D plain weave fabric	35			32.8/30.8
3D-40-8/0	3D 100% binding yarn	40		970	39/35.8
3D-40-8/4	3D 66.7% binding & 33.3% stuffer	40		970	39.7/37.8
3D-40-8/8	3D 50% binding & 50 % stuffer	40		970	39.3/37.8
3D-40-4/8	3D 33.3% binding and 66.7% stuffer	40		970	38.2/37.2

7.3 Results and Discussion

7.3.1 Back Face Signature (BFS) values

After each panel ballistic test, in the non-perforation case, the BFS values were scanned using a hand scanner in the backing material. **Figure 7.3** only shows panels' face with no perforation while ballistic tests at different shots. However, the scanning, modelling and measuring parameters along with proper procedure are discussed in the methodology part.
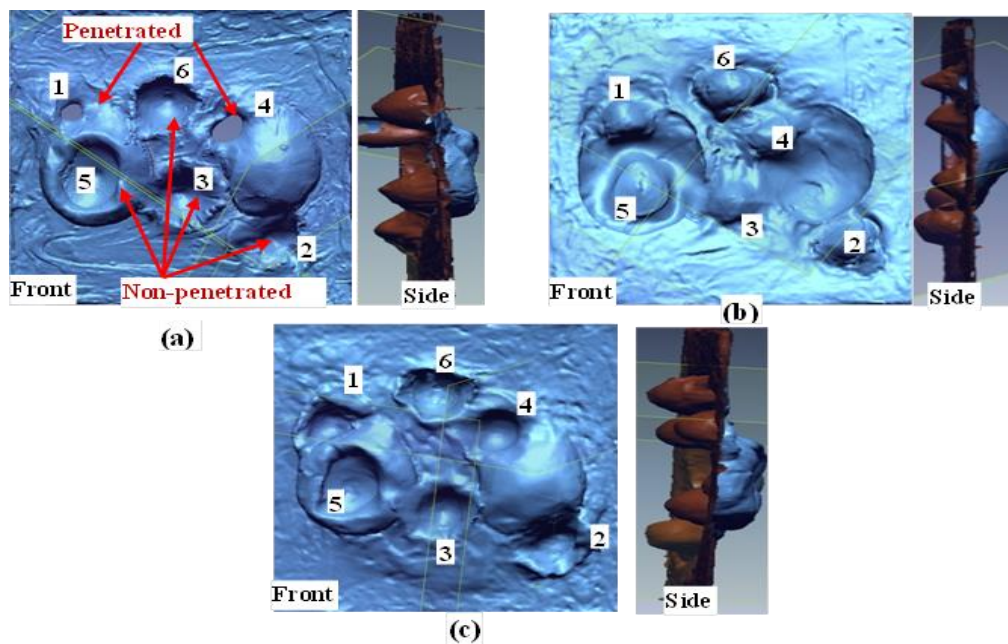
Figure 7.3 Front and back scanned pictures of BFS indentation on backing clay for sample 3D-40-8:0 (a) 3D-40-8/4 (b) and 3D-40-8/8 (c)

The average BFS diameter and its maximum depth values for the different tested panels are indicated in **Figure 7.4** and **Figure 7.5** respectively. Based on the observations, the different warp yarn orientation and its ratios inside the structures show a great influence and improvement on the panel's BFS depth and diameters. In general, involving higher proportions

of either binder or stuffer warp yarn inside the 3D warp interlock fabrics brought lower ballistic performance. For example, a sample with a higher stuffer yarn proportion amount (sample 3D-40- 4/8) faces complete penetration in all shot points than the other 3D warp interlock fabrics. Moreover, another sample made of 3D warp interlock fabrics with 100% binder warp yarn (sample 3D-40-8/0) were penetrated at the two-shot points, shot point 1 and 4. On the contrary, 3D warp interlock fabrics samples made with equal or a bit higher interchange ratio of the binding: stuffer warp yarn inside the 3D fabric shows lower trauma depth values. For instance, sample 3D-40-8/4 and 3D-40-8/8 shows no perforation with less trauma depth values of the maximum allowed standard values (44 mm). However, except in target shot point 5, sample 3D-40-8/4 shows lower trauma depth as compared to its counterpart panel made with the same number of 3D warp interlock fabric layers but different warp yarn interchange ratio, sample 3D-40-8/8. Numerically, 3D-40-8/4 shows the minimum and maximum trauma value of 20.5 mm and 32 mm in shot 4 and 6 respectively. Sample 3D-40-8/8 also shows the minimum and maximum trauma values of 23 mm and 36 mm in shots 4 and 2 respectively. Sample 3D-40-8/0 faced penetration at two-shot locations (shot 1 and shot 4) which are located on edges of the right and left deformed bust shapes.
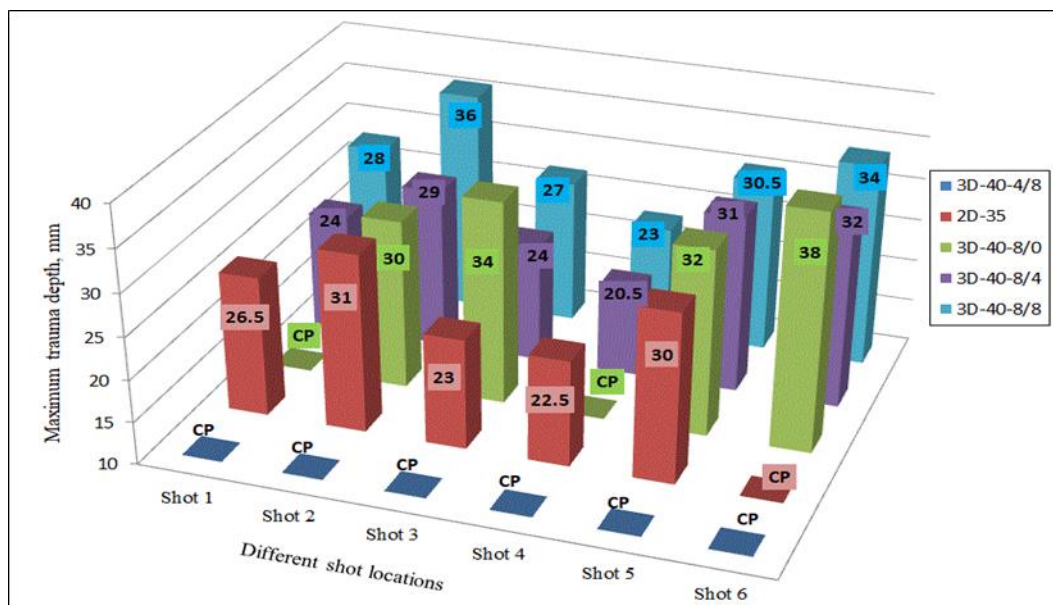
Figure 7.4 Maximum BFS depth for different 3D warp interlock variants and 2D plain weave p-aramid fabrics at different shoot locations (^{CP}- *represents the penetrated panel at the specified shot point)*

Whereas, sample 3D-40-4/8 were fully penetrated in all the shot points. Besides, the type of fabric constructions (2D and 3D woven) used in the panels was also observed as one of the factors that affect the trauma measurements. Samples made of 2D woven fabrics with an approximately equal areal density of the other 3D warp interlock fabrics penetrated in one shot point shot 6. Similarly, except for shooting locations 3 and 5, sample 3D-40-8/4 also shows lower trauma depth values as compared to sample 2D-35. The BFS depth values for the 3D warp interlock fabric structure made with various warp yarn interchange ratios were also

revealed higher and nearly similar values among moulded shot points (shot 5) compared to the majority of other non-moulded shot location **Figure 7.4**.

For example, except 3D-40-4/8 in which all are penetrated, the maximum BFS depth for the 3D-40-8/0, 3D-40-8/4, 3D-40-8/8 and 2D-35 were recorded 32, 31, 30.5 and 30 mm respectively at the moulded area of shot point 5. Unlike other non-moulded shot point areas, such back-face signature depth increments in the moulded area are due to occurrences of fabric density (thickness) reduction and yarn filament damages during the forming process by stretching the fabric. Moreover, the influences of warp yarn interchange ratio in 3D warp interlock fabric and woven fabric types (2D and 3D woven) on average BFS diameter values were also investigated as shown in **Figure 7.5.** According to the investigations, sample 3D-40-8/4 shows lower BFS diameter compared to all other samples made with 3D warp interlock weave fabric architectures. On the contrary, sample 3D-40-8/0 revealed the highest BFS diameter compared to its entire counterpart 3D warp interlock fabric sample, except sample 3D-40-4/8 where all of its target position got penetrated.
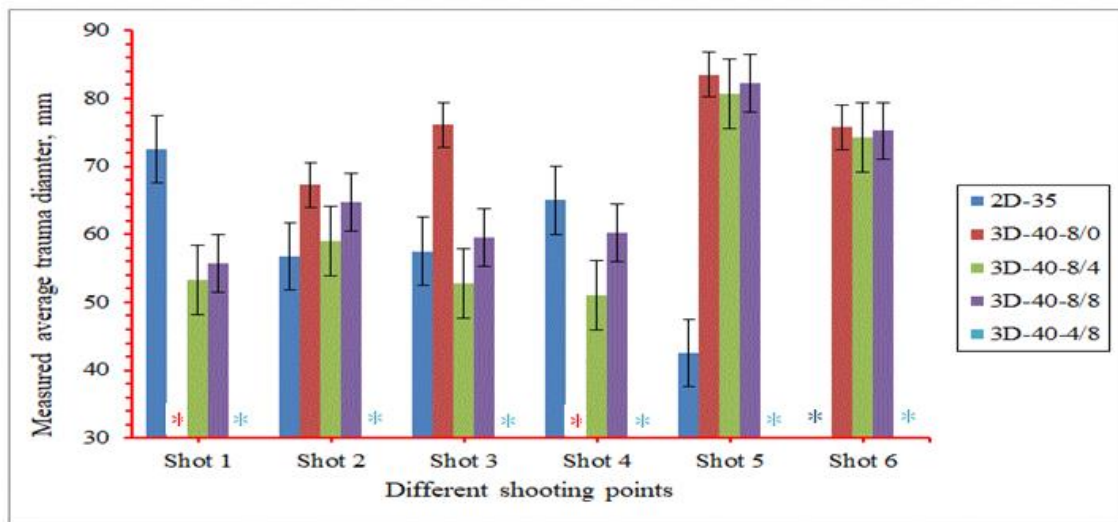
Figure 7.5 Measured averaged BFS diameter for different 3D warp interlock variants and 2D plain weave p-aramid fabrics at different shoot locations, (*All shots were penetrated for 3D-40-4/8,*shot 6 penetrated the 2D-35, and *shot 1 & 4 penetrated the 3D-40-8/0)

Except for its penetration at shot points 6, sample made with 2D plain weave fabric, 2D-35, and records lower BFS diameter at shot 2 and 5, but higher at shot points 1 and 4 as compared to samples made of 3D warp interlock structures. Specifically, except shot 6, sample 2D-35 revealed lower BFS values than the 3D-40-8/0 and 3D-40-4/, but higher values than sample 3D-40-8/4 followed by 3D-40-8/8 in the majority of the target shot. Moreover, among all the 2D and 3D warp interlock fabric samples, 3D-40-8/4 revealed much lower BFS diameter in the majority of the target shot. The conditions of the sample (moulded and non-moulded target situations) could also reduce the ballistic performances and increased the BFS depth of the final panels at the specified target points.

7.3.2   Energy absorption capabilities of 3D warp interlock fabrics

One of the methods to understand the ballistic impact phenomenon of the target knows exactly the energy absorbing mechanisms. Mostly, the impact energy of ballistic fabric panels with high-speed projectile will be converted into various forms including sound, heat, but the majority to kinetic energy. Such kinetic energy will be either absorbed by the fabric panels or transmitted to the back and creates trauma indentations. So, enhancing such absorbing capability of the fabric could reduce the creation of trauma and injury at the back of the panels. Among the different factors, material type, fabric structure, fabric finishing, fabrics areal density, panel arrangement areal density, etc. are some of the major parameters which could influence the energy-absorbing capabilities of the final fabric panels. Besides, shock wave propagations on the panel surface could be also generated by the impact energy. Such dynamic impact mechanisms bring the probability of destructing different fabric elements including filaments, fibres, and yarns. Except for fully penetrated target shot points, different BFS measurements for the different samples were computed. According to the NIJ standard, BFS volumes of each shot helps to compute the energy transmitted and absorbed values for each target and corresponding shot points. Higher trauma volume measurement at the back of the fabric could indicate a higher amount of energy has been transmitted to the back of the panels and vice-versa. **Figure 7.6(a) and (b)** shows the energy transmitted and absorbed values of 3D warp interlock panels made with different binder: stuffer warp yarn interchange ratio and compared with 2D plain weave p-aramid fabrics. However, the initial impact energy for all samples and their corresponding impact point might be different due to the different impact velocity applied. This means that the energy absorbed by the panel and energy transmitted to the backing panels might not be considered as good performance measurements for each sample. For better performance comparison, it is better to normalize the energy absorbing capacity of each sample with their corresponding shot points based on the initial total impact energy. **Figure 7.7** shows the energy-absorbing capacity (%) of each sample made of the different binding: stuffer interchange ratio of 3D warp interlock fabrics and 2D plain weave fabric at different shot points.
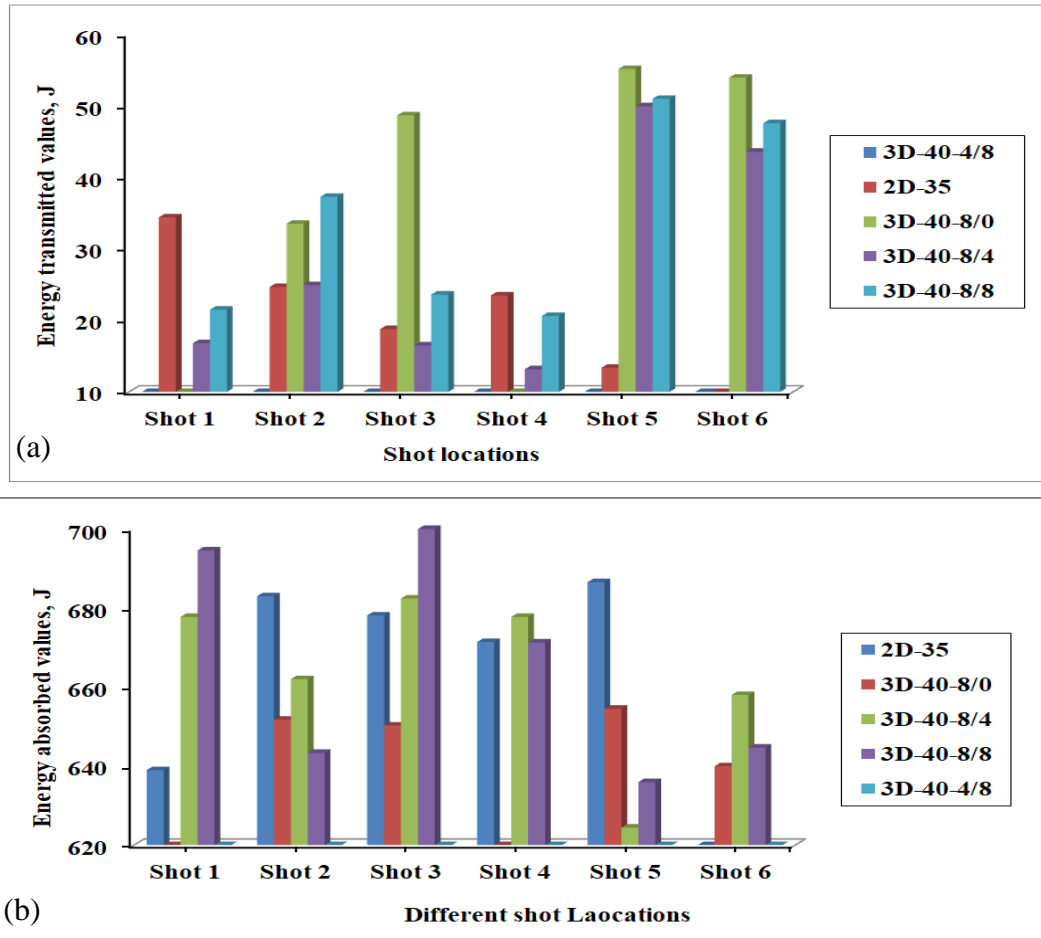
Figure 7.6 a) Energy transmitted, (b) Energy absorbed by different 3D warp interlock and 2D plain weave p-aramid fabric panels at different shoot locations, (*All shots penetrated sample 3D-40-4/8, * shot six penetrated sample 2D-35, and *shot 1 & 4 penetrated *sample 3D-40-8/0)*

Different energy absorption percentage values were also observed at different shot points within the same samples. Sample 3D-40-8/4 shows a higher percentage of energy-absorbing capability in majority target shot points of both moulded and non-moulded target areas as compared to other samples made with 3D warp interlock fabrics. Moreover, in the normalized graph, 3D-40-8/4 also revealed better absorbing capacity at target shot ppoints1, 3, 4 and 6 as compared to samples made with 2D plain weave, 2D-35. The maximum and minimum absorbed energy capabilities (%) of 3D-40-8/4 were recorded as 98.1% and 92.6 % in target shot point 4 and 5 respectively. Even though 3D warp interlock fabric shows good moulding ability [33][166], the energy capability of the 3D-40-8/4 was reduced in the moulded area (shot 5). This might be due to its low moulding recovery behaviours which in turn minimizes the fabric thickness along tensioning of fibres on the specific moulded area. Such a mechanism could reveal the reduction of the energy-absorbing capability and hinders the ballistic performances of that particular region. Moreover, sample 3D-40-8/8 revealed 97%, 94.5%, 94.5%, 96.7%, 97, 92.6% and 93.1% energy-absorbing percentage for shot 1, 2,3,4,5, and 6 respectively. Unlike shots 1 and 4 where full penetrations occurred, sample 3D-40-8/8 also recorded 95%, 93%, 92.2% and 92% for shot points 2, 3, 5 and 6 respectively. Whereas sample 2D-35, except penetration at shot 6, exhibited 94.89%, 96.52%, 97.3%, 96.62%, 98.09% energy absorption capability for shot 1, 2,

3, 4 and 5 respectively. Unlike our previous studies [353], samples made of 2D plain weave fabric shows higher energy absorbing capabilities on the moulded area of the panel (shot 5) than samples made with 3D warp interlock fabrics. This might be due to quick moulding recovering of the panels at moulded bust areas before ballistic testing. Based on the result, it is indicated that, like other parameters such as fibre type, fabric architecture, panel system, etc., the energy absorbing capacity of panels made of 3D warp interlock fabrics was greatly affected by the warp yarn interchange ratio inside the architecture as well.
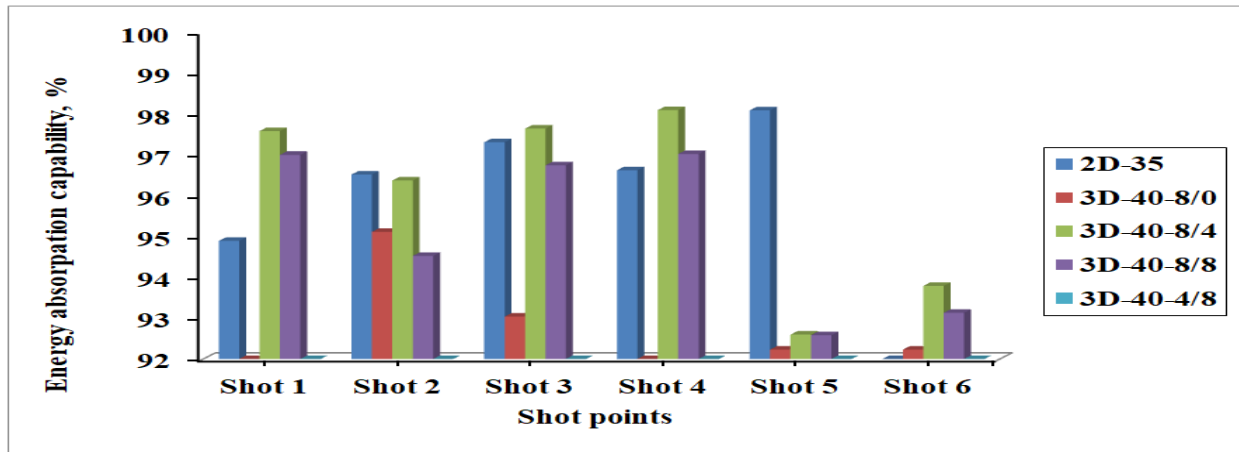
Figure 7.7 Energy-absorbing capability (%) for 3D and 2D fabric samples at different shot locations, (*All shots penetrated sample 3D-40-4/8, * shot six penetrated sample 2D-35, and *shot 1 & 4 penetrated sample 3D-40-8/0)

7.3.3 Post-Mortem analysis on impacted panels and projectiles

Sample panels responsible for arresting the projectile - The number of panels at which the bullet stopped while testing the 3D warp interlocks fabrics considering various shot points was computed. Regardless of the penetration level of the bullet, the number of panels where the bullet trapped was considered for better understanding and comparisons.

The four variants of 3D warp interlocks fabrics which are made of the different binding: stuffer ratios were considered for analysis. However, since sample 3D-40-4/8 in all shot points and sample 3D-40-8/0 in shot points 1 and 4 were penetrated, the values in the specific positions were excluded while comparing and discussing the projectile arresting panels and its post-mortem analysis. **Figure 7.8** shows the pictures of the striking faces of the 1st and 8th panels of the different samples at various shot points.
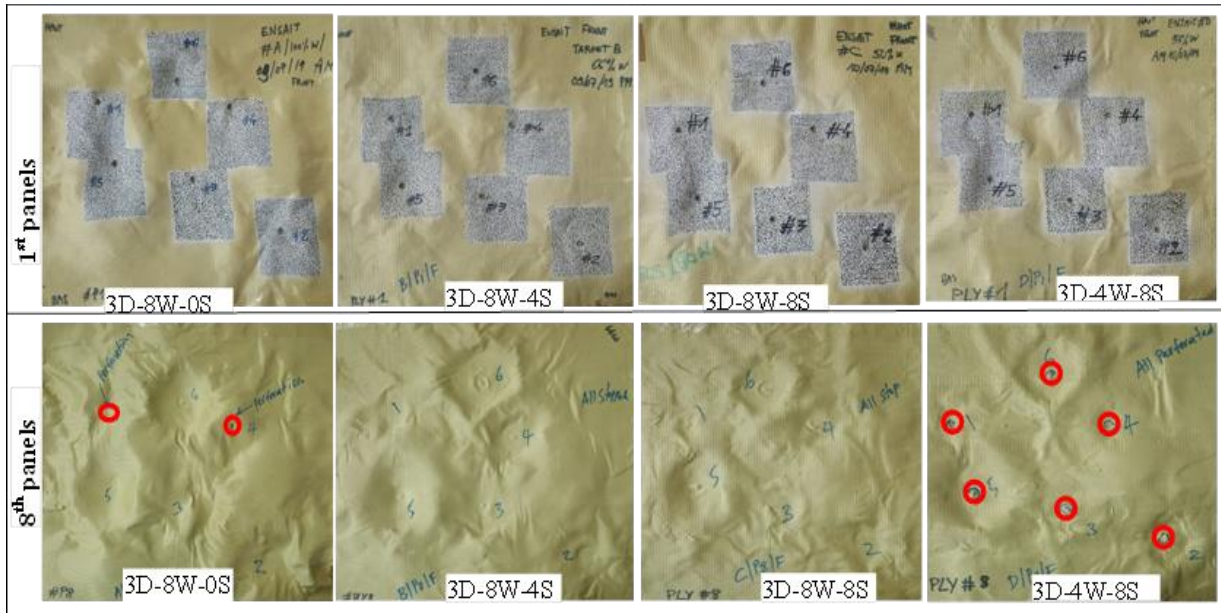
Figure 7.8 The striking faces of the 1st and 8th panel of the tested samples with various shot points

The different trapped projectiles were also carefully collected and measured its length and diameter for the post-mortem analysis of projectile deformations. Some of the trapped projectiles at various shot points by different panels are shown in **Figure 7.9.**

Figure 7.9 Examples of the trapped projectiles in some sample panel

In this section, the number of panels involved to stop the projectile by the different samples at the different shot points will be also discussed. **Figure 7.10** shows the responsible number for the different 3D warp interlock fabric panels to arrest the projectile at the designated shot points. Based on the result, sample 3D-40-8/4 and 3D-40-8/8 revealed the same number of panels which is responsible to halt the projectile in the majority of the shot points. For example, those samples were involved 5 panels at shot points 1 and 2 to arrest the projectile. Whereas, 4 and 2 panels were accountable to arrest the projectile by the mentioned two samples at shot points 3 and 5 respectively. Sample 3D-40-8/8 uses a lesser number of panels to stop the projectile at shot points 4 and 6 as compared to sample 3D-40-8/4. Besides, sample 3D-40-8/0, except shot

point 2, involved a higher number of panels in the projectile arresting mechanism than sample 3D-40-8/4 and 3D-40-8/8. Without considering the whole penetrated samples, 3D-40-4/8, and 3D-40-8/0 at shot points 1 and 4, the sample 3D-40-8/0 recorded the highest number of panels (7 panels) to stop the projectile at shot point 3 as compared to all other samples. On the contrary, sample 3D-40-8/4 and 3D-40-8/8 contributed the minimum number of panels (2) to halt the impacted projectile at shot point 5. However, the number of panels required by the majority of samples to stop the projectiles at different shot points located between 4 to 6 panels. (In this investigation, even if it is not much significant, the moulding process also affected the ballistic resistance of the sample). As discussed in the previous chapter, this might be due to both the reduction of the areal density of the fabric and some yarn failures at the moulded area.) In conclusion, the different warp yarn interchange ratio inside the 3D warp interlock structure greatly influences the number of panels required in the samples to stop the projectiles regardless of the shot points. The more balanced the proportions of the binder and stuffer warp yarn inside the warp interlock fabric, the better ballistic performance with less number of panel penetration was achieved. For example, a sample with 50% of each binding and stuffer warp yarn, 3D-40-8/8, revealed a minimum number of panels required to halt the projectile followed by sample 3D-40-8/4 in the majority of shot points. In contrary, a sample with less balanced warp yarn proportion, 3D-40-4/8, and 3D-40-8/0, needs a higher number of panels to resist the projectile.
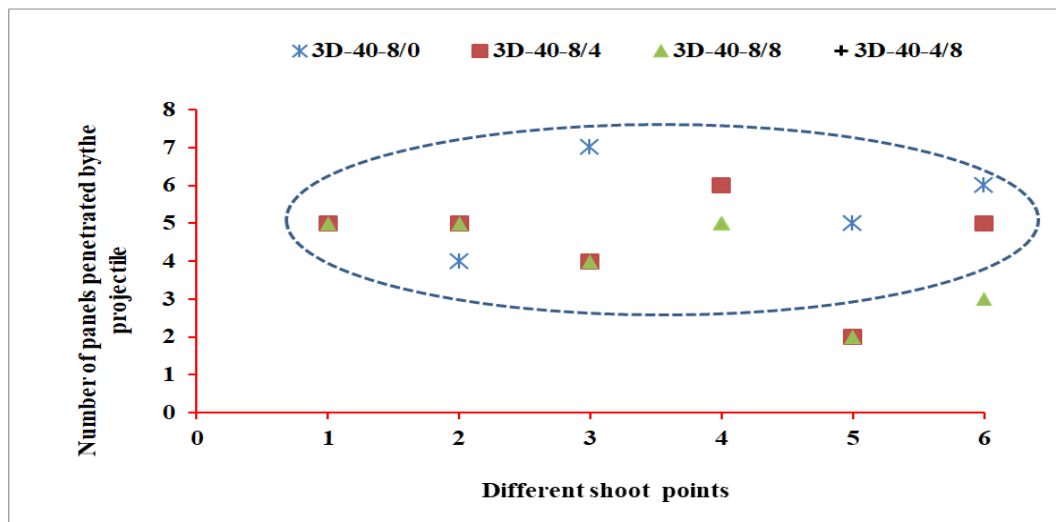
Figure 7.10 3D warp interlocks panel's number responsible to stop the projectile *(*All shots were penetrated for sample 3D-40-4/8, and shot 1 & 4 penetrated sample 3D-40-8/0)*

Post-mortem analysis of projectile deformations – As discussed earlier, the trapped debris at different shot points of the non-penetrated sample panels can be measured and analysed. In the current ballistic test, the trapped debris from four samples made of 3D warp interlock fabrics made with different warp yarn interchange ratios and one sample of 2D plain weave fabrics were considered. A total of 30 shots, 6 shots for every 5 samples, were used according to NIJ standard. However, among the 30 projectile, a total of 9 projectiles (6 projectiles from sample 3D-4W-8S, 2 projectiles from sample 3D-8W-0S and 1 projectile from sample 2D-35) were not considered due to it penetrates throughout the panel. The rest 21 debris after the ballistic test

was measured using precise Vernier scale. Some of the shapes and measurements of the debris after impact are shown in **Figure 7.11.**
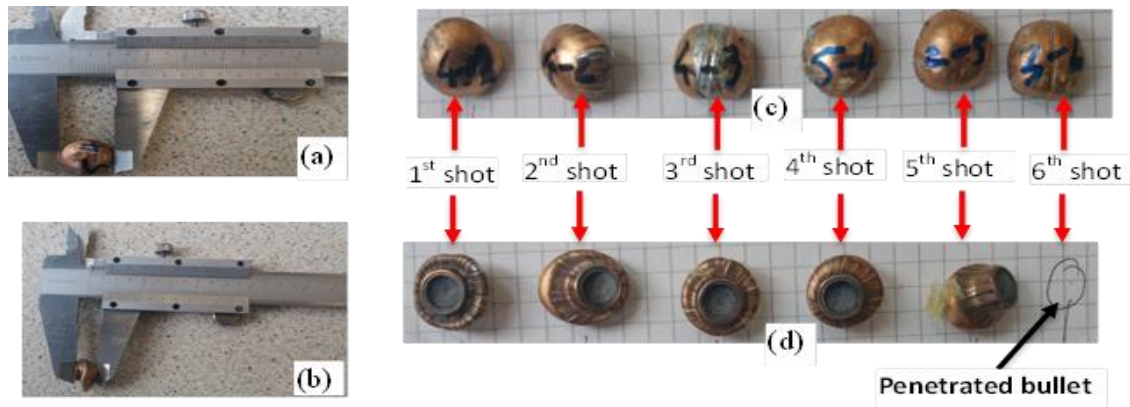
Figure 7.11 Debris measurement (a) Diameter, (b) Length, and shapes for (c) 3D-8W-8S and (d) 2D-PWF panels after impact

Unlike the debris measurement values, its deformational percentages both in the length and diameter direction give a better comparison in the different samples at various shot points. **Figure 7.12** presented the deformational percentages of the debris length and diameter respectively against the original projectile measurement for the different samples. In general, unlike the debris length, the diameter of the debris possesses an increment compared to the original projectile measurement values.

Based on the result, the projectile impacted onto the sample 3D-40-8/4 panels, except shot 5, faced much higher longitudinal deformation compared to the other sample panels in the majority of impact points. Besides, the sample 3D-40-8/4 also deformed the projectile with the maximum longitudinal deformation percentage (68%) at shot point 2 than the other impacted projectiles. On the contrary, minimum longitudinal deformation percentages of projectile were recorded at shot 5 of sample 2D-35. Unlike its penetration in shot point 1, sample 3D-40-80 shows the similar projectile deformational percentage (%) at shot points 2 and 3, but possesses lower values in shot points 5 and 6 compared to sample 3D-40-8/8. In general, projectile deformations values were random and there was not a clear indication that it is influenced by the warp yarn interchange ratio inside the 3D warp interlock fabrics. However, a sample made of 3D warp interlock fabrics with more balanced warp yarn interchange ratio shows better projectile deformation than sample made of 2D plain weave fabrics. Unlike the previous research work (chapter 6), the location of the impact shows no significant effect on the post-impact projectile deformations of the samples.
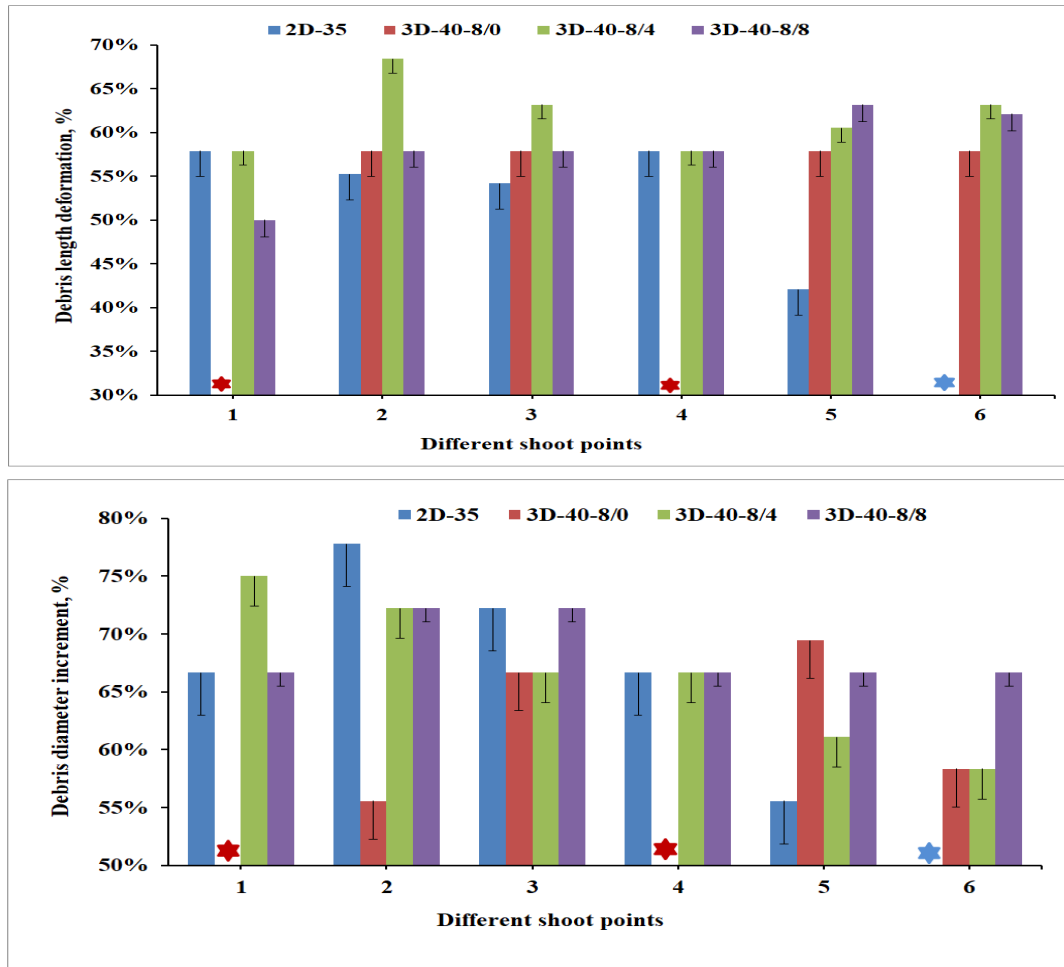
Figure 7.12 The projectile deformational percentage for samples at various shot points. (*All shots were penetrated for sample 3D-40-4/8, sample 3D-4W-8/0 penetrated at Shoot 1 & 4 (*) and sample 2D-35 penetrated at Shoot 6(*)*)

7.3.4 Surfaces strains at global and local points of the panel

The distribution of strain on the surface of the panel layer during the ballistic impact is very important not only to understand how the fabric material responses and its energy distribution on the surface but also help to improve the performances of the fabrics. The two cameras were therefore installed to record the impact event in the front with an angle (45°) from the hot axis. These cameras allow for the observation of the whole impacted process of the local impact area. Besides, the two cameras were also coordinated with the proper timing of the shot to record properly the impact events. In general, the recording was started 0.018ms before the bullet touches the target and recorded around a total of 3.6ms. Later, the two camera video was synchronized together to give the stereoscopic video. The recorded data by the high-speed camera was processed by the TEMA viewer with track eye motion analysis software and then exported in the form of stereoscopic mages. This high-speed3D photograph at fraction of microsecond frame greatly helps to study in detail the dynamic response of the panel and surface strain analysis. Even though it is possible to generate a huge amount of images, only some of the Stereoscopic digital images with the real fabric surface image were used to unveil and analyse the local and global strain, wave propagations and failure modes of the panels. We

also excluded samples 3D-4W-8S since it was fully penetrated by the projectile in all the shot points. Moreover, shot points1, 3 and 5 were primarily considered in the majority of image analysis to better understand the ballistic event both in the moulded and non-moulded regions of the panel. **Figure 7.13** shows the strain image sequences of the impacted panel, sample 3D-8W-0S, 3D-8W-4S and 3D-8W-8S, with selected time at shot point 3. In general, the presented panel shows different surface strains but almost similar panel penetrations sizes throughout the events at the given shot points. Based on the observations, sample 3D-40-8/4 still involved predominantly the primary yarns at 0.36ms after impact. On the contrary, considering the same after impact time (0.36ms), both sample 3D-40-8/0 and 3D-40-8/8 involve the primary and secondary regions to resist the ballistic impacts.
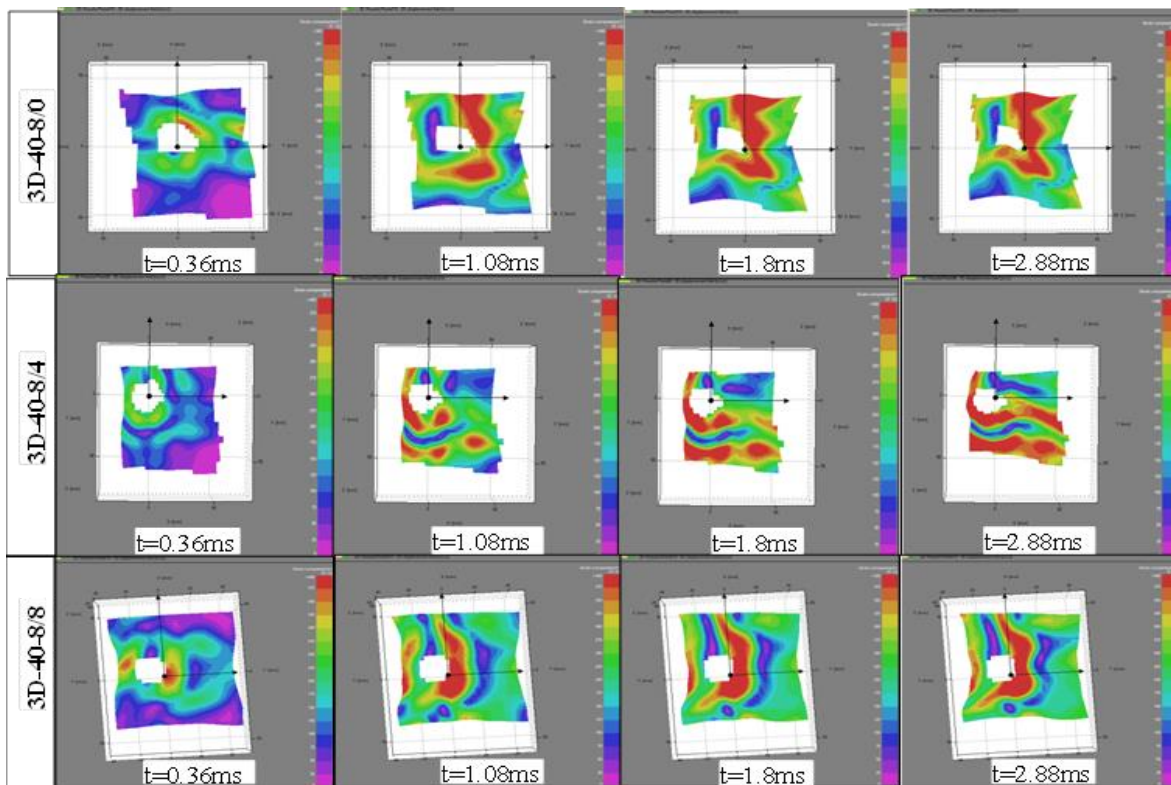
Figure 7.13 Image sequences of an impacted panel at front with selected time at shot point 3

However, the strain propagations were still accumulated around the local impact regions. Of course as the after impact time went further; all the tested samples involved both the primary and secondary yarns. Interestingly, similar trends of the wave propagations were observed within the same sample panels as time after impact goes further from 0.36ms to 2.88ms. However, the wave propagations trend and its effect on the panel's surface strain were realized in different directions among the samples. For example, the wave propagations in the panel surface of sample 3D-40-8/0 seem well concentrated in certain areas near the local impact points and contours of the penetrated panel. Besides, the local strains were found well distributed both in the weft (horizontal) and warp (vertical) directions. On the contrary, the higher surface strain by the wave propagations of sample 3D-40-8/4 through time was distributed in different regions both near and away from the impact points. The high surface strains of this panel were seen along the weft (horizontal) directions. As shown in **Figure 7.13,** sample 3D-40-8/8 also shows

its own high strain values location and directions. In this panel, similar to sample 3D-40-8/0, the high stain was more concentrated around the local impact point but propagates with different intensity in the warp (vertical) at time goes.

The different images of the impacted panels for the other shot points were also captured. By considering the various shot points, different panel surface strain patterns, direction, and failure modes might be obtained in the panels. This helps to properly compare the responses of the panel at the specific target points, i.e. moulded and non-moulded shot points. In addition to the previous discussion considering impact at a non-moulded area (shot points 3), **Figure 7.14** shows the image sequences of an impacted panel with selected time at a moulded area (shot point 5). Here only the two non-penetrated sample panel by all the shots, sample 3D-8W-4S and 3D-8W-8S were considered. In this particular shot point, sample 3D-8W-4S revealed higher surface strain which is located away from the penetrated contour area of the panel and mostly concentrated toward the four corners of the outer impacted regions.

Even though the surface strain of sample 3D-8W-8S shows a similar trend and directions as of sample 3D-8W-4S, however, it also revealed higher surface strain intensity on the specified panel surface. Besides, the panel penetration sizes of sample 3D-8W-8S were also found similar as compared to sample 3D-8W-4S in their respective impact timing. For close observation and better discussion, the two tested but not penetrated samples, 3D-8W-8S and 3D-8W-4S, were also presented their conditions at the beginning and end of the impact period considering shot points 1, 3 and 5.
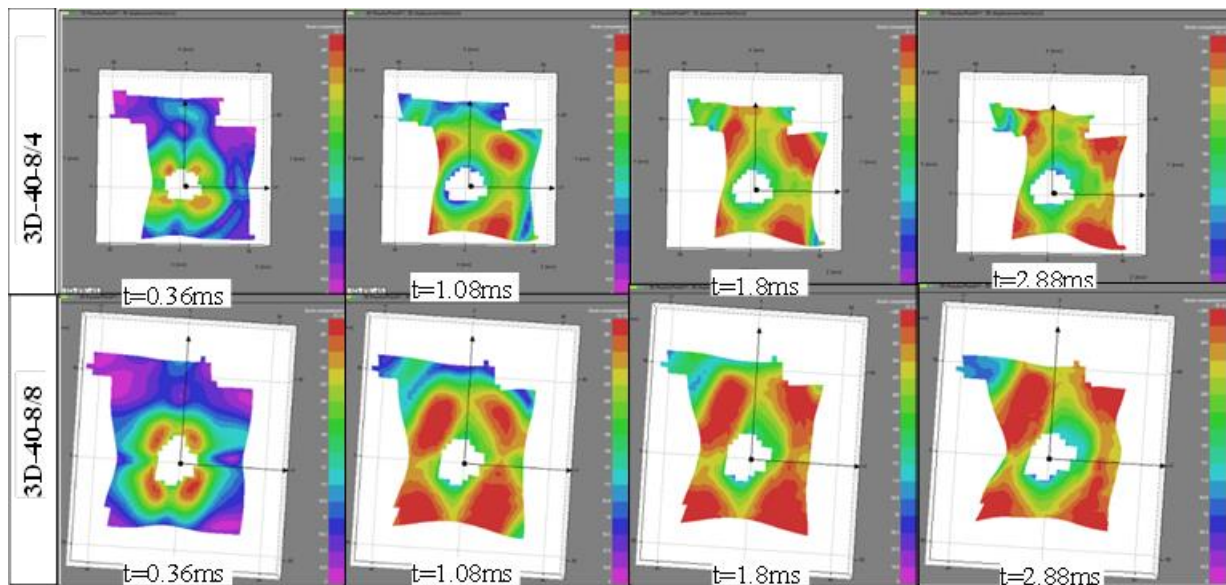
Figure 7.14 Image sequences of an impacted panel at front with selected time at shot 5

Figure 7.15, Figure 7.16 and Figure 7.17 shows the deformed state of 3D-8W-8S and 3D-8W-4S panels with their local strain at 0.18ms after impact at shot point 1, 3 and 5 respectively. Based on the high-speed camera images, the surface strain was initiated at t≈0.180ms after impact by the projectile wave for the mentioned tests. This is the reason why we consider t=0.18ms for the start of the impact to observe the different impacted samples. The samples were presented in the front and side views with the stereoscopic fabrics images. **Figure 7.15**

shows the deformed panels (3D-40-8/4 and 3D-40-8/8) with surface strain at the instant (t=0.18ms) at shot 1.
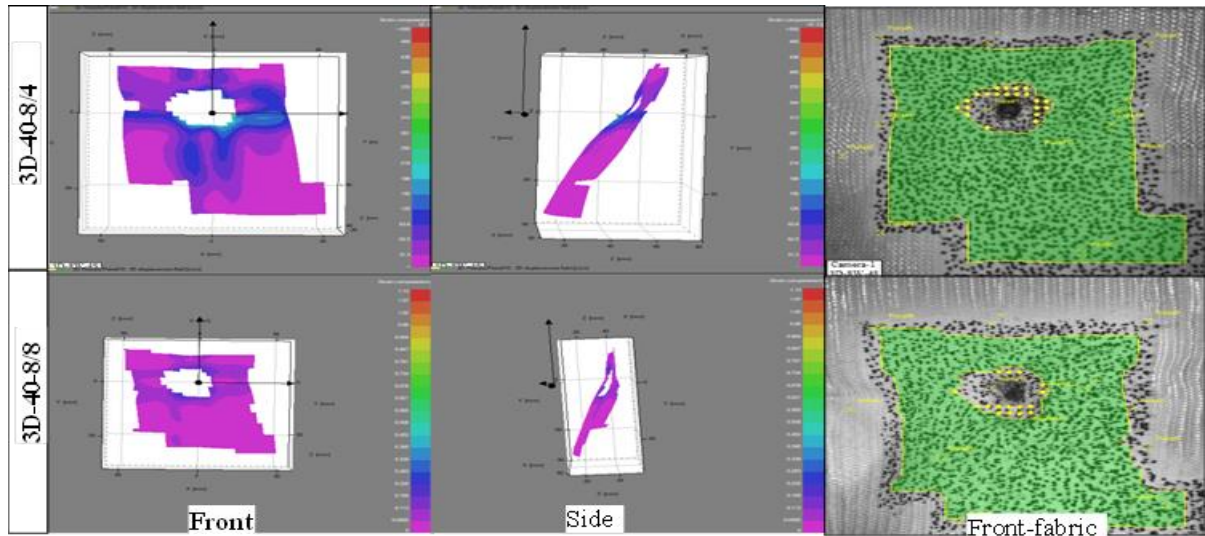
Figure 7.15 Deformed state of panels at 0.18ms after impact at shot point 1

According to the observations, both samples show surface strain on the panel, however, sample 3D-40-8/4 involved a higher amount of primary yarns in both directions as compared to sample 3D-40-8/8 at the specified impacting time. This means that 3D-40-8/8 needs much more time to detect the strain than the 3D-40-8/4. However, as shown in the fabric images, the penetrated hole for both samples displays similar size and shapes. **Figure 7.16** shows the deformed panel (3D-40-8/4 and 3D-40-8/8) images with an instant time (t=0.18ms) after impact at shot point 3.
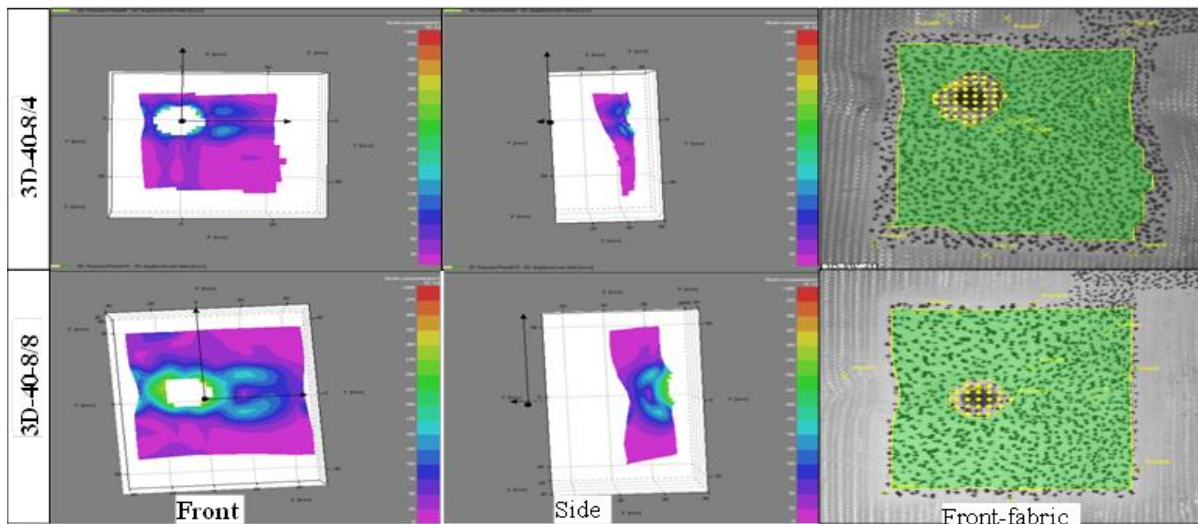
Figure 7.16 Deformed state of panels at 0.18ms after impact at shot point 3

Unlike the shot point-1, even though both samples involved primary yarn well, sample 3D-40-8/8 faces higher strain values than 3D-40-8/4 at shot point 3. The higher and instant involvements of primary yarn after impact might be due to the high surface tension of the panel at this shot point. This result is because of higher straightening (less undulation) of the yarn

during the forming process in the particular impact area as compared to shot point 1. However, unlike the 3D-40-8/8, sample 3D-40-8/4 shows similar strain images both in shot points 1 and 3. **Figure 7.17** also shows the tested panel (3D-40-8/4 and 3D-40-8/8) images with an instant time (t=0.18ms) after impact at shot point 5.
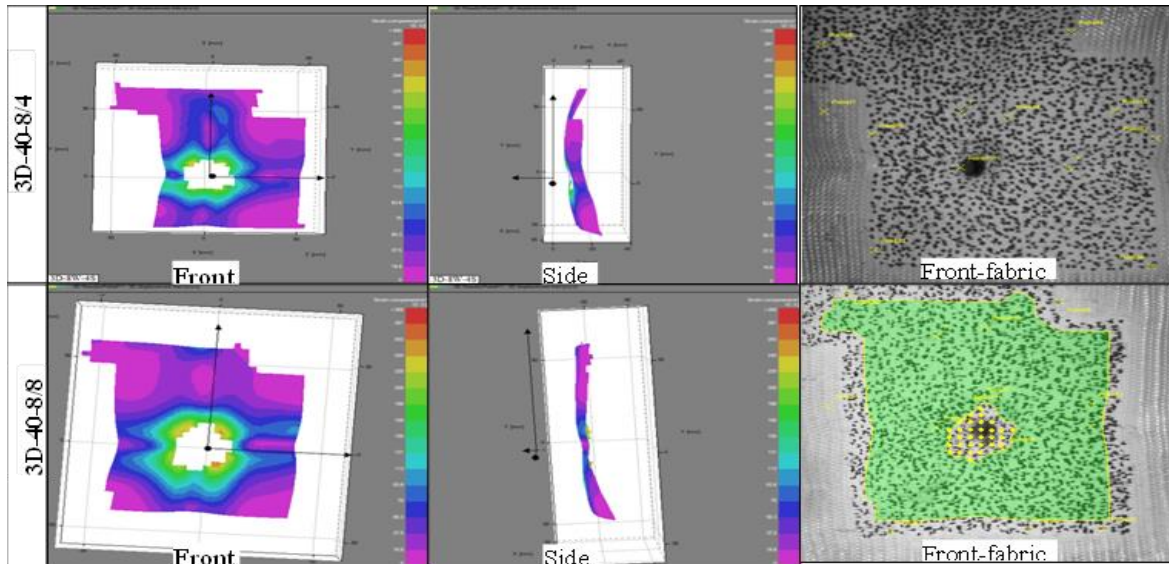
Figure 7.17 Deformed state of panels at 0.18ms after impact at shot point 5

In this particular shot point, both samples involved higher involvement of the primary regions with approximately equal strain values around the impact regions. In general, sample 3D-40-8/8 shows higher panel surface strain with shot point 5 as compared to shot point 3 during the first few microseconds after impact (t=0.18ms). However, with the same impact timing, the panel revealed the lowest level of surface strain at shot point 1. Sample 3D-40-8/8 also faces higher strain while wave propagation on the surface at shot point 5 at the start of the impact. In contrary, the samples have seen with smaller compared to shot 5 but approximately similar surface strain intensity at shot point and 3 in the same impact timing. For both samples, higher intensity of the surface strain was achieved at shot 5 than the other shot points with the same impact time (t=0.18ms). Even the strain values by the impact wave propagation were found higher in shot 3 as compared to shot point 1. This is due to the effect of the conditions of the shot areas while impacting. Generally, the surface strain values were more observed at the shot points where it is located on the panel which faces higher tensioning of yarns including the moulded panel areas than the panel region having higher undulations of yarn(non-moulded regions). For a complete understanding of impact phenomena, the samples' surface strain at the end of the impact process was also investigated with similar shot points, 1, 3 and 5. **Figure 7.18, Figure 7.19** and **Figure 7.20** show the deformed state of both 3D-8W-8S and 3D-8W-4S panels with their local strain at final microseconds of the impact t=3.6ms) at shot point 1, 3 and 5 respectively. This phenomenon greatly helps to observe the final states of the impacted samples not only in terms of the local surface strain but also to see the global strain and failure modes. **Figure 7.18** illustrated the deformed panel (3D-40-8/4 and 3D-40-8/8) images with an instant time (t=3.6ms) after impact at shot point 1. According to the observations, sample 3D-40-8/4

shows higher strain surfaces just below the impacted location in the horizontal direction not only at the indicated after impact time (t=3.6ms) but also for an extended impact durations.
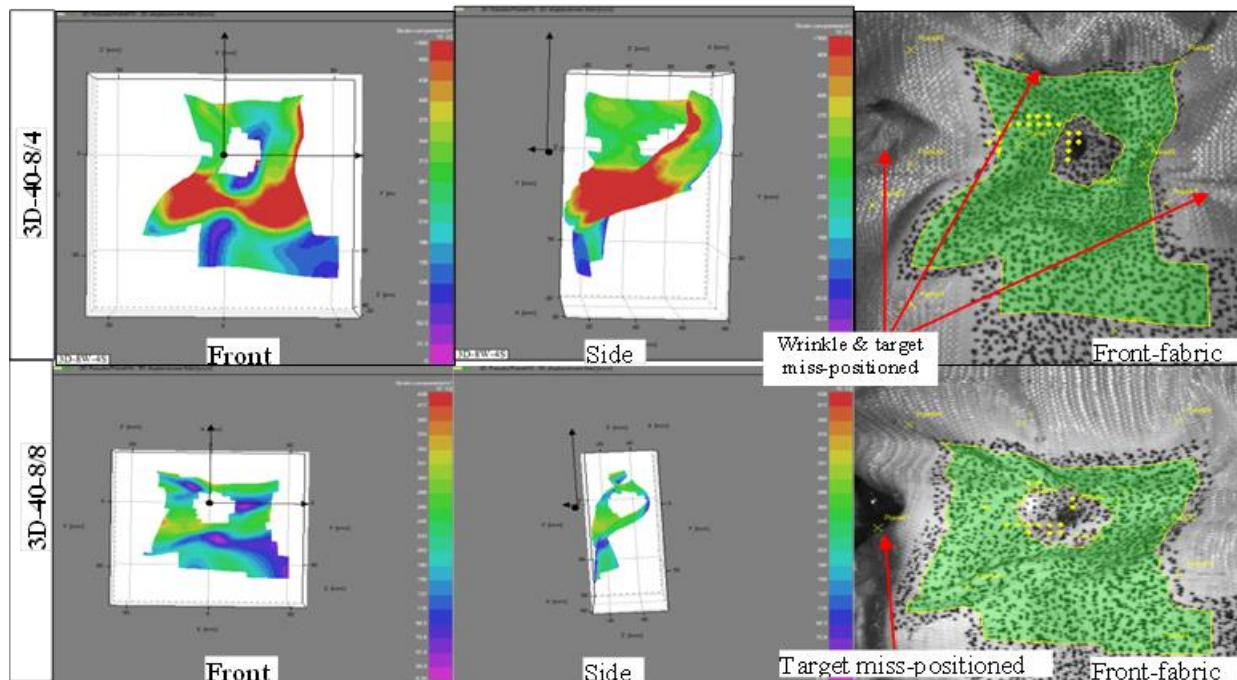
Figure 7.18 Deformed state of panels at 3.6ms after impact at shot point 1

Besides, global failures in the form of fabric wrinkling, shrinkage and miss-position of the target in all directions were observed as shown in the fabric images. On the contrary, sample 3D-40-8/8 revealed uniform distributions of wave propagation with lower surface strain values throughout the impacted local areas. In the global response, it also shows less fabric surface wrinkling but faces miss-position of the target on the right sides. Similarly, **Figure 7.19** also displays the deformed panel (3D-40-8/4 and 3D-40-8/8) images with the time (t=3.6ms) after impact at shot point 3. Based on the stereoscopic image observations of the panel at the specific impact time and locations, both sample types were suffered from a huge amount of surface strains as the impact wave propagates. However, each sample panel tends to create strains in a specific but different direction while resisting the ballistic impact. For example, in the sample 3D-40-8/4, a higher surface strain with different layers along the weft (horizontal) direction near the impact position and far edges of the impact positions were observed. Similarly, the other sample, 3D-40-8/8, also revealed a patterned surface strain but were flown along the warp (vertical) directions mostly near to the impact points. Even though 3D-40-8/8 shows higher than 3D-40-8/4, both sample type shows fewer values not only global surface strain but also wrinkling and miss-positions of the target at shot point 3 compared to shot point 1as shown in fabric photographs. The local, global surface strains and other failure modes of the two samples were also observed at impact position of the moulded area, shot point 5. This help to provide a better understanding of the effect of the impact position in terms of surface strain and other failures modes. **Figure 7.20** shows the panels (3D-40-8/4 and 3D-40-8/8) deformation images at the time after impact (t=3.6ms) of shot point 5. As illustrated on the front faces of the surface strain, 3D-40-8/4 shows higher surface strain around far corners of the local impact points.

Similarly, sample 3D-40-8/4 similarly faces surface strain in similar positions of sample 3D-40-8/4 but with higher values. Both samples also face severe not only wrinkling and folding of the panel surface but also miss-positioning of the panel toward the centre in all direction. Shot point 1 and 5 faces higher global strain in both samples as compared to shot point 3.
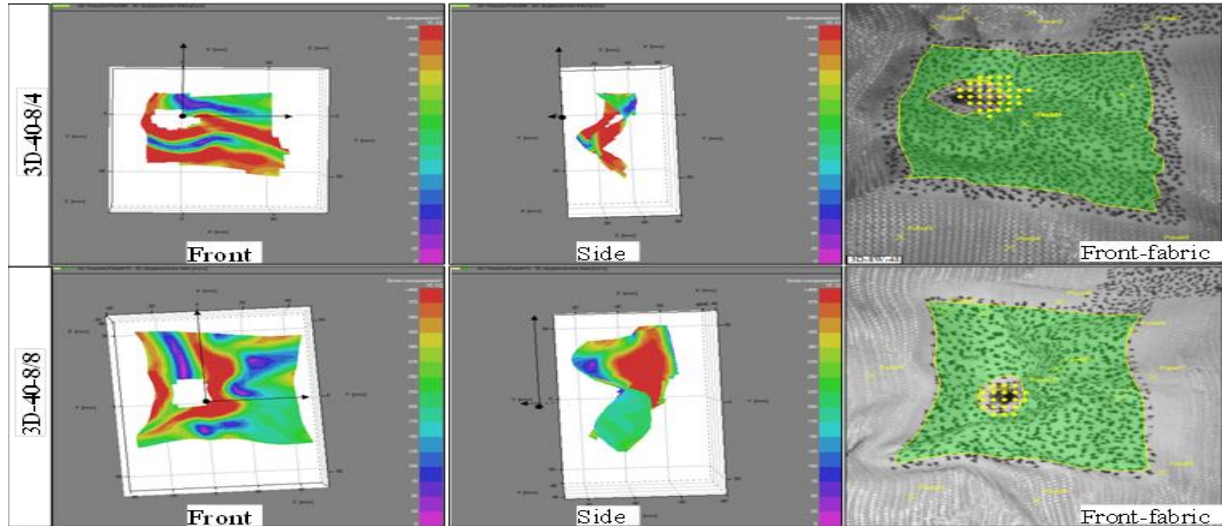
Figure 7.19 Deformed state of panels at 3.6ms after impact at shot point 3

In the final remark, the global and local strain at and around the impact regions were greatly affected not only by the type of the 3D warp interlock fabric variant but also by the impact shot points. Ballistic impact at the moulded areas (shot 5) brings not only higher local and global surface strain but also wrinkling and miss-positioned of the panels toward the centre for both types of the samples at the instant (t=0.18ms) and last (t=3.6ms) impact. 3D-40-8/4 shows higher surface local and global strains at shot point 1 and 3, but less global strain at shot point 3.
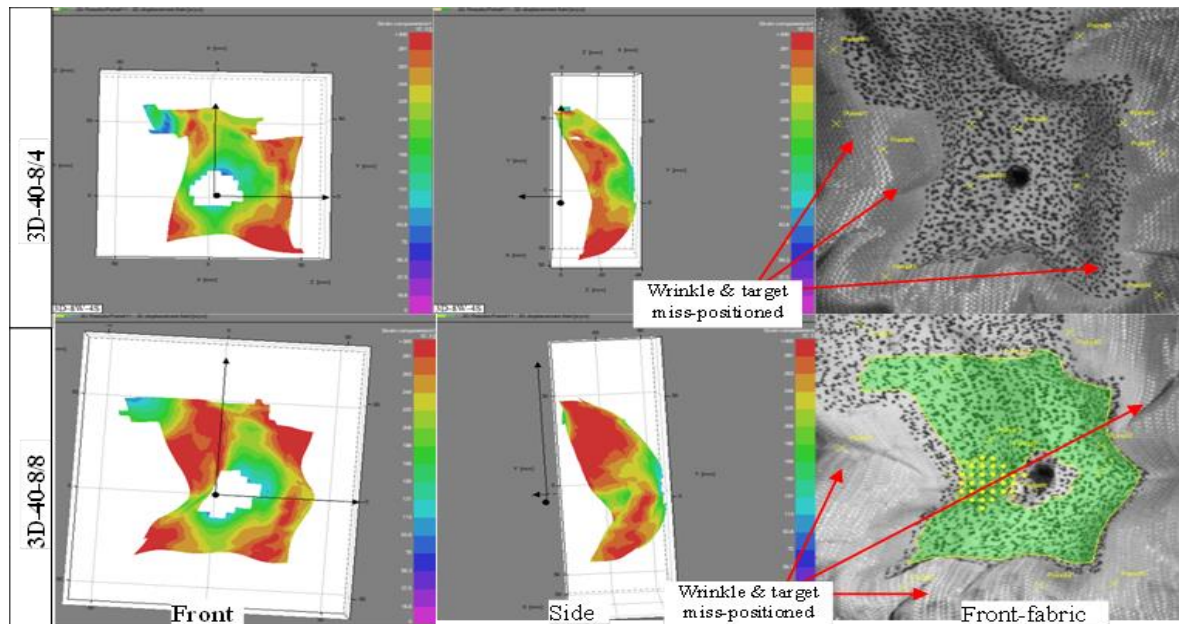
Figure 7.20 Deformed state of panels at 3.6ms after impact at shot point 5

7.4 Conclusion

The purpose of this chapter was to experimentally investigate the ballistic performances of the already designed and manufactured 3D warp interlock fabrics. As discussed in material section, the 3D warp interlock architecture which consists of 8/0, 8/6, 8/8 and 4/8 of binding: stuffer warp yarn interchange ratio was designed and manufactured using ARM semi-automatic dobby loom in GEMTEX lab with different warp yarn interchange ratios. The 2D plain weave fabrics (CT-709) delivered from Teijin Company made of the same types of material and yarn densities were also investigated for comparisons. The different samples from both 2D plain weave and the developed four variants of 3D warp interlock fabrics with the dimensions of 50 cm x 50 cm were prepared in non-stitched form. Before testing, like the previous study, each panel was moulded at the pre-defined position with the help of the adapted bust-shaped punch forming bench. This helps to mould the panel target to mimic the frontal shape of the women upper torso. Each panel was then placed properly and tied at the four edges of the box which is filled with conditioned backing clay having inverted shapes of the moulded panel for accommodation bust. The panels were tested according to the NIJ Level-IIIA standard. Based on the result, the following conclusions were drawn:

➢ Fabric samples made of 100% binder warp yarn (3D-40-8/0) were perforated at 2 different shot points, whereas sample made with 33.3% binder and 66.7% binder warp yarn (3D-40-4/8) faces complete penetration in all (6) shooting points. On the contrary, samples made either 50% binder and 50% stuffer (3D-40-8/8) and fabric sample with 66.7% binder and 33.3% stuffer warp yarn (3D-40-8/4) did not face any perforation at all. Besides, the type of fabric constructions (2D and 3D) also affected the BFS measurements. Samples made of 2D woven fabrics with an approximately equal areal density of the other 3D warp interlock fabrics were penetrated in shot point 6. Similarly, except for shot points 3 and 5, sample 3D-40-8/4 shows lower BFS values as compared to sample 2D-35.

➢ The investigation also revealed that sample 3D-40-8/4 revealed better BFS depth and diameter measurement in the majority of shot points than the samples including 2D-35 followed by sample 3D-40-8/8. Except for its penetration at shot point 6, sample 2D-35 shows nearly equivalent BFS depth values but lower BFS diameter than sample 3D-40-8/4. On the contrary, sample 3D-40-8/0 record the highest BFS diameter compared to all 3D warp interlock fabric samples, except 3D-40-4/8 where its entire target points got penetrated.

➢ A significant difference in energy-absorbing capability (%) was observed among the different samples made of 3D warp interlock fabrics with different warp interchange ratio and 2D fabric at different target points. For example, the energy absorbing percentage values were also found higher for 3D-40-8/4 than sample 3D-40-8/8 and 2D-35 for majority shot points. In general, samples from 3D warp interlock fabrics which comprise the highest binder or stuffer warp yarn ratio face lowest ballistic performances.

➢ Both the post-mortem analysis of projectile deformations and the number of panels involved to stop the projectile were also influenced by the warp yarn interchange ratios inside the 3D warp interlock fabrics. Based on the result, sample 3D-40-8/4 and 3D-40-8/8 revealed the same and a minimum number of panels responsible to halt the projectile in the majority of the shot points as compared to other samples. For example, they involved 5 panels at shot

points 1 and 2 to arrest the projectile. Besides, only 4 and 2 panels were accountable to arrest the projectile by the mentioned two samples at shot points 3 and 5 respectively. Sample 3D-40-8/8 uses a lesser number of panels to stop the projectile at shot points 4 and 6 as compared to sample 3D-40-8/4.

➢ The global and local strain values from the high-speed images were also greatly affected not only by the type of the 3D warp interlock fabric variant but also by the impact shot points. Sample 3D-40-8/4 shows higher surface local and global strains at shot point 1 and 3, but less global strain at shot point 3. Moreover, sample 3D-40-8/8 shows less global and local strains at shot points 3 and 1 respectively compared with other impact points. Ballistic impact at the moulded areas (shot 5) brings not only higher local and global surface strain but also wrinkling and miss-positioned of the panels toward the centre for both types of the samples at the instant (t=0.18ms) and last (t=3.6ms) impact.

8 General Conclusions and future perspectives

8.1 Thesis Summary and General Conclusion

8.1.1 Thesis Summary

The main aim of this thesis work was generating a seamless women's soft body armour multi-panel pattern on the 3D women virtual mannequin using the 3D design process. It is also extended the study on realising its good ballistic performance and fitness by applying the appropriate 3D warp interlock fabric structure using dome-formations principles. Various systematic 3D designing approaches on the virtual environment, engineering and investigations of different 3D warp interlock fabrics variants were performed to achieve the thesis objectives**.** A brief introduction on different concept and information's along with the thesis objective were provided in the introduction part. Following the general introduction, **Chapter One** covered the state of the art. The states of the art were presented into two parts for better understanding and explanations of the relevant information. The first part was focused to explore and provides brief background, valuable information and the related research studies in the area of body armour and its categories, ballistic testing and evaluation methods, ballistic material, ballistic impact mechanisms, factors which affects the fabric ballistic performances etc. The second part dealt with the 3D design process, modelling and pattern generation system for bra's and women body armour, current developments and designing techniques of women body armour, etc. Later, **Chapter Two** mainly explores and focuses on explaining the different methods, research design, fabric manufacturing, testing procedure and apparatus adopted to achieve the aims and objectives of the different research lines in this thesis. Moreover, the different materials including the 2D plain weave fabrics, and the design, development and manufacturing process of different 3D warp interlock fabrics was outlined for further investigations. The main part of the thesis works was presented in **Chapter Three, Four, Five and Six**. It consists of the various research results and outcomes in different research lines both in the garment modelling and experimental work. The first chapter, **Chapter Three**, which also consists of three sub-chapters, deals with modelling, designing and pattern generation's systems for developing a multi-layer seamless woman body armour panel through a moulding process. The first sub-chapter devised the new approaches to simulate the women adaptive bust on a 3D virtual mannequin (having 90B cup size) using the 3D design process. Later, the second sub-chapter discussed on associating of the adaptive bust cup with other frontal parts of 3D women virtual mannequin. This helps to develop a 2D block pattern for 1st layers of women seamless soft body armour panel by using a reverse engineering process (2D-3D-2D pattern generation). Finally, due to the body armour panel composed of multi-layers, the third sub-chapter proposes a new systematic 3D design approach through parametrization process based on each layer's thickness for generating the pattern for each successive panel layers. This sub-chapter also includes some experimental validation of such 3D design approach and its manufacturing system by developing seamless women soft body armour.

The next chapter, **Chapter Four**, comprehensively investigates the influences of yarn density on the different mechanical characterizations and moulding behaviours of the engineered 3D orthogonal warp interlock fabrics variants and compared with counterpart 2D plain weave fabrics of the same fabric density made of 168Tex p-aramid Kevlar yarn. The investigations revealed that the bending rigidity of 3D warp interlock fabrics with higher fabric areal density shows higher values than low fabric areal density. The tensile strength of 3D warp interlock fabric was also influenced by the yarn densities in the respective directions. As the yarn density in their respective warp or/and weft directions increases, maximum tensile load with maximum strain also increases in specific directions. Even though the overall fabric density showed an effect on the deformability, the drawing-in values in specific direction were mainly influenced by the respective yarn densities. In general, the topic concludes that fabric and the respective yarn density of 3D warp interlock fabrics can influence greatly the tensile, bending and moulding properties. Therefore, those parameters should be considered and carefully considered while applying in various technical textile applications i.e., soft body armour.

The next chapter, **Chapter five**, deals on the investigation and discussions of the effects of the warp yarn interchange ratios inside the 3D warp interlock p-aramid architectures on its overall mechanical behaviours. 3D warp interlock variants with the same structural characteristics but different binding: stuffer warp yarn ratios were manufactured and some quasi-static mechanical tests were carried out. The result shows that the warp yarn interchange ratios showed a significant influence on the tensile properties of the 3D warp interlock fabrics. Fabrics with higher stuffer warp yarn (3D-4W-8S) revealed higher tensile modulus (*E*) than fabrics with lower stuffer yarn proportion due to the improved stiffness and fewer waviness behaviours. Besides, fabrics with balanced proportions of stuffer and binding warp yarn (3D-8W-8S) exhibited two tensile peak points at failures because of the actual length difference between the two warp yarns during weaving. Unlike the warp directions, the different fabric load-strain curve in weft direction performed almost as a linear and progressive curve with approximately similar trends. This is due to possessing the same weft yarn compositions and yarn density among all the fabrics. The fabrics with higher binding warp yarn possess higher tensile strain at failure due to higher undulating properties of binder warp yarn inside the fabric architecture. Moreover, 3D warp interlock fabrics which comprise more stuffer warp yarn also possesses the highest flexural rigidity as compared to fabrics with low or no stuffer warp yarns in the warp direction. Whereas, fabrics that only involved binding warp yarn (3D-8W-0S) revealed the lowest flexural rigidity. Moreover, the flexural rigidity in weft direction has been also slightly influenced by the warp yarn compositions and found higher than the respective warp direction due to its less waviness and straight properties than warp yarns. Besides, the influences of the warp yarn interchange ratio on the formability behaviours of the developed 3D warp interlock p-aramid fabrics were also investigated and analysed. According to the result, different forming characteristics of 3D warp interlock fabrics were influenced by the warp yarn interchange ratios. For example, the increments of the stuffer warp yarn interchange ratio exhibit an impact and directly proportional to the stamping force while forming. Sample with higher stuffer yarn ratio possesses less yarn undulation in the warp direction which in turn needs a higher amount of punching loads to deform the preforms to the maximum deformational depth. Besides, in-plane

shear angles were observed higher in the majority of the region for warp interlock fabric with lower binder yarn ratio. Furthermore, fabric structure with higher stuffer yarn ratio also revealed the higher drawing-in values than no or less stuffer yarn. The warp yarn interchange ratio also showed a great influence on the forming recovery properties of 3D warp interlock fabric. The involvement of a higher stuffer warp yarn interchange ratio possesses a higher deformational recovery percentage at maximum depth as compared to fabric with a lower stuffer yarn interchange ratio.

The next two chapters, **Chapter Six and Seven** deals on the ballistic impact performances evaluations of the 3D warp interlock fabrics. The first one discusses the development, investigation and analyses the various 3D warp interlocks fabrics impact performances considering different parameters according to the NIJ standard Level IIIA for seamless woman body armour panel. It also investigates and analyses its performances as compared with the most commonly used traditional 2D plain weave fabrics. In general, the result shows that the woven fabric type (2D and 3D woven), panel impact conditions and the number of layers show a great effect on ballistic impact performances of the panels. Unlike a higher number of layers, 2D plain weave fabric panels revealed higher energy absorption with corresponding 3D interlock O-L p-aramid fabric at a lower number of layers due to its rigid and stiffness property. Based on the limitations of the 3D warp interlock fabric toward the ballistic performance, new variants were designed, manufactured and investigate against the ballistic performance in **Chapter Seven.** During the investigation, the ballistic performances of the 3D warp interlock were enhanced through considering the different warp yarn ratios inside the fabric structures. The ballistic test result show that 3D warp interlock fabrics made with equal or a bit higher interchange ratio of binding: stuffer warp yarn inside the 3D fabric, i.e. 66.7% binder and 33.3% stuffer warp yarn revealed much lower BFS values and higher energy absorbing capability with a minimum number of panels layer penetrations as compared with both the corresponding 2D plain weave and other 3D warp interlock fabric variants. This would be a great achievement for developing women seamless soft body armour which comprises with better ballistic resistance and fit against NIJ-standard Level IIIA.

8.1.2 General Conclusion

Unlike the men's, women soft body armour faces problems in terms of not only its garment design but also finding proper materials to accommodate their morphological shape without affecting its performances are in great demand. This thesis work aimed to develop seamless women soft body armour with better ballistic protection and fitness. To achieve this both a systematic new pattern generation system and engineering the proper ballistic materials were involved.

The 3D design process using the CAD knowledge was used on the specific sizes (90B cup size) of women virtual mannequin for generating the different layers of pattern. The general conclusion in this part includes:

➢ An adaptive bust was successfully developed using a novel 3D design process with the help of computer-aided design (CAD) knowledge on the 3D women virtual model with specific size (90B). The developed adaptive bust greatly helps to directly conceive and generates 3D

patterns of corsetry (bra) on the 3D bust for women having the same size but different cup sizes. Moreover, the determination of different volumes of the bust will greatly help for curtailing the current corset problem, i.e. comfort and fitness.

➢ Besides corset (bra) pattern generation, the adaptive bust in association with the women frontal body, it was extended to design fitted and comfortable women's soft body armour with better bust area accommodation. To achieve an efficient reverse engineering approach (2D-3D-2D pattern generation system) were devised and applied on the associated frontal 3D woman adaptive bust virtual mannequin (90B size bust cup) to generate appropriate 2D block patterns for the first-panel layer. The generated patterns were mainly aimed to develop the woman seamless soft body armour panel without involving the dart through the dome-formation process on the bust area. According to the material deformation analysis based on a 3D-to-2D flattened pattern, the generated flattened pattern reveals better shape to accommodate the deformation with low distortion throughout the fabric surface while flattening.

➢ Since body armour panel comprises the multiple layers, a systematic 3D design approach through parametrization process based on the thickness of each layer was applied on the conceived 3D virtual adaptive woman mannequin to generate 3D block patterns for the frontal panel of each successive layer. The methods reference the developed block pattern of the first layer as a base. The 3D pattern was then flattened and validated by manufacturing the frontal soft body armour panel using 3D warp interlock fabrics through the dome-formation process on the adapted bust-shaped punching bench. Based on the observations, the proposed 3D design approach was found good to generate multi-layer panels block pattern for better shape and fitness of the final garment.

Besides, introducing 3D warp interlock fabrics for women body armour design becomes promising, this thesis has made a great effort to identify and develop the structure which could give both good shaping of the women body shape (moulding ability) based on the developed pattern and improved ballistic performances. For this, two phases of 3D warp interlock fabric design and manufacturing campaign were carried out considering different parameter. The fabric structures were characterised by their mechanical and moulding behaviours. Moreover, all the produced fabrics structures were tested against ballistic performances based on NIJ-standard Level-IIIV and compare with the traditional 2D plain weave fabrics. Based on our investigations the following conclusions are drawn:

➢ The bending rigidity of 3D warp interlock fabrics with higher fabric areal density shows higher values than low fabric areal density. Moreover, the fabric becomes very stiff and faces resistant to bend in the higher yarn density direction.

➢ The tensile strength of 3D warp interlock fabric was also influenced by the yarn densities in the respective directions. As the yarn density in their respective warp or/and weft directions increases, maximum tensile load with maximum strain also increases in specific directions.

➢ Even though the overall fabric density showed an effect on the deformability, the drawing-in values in specific direction were mainly influenced by the respective yarn densities.

➢ Besides, even though there was no clear relationship between the in-plane shear and its recovery values with the fabric density, in general, the higher the fabric density reduced

the in-plane shear angle and its recovery of the sub-region. This might be as the yarn density increases; the yarn comes closer and compresses each other to create a more rigid fabric with high frictional resistance between them. This helps to resist the shear angle formation and recovery from the deformed positions.

➢ In general, fabric and the respective yarn density of 3D warp interlock fabrics influenced greatly the tensile, bending and moulding properties where those parameters should be considered and should be carefully considered while applying in various technical textile applications i.e., soft body armour.

➢ The different panels made with various layers 3D warp interlock (O-L) p-aramid fabrics were also arranged and moulded to resemble the frontal women's body shape before ballistic impact tested against NIJ-Level IIIA. Based on the non-perforation evaluations, type of fabrics (2D/3D), number of panel layers and shot point conditions (moulded/flat) affects the BFS measurement and energy capabilities of the final panels. Due to its structural compactness and rigidity, 2D plain p-aramid fabrics revealed good ballistic performance, lower BFS measurement and less number of layers to halt the projectile as compared to 3D warp interlock fabrics. Besides, the panel energy absorption at the non-moulded shot point revealed better than the moulded shot points due to the compactness and rigidity of the panel in the specified area has been compromised and ultimately gives lower ballistic performances. On the contrary, the 3D warp interlock fabric displays better shaping ability according to the women contour while designing the body armor than its counterpart 2D plain weave p-aramid fabric.

➢ Besides, due to the involvement of many primary yarns, stiffness and close yarns in the weave structure makes the 2D plain weave fabric panel to possess a higher level of local surface damages, wider cone deformations and lesser bowing of yarn was substantially observed than 3D warp interlock fabric panels at a similar number of layers and shooting points.

Considering the above result, four possible variants of 3D warp interlock fabric with the same structural characteristics but different (8/0, 8/6, 8/8 and 4/8) binder: stuffer warp yarn interchange were manufactured using ARM semi-automatic dobby loom in GEMTEX lab to evaluate its overall performance. Based on the experimental investigation on its quasi-static mechanical, moulding ability and ballistic impact tests, the following conclusions were drawn:

➢ The warp yarn interchange ratios inside the 3D warp interlock fabrics structure also showed a significant influence on its tensile, flexural rigidity, crimp percentage and formability and its recovery against hemispherical punch and ballistic performances.

Fabrics with higher stuffer warp yarn (3D-4W-8S) revealed higher tensile modulus (E) than fabrics with lower stuffer yarn proportion due to the improved stiffness and less waviness behaviours. Besides, fabrics with balanced proportions of stuffer and binding warp yarn (3D-8W-8S) exhibited two tensile peak points at failures because of the actual length difference between the two warp yarns during weaving. Unlike the warp directions, the different fabric load-strain curve in weft direction performed almost as a linear and progressive curve with approximately similar trends. This is due to possessing the same weft yarn compositions and yarn density among all the fabrics. The fabrics with higher binder warp yarn possess higher tensile strain at failure due to higher undulating properties

of binder warp yarn inside the fabric architecture. 3D-8W-0S possesses higher tensile strain at failure (12.88%) than weft directions (5.88%), whereas, 3D-4W-8S record approximately equal tensile strain at failure both in the warp and weft direction (4.88%) due to having similar undulation of warp and weft yarns inside the fabrics structures. Unlike warp directions, the maximum tensile strain (εmax) and load (σmax) at failures in weft directions were slightly affected by the warp yarn even it possesses the same weft yarn compositions inside 3D fabrics architecture. 3D-8W-0S and 3D-8W-4S were failed at the tensile strain values of approximately around 5.88% and 7.8% and Sample C and D failed at the strain values of 7.55% and 4.8%.

➢ 3D warp interlock fabrics which comprise more stuffer warp yarn also possesses the highest flexural rigidity as compared to fabrics with low or no stuffer warp yarns in the warp direction. Whereas, fabrics that only involved binding warp yarn (3D-8W-0S) revealed the lowest flexural rigidity. Moreover, the flexural rigidity in the weft direction has been also slightly influenced by the warp yarn compositions and found higher than the respective warp direction due to its less waviness and straight properties than warp yarns.

➢ Variants with higher stuffer warp yarn ratio absorb a higher amount of punching loads while deformed at the maximum depth due to possessing less yarn undulation in the warp direction. Higher in-plane shear angles and drawing-in values were also observed in the majority of the region for variants having higher stuffer yarn ratio. The forming recovery of the fabrics was also influenced by the involvements of different warp yarn interchange ratio. The higher the stuffer warp yarn interchange ratio inside the fabric structure, the better the deformational recovery percentage at maximum displacement was achieved. Specifically, 3D-4S-8W revealed the maximum drawing-in recovery percentage of 43.13% and 46.98% in the machine (warp) and cross (weft) direction respectively around the preform peripheral edges. On the contrary, samples with higher binder warp yarn; 3D-8W-0S show the maximum drawing-in recovery percentages values of 31.21 % and 34.99% in the machine (warp) and cross (weft) direction respectively.

➢ Different samples made of 35 layers 2D plain weave (CT-709) fabric and 40 layers of the different developed 3D warp interlock p-aramid fabrics were prepared in a non-stitched form and moulded with adapted bust-shaped punch forming bench at a bust position to mimic the frontal shape of the women upper torso before the ballistic test. According to the ballistic test with NIJ Level-IIIA standard, a sample with 100% binder warp yarn (3D-40-8/0) perforated at 2 different shot points, whereas sample made with 33% binder and 66.7% binder warp yarn (3D-40-4/8) faces complete penetration in all (6) shooting points. On the contrary, samples made of 50% binder and stuffer warp yarn (3D-40-8/8) and sample with 66.7% binder and 33.3% stuffer warp yarn (3D-40-8/4) did not face any perforation. Sample 3D-40-8/4 revealed better BFS depth and diameter measurement in the majority of shot points than other variants including 2D-35 followed by 3D-40-8/8. Except for its penetration at shot point 6, sample 2D-35 shows nearly equivalent BFS depth values but lower BFS diameter than sample 3D-40-8/4. However, sample 3D-40-8/0 record highest BFS diameter compared to all 3D warp interlock fabric samples, except 3D-40-4/8 where its entire target points got penetrated. Moreover, sample 3D-40-8/4 revealed higher energy absorbing percentage values than sample 3D-40-8/8 and 2D-35 for majority

shot points. Samples from 3D warp interlock fabrics which comprise the highest binder or stuffer warp yarn ratio face lowest ballistic performances. The warp yarn interchange ratios inside the 3D warp interlock fabrics also affected the projectile deformations and number of panels responsible to stop the projectile. Based on the computations, sample 3D-40-8/4 and 3D-40-8/8 revealed the same and the minimum number of panels responsible to halt the projectile in the majority of the shot points as compared to other samples. However, sample 3D-40-8/8 shows superior in using lesser number of panels to stop the projectile at shot points 4 and 6 as compared to sample 3D-40-8/4. From the high-speed images, higher local and global surface strains were observed at shot point 1 and 3, but less global strain at shot point 3. On the contrary, sample 3D-40-8/8 revealed lesser global and local strains at shot point 3 and 1 respectively than the other impact points. Ballistic impact at the moulded areas (shot 5) brings not only higher local and global surface strain but also wrinkling and miss-positioned of the panels toward the centre for all samples at the instant (t=0.18ms) and last (t=3.6ms) impact int.

8.2 Challenges and future perspectives

8.2.1 Challenges

➢ Modelling and body armour pattern was generated only for one size of women body (90 B) with different adaptive bust due to time limitations.
➢ The developed pattern was evaluated its fitness through manual deformation of the 3D warp interlock fabrics and by observation on the real mannequin (Comfort was not studied)
➢ The production of 3D warp interlock fabrics at the lab scale took more time and energy. It was also very difficult to control the weaving condition and quality of the product.
➢ The ballistic performance of the panels was carried out only for the standard NIJ-Level IIIV.
➢ The local and global surface strains of the tested 3D warp interlock fabric were analyses by observing the image taken through a high-speed camera.
➢ Moulding of the panel to mimic the frontal body needs an advanced way of dome-formation principles and techniques.

8.2.2 Future works

➢ Modelling, Designing and pattern generation system of soft body armour panel for the different women body sizes makes it women armour solutions very complete.
➢ The experimental investigations of the quasi-static and dynamic ballistic impact phenomena of the fabrics should be also carried out with numerical simulation for complete understanding and better performance optimizations.
➢ Apart from ballistic performances and fitness of the body armour, further evaluation of comfort is very important. This could help to provide sufficient breathability for extended use, especially during high temperatures, and must not interfere with or restrict the user's mobility.
➢ However, it is very challenging to balance the level of protection required for specific threat type(s) against weight, comfort and flexibility, cost, environmental exposure (heat,

ultraviolet light, moisture, etc.), and service life. Mostly multi-layer soft body armour vests are very heavy in weight, rigid and create uncomfortable to wear and also even have an impact on the mobility of the personnel. Developing soft body armour by reducing the weight of material using different advanced technology will enhance its comfort level.

➤ Even though the new design approach for multi-layer woman body armour panel layer offers better pattern block projection, an improvement in the manufacturing process in terms of making scientific dome-formation process is required.

➤ The mechanical moulding process on the dry fabric could help only to determine and understand the capability of the fabrics to be deformed with different characteristics. However, it is intended to use for final women soft body armour development, different mechanism to sustain the moulded area for an extended period will be the future aspects.

8.3 Contributions and publications

 I. List of journal publications (* = Corresponding author)

2018

1. **Mulat A. Abtew***, F. Boussu, P. Bruniaux, C. Loghin, I. Cristian, Y. Chen and L. Wang 'Forming characteristics and surface damages of stitched multi-layered para-aramid fabrics with various stitching parameters for soft body armour design', *Composites Part A: Applied Science and Manufacturing (Elsevier)*, 109(2018); 517–537 (IF = 6.282) doi.org/10.1016/j.compositesa.2018.02.037

2. **Mulat A. Abtew***, F. Boussu, P. Bruniaux, C. Loghin, I. Cristian, Y. Chen and L. Wang, 'Influences of fabric density on mechanical and moulding behaviours of 3D warp interlock para-aramid fabrics for soft body armour application, *Composite Structure (Elsevier),* 204(2018); 402–418 (IF = 4.829). doi.org/10.1016/j.compstruct.2018.07.101

3. **Mulat A. Abtew***, P. Bruniaux, F.Boussu, C. Loghin, I. Cristian, Y. Chen and L. Wang, 'A systematic pattern generation system for manufacturing customized seamless multi-layer female soft body armour through dome-formation (moulding) techniques using 3D warp interlock fabrics,' *Journal of Manufacturing Systems (Elsevier)*, 49(2018);61–74 (IF = 3.699) doi.org/10.1016/j.jmsy.2018.09.001

4. **Mulat A. Abtew***, P. Bruniaux, F. Boussu, C. Loghin, I. Cristian and Y. Chen, 'Development of comfortable and well-fitted bra pattern for customized female soft body armour through 3D design process of adaptive bust on virtual mannequin,' *Computers in Industry (Elsevier)*,100(2018);7–20 (IF=4.769). doi.org/10.1016/j.compind.2018.04.004

5. **Mulat A. Abtew***, P. Bruniaux, F. Boussu, C. Loghin, I. Cristian, Y. Chen and L. Wang 'Female seamless soft body armour pattern design system with innovative reverse engineering approaches, *International Journal of Advanced Manufacturing Technology*, 98(2018); 2271–2285 (IF = 2.601) doi.org/10.1007/s00170-018-2386-y

2019

1. **Mulat A. Abtew***, F. Boussu, P. Bruniaux, C. Loghin, and I.Cristian, 'Ballistic impact mechanisms - A review on textiles and fibre-reinforced composites impact responses,

Composite structure (Elsevier), 223, Sept 2019, 110966; (IF = 4.829) doi.org/10.1016/j.compstruct.2019.110966

2. **Mulat A. Abtew***, F. Boussu, P. Bruniaux, C. Loghin, I.Cristian, 'Engineering of 3D warp interlock p-aramid fabric structure and its energy absorption capabilities against ballistic impact for body armour applications, *Composite structure (Elsevier)*, 225 (2019), 111179; (IF = 4.829). https://doi.org/10.1016/j.compstruct.2019.111179

3. **Mulat A. Abtew***, F. Boussu, P. Bruniaux, C. Loghin, I.Cristian, Y. Chen and L. Wang, 'Ballistic impact performance and surface failure mechanisms of 2D and 3D woven p-aramid multi-layer fabrics for lightweight women ballistic vest applications,' *Journal of industrial textile (SAGE)*,0(0)(2019);1–33(IF=1.88). DOI: 10.1177/1528083719862883

4. **Mulat A. Abtew*****,** Pascal BRUNIAUX and François BOUSSU, 'Customizations of women bullet-proof jacket through 3D design process, TEXT LEATH REV 2 (1) 2019 23-31. Doi: 10.31881/TLR.2019.20

5. **Mulat A. Abtew***, C. Loghin, I. Cristian, F.Boussu and P. Bruniaux, 'Mouldability and its recovery properties of plain-woven p-aramid fabric for soft body armour applications' *FIBRES & TEXTILES in Eastern Europe*, 2019; 27, 6(138): 54-62. DOI: 10.5604/01.3001.0013.4468 (IF = 0.57).

6. **Mulat A. Abtew***, P. Bruniaux, F. Boussu, C. Loghin, I. Cristian, Y. Chen and L. Wang 'Three-dimensional (3D) warp interlock p-aramid fabrics for the development of seamless female soft body armour with better flexibility and ballistic impact performance,' current applied physics, under review.

7. **Mulat A. Abtew***, P. Bruniaux, F. Boussu, C. Loghin, I. Cristian, Y. Chen and L. Wang, 'Fabrication and characterizations of dry 3D warp interlock para-aramid fabric structures for composite and ballistic applications,' Composite part A: Applied science and manufacturing, under review.

8. **Mulat A. Abtew***, P. Bruniaux, F. Boussu, C. Loghin and I. Cristian, 'Influences of warp yarn interchange ratio on the formability of dry 3-dimensional (3D) warp interlock p-aramid fabric structure, Composite par B: Engineering, under review.

9. **Mulat A. Abtew***, P. Bruniaux, F. Boussu, C. Loghin, I. Cristian, Y. Chen and L. Wang, 'Yarn degradation during weaving process and its effect on the mechanical behaviours of 3D warp interlock p-aramid fabric for industrial applications' Journal of Industrial textile, under review.

II.   Conference proceeding publications, oral and poster presentations (* = Corresponding author and [†] = **presenter)**

2017

1 **Mulat A. Abtew***[†], P. Bruniaux and F. Boussu, 'Development of adaptive bust for female soft body armour using 3D warp interlock fabrics: 3D design process,' IOP Conf. Series: Materials Science and Engineering 254 (2017) 05200.Doi:10.1088/1757-899X/254/5/052001 (AUTEX 2017-Corfu, Greece).

2 **Mulat A. Abtew***[†], P. Bruniaux and F. Boussu, 'Experimental investigation of 2D/3D aramid fabric forming capabilities for female body armour design', CLOTECH-2017, Lodz, Poland).

2018

1. **Mulat A. Abtew***, F. Boussu[†], P. Bruniaux, C. Loghin, I. Cristian, Y. Chen and L. Wang, 'Experimental investigation of effects of stitching orientation on forming behaviours of 2D P-aramid multilayer woven preform,' AIP Conference Proceedings 1960, 020001 (2018). doi: 10.1063/1.5034802, ESAFORM-18, Palermo, Italy.

2. **Mulat A. Abtew***[†], C Loghin, I Cristian, F Boussu, P Bruniaux, Y Chen and L Wang, 'Two Dimensional (2D) P-Aramid Dry Multi-Layered Woven Fabrics Deformational Behaviour for Technical Applications, IOP Conf. Series: Materials Science and Engineering 374 (2018) 012055. Doi:10.1088/1757-899X/374/1/012055, Euroinvent ICIR-18, Iasi, Romania.

3. **Mulat A. Abtew***[†], F. Boussu, P. Bruniaux, C. Loghin, I. Cristian, Y. Chen and L. Wang', Effects of fabric density on bending behaviour of 3D warp interlock fabrics for composite and body armour', AUTEX-2018, Istanbul, Turkey.

4. **Mulat A. Abtew***, P. Bruniaux, F. Boussu[†], C. Loghin, I. Cristian, Y. Chen and L. Wang Formability behaviour of 3D warp interlocks P-aramid Fabric for soft body armour design, TEXCOMP-13, Milan, Italy.

5. Mulat A. Abtew*[†], P. Bruniaux, F. Boussu, C. Loghin, I. Cristian, Y. Chen and L. Wang 3D warp interlock p-aramid fabrics and its mouldability property for female ballistic vest design" 7-9 November 2018 17th Romanian Textiles and Leather Conference – CORTEP 2018, Iasi, Romania.

2019

1. **Mulat A. Abtew***[†], C Loghin, I Cristian, F Boussu, P Bruniaux, Y Chen and L Wang, '3D warp interlocks p-aramid fabrics for composite reinforcement and ballistic vest applications: Effect of yarn density on its formability characteristics, IOP Conf. Series: Materials Science and Engineering 572 (2019) 012078. Doi:10.1088/1757-899X/572/1/012078 (Euroinvent ICIR-19, Iasi, Romania.

2. **Mulat A. Abtew***[†], P. Bruniaux and François Boussu, 'Customizations of women bullet-proof jacket through 3D design process', Textile Science & Economy-19, Zagreb, Croatia.

3. **Mulat A. Abtew***, F. Boussu[†], P. Bruniaux, C. Loghin and I. Cristian, '3D warp interlock fabric structure as a new material for women ballistic protective vest design', Proceedings of the 19th world textile conference-Autex-2019, Belgium-Ghent.

4. **Mulat A. Abtew***[†], C Loghin, I Cristian, F Boussu, P Bruniaux, Y Chen and L Wang, 'Effects of woven fabric types on ballistic impact performance for seamless women soft body armour design' proceeding of Light-weight amour and security, LWAG-2019, Roubaix, France.

5. **Mulat A. Abtew***[†], P. Bruniaux, F. Boussu, C. Loghin, I. Cristian, Y. Chen and L. Wang, '3D design process with reverse engineering approach for seamless women soft body

armour pattern generation and its development using 3D warp interlock fabrics, Mechanics of Living Materials and Composites, M2VC-2019, March 29, 2019, ENSAIT-GEMTEX, Roubaix, ENSAIT.

6. **Mulat A. Abtew***[†], C Loghin, I Cristian, F Boussu, P Bruniaux, Y Chen and L Wang, 'Three-dimensional (3D) warp interlock p-aramid fabrics for the development of seamless female soft boy armour with better flexibility and ballistic impact performance',(AAAFM-UCLA -2019, Advanced Materials Conference, Los Angeles, USA.

III.   Chapters in a Book (* = Corresponding author)

1. **Mulat .A. Abtew***, P. Bruniaux, F. Boussu, C. Loghin, I.Cristian, Y. Chen and L. Wang, '3D woven fabrics for the women soft body armour applications,' under review for the book' Advanced weaving Technology, will be published by Springer.

VI.   Recent papers by the author not related to the thesis topic (* = Corresponding author)

1. **Mulat .A. Abtew***, Subhalakshmi Kropi, Hong Yan, Linzi Pu, 'Implementation of Statistical Process Control (SPC) in the Sewing Section of Garment Industry for Quality Improvement, *Autex Research Journal*, (2018) 18(2):160-172 DOI: 10.1515/aut-2017-0034
2. **Mulat .A. Abtew***, Annu Kumari, Ambika Mehtre and Yan Hong, 'Statistical analysis of standard allowed minute (sam) on sewing efficiency in apparel industry,' *Autex Research Journal, (2018).* DOI 10.2478/aut-2019-0045.
3. Linzi Pu, Hong Yan, Melissa Wagner, peiguo wang* and **Mulat .A. Abtew,**'Raincoat design for children for age group 7–8 years: A design development case study,' Industria textile, (2018), 69(5):394–399.

9 References

[1]   Bajaj P. Ballistic protective clothing : An overview. *Indian J Fibre Text Res* 1997; 22: 274–291.

[2]   Xiaogang Chen and Dan Yang. Use of 3D Angle-Interlock Woven Fabric for Seamless Female Body Armour : Part I : Ballistic Evaluation. *Text Res J* 2010; (0): 1–8.

[3]   Bailer B. Magazine. *Concealable Body Armor Gets More Comfortable*, 2013http://www.policemag.com/channel/patrol/articles/2013/07/concealable-body-armor-gets-more-comfortable.aspx (2013).

[4]   Richard A. Carlson. *Pleated ballistic package for soft body armour*. US20100313321 A1, USA, 2010.

[5]   Messiry M El, El-tarfawy S. Performance of Weave Structure Multi-Layer Bulletproof Flexible Armor. In: *The 3rd conference of the National Campaign for Textile Industries,NRC Cairo, '"Recent Manufacturing Technologies and Human and Administrative Development"'*. Cairo, 2015, pp. 218–225.

[6]   Wanger L. Military and law enforcement applications. In: Bhatnagar A (ed) *Lightweight Ballistic Composites*. Abington Hall, Abington, Cambridge CB1 6AH, England: Woodhead Publishing, pp. 1–25.

[7]   Smith WC. *An overview of protective clothing-markets, materials, needs*. Greer, SC, USA, 1999.

[8]   Bhatnagar A, Arvidson B, Pataki W. *Lightweight Ballistic Composites, Military and Law-Enforcement Applications*. Woodhead Publishing, 2006, p. 213-214, 2006.

[9]   Eurostat. Police, court and prison personnel statistics. *https://ec.europa.eu/eurostat/statisticsexplained/index.php?title=Police,_court_and_prison_personnel_statistics#One_in_five_police_officers_is_a_woman*.

[10]   Hargreaves J, Cooper J, Woods E, et al. Police Workforce, England and Wales. *Statistical bulletin 05/16*, 2016, pp. 1–38.

[11]   International Women's Day, police Scotland. *Police Scotland 8 march 2017, Retrived 26 July 2016*.

[12]   Police Service of Northern Ireland (PSNI). Workforce Composition Statisticshttps://www.psni.police.uk/inside-psni/Statistics/workforce-composition-statistics/ (2017, accessed 26 July 2017).

[13]   Crime in the United States 1995. FBIhttps://ucr.fbi.gov/crime-in-the-u.s/1995 (2016).

[14]   Crime in the United States 2005. *Gender*www2.fbi.gov (2006).

[15]   Crime in the United States 2014. *Police Employee Data*https://ucr.fbi.gov/crime-in-the-u.s/2014/crime-in-the-u.s.-2014/police-employee-data/main (2014).

[16]   Zufle TT. *Body Armour For Women*. 4,578,821, USA patent, 1986.

[17]   Mellian SA. *Body Armor for Women*. US4183097 A, US, 1980.

[18]   Nelson JS, Price AL. *Ballistic vest*. US 5619748 A, US, 1997.

[19]   Hussein M, Parker G. *Ballistic protective wear for the female torso*. US6281149 B1, US, 2001.

[20]   McQueer PS. *Woman's bullet-resistant undergarment*. US20110277202 A1, USA, 2011.

[21]   Vives M. *Ballistic protection armour*. US5221807 A, USA, 1993.

[22]   Carlson RA, Hills C. *Female armour system*. US20120174275 A1, US Patent: US20120174275 A1, 2012.

[23]   Dyer PA. *Ballistic protective insert for use with soft body armour by female personnel*. US5020157 A, 1991.

[24] Yang D, Chen X. Multi-layer pattern creation for seamless front female body armor panel using angle-interlock woven fabrics. *Text Res J* 2017; 87: 1–6.

[25] Abtew MA, Boussu F, Bruniaux P, et al. Forming characteristics and surface damages of stitched multi-layered para-aramid fabrics with various stitching parameters for soft body armour design. *Compos Part A Appl Sci Manuf* 2018; 109: 517–537.

[26] Haanappel SP, Ten Thije RHW, Sachs U, et al. Formability analyses of uni-directional and textile reinforced thermoplastics. *Compos Part A Appl Sci Manuf* 2014; 56: 80–92.

[27] Vanclooster K, Lomov S V, Verpoest I. On the formability of multi-layered fabric composites. *Proc 17th Int Conf Compos Mater* 2009; 1–10.

[28] Chen S, Endruweit A, Harper LT, et al. Forming simulations of multi-layered woven preforms assembled with stitch yarns. In: *ECCM16 - 16th European Conference On Composite Materials, Seville, Spain, 22-26 June*. 2014.

[29] T.K. LPB and G. *Apparel Sizing And Fit*. UK: Oxford, 2002.

[30] Cichocka A, Bruniaux P. Approach To The Modelling Of Virtual Mannequins Of Human Body For Garment Industry In 3D. In: *10th World Textile Conference, Autex*. Vilnius Lithuania: AUTEX, 2011.

[31] Bruniaux P. 3D Pattern-Making On Adaptive Morphotype Mannequin. In: *14th Romanian Textiles and Leather Conference – CORTEP 2012,*. Sinaia.

[32] Cuong Ha-Minh, Boussu F, Kanit T, et al. Effect of Frictions on the Ballistic Performance of a 3D Warp Interlock Fabric : Numerical Analysis. *Appl Compos Mater* 2012; 19: 333–347.

[33] Chen X, Lo W-Y, Tayyar AE. Mouldability of Angle-Interlock Woven Fabrics for Technical Applications. *Text Res J* 2002; 72: 195–200.

[34] Boussu F, Legrand X, Nauman S, et al. Mouldability of angle interlock fabrics. In: *FPCM -9, the 9th International Conference on Flow Processes in Composite Materials*. Montréal (Québec), Canada, 2008.

[35] Chen X, Yang D. Use of Three-dimensional Angle-interlock Woven Fabric for Seamless Female Body Armor : Part II : Mathematical Modeling. *Text Res J* 2010; Vol 80: 1589–1601.

[36] Roedel C, Chen X. Innovation and Analysis of Police Riot Helmets with Continuous Textile Reinforcement for Improved Protection. *J Inf Comput Sci* 2007; 2: 127–136.

[37] Zahid B, Chen X. Manufacturing of single-piece textile reinforced riot helmet shell from vacuum bagging. *J Compos Mater* 2012; 47: 2343–2351.

[38] Yang D, Chen X, Sun D, et al. Ballistic performance of angle-interlock woven fabrics. *J Text Inst* 2017; 108: 586–596.

[39] Roylance D, Wilde A, Tocci G. Ballistic Impact of Textile Structures. *Textile Research Journal* 1973; 43: 34–41.

[40] Karahan M, Jabbar A, Karahan N. Ballistic impact behavior of the aramid and ultra-high molecular weight polyethylene composites. *J Reinf Plast Compos* 2015; 34: 37–48.

[41] Roylance D, Wang SS. Influence of fibre properties on ballistic penetration of textile panels. *Fibre Science and Technology* 1981; 14: 183–190.

[42] Cunniff PM. An Analysis of the System Effects in Woven Fabrics Under Ballistic Impact. *Text Res J* 1992; 62: 495–509.

[43] Briscoe BJ, Motamedi F. The ballistic impact characteristics of aramid fabrics: The influence of interface friction. *Wear* 1992; 158: 229–247.

[44] Tan VBC, Tay TE, Teo WK. Strengthening fabric armour with silica colloidal suspensions. *Int J Solids Struct* 2005; 42: 1561–1576.

[45] Karahan M. Comparison of Ballistic Performance and Energy Absorption Capabilities of Woven and Unidirectional Aramid Fabrics. *Text Res J* 2016; 78: 718–730.

[46] Chen X, Sun D, Wang Y, et al. 2D / 3D Woven Fabrics for Ballistic Protection. In: *4th World Conference on 3D Fabrics and Their Applications ; 10 Sep 2012-11 Sep 2012; Aachen, Germany. Manchester: TexEng/RWTH Aachen*. 2012, pp. 1–12.

[47] Othman AR, Hassan MH. Effect of different construction designs of aramid fabric on the ballistic performances. *Mater Des* 2013; 44: 407–417.

[48] Cork CR, Foster PW. The ballistic performance of narrow fabrics. *Int J Impact Eng* 2007; 34: 495–508.

[49] Zhang D, Sun Y, Chen L, et al. Influence of fabric structure and thickness on the ballistic impact behavior of Ultrahigh molecular weight polyethylene composite laminate. *Mater Des* 2014; 54: 315–322.

[50] Yavaşa MO, Avcıa A, Şimşirb M, et al. Ballistic performance of Kevlar49/ UHMW-PEHB26 Hybrid Layered- Composite. *Int J Eng Res Dev* 2015; 7: 1–20.

[51] Montgomery TG, Grady PL, Tomasino C. The Effects of Projectile Geometry on the Performance of Ballistic Fabrics. *Text Res J* 1982; 442–450.

[52] Shim VPW, Tan VBC, Tay TE. Modelling deformation and damage characteristics of woven fabric under small projectile impact. *Int J Impact Eng* 1995; 16: 585–605.

[53] Tan VBC, Lim CT, Cheong CH. Perforation of high-strength fabric by projectiles of different geometry. *Int J Impact Eng* 2003; 28: 207–222.

[54] Park Y, Kim YH, Baluch AH, et al. Numerical simulation and empirical comparison of the high velocity impact of STF impregnated Kevlar fabric using friction effects. *Compos Struct* 2015; 125: 520–529.

[55] Park JL, Yoon B il, Paik JG, et al. Ballistic performance of p-aramid fabrics impregnated with shear thickening fluid; Part I – Effect of laminating sequence. *Text Res J* 2012; 82: 527–541.

[56] Park JL, Yoon B il, Paik JG, et al. Ballistic performance of p-aramid fabrics impregnated with shear thickening fluid; Part II – Effect of fabric count and shot location. *Text Res J* 2012; 82: 542–557.

[57] Sun D, Chen X. Plasma modification of Kevlar fabrics for ballistic applications. *Text Res J* 2012; 82: 1928–1934.

[58] Lee YS, Wetzel ED, Wagner NJ. The ballistic impact characteristics of Kevlar® woven fabrics impregnated with a colloidal shear thickening fluid. *J Mater Sci* 2003; 38: 2825–2833.

[59] Lee BW, Kim IJ, Kim CG. The influence of the particle size of silica on the ballistic performance of fabrics impregnated with silica colloidal suspension. *J Compos Mater* 2009; 43: 2679–2698.

[60] Park JL, Chi Y, Kang TJ. Ballistic performance of hybrid panels composed of unidirectional/woven fabrics. *Text Res J* 2013; 83: 471–486.

[61] Wang Y, Chen X, Young R, et al. An Experimental study of ply orientation on ballistic impact resistance of multi-ply fabric panels. *Compos Part B Eng* 2015; 68: 259–265.

[62] Yanyan C, Xiaogang C, Sheel DW, et al. Surface modification of aramid fibers by atmospheric pressure plasma-enhanced vapor deposition. *Text Res J* 2014; 84: 1288–1297.

[63] Chu Y, Chen X, Wang Q, et al. An investigation on sol–gel treatment to aramid yarn to increase inter-yarn friction. *Appl Surf Sci* 2014; 320: 710–717.

[64] Ha-Minh C, Boussu F, Kanit T, et al. Effect of frictions on the ballistic performance of a 3D warp interlock fabric: Numerical analysis. *Appl Compos Mater* 2012; 19: 333–347.

[65] Tan VBC, Lim CT, Cheong CH. Perforation of high-strength fabric by projectiles of different geometry. *Int J Impact Eng* 2003; 28: 207–222.

[66] Wang Y, Chen X, Young R, et al. Finite element analysis of effect of inter-yarn friction

on ballistic impact response of woven fabrics. *Compos Struct* 2016; 135: 8–16.

[67]   Duan Y, Keefe M, Bogetti TA, et al. Modeling friction effects on the ballistic impact behavior of a single-ply high-strength fabric. *Int J Impact Eng* 2005; 31: 996–1012.

[68]   Duan Y, Keefe M, Bogetti TA, et al. Modeling the role of friction during ballistic impact of a high-strength plain-weave fabric. *Compos Struct* 2005; 68: 331–337.

[69]   Zeng XS, Tan VBC, Shim VPW. Modelling inter-yarn friction in woven fabric armour. *Int J Numer Methods Eng* 2006; 66: 1309–1330.

[70]   Chu Y, Min S, Chen X. Numerical study of inter-yarn friction on the failure of fabrics upon ballistic impacts. *Mater Des* 2017; 115: 299–316.

[71]   Karbalaie M, Yazdanirad M, Mirhabibi A. High performance Dyneema® fiber laminate for impact resistance/macro structural composites. *J Thermoplast Compos Mater* 2012; 25: 403–414.

[72]   Shanazari H, Liaghat G, Hadavinia H, et al. Analytical investigation of high-velocity impact on hybrid unidirectional / woven composite panels. *J Thermoplast Compos Mater* 2015; 1–9.

[73]   Chen X, Zhou Y, Wells G. Numerical and experimental investigations into ballistic performance of hybrid fabric panels. *Compos Part B Eng* 2014; 58: 35–42.

[74]   Seltzer R, González C, Muñoz R, et al. X-ray microtomography analysis of the damage micromechanisms in 3D woven composites under low-velocity impact. *Compos Part A Appl Sci Manuf* 2013; 45: 49–60.

[75]   Chen X, Chaudhry I. Ballistic protection. In: Scott R (ed) *Textiles for Protection*. Cambridge: Woodhead Publishing Limited, 2005, p. 229.

[76]   Saxtorph M. *Warriors and Weapons of Early Times*. New York: Macmillan Co., 1972.

[77]   Sun D. *Ballistic performance evaluation of woven fabrics based on experimental and numerical approaches*. Elsevier Ltd. Epub ahead of print 2016. DOI: 10.1016/B978-1-78242-461-1.00014-5.

[78]   David N V., Gao X-L, Zheng JQ. Ballistic Resistant Body Armor: Contemporary and Prospective Materials and Related Protection Mechanisms. *Appl Mech Rev* 2009; 62: 050802.

[79]   Zee RH, Hsieh CY. Energy absorption processes in fibrous composites. *Mater Sci Eng A* 1998; 246: 161–168.

[80]   Zhang YD, Wang YL, Huang Y, et al. Preparation and Properties of Three-dimensional Braided UHMWPE Fiber Reinforced PMMA Composites. *J Reinf Plast Compos* 2006; 25: 1601–1609.

[81]   Dong Z, Sun CT. Testing and modeling of yarn pull-out in plain woven Kevlar fabrics. *Compos Part A Appl Sci Manuf* 2009; 40: 1863–1869.

[82]   Karahan M, Ulcay Y, Eren R, et al. Investigation into the Tensile Properties of Stitched and Unstitched Woven Aramid/Vinyl Ester Composites. *Text Res J* 2010; 80: 880–891.

[83]   Erlich DC, Shockey DA, Simons JW. Slow Penetration of Ballistic Fabrics. *Text Res J* 2003; 73: 179–184.

[84]   Zahid B, Chen X. Impact performance of single-piece continuously textile reinforced riot helmet shells. *J Compos Mater* 2014; 48: 761–766.

[85]   Nayak N, Banerjee A, Datta D. Ultrasonic assessment of bullet inflicted damage in aramid laminated composites. *Def Sci J* 2012; 62: 153–158.

[86]   Jang BZ, Chen LC, Hwang LR, et al. The response of fibrous composites to impact loading. *Polym Compos* 1990; 11: 144–157.

[87]   Yang Y, Chen X. Investigation of energy absorption mechanisms in a soft armor panel under ballistic impact. *Text Res J* 2017; 87: 2475–2486.

[88]   Chen X, Yang D. Use of 3D Angle-Interlock Woven Fabric for Seamless Female Body

Armour: Part 1: Ballistic Evaluation. *Text Res J* 2010; 80: 1581–1588.

[89] Öberg EK, Dean J, Clyne TW. Effect of inter-layer toughness in ballistic protection systems on absorption of projectile energy. *Int J Impact Eng* 2015; 76: 75–82.

[90] Yang Y, Chen X. Investigation on energy absorption efficiency of each layer in ballistic armour panel for applications in hybrid design. *Compos Struct* 2017; 164: 1–9.

[91] Zohdi TI. Modeling and simulation of progressive penetration of multilayered ballistic fabric shielding. *Comput Mech* 2002; 29: 61–67.

[92] Joo K, Kang TJ. Numerical Analysis of Energy Absorption Mechanism in Multi-ply Fabric Impacts. *Text Res J* 2008; 78: 561–576.

[93] Learmont HS. *Soft armor*. patent number US 7,251,835 B2, US, 2007. Epub ahead of print 2007. DOI: 10.1126/science.Liquids.

[94] Karahan M, Kuş A, Eren R. An investigation into ballistic performance and energy absorption capabilities of woven aramid fabrics. *Int J Impact Eng* 2008; 35: 499–510.

[95] Liu J, Long Y, Ji C, et al. Influence of layer number and air gap on the ballistic performance of multi-layered targets subjected to high velocity impact by copper EFP. *Int J Impact Eng* 2018; 112: 52–65.

[96] Crouch IG. Body armour – New materials, new systems. *Def Technol* 2019; 15: 241–253.

[97] Nayak R, Crouch I, Kanesalingam S, et al. Body armor for stab and spike protection , Part 1 : Scientific literature review. *Text Res J* 2017; 0: 1–21.

[98] Azrin Hani AR, Roslan A, Mariatti J, et al. Body armor technology: A review of materials, construction techniques and enhancement of ballistic energy absorption. *Adv Mater Res* 2012; 488–489: 806–812.

[99] Laible RC. *Fibrous armor. In: Laible RC (ed.) Ballistic materials and penetration mechanics*. Newyork, USA: Elsevier Applied Science. Epub ahead of print 1980. DOI: 10.1097/00000433-198206000-00020.

[100] Chen X, Zhou Y. Technical textiles for ballistic protection. In: *Handbook of Technical Textiles*. Elsevier Ltd., pp. 169–192.

[101] Wittman RE, Rolsten RF. Armor – of Men and Aircraft. In: *12th National SAMPE Symposium, SAMPE*. 1967.

[102] Tam T, Bhatnagar A. High performance ballistic fibers. In: Bhatnagar A (ed) *Lightweight ballistic composites, Military and law-enforcement applications*. Abington Hall, Abington, Cambridge CB1 6AH, England,: Woodhead Publishing Limited, 2006, pp. 189–209.

[103] Yang HH. *Kevlar Aramid Fiber*. Chichester: John Wiley & Sons, 1993.

[104] Horrocks AR, Kandola BK. Flammability and fire resistance of composites. In: *Design and manufacture of textile composites*. Abington Hall, Abington, Cambridge CB1 6AH, England: Woodhead Publishing Limited, 2005, pp. 30–363.

[105] Finckernor, M. M. Comparison of High-Performance Fiber Materials Properties in Simulated and Actual Space Environments. *NASA Tech Rep*https://ntrs.nasa.gov/search.jsp?R=20170006996&hterms=polymer+composite+radiation&qs=Ntx%3Dmode%2520matchallpartial%26Ntk%3DAll%26Ns%3DPublication-Date%7C1%26N%3D0%26No%3D10%26Ntt%3Dpolymer%2520composite%2520radiation (2017).

[106] HA-MINH C. *Comportement mécanique des matériaux tissés soumis à un impact balistique : approches expérimentale, numérique et analytique*. UNIVERSITÉ DE LILLE 1, 2011.

[107] Gruschwitz Textilwerke AG. Ultra High Molecular Weight Polyethylene Fiber from DSM Dyneema. *Tech DataSheet*; 49https://issuu.com/eurofibers/docs/name8f0d44 (2016).

[108] Shim VPW, Tan VBC, Tay TE. Modelling deformation and damage characteristics of woven fabric under small projectile impact. *Int J Impact Eng* 1995; 16: 585–605.

[109] Bhatnagar A. *Lightweight ballistic composites - Military and law-enforcement applications*. Cambridge, , England: Woodhead Publishing Limited, 2006.

[110] Spectra® fiber1000. *https://www.packagingcomposites-honeywell.com/spectra/product-info/spectra-fiber/*.

[111] Percha PA. *Mater Res Soc Symp Proc, 134, 307*. 1989.

[112] Toyobo. BPO fibers. *http://www.toyobo.co.jp/e/seihin/kc/pbo/technical. pdf, Toyobo Co., pp 2-18* 2001; 2–18.

[113] AP. New York Times, New York. *P A37*, 2003.

[114] Walsh PJ, Hu X, Cunniff P, et al. Environmental effects on poly-p-phenylenebenzobisoxazole fibers. I. Mechanisms of degradation. *J Appl Polym Sci* 2006; 102: 3517–3525.

[115] Yang H. *Kevlar aramid fiber*. New York: John Wiley & Sons Ltd, 1993.

[116] Dey SK, Xanthos M. Glass Fibers. *Funct Fill Plast* 2010; 21: 141–162.

[117] Wallenberger F, Watson J, Li H. Glass Fibers. In: *ASM Handbook composites*. Ohio, 2001. Epub ahead of print 2001. DOI: 10.1143/JJAP.48.070215.

[118] Lowenstein KL. *The Manufacturing Technology of Continuous Glass Fibres*. 3rd editio. Amsterdam, the Netherlands, 1993.

[119] Wallenberg FT, Watson JC, Li H. Glass Fibers. In: *Constituent Materials in ASM Handbook*. Materials Park, OH: ASM International, Materials Information Society, 2001, pp. 21, 27–34.

[120] Wallenberger FT, Bingham PA. *Fiberglass and Glass Technology: Energy-Friendly Compositions and Applications*. Newyork, USA: Springer, 2010.

[121] Donnet JB, Bansal RC. *Carbon Fibers*. New York: Marcel Dekker Inc, 1990. Epub ahead of print 1990. DOI: 10.1016/B0-12-227410-5/00082-X.

[122] Buckley J, Edie DD. *Carbon-carbon materials and composites*. New Jersey: Noyes Publications, 1993.

[123] Yadav S, Ravichandran G. Penetration resistance of laminated ceramic/polymer structures. *Int J Impact Eng* 2003; 28: 557–574.

[124] Karandikar PG. A review of ceramics for armor applications. In: *Advances in Ceramic Armor IV, vol. 29*. The American Ceramic Society, 2009, pp. 163–175.

[125] Silva M V., Stainer D, Al-Qureshi H a., et al. Alumina-Based Ceramics for Armor Application: Mechanical Characterization and Ballistic Testing. *J Ceram* 2014; 2014: 1–6.

[126] Gonçalves DP, De Melo FCL, Klein AN, et al. Analysis and investigation of ballistic impact on ceramic/metal composite armour. *Int J Mach Tools Manuf* 2004; 44: 307–316.

[127] Skaggs SR. A Brief History of Ceramic Armor Development. In: *Ceramic Engineering and Science Proceedings*. The American Ceramic Society, 2003, pp. 337–349.

[128] Klement R, Krestan J, Rolc S. Ceramic materials for ballistic protection. *Key Eng Mater* 2009; 409: 291–294.

[129] Hearle J. A new generation of fibres:Introduction. In: *Hearle, JWS (ed.) High performance fibers*. Cambridge, UK: Woodhead Publishing Ltd, 2001.

[130] Fernanda Santos da Luza, Edio Pereira Lima Juniora LHLL, Monteiroa SN. Ballistic Test of Multilayered Armor with Intermediate Epoxy Composite Reinforced with Jute Fabric. *Mater Res* 2015; 18: 170–177.

[131] Pratheep Kumar A, Singh RP, Sarwade BD. Degradability of composites, prepared from ethylene-propylene copolymer and jute fiber under accelerated aging and biotic environments. *Mater Chem Phys* 2005; 92: 458–469.

[132] Bilisik K. Two-dimensional (2D) fabrics and three-dimensional (3D) preforms for ballistic and stabbing protection: A review. *Text Res J* 2017; 87: 1–30.

[133] Lane RA. High performance fibers for personnel and vehicle armor systems. *AMPTIAC Q* 2005; 9: 10.

[134] Bilisik K. Three-dimensional braiding for composites: A review. *Text Res J* 2013; 83: 1414–1436.

[135] Kadir Bilisik A, Turhan Y. Multidirectional Stitched Layered Aramid Woven Fabric Structures and their Experimental Characterization of Ballistic Performance. *Text Res J* 2009; 79: 1331–1343.

[136] Bilisik K, Korkmaz M. Multilayered and Multidirectionally-stitched aramid Woven Fabric Structures : Experimental Characterization of Ballistic Performance by Considering the Yarn Pull-out Test. *Text Res J* 2010; 80: 1697–1720.

[137] Chitrangad. *Hybrid ballistic fabric*. USA Patent 5187003 A, 1993.

[138] BL L, TF W, ST W, et al. Penetration failure mechanisms of Armor-Grade Fiber. *J Compos Mater* 2001; 35: 1605–33.

[139] Prosser RA, Cohen SH, Segars RA. Heat as a Factor in the Penetration of Cloth Ballistic Panels by 0.22 Caliber Projectiles. *Text Res J* 2000; 70: 709–722.

[140] Lee BL, Song JW, Ward JE. Failure of Spectra® Polyethylene Fiber-Reinforced Composites under Ballistic Impact Loading. *J Compos Mater* 1994; 28: 1202–1226.

[141] Montgomery TG, Grady PL. The Effects of Projectile Geometry on the Performance of Ballistic Fabrics. *Text Res J* 1982; 52: 442–450.

[142] Liang Z, Lee HK, Suaris W. Micromechanics-based constitutive modeling for unidirectional laminated composites. *Int J Solids Struct* 2006; 43: 5674–5689.

[143] Bilisik K, Karaduman NS, Bilisik NE, et al. Three-dimensional fully interlaced woven preforms for composites. *Text Res J* 2013; 83: 2060–2084.

[144] Yan C-F, Caiazzo AA. *3D woven composite for new and innovative impact and penetration resistance systems*. 2001.

[145] Flanagan MP, Zikry MA, Wall JW, et al. An Experimental Investigation of High Velocity Impact and Penetration Failure Modes in Textile Composites. *J Compos Mater* 1999; 33: 1080–1103.

[146] Grogan J, Tekalur SA, Shukla A, et al. Ballistic resistance of 2D and 3D woven sandwich composites. *J Sandw Struct Mater* 2007; 9: 283–302.

[147] Lefebvre M, Boussu F. High energy absorption of warp interlock fabrics : Application to high speed impact of fragments. In: *DYMAT International Conferences*. EDP Sciences, 2009, pp. 429–435.

[148] Boussu F, Cristian I, Nauman S. General definition of 3D warp interlock fabric architecture. *Compos Part B Eng* 2015; 81: 171–188.

[149] Lee B, Leong KH, Herszberg I. Effect of weaving on the tensile properties of carbon fibre tows and woven composites. *J Reinf Plast Compos* 2001; 20: 652–670.

[150] Callus PJ, Mouritz AP, Bannister MK, et al. Tensile properties and failure mechanisms of 3D woven GRP composites. *Compos Part A Appl Sci Manuf* 1999; 30: 1277–1287.

[151] Das S, Jagan S, Shaw A, et al. Determination of inter-yarn friction and its effect on ballistic response of para-aramid woven fabric under low velocity impact. *Compos Struct* 2015; 120: 129–140.

[152] Yang CC, Ngo T, Tran P. Influences of weaving architectures on the impact resistance of multi-layer fabrics. *Mater Des* 2015; 85: 282–295.

[153] Karahan M. Comparison of Ballistic Performance and Energy Absorption Capabilities of Woven and Unidirectional Aramid Fabrics. *Text Res J* 2008; 78: 718–730.

[154] Bandaru AK, Vetiyatil L, Ahmad S. The effect of hybridization on the ballistic impact

behavior of hybrid composite armors. *Compos Part B Eng* 2015; 76: 300–319.

[155] Nguyen LH, Ryan S, Cimpoeru SJ, et al. The effect of target thickness on the ballistic performance of ultra high molecular weight polyethylene composite. *Int J Impact Eng* 2015; 75: 174–183.

[156] Byun JH, Chou TW. Elastic Properties of Three- dimensional Angle-interlock Fabric Preforms. *J Text* 1990; 81: 538–548.

[157] Abtew MA, Loghin C, Cristian I, et al. Two Dimensional (2D) P-Aramid Dry Multi-Layered Woven Fabrics Deformational Behaviour for Technical Applications. *IOP Conf Ser Mater Sci Eng* 2018; 374: 1–12.

[158] Abtew MA, Bruniaux P, Boussu F, et al. Female seamless soft body armor pattern design system with innovative reverse engineering approaches. *Int J Adv Manuf Technol* 2018; 98: 2271–2285.

[159] De Luycker E, Morestin F, Boisse P, et al. Simulation of 3D interlock composite preforming. *Compos Struct* 2009; 88: 615–623.

[160] Khokar N. 3D-Weaving: Theory and Practice. *J Text Inst* 2001; 92: 193–207.

[161] Gokarneshan N, Alagirusamy R. Weaving of 3D fabrics: A critical appreciation of the developments. *Text Prog* 2009; 41: 1–58.

[162] Zahid B, Chen X. Development of a Helmet Test Rig for Continuously Textile Reinforced Riot Helmets. *Int J Text Sci* 2013; 2: 12–20.

[163] Min S. *Engineering Design of Composite Military Helmet Shells Reinforced by Continuous 3D Woven Fabrics*. 2016.

[164] Mih S, Roedel C, Zahid B, et al. Moulding of single-piece woven fabrics for protective helmets – A review and future work. In: *Moulding of single-piece woven fabrics for protective helmets – A review and future work*. Aachen: TexEng/RWTH Aachen, 2012.

[165] Dufour C, Wang P, Boussu F, et al. Experimental Investigation About Stamping Behaviour of 3D Warp Interlock Composite Preforms. *Appl Compos Mater* 2014; 21: 725–738.

[166] Abtew MA, Boussu F, Bruniaux P, et al. Influences of fabric density on mechanical and moulding behaviours of 3D warp interlock para-aramid fabrics for soft body armour application. *Compos Struct* 2018; 204: 402–418.

[167] Naik NK, Shrirao P, Reddy BCK. Ballistic impact behaviour of woven fabric composites: Formulation. *Int J Impact Eng* 2006; 32: 1521–1552.

[168] Cheeseman BA, Bogetti TA. Ballistic impact into fabric and compliant composite laminates. *Compos Struct* 2003; 35: 161–173.

[169] Yang D. *Design , Performance and Fit of Fabrics for Female Body Armour*. University of Manchester, 2011.

[170] Smith JC, Mccrackin FL, Schiefer HF. Stress-Strain Relationships in Yarns Subjected to Rapid Impact Loading:Part V: Wave Propagation in Long Textile Yarns Impacted Transversely. *Text Res J* 1958; 28: 288–302.

[171] Roylance D. Wave Propagation in a viscoelactic fibre subjected to transverse impact. *J Appl Mech* 1973; 40: 143–148.

[172] Roylance D. Ballistics of Transversely Impacted Fibers. *Textile Research Journal* 1977; 47: 679–684.

[173] Petterson DR, Stewart GM, Odell FA, et al. Dynamic Distribution of Strain in Textile Materials Part I: Experimental Methods and Preliminary Results on Single Yarns. *Text Res J* 1960; 30: 411–421.

[174] FREESTON, W. DENNEY J, WILLIAM D., CLAUS J. Strain-Wave Reflections During Ballistic Impact of Fabric Panels. *Text Res J* 1973; 43: 348–351.

[175] Yang EC, Ngo TD, Ruan D, et al. Impact Resistance and Failure Analysis of Plain

Woven Curtains. *Int J Prot Struct* 2015; 6: 113–136.

[176] Laible R. Fibrous armor. In: Laible R (ed) *Ballistic materials and penetration mechanics*. New York, USA: Elsevier Applied Science, 1980.

[177] Roylance D. Stress Wave Propagation in Fibres: Effect of Crossovers. *Fibre Sci Technol* 1980; 13: 385–395.

[178] Roylance DK. Wave Propagation in a Viscoelastic Fiber Subjected to Transverse Impact. *J Appl Mech* 1973; 40: 143–148.

[179] Pandya KS, Pothnis JR, Ravikumar G, et al. Ballistic impact behavior of hybrid composites. *Mater Des* 2013; 44: 128–135.

[180] Shaktivesh, Nair NS, Sesha Kumar C V., et al. Ballistic impact performance of composite targets. *Mater Des* 2013; 51: 833–846.

[181] Haijun X, Lulu L, Guangtao C, et al. Impact response and damage evolution of triaxial braided carbon/epoxy composites. Part I: Ballistic impact testing. *Text Res J* 2013; 83: 1703–1716.

[182] Shaktivesh, Nair NS, Naik NK. *Ballistic impact behavior of 2D plain weave fabric targets with multiple layers: Analytical formulation*. 2015. Epub ahead of print 2015. DOI: 10.1177/1056789514524074.

[183] Jia X, Sun B, Gu B. A numerical simulation on ballistic penetration damage of 3D orthogonal woven fabric at microstructure level. *Int J Damage Mech* 2012; 21: 237–266.

[184] Naik NK, Doshi AV. Ballistic impact behaviour of thick composites: Parametric studies. *Compos Struct* 2008; 82: 447–464.

[185] Udatha P, Sesha Kumar C V., Nair NS, et al. High velocity impact performance of three-dimensional woven composites. *J Strain Anal Eng Des* 2012; 47: 419–431.

[186] Timoshenko S, Goodier J. *Theory of elasticity*. New York: McGraw-Hill Inc. Epub ahead of print 1951. DOI: 10.1016/B978-0-08-057069-3.50001-2.

[187] Leigh Phoenix S, Porwal PK. A new membrane model for the ballistic impact response and V50 performance of multi-ply fibrous systems. *Int J Solids Struct* 2003; 40: 6723–6765.

[188] Anderson Jr. CE, Gooch WA. Numerical simulations of dynamic X-ray imaging experiments of 7.62 mm APM2 projectiles penetrating B4C. In: *Proceedings of the 19th International Symposium of Ballistics*. Interlaken, Switzerland, 2001, pp. 1423–1429.

[189] Morye SS, Hine PJ, Duckett RA, et al. Modelling of the energy absorption by polymer composites upon ballistic impact. *Compos Sci Technol* 2000; 60: 2631–2642.

[190] Guoqi Z, Goldsmith W, Dharan CKH. Penetration of laminated Kevlar by projectiles-I. Experimental investigation. *Int J Solids Struct* 1992; 29: 399–420.

[191] Cantwell WJ, Morton J. Impact perforation of carbon fibre reinforced plastic. *Compos Sci Technol* 1990; 38: 119–141.

[192] Yang C, Tran P, Ngo T, et al. Effect of Textile Architecture on Energy Absorption of Woven Fabrics Subjected to Ballistic Impact. *Appl Mech Mater* 2014; 553: 757–762.

[193] Grujicic M, Bell WC, Glomski PS, et al. Filament-level modeling of aramid-based high-performance structural materials. *J Mater Eng Perform* 2011; 20: 1401–1413.

[194] Grujicic M, Hariharan A, Pandurangan B, et al. Fiber-level modeling of dynamic strength of kevlar® KM2 ballistic fabric. *J Mater Eng Perform* 2012; 21: 1107–1119.

[195] Chandekar GS, Kelkar AD, Mohan R V, et al. Comparative study of different weave architectures of woven textile composites under low velocity impact loading. In: *Proceedings of IMECE2008*. Boston, Massachusetts, USA, 2017, pp. 1–5.

[196] Backert S. The Relationship Between the Structural Geometry of a Textile Fabric and Its Physical Properties: Part II: The Mechanics of Fabric Abrasion. *Text Res J* 1951; 21: 453–468.

[197] SCELZO WA, BACKER S, BOYCE MC. Mechanistic Role of Yarn and Fabric Structure in Determining Tear Resistance of Woven Cloth Part I: Understanding Tongue Tear. *Text Res J* 1994; 64: 291–304.

[198] Teixeira NA, Platt MM, Hamburger WJ. Mechanics of Elastic Performance of Textile Materials:Part XII: Relation of Certain Geometric Factors to the Tear Strength of Woven Fabrics. *Text Res J* 1955; 25: 838–861.

[199] Matusiak M, Sikorski K. Influence of the structure of woven babrics on their thermal insulation properties. *J Fibres Text* 2011; 19: 46–53.

[200] Suppakul P, Bandyopadhyay S. The effect of weave pattern on the mode-I interlaminar fracture energy of E-glass/vinyl ester composites. *Compos Sci Technol* 2002; 62: 709–717.

[201] Grujicic M, Yavari R, Snipes JS, et al. The effect of plain-weaving on the mechanical properties of warp and weft p-phenylene terephthalamide (PPTA) fibers/yarns. *J Mater Sci* 2014; 49: 8272–8293.

[202] Chu CK, Chen YL. Ballistic-proof effects of various woven constructions. *Fibres Text East Eur* 2010; 83: 63–67.

[203] Tran P, Ngo T, Yang EC, et al. Effects of architecture on ballistic resistance of textile fabrics: Numerical study. *Int J Damage Mech* 2014; 23: 359–376.

[204] Zhou Y, Chen X. A numerical investigation into the influence of fabric construction on ballistic performance. *Compos Part B Eng* 2015; 76: 209–217.

[205] Kędzierski P, Popławski A, Gieleta R, et al. Experimental and numerical investigation of fabric impact behavior. *Compos Part B Eng* 2015; 69: 452–459.

[206] Sun D, Chen X, Wells G. Engineering and analysis of gripping fabrics for improved ballistic performance. *J Compos Mater* 2014; 48: 1355–1364.

[207] Shimek ME, Fahrenthold EP. Effects of Weave Type on Ballistic Performance of Fabrics. *AIAA J* 2012; 50: 2558–2565.

[208] Içten BM, Karakuzu R. Effects of weaving density and curing pressure on impact behavior of woven composite plates. *J Reinf Plast Compos* 2008; 27: 1083–1092.

[209] Min S, Chai Y, Chu Y, et al. Effect of Panel Construction on the Ballistic Performance of Multiply 3D through-the-Thickness Angle-Interlock fabrIc Reinforced Composites. *Polym Artic* 2019; 11: 1–13.

[210] Laib Le RC, Figu Cia F, Street K, et al. The Application of High-Modulus Fibers to Ballistic Protection. *J Macromol Sci Part A - Chem* 1973; 7: 295–322.

[211] Lim JS. Ballistic Behavior of Heracron®-Based Composites: Effect of the Number Multifilaments on High-Speed Projectiles. *Model Numer Simul Mater Sci* 2013; 03: 84–89.

[212] Nilakantan G, Keefe M, Wetzel ED, et al. Effect of statistical yarn tensile strength on the probabilistic impact response of woven fabrics. *Compos Sci Technol* 2012; 72: 320–329.

[213] Rao MP, Duan Y, Keefe M, et al. Modeling the effects of yarn material properties and friction on the ballistic impact of a plain-weave fabric. *Compos Struct* 2009; 89: 556–566.

[214] Ha-Minh C, Imad A, Boussu F, et al. Numerical study on the effects of yarn mechanical transverse properties on the ballistic impact behaviour of textile fabric. *J Strain Anal Eng Des* 2012; 47: 524–534.

[215] Dischler L. *Bullet resistant fabric and methods of manufacture*. US patent 5,225,241, USA, 1993.

[216] Chitrangad, Midlothian V, Rodriguez-Parada JM. *Flourinated finishes for aramids*. US Patent Number: 5,266,076., 1993. Epub ahead of print 1993. DOI: 10.1016/j.(73).

[217] Rebouillat S. *Surface treated aramid fibers and a process for making them*. US patent number 5,443,896, USA, 1993.

[218] Jantharat P, Mccuiston R, Gamonpilas C, et al. Influence of the Laminate Configurations of Transparent Armor on its Ballistic Protection. *Key Eng Mater* 2014; 608: 253–258.

[219] Min S, Chen X, Chai Y, et al. Effect of reinforcement continuity on the ballistic performance of composites reinforced with multiply plain weave fabric. *Compos Part B* 2016; 90: 30–36.

[220] Pol MH, Liaghat G, Hajiarazi F. Effect of nanoclay on ballistic behaviour of woven fabric composites: Experimental investigations. *J Compos Mater* 2012; 47: 1563–1573.

[221] Park JL, Chi YS, Kang TJ. Ballistic performance of hybrid panels composed of unidirectional/woven fabrics. *Text Res J* 2013; 83: 471–486.

[222] Wang Y, Chen X, Young R, et al. A numerical study of ply orientation on ballistic impact resistance of multi-ply fabric panels. *Compos Part B Eng* 2015; 68: 259–265.

[223] Min S, Chu Y, Chen X. Numerical study on mechanisms of angle-plied panels for ballistic protection. *Mater Des* 2016; 90: 896–905.

[224] Kang TJ, Lee S ho. Effect of Stitching on the Mechanical and Impact Properties of Woven Laminate Composite. *J Compos Mater* 1994; 28: 1574–1587.

[225] Hosur MV, Vaidya UK, Ulven C, et al. Performance of stitched / unstitched woven carbon / epoxy composites under high velocity impact loading. *Compos Struct* 2004; 64: 455–466.

[226] Tan KT, Yoshimura A, Watanabe N, et al. Effect of stitch density and stitch thread thickness on damage progression and failure characteristics of stitched composites under out-of-plane loading. *Compos Sci Technol* 2013; 74: 194–204.

[227] Wood MDK, Sun X, Tong L, et al. The effect of stitch distribution on Mode I delamination toughness of stitched laminated composites - experimental results and FEA simulation. *Compos Sci Technol* 2007; 67: 1058–1072.

[228] Ahmad MR, Yunus W, Ahmad W, et al. Effect of fabric stitching on ballistic impact resistance of natural rubber coated fabric systems. *Mater Des* 2008; 29: 1353–1358.

[229] Nilakantan G, Wetzel ED, Bogetti TA, et al. Finite element analysis of projectile size and shape effects on the probabilistic penetration response of high strength fabrics. *Compos Struct* 2012; 94: 1846–1854.

[230] Valdi MHT, Atrechian MR, Shalkoohy AJ, et al. Numerical investigation of the effect of projectile mass and drop height from water surface on pinch-off time and depth. *J Mar Sci Technol* 2018; 26: 408–420.

[231] Cunniff PM. The V50 performance of body armor under oblique impact. *Proc 18th Int Symp ...* 1999; 814–821.

[232] C. T. Lim C. H. Cheong VBCT. Perforation of High-Strength Double Ply Fabric System by Varying Shaped Projectiles. *Int J Impact Eng* 2002; 27: 577–591.

[233] Tan VB., Lim C., Cheong C. Perforation of high-strength fabric by projectiles of different geometry. *Int J Impact Eng* 2003; 28: 207–222.

[234] Rodríguez Millán M, Moreno CE, Marco M, et al. Numerical analysis of the ballistic behaviour of Kevlar® composite under impact of double-nosed stepped cylindrical projectiles. *J Reinf Plast Compos* 2016; 35: 124–137.

[235] Talebi H, Wong S V, Hamouda AMS. Finite element evaluation of projectile nose angle effects in ballistic perforation of high strength fabric. *Compos Struct* 2009; 87: 314–320.

[236] Hudspeth M, Chu JM, Jewell E, et al. Effect of projectile nose geometry on the critical velocity and failure of yarn subjected to transverse impact. *Text Res J* 2017; 87: 953–972.

[237] Phoenix S, Heisserer U, van der Werff H, et al. Modeling and Experiments on Ballistic Impact into UHMWPE Yarns Using Flat and Saddle-Nosed Projectiles. *Fibers* 2017; 5: 8.

[238] Tan VBC, Khoo KJL. Perforation of flexible laminates by projectiles of different geometry. *Int J Impact Eng* 2005; 31: 793–810.

[239] Feaga MK. The Effect of Projectile Strike Velocity on the Performance of Polyurea Coated RHA Plates. *Theses Diss*.

[240] Ansari MM, Chakrabarti A. Influence of projectile nose shape and incidence angle on the ballistic perforation of laminated glass fiber composite plate. *Compos Sci Technol* 2017; 142: 107–116.

[241] Ulven C, Vaidya UK, Hosur M V. Effect of projectile shape during ballistic perforation of VARTM carbon/epoxy composite panels. *Compos Struct* 2003; 61: 143–150.

[242] Rajagopal A, Naik NK. Oblique ballistic impact behavior of composites. *Int J Damage Mech* 2014; 23: 453–482.

[243] Chu CK, Chen YL, Hseu GC, et al. The study of obliquity on the ballistic performance of basket fabric composite materials. *J Compos Mater* 2007; 41: 1539–1558.

[244] Shim VPW, Guo YB, Tan VBC. Response of woven and laminated high-strength fabric to oblique impact. *Int J Impact Eng* 2012; 48: 87–97.

[245] Nilakantan G, Nutt S. Effects of fabric target size, shape, and clamping on the v50 ballistic impact performance of aramid soft body armor. In: *SAMPE Conference Proceedings*. Seattle, WA, pp. 1–15.

[246] Nilakantan G, Nutt S. Effects of fabric target shape and size on the V50 ballistic impact response of soft body armor. *Compos Struct* 2014; 116: 661–669.

[247] Nilakantan G, Nutt S. Effects of clamping design on the ballistic impact response of soft body armor. *Compos Struct* 2014; 108: 13–150.

[248] Zhang TG, Satapathy SS, Vargas-Gonzalez LR, et al. Effect of boundary conditions on the back face deformations of flat UHMWPE panels. In: *CAMX 2014 - The Composites and Advanced Materials Expo*. 2014.

[249] Cepuš E, Shahkarami A, Vaziri R, et al. Effect of boundary conditions on the ballistic response of textile structures. In: *ICCM-12 conference*. Parishttp://www.iccm-central.org/Proceedings/ICCM12proceedings/site/papers/pap695.pdf (1999).

[250] Singletary J, Steinruck T, Fitzgerald P. Effects of boundary conditions on v50 and zone of mixed results of fabric armor targets. In: *23rd International Symposium on ballistics*. Tarragona, 2007, pp. 865–871.

[251] Ha-Minh C, Boussu F, Kanit T, et al. Analysis on failure mechanisms of an interlock woven fabric under ballistic impact. *Eng Fail Anal* 2011; 18: 2179–2187.

[252] Zhang GM, Batra RC, Zheng J. Effect of frame size, frame type, and clamping pressure on the ballistic performance of soft body armor. *Compos Part B Eng* 2008; 39: 476–489.

[253] Zeng XS, Shim VPW, Tan VBC. Influence of boundary conditions on the ballistic performance of high-strength fabric targets. *Int J Impact Eng* 2006; 32: 631–642.

[254] Brantner SB. policeone.com. *Police History: The evolution of women in American law enforcement*https://www.policeone.com/police-history/articles/8634189-Police-History-The-evolution-of-women-in-American-law-enforcement/ (2015, accessed 23 December 2016).

[255] MONRIQUE Michèle. *Place des femmes dans la professionnalisation des armées*http://www.c2sd.sga.defense.gouv.fr/IMG/pdf/c2sd_synth_loriot_choix_femmes.pdf (2004).

[256] Boussu F, Bruniaux P. Customization of a lightweight ballistic vest for the female form. In: *Advances in military textiles and personal equipment.: Woodhead Publishing*. 2012, pp. 167–195.

[257] Boussu F, Ragot A, Kulinska M, et al. Customization of a lightweight ballistic vest. In: *2nd International Scientific Conference Textiles of the Future*. 2008.

[258] Moureaux B, Pfister F V, Van Zijl NA. *Specially shaped multilayer armor*. US5943694 A, USA: Google Patentshttps://www.google.sm/patents/US5943694 (1999).

[259] Hostettler IF, Rhum D, Forman MR, et al. (12) United States Patent subiectto any disclaimer : the term of this. 1.

[260] Teijin Aramid. *Ballistics material handbook*. 2016.

[261] Dong Z, Jiang G, Wu Z, et al. 3D parametric human modeling for warp-knitted seamless garment. *Int J Cloth Sci Technol* 2015; 27: 532–548.

[262] Mahbub R, Wang L, Arnold L. Design of knitted three-dimensional seamless female body armour vests. *Int J Fash Des Technol Educ* 2014; 7: 198–207.

[263] Smith BL, Chung L. Ting. *Molded torso-conforming body armor including method of producing same*. Patent No: US 2009/0255022 A1, US, 2009.

[264] Mccartney J, Hinds BK, Seow BL, et al. Dedicated 3D CAD for garment modelling. *J Mater Process* 2000; 107: 31–36.

[265] Yip, J., & Yu W. Intimate apparel with special functions. In: *Innovation and Technology of Women's Intimate Apparel,*. 2006, pp. 171–195.

[266] Taylor P, Sadat A, Sayem M, et al. 3D CAD systems for the clothing industry. *Int J Fash Des , Technol Educ* 2013; 3: 37–41.

[267] Huang HQ, Mok PY, Kwok YL, et al. Block pattern generation: From parameterizing human bodies to fit feature-aligned and flattenable 3D garments. *Comput Ind* 2012; 63: 680–691.

[268] Meng Y, Mok PY, Jin X. Computer aided clothing pattern design with 3D editing and pattern alteration. *CAD Comput Aided Des* 2012; 44: 721–734.

[269] Liu YJ, Zhang DL, Yuen MMF. A survey on CAD methods in 3D garment design. *Comput Ind* 2010; 61: 576–593.

[270] Chu C-H, Tsai Y-T, Wang CCL, et al. Exemplar-based statistical model for semantic parametric design of human body. *Comput Ind* 2010; 61: 541–549.

[271] Lin Y, Wang MJ. Constructing 3D human model from front and side images. *Expert Syst Appl* 2012; 39: 5012–5018.

[272] Wang CCL. Parameterization and parametric design of mannequins. *Comput Des* 2005; 37: 83–98.

[273] Wang C, Zhang Y, Sheung H. From designing products to fabricating them from planar materials. *IEEE Comput Graph Appl* 2010; 30: 74–85.

[274] Baek S-Y, Lee K. Parametric human body shape modeling framework for human-centered product design. *Comput Des* 2012; 44: 56–67.

[275] Cichocka A, Bruniaux P, Frydrych I. 3D Garment Modelling - Creation of a Virtual Mannequin of the Human Body. *Fibres Text East Eur* 2014; 22: 123–131.

[276] Fontana M, Rizzi C, Cugini U. 3D virtual apparel design for industrial applications. *Comput Des* 2005; 37: 609–622.

[277] Wang CCL, Wang Y, Yuen MMF. Design automation for customized apparel products. *Comput Des* 2005; 37: 675–691.

[278] McGhee DE, Steele JR. Optimising breast support in female patients through correct bra fit. A cross-sectional study. *J Sci Med Sport* 2010; 13: 568–572.

[279] McGhee D, Steele J. Breast volume and bra size. *Int J Cloth Sci Technol* 2011; 23: 351–360.

[280] Chan C, Yu W, Newton E. Evaluation and analysis of bra design. *Des J* 2001; 4: 33–40.

[281] Hardaker CHM, Fozzard GJW. The bra design process – a study of professional practice. *Int J Cloth Sci Technol* 1997; 9: 311–325.

[282] White J, Scurr J. Evaluation of professional bra fitting criteria for bra selection and fitting in the UK. *Ergonomics* 2012; 55: 704–711.

[283] Zheng R, Yu W, Fan J. Development of a new chinese bra sizing system based on breast anthropometric measurements. *Int J Ind Ergon* 2007; 37: 697–705.

[284] Lee H, Hong K, Ae E. Measurement protocol of women ' s nude breasts using a 3D scanning technique. *Appl Ergon* 2004; 35: 353–359.

[285] Kovacs L, Eder M, Hollweck R, et al. Comparison between breast volume measurement using 3D surface imaging and classical techniques. *Breast* 2007; 16: 137–145.

[286] Kayar R, Civelek S, Cobanoglu M, et al. Five methods of breast volume measurement: A comparative study of measurements of specimen volume in 30 mastectomy cases. *Breast Cancer Basic Clin Res* 2011; 5: 43–52.

[287] Wang JP, Zhang WY. An approach to predicting bra cup dart quantity in the 3D virtual environment. *Int J Cloth Sci Technol* 2007; 19: 361–373.

[288] Colaianni M, Siegl C, Penkunas S, et al. Volume Extraction from Body Scans for Bra Sizing. In: *6th International Conference on 3D Body Scanning Technologies, Lugano, Switzerland*. Lugano, Switzerland, 2015. Epub ahead of print 2015. DOI: 10.15221/15.106.

[289] Krenzer G, Starr C, Branson D. Development of a sports bra prototype patternworks International Best Solution to a Patternmaking Problem, 2000. *Cloth Text Res J* 2005; 23: 131–134.

[290] Oh S, Chun J. New Breast Measurement Technique and Bra Sizing System Based on 3D Body Scan Data. *J Erg Soc Korea 2014;* 2014; 33: 299–311.

[291] Wu L, Yick K, Ng S, et al. Parametric design and process parameter optimization for bra cup molding via response surface methodology. *Expert Syst Appl* 2012; 39: 162–171.

[292] Yick KL, Ng SP, Zhou XJ, et al. Wire Frame Representation of 3D Moulded Bra Cup and Its Application to Example-based Design. *Fibers Polym* 2008; 9: 653–658.

[293] Johnson CE. *Size adjustable bra structure*. US5863236 A, USA: Google Patentshttps://www.google.com/patents/US5863236 (1999).

[294] Loftin B. *Moulded Brassier*. No. 3,202,565, Celanese Corporation of America: US patent, 1965.

[295] Taylor P, Shin K, Ng SP, et al. A geometrically based flattening method for three-dimensional to two-dimensional bra pattern conversion. *Int J Fash Des , Technol Educ* 2010; 3: 37–41.

[296] Lee C-S, Cheng-Wen L. The application of codesign in new bra product innovations. *Int J Cloth Sci Technol* 2010; 22: 211–227.

[297] Ashdown SP. An investigation of the structure of sizing systems A comparison of three multidimensional optimized sizing systems generated from anthropometric data with the ASTM standard D5585-94. *Int J Cloth Sci Technol* 1998; 10: 324–341.

[298] Armstrong H. *Pattern Marking for Fashion Designer*. Harper Collins, New York, 1987.

[299] Page K, Steele J. Breast Motion and Sports Implications for Future Research. *Sport Med* 1999; 27: 205–211.

[300] Lee HY, Hong K. Optimal brassiere wire based on the 3D anthropometric measurements of under breast curve. *Appl Ergon* 2007; 38: 377–384.

[301] Pechter EA. Method for Determining Bra Size and Predicting Postaugmentation Breast Size. In: Shiffman MA (ed) *Breast Augmentation Principles and Practice*. Springer Berlin Heidelberg, 2009, pp. 77–83.

[302] Chevalier C, Kerisit C, Boussu F, et al. A new experimental setup to characterize the dynamic mechanical behaviour of ballistic yarns. *Meas Sci Technol* 2016; 27: 105902.

[303] Yadav R, Naebe M, Wang X, et al. Body armour materials: from steel to contemporary biomimetic systems. *RSC Adv* 2016; 6: 115145–115174.

[304] Bilisik K. Two-dimensional (2D) fabrics and three-dimensional (3D) preforms for ballistic and stabbing protection: A review. *Text Res J* 2016; 0: 1–30.

[305] Sun D, Chen X. Three-dimensional textiles for protective clothing. In: *Advances in 3D*

Textiles. 2015, pp. 341–360.

[306] Tong L, Mouritz AP BM. Manufacture of 3D fibre preforms. In: *3D Fibre Reinforced Polymer Composites*. Elsevier Science Ltd, 2002, pp. 13–15.

[307] Cox BN, Dadkhah MS. The Macroscopic Elasticity of 3D Woven Composites. *J Compos Mater* 1995; 29: 785–819.

[308] Lee L, Rudov-Clark S, Mouritz AP, et al. Effect of weaving damage on the tensile properties of three-dimensional woven composites. *Compos Struct* 2002; 57: 405–413.

[309] AFNOR. NF ISO-7211-3. Textiles-woven fabrics – construction – methods of analysis, part 3 : determination of crimp of yarn in fabric. 2017; 1–24.

[310] AFNOR.EN NF ISO 5084. Textiles–determination of thickness of textiles and textile products. 1996; 1–5.

[311] AFNOR. EN N 12127. Textiles–fabrics – determination of mass per unit area using small samples. 1998; 1–10.

[312] AFNOR. NF EN ISO 13934-1. Tensile properties of fabrics, part 1 : determination of maximum force and elongation at maximum force using the strip method. 2013; 10.

[313] Zhong T, Hu H. Formability of weft-knitted fabrics on a hemisphere. *Autex Res J* 2007; 7: 245–251.

[314] Bekampiene P, Domskiene J. Experimental analysis of the influence of stress concentrators on the buckling of woven materials under uniaxial tension. *Int J Mater Form* 2010; 3: 211–214.

[315] Mozafary V, Payvandy P, Bidoki S, et al. Predicting the Influence of Seam Design on Formability and Strength of Nonwoven Structures Using Artificial Neural Network. *Fibers Polym* 2013; 14: 1535–1540.

[316] Najjar W, Legrand X, Dal Santo P, et al. Analysis of the blank holder force effect on the preforming process using a simple discrete approach. *Key Eng Mater* 2013; 554–557: 441–446.

[317] Najjar W, Legrand X, Pupin C, et al. A simple discrete method for the simulation of the preforming of woven fabric reinforcement. *Key Eng Mater* 2012; 504: 213–218.

[318] Dufour C, Boussu F, Wang P, et al. Experimental Forming Studies on 3D Warp Interlock Fabrics. *Eccm16 - 16Th Eur Conf Compos Mater*.

[319] U.S. Department of Justice, ballistic Resistance of Body Armor, NIJ Standard-0101.06. *Law Enforc Correct Stand Test Progr* 2000; 1–67.

[320] Prather R, Swann C, Hawkins C. *Backface Signatures of Soft Body Armors and the Associated Trauma Effects*. 1977.

[321] Le Pechoux B, Ghosh TK. *Apparel Sizing and Fit*. The Textile Institute, Textile Progress. Volume 32, Number 1, ALDEN, Oxford, UK, 2002.

[322] Anderson J, Chandler S, Mason M, et al. Scientific Analysis Reveals Major Differences in the Breast Size of Women in Different Countries. *J Female Heal Sci JFHTD13098*; 268–283.

[323] Zheng R, Yu W, Fan J. Breast measurement and sizing. In: *Innovation and Technology of Women's Intimate Apparel*. 2006, pp. 28–58.

[324] Loker S, Ashdown SP, Cowie L, et al. Consumer interest in commercial applications of body scan data. *J Text Apparel, Technol Manag* 2004; 4: 1–13.

[325] Chiappetta J. *La coupe à plat n°2, La lingerie féminine et le maillot de bain*. Les Presses du Midi, ISBN : 2-87867-124-4, France (1999), pp. 9-29.

[326] Barker J, Black C. Ballistic vests for police officers : using clothing comfort theory to analyse personal protective clothing. *Int J Fash Des , Technol Educ* 2009; 37–41.

[327] Li J, Zhang D, Lu G, et al. Flattening triangulated surfaces using a mass-spring model. *Int J Adv Manuf Technol* 2005; 25: 108–117.

[328] McCartney J, Hinds BK, Seow BL. Flattening of triangulated surfaces incorporating darts and gussets. *CAD Comput Aided Des* 1999; 31: 249–260.

[329] Wang CCL, Smith SS-F, M.F.Yuen M. Surface flatting based on energy model. *Comput Des* 2002; 34: 823–833.

[330] Amirbayat J, Hearle JWS. The anatomy of buckling of textile fabrics: Drape and conformability. *J Text Inst* 1989; 80: 51–70.

[331] Bruniaux P. 3D Pattern-Making On Adaptive Morphotype Mannequin. In: *14th Romanian Textiles and Leather Conference – CORTEP, 2012, 6 - 8 September* . Sinaia.

[332] Abtew MA, Bruniaux P, Boussu F, et al. Development of comfortable and well-fitted bra pattern for customized female soft body armor through 3D design process of adaptive bust on virtual mannequin. *Comput Ind* 2018; 100: 7–20.

[333] Abtew MA, Bruniaux P, Boussu F. Development of adaptive bust for female soft body armour using three dimensional (3D) warp interlock fabrics: Three dimensional (3D) design process. *IOP Conf Ser Mater Sci Eng* 2017; 254: 052001.

[334] Cichocka A, Bruniaux P, Koncar V. Modelling of Virtual Garment Design in 3D. *Res J Text Appar* 2007; 11: 55–63.

[335] Cichocka A, Bruniaux P. Comparison of traditional 2D and virtual patterns design in 3D VIRTUAL pattern design. In: *NASTEC6-2008, 13-15 August, McGill University, Montreal, canada.* 2008.

[336] Sun D, Chen X, Wells G. Engineering and analysis of gripping fabrics for improved ballistic performance. *J Compos Mater* 2013; 0: 1–10.

[337] Zufle TT. *Body armor for women*. US 4578821 A, US Patent: US 4578821 A, 1986.

[338] Süle G. Investigation of bending and drape properties of woven fabrics and the effects of fabric constructional parameters and warp tension on these properties. *Text Res J* 2012; 82: 810–819.

[339] Brandt J, Drechsler K, Arendts FJ. Mechanical performance of composites based on various three-dimensional woven-fibre preforms. *Compos Sci Technol* 1996; 56: 381–386.

[340] Chou S, Chen HC, Chen HE. Effect of weave structure on mechanical fracture behavior of three-dimensional carbon fiber fabric reinforced epoxy resin composites. *Compos Sci Technol* 1992; 45: 23–35.

[341] Stig F, Hallström S. Assessment of the mechanical properties of a new 3D woven fibre composite material. *Compos Sci Technol* 2009; 69: 1686–1692.

[342] Wang Y. Effect of Fabric Structures on the Mechanical Properties of 3-D Textile Composites. *J Ind Text* 2006; 35: 239–256.

[343] Behera BK, Dash BP. An Experimental Investigation into the Mechanical Behaviour of 3D Woven Fabrics for Structural Composites. 2014; 15: 1950–1955.

[344] Nasrun FMZ, Yahya MF, Ghani SA, et al. Effect of Weft Density and Yarn Crimps Towards Tensile Strength of 3D Angle Interlock Woven Fabric. *AIP Conf Proc* 2016; 020003: 1–6.

[345] Lv L, Zhang X, Ye F, et al. Fabrication and mechanical performance of 3D woven basalt fiber composite materials. *Funct Mater* 2017; 1: 76–81.

[346] Peerzada MH, Abbasi S, Khatri A. Tensile Behavior Analysis on Different Structures of 3D Glass Woven Perform for Fibre Reinforced Composites. 2013; 32: 121–124.

[347] Tong L, Mouritz AP BM. *3D fibre reinforced composite materials*. London: Elsevier Applied Science, 2002. Epub ahead of print 2002. DOI: https://doi.org/10.1016/B978-008043938-9/50020-X.

[348] Cooper DNE. The stiffness of woven textiles. *J Text Inst Trans* 1960; 51: T317–T335.

[349] Boisse P, Hamila N, Vidal-Sallé E, et al. Simulation of wrinkling during textile

composite reinforcement forming. Influence of tensile, in-plane shear and bending stiffnesses. *Compos Sci Technol* 2011; 71: 683–692.

[350] Prodromou AG, Chen J. On the relationship between shear angle and wrinkling of textile composite preforms. *Compos Part A Appl Sci Manuf* 1997; 28: 491–503.

[351] Skelton J. Textile materials: recovery from imposed deformation. *Science (80-)* 1972; 177: 657–663.

[352] Moure MM, Feito N, Aranda-Ruiz J, et al. On the characterization and modelling of high-performance para-aramid fabrics. *Compos Struct* 2019; 212: 326–337.

[353] Abtew MA, Boussu F, Bruniaux P, et al. Engineering of 3D warp interlock p-aramid fabric structure and its energy absorption capabilities against ballistic impact for body armour applications. *Compos Struct* 2019; 225: 111179.

[354] Abtew MA, Boussu F, Bruniaux P, et al. Ballistic impact performance and surface failure mechanisms of two-dimensional and three-dimensional woven p-aramid multi-layer fabrics for lightweight women ballistic vest applications. *J Ind Text* 2019; 0: 1–3.

[355] Mishra R, Behera BK. 3-Dimensional weaving. *Indian J Fibre Text Res* 2008; 33: 274–287.

[356] Khokar N. 3D-Weaving: Theory and Practice. *J Text Inst* 2001; 92: 193–207.

[357] Abtew MA, Bruniaux P, Boussu F, et al. A systematic pattern generation system for manufacturing customized seamless multi-layer female soft body armour through dome-formation (moulding) techniques using 3D warp interlock fabrics. *J Manuf Syst* 2018; 49: 61–74.

[358] Dufour C, Boussu F, Wang P, et al. Forming behaviour of 3D warp interlock fabric to produce tubular cross composite part. In: *14th AUTEX World Textile Conference*. Bursa, Turkey, 2014.

[359] Corbin AC, Boussu F, Ferreira M, et al. Influence of 3D warp interlock fabrics parameters made with flax rovings on their final mechanical behaviour. *J Ind Text* 2018; 0: 1–22.

[360] Chen X, Spola M, Paya JG, et al. Experimental Studies on the Structure and Mechanical Properties of Multi-layer and Angle-interlock Woven Structures. *J Text* 1999; 90: 91–99.

[361] Chen X, Zanini I. An experimental investigation into the structure and mechanical properties of 3D woven orthogonal structures. *J Text Inst* 1997; 88: 449–464.

[362] Gu H, Zhili Z. Tensile behavior of 3D woven composites by using different fabric structures. *Mater Des* 2002; 23: 671–674.

[363] Behera BK, Dash BP. Mechanical behavior of 3D woven composites. *Mater Des* 2015; 67: 261–271.

[364] Dai S, Cunningham PR, Marshall S, et al. Influence of fibre architecture on the tensile , compressive and flexural behaviour of 3D woven composites. *Compos PART A* 2015; 69: 195–207.

[365] Umer R, Alhussein H, Zhou J, et al. The mechanical properties of 3D woven composites. *J Compos Mater* 2017; 51: 1703–1716.

[366] Corbin AC, Kececi A, Boussu F, et al. Engineering Design and Mechanical Property Characterisation of 3D Warp Interlock Woven Fabrics. *Appl Compos Mater* 2018; 25: 811–822.

[367] Isa MT, Ahmed AS, Aderemi BO, et al. Effect of fiber type and combinations on the mechanical, physical and thermal stability properties of polyester hybrid composites. *Compos Part B Eng* 2013; 52: 217–223.

[368] Bandaru AK, Patel S, Sachan Y, et al. Mechanical characterization of 3D angle-interlock Kevlar/basalt reinforced polypropylene composites. *Polym Test* 2016; 55: 238–246.

[369] Bandaru AK, Sachan Y, Ahmad S, et al. On the mechanical response of 2D plain woven

and 3D angle-interlock fabrics. *Compos Part B Eng* 2017; 118: 135–148.

[370] Dahale M, Neale G, Lupicini R, et al. Effect of weave parameters on the mechanical properties of 3D woven glass composites. *Compos Struct* 2019; 223: 110947.

[371] Boussu F, Picard S, Soulat D. Interesting mechanical properties of 3D warp interlock fabrics. In: Al YK et (ed) *Narrow and Smart Textiles*. Springer International Publishing, 2018, pp. 21–31.

[372] Dash AK, Behera BK. Role of stuffer layers and fibre volume fractions on the mechanical properties of 3D woven fabrics for structural composites applications. *J Text Inst* 2019; 110: 614–624.

[373] Rao MP, Sankar B V., Subhash G. Effect of Z-yarns on the stiffness and strength of three-dimensional woven composites. *Compos Part B Eng* 2009; 40: 540–551.

[374] Umair M, Hamdani STA, Asghar MA, et al. Study of influence of interlocking patterns on the mechanical performance of 3D multilayer woven composites. *J Reinf Plast Compos* 2018; 37: 429–440.

[375] Labanieh AR, Liu Y, Vasiukov D, et al. Influence of off-axis in-plane yarns on the mechanical properties of 3D composites. *Compos Part A Appl Sci Manuf* 2017; 98: 45–57.

[376] Zhang D, Sun M, Liu X, et al. Off-axis bending behaviors and failure characterization of 3D woven composites. *Compos Struct* 2019; 208: 45–55.

[377] Kuo WS, Fang J, Lin HW. Failure behavior of 3D woven composites under transverse shear. *Compos Part A Appl Sci Manuf* 2003; 34: 561–575.

[378] Mouritz AP, Bannister MK, Falzon PJ, et al. Review of applications for advanced three-dimensional fibre textile composites. *Compos Part A Appl Sci Manuf* 1999; 30: 1445–1461.

[379] Abtew MA, Boussu F, Bruniaux P, et al. Experimental investigation of effects of stitching orientation on forming behaviors of 2D P-aramid multilayer woven preform. In: *AIP Conference Proceedings*. 2018, pp. 1–8.

[380] Purushothaman Pa, Coimbatore G, Ramkumar SS. Soft Body Armor for Law Enforcement Applications. *J Eng Fiber Fabr* 2013; 8: 97–103.

[381] Pirvu C, Deleanu L, Lazaroaie C. Ballistic tests on packs made of stratified aramid fabrics LFT SB1. In: *IOP Conference Series: Materials Science and Engineering*, p. 012099.

[382] Prabhakaran RTD, Andersen TL, Markussen CM, et al. Tensile and Compression Properties of Hybrid Composites - A Comparative Study. *19th Int Conf Compos Mater (ICCM 19)* 2013; 1029–1035.

[383] Zweben C. Tensile strength of hybrid composites. *J mat* 1977; 12: 1325–1337.

[384] MANDERS PW, BADER MG. The strength of hybrid glass/carbon fibre composites. *J Mater Sci* 1981; 16: 2233–2245.

[385] Legrand X, Boussu F, Nauman S, et al. Forming behaviour of warp interlock composite. *Int J Mater Form* 2009; 2: 177–180.